CATACLYSMIC VARIABLES IN GLOBULAR CLUSTERS AND LOW MASS X-RAY BINARIES

A Thesis submitted
to the University of Oxford
in the partial fulfilment of
the requirements
for the degree of
Doctor of Philosophy

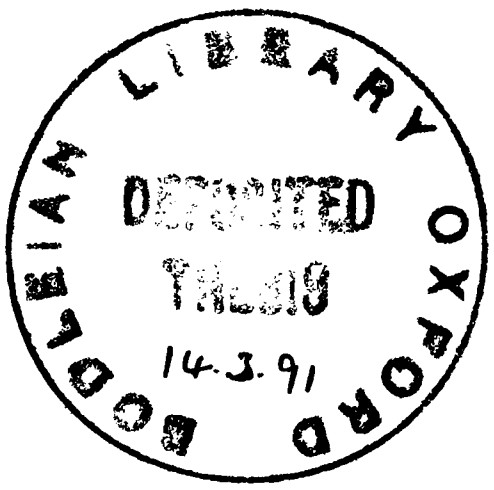

by
Graham Machin
Linacre College
Michealmas Term 1990

Cataclysmic Variables in Globular Clusters and Low Mass X–ray Binaries

Graham Machin
Linacre College
Oxford

A Thesis submitted to the University of Oxford in partial fulfilment of the requirements for the degree of Doctor of Philosophy.

Michaelmas 1990

Abstract

An introduction is given to cataclysmic variables (CVs), low mass X–ray binaries (LMXBs) and globular clusters. The radio properties of LMXBs are reviewed. I present optical spectroscopy and photometry of the globular cluster CV candidates, V4 in M30, V101 in M5, the CV candidates in M71 and of the LMXB 4U0614+09. VLA observations of the globular cluster X–ray sources in NGC7078, NGC6712, NGC6624 and NGC1851 and a "snapshot" of the galactic LMXB 4U2129+47 are presented.

The quiescent colours of V4 indicate that its orbital period is <5 hours. Its radial velocity, quiescent and outburst magnitudes show that it is probably not a cluster member. A hump in the light curve of V101, its quiescent colours, outburst magnitude and the results of quiescent state time resolved spectroscopy are all consistent with an orbital period of ~5–8 hours. V101 is the only CV whose photometric properties are compatible with cluster membership. Spectroscopy of the two brightest CV candidates in M71 shows that they are subdwarf B stars. The nature of the remaining candidates is discussed.

Radio counterparts to the X–ray sources in NGC7078 and NGC6712 are discovered. The observed emission is interpreted in terms of the synchrotron emission mechanism. Upper limits are placed on radio emission from the X–ray sources in NGC6624 and NGC1851 and from the galactic LMXB 4U2129+47.

4U0614+09 displays photometric variability on two timescales; 10 days and 1 hour. The former is interpreted as a precessing accretion disc whilst the latter could be either long timescale QPO or the orbital period. The optical spectrum is unusual because it only displays the Bowen blend (λ4640–4660) emission feature not He II λ4686. Possible explanations for this behaviour are discussed. Simultaneous optical and X–ray photometry shows that the optical flux was anticorrelated with the X–ray emission.

Contents

Chapter 1

Introduction

1.1 Preamble

Many stars (>50% Batten 1967) are found in binary systems. The orbital periods of such systems range from a few minutes to many years. The objects under investigation in this thesis are all short period (P~few hours) interacting binary stars, consisting of a degenerate component (that is a white dwarf, neutron star or black hole) and a low mass dwarf, the latter filling its Roche lobe. Matter is transferred to the degenerate object by Roche lobe overflow giving rise to a whole host of interesting observational phenomena, such as X–ray bursts and rapid large scale optical variability. Interacting binary stars which are comprised of a low mass secondary ($\leq$1 $M_{\odot}$) and a white dwarf primary are known as cataclysmic variables (CVs). Where the primary is a neutron star the systems are known as low mass X–ray binaries (LMXBs).

The thesis is structured in the following way:

Chapter One gives an introduction to the basic accretion process, white dwarf and neutron star binaries, globular clusters and radio observations of LMXBs and globular clusters.

In Chapters Two, Three and Four I will describe the results of observations of globular cluster CVs and globular cluster CV candidates. These observations are necessary for several reasons. Firstly, many CVs are thought to exist in globular clusters formed by the tidal capture mechanism (Fabian *et al.* 1975).

However relatively few, as yet, have been found and therefore it is important to search for new candidates to test this prediction. Secondly, the observational characteristics of the known candidate globular cluster CVs are poorly known and therefore require further study. Thirdly, the globular cluster CV population could have different observational and physical properties to its galactic counterpart. This might be due to the CVs in globular clusters having a different metallicity to the field CVs.

In Chapter Two new observations of the known globular cluster CV, V4 in M30 are presented along with a re–interpretation of its observed properties. In Chapter Three the results of photometry and low resolution spectroscopy of the globular cluster CV, V101 in M5 are presented. In Chapter Four I will present the results of photometry and spectroscopy of CV candidates in the globular cluster M71.

In Chapter Five I present the results of deep VLA imaging of four globular cluster LMXBs and a "snapshot" VLA observation of a radio emitting field LMXB. There are several reasons for conducting a survey for radio counterparts to globular cluster LMXBs. Firstly, many field LMXBs are known to emit radio radiation. To fully compare the field LMXBs with globular cluster LMXBs it is necessary to establish whether the globular cluster LMXBs actually emit radio radiation and in what form. Secondly it is very difficult to identify the optical counterparts to globular cluster LMXBs because of the extremely crowded nature of the field and the large size of the X–ray error boxes. Radio synthesis imaging can improve this accuracy by approximately an order of magnitude thereby reducing the number of possible candidate stars. Prior to these observations no radio emission had been found from any globular cluster LMXB.

The galactic plane LMXB 4U0614+09 has been only poorly studied. In an at-

tempt to remedy this situation an extensive photometry campaign (1986–1989) on the object has been performed to try to discover its orbital period. Also low resolution spectroscopy and simultaneous X–ray and optical photometry has been obtained in order to investigate the system's physical and observational characteristics. The results of these observations are described in Chapter Six.

1.2 Basic Accretion Physics

The lifetime of a star and its ultimate fate is critically dependent upon its mass. Stars with mass $M \leq 4\ M_{\odot}$ evolve reasonably gently through the main sequence, red giant and planetary nebula phases eventually ending up as white dwarfs. These compact stellar remnants are supported against further gravitational collapse by electron degeneracy pressure. Stars with mass $M \geq 8\ M_{\odot}$ evolve rapidly, eventually destroying themselves with a supernova explosion leaving behind a neutron star remnant. Both white dwarfs and neutron stars have been observed and are well established end–points of stellar evolution.

When white dwarfs or neutron stars are found in binary systems the possibility of accretion onto the compact object arises. The basics of the accretion process were first formulated by Edouard Roche when he considered the orbit of a test particle in the gravitational potential of two massive bodies orbiting one another. Though at the time he was concerned with the destruction or survival of planetary satellites the results he obtained are more widely applicable. The formulation assumes (1) the test particle does not perturb the orbits of the massive bodies, (2) that the massive bodies move in circular Keplerian orbits about one another and (3) the two bodies can be treated as point masses. When one calculates the orbits of the test particle one arrives at a sequence of allowed

paths such as those shown in Figure 1.2.1.

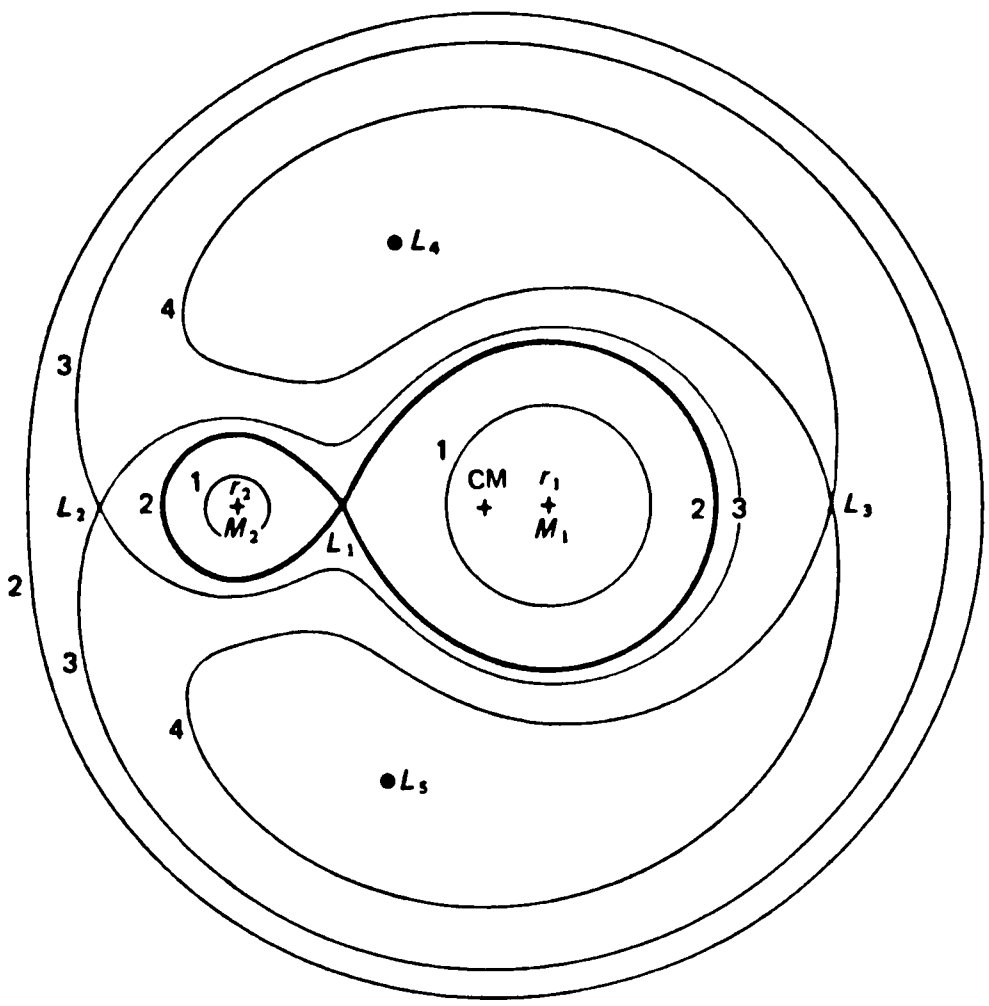

Figure 1.2.1: Sections in the orbital plane of the Roche equipotentials (adapted from Frank, King and Raine 1985). The centre of mass (CM) is marked as are the Lagrangian points L1–L5.

As can be seen quite complicated orbits are allowed. Far from the two stars the test particle executes an approximately circular orbit. This is because it effectively sees a point mass at the centre of the system. Similarly, close to each star the orbits of the test particle are circular; ie. the potential of one star is essentially unperturbed by the presence of the other. Inbetween there is somewhat complicated behaviour. The possible orbits of the test particle have several stationary (or saddle) points known as Lagrangian points (L1–L5). The orbit of the test particle which encloses one star and which passes through L1 (the inner Lagrangian point) is known as the Roche lobe of that star. All binary stars have Roche geometry such as this.

If one of the stars fills its Roche lobe then matter will be transferred through the L1 point and it will eventually be captured by the other star (this is shown schematically in Figure 1.2.2(a)–(c)). This type of binary star is known as a semi–detached system (Figure 1.2.2(b)). Mass transfer will continue until the mass losing star becomes smaller than its Roche lobe.

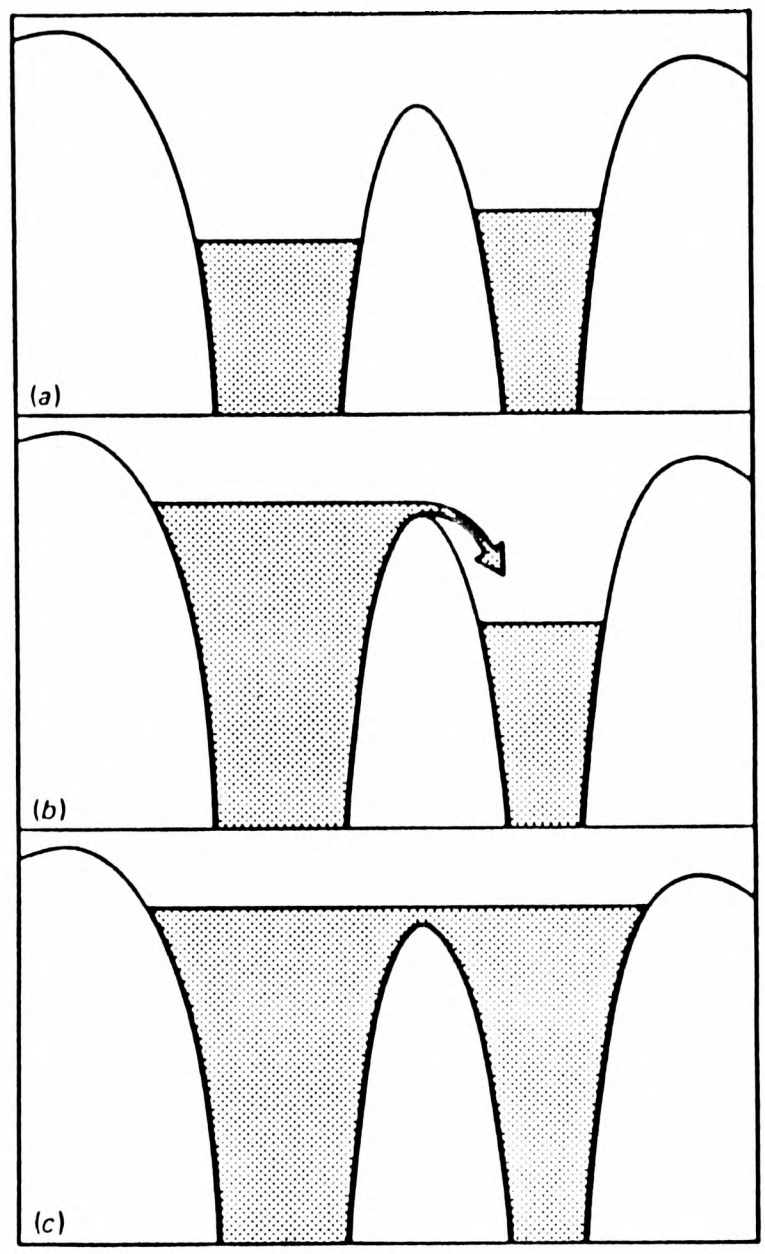

Figure 1.2.2: This shows the Roche potential (y–axis) versus the distance between the two stars (x–axis). Figure 1.2.2(a) shows a detached stellar system with both components remaining inside their Roche lobes. Figure 1.2.2(b) shows a semi–detached system where matter flows through the L1 point down the potential well onto the other star. Figure 1.2.2(c) shows a contact binary where both stars fill their Roche lobe and share a common envelope (Wade and Ward 1985).

Accretion of matter onto the surface of a compact object leads to the release of vast quantities of gravitational potential energy. The accretion luminosity (L_{acc}) is given by,

$$L_{acc}=GM\dot{M}/R \quad \text{erg s}^{-1} \qquad 1.2.1$$

where R and M are the radius and mass of the compact object respectively and $\dot{M}$ the mass accretion rate. L_{acc} is eventually released in the form of electromagnetic radiation. For example a typical solar mass neutron star with R$\sim$10 km and mass accretion rate of $\sim 10^{-10}$ $M_{\odot}$ yr^{-1} will have an accretion luminosity of $L_{acc}\sim 10^{37}$ erg s^{-1}. If it is assumed that the emission is blackbody and hence obeys Stefans law (equation 1.2.2) then an estimate of the blackbody temperature can be made,

$$L_{acc}=4\pi R^2 \sigma T^4 \qquad 1.2.2$$

which gives T$\sim 10^7$ K. Wiens displacement law shows that the peak of emission for a blackbody at this temperature is $\sim$3 Å ; ie. the peak of emission is in the X–ray waveband. Note that a white dwarf has R$\sim 10^4$ km and hence L_{acc} would be a 1000 times less than this case.

Matter that passes through the L1 point cannot be accreted directly onto the surface of the compact object since it possesses angular momentum. The angular momentum forces the material into a Keplerian orbit around the compact object such that the orbit has the same specific angular momentum as the gas had on passing through L1. The orbit will be circular since it lies well within the Roche lobe of the accreting star and hence a ring of material forms around the compact object. The orbiting material must shed its angular momentum before it can accrete onto the compact object. Dissipative processes such as viscous

interactions between fluid elements within the ring converts some of the orbital energy into internal energy of the ring. The ring of gas heats up and radiates energy away. To fuel this loss of energy the material moves closer towards the accreting object with its specific angular momentum decreasing. To conserve angular momentum a corresponding amount of material must move outwards with its specific angular momentum increasing. This causes the ring to spread out and form an accretion disc.

Examples of weakly or non–magnetic disc forming systems are dwarf novae (DN), which are a subclass of CVs, and LMXBs.

Modelling the physics of the accretion disc is extremely difficult and many approximations have to be made. The most important approximation is the parameterization of the disc viscosity, ν, into one parameter $\alpha = \nu / c_s H$ where c_s is the sound speed within the plasma and H the disc thickness (Shakura and Sunyaev 1973). This has enabled reasonably realistic models of disc systems to be constructed with the lack of understanding of the viscosity being isolated in the α parameter.

Accretion via an accretion disc is modified if the compact object possesses a strong magnetic field. A disc in some of these "magnetic systems" is unable to form at all because the ram pressure of the infalling material is less than the magnetic pressure of the B–field. In these cases the matter joins onto the magnetic field lines and is directly accreted onto the magnetic poles of the accreting object. Examples of strongly magnetized systems are Polars (AM Her) and the binary X–ray pulsars. These two situations are shown schematically in Figure 1.2.3.

Accretion onto a compact object does not have to occur by Roche lobe overflow.

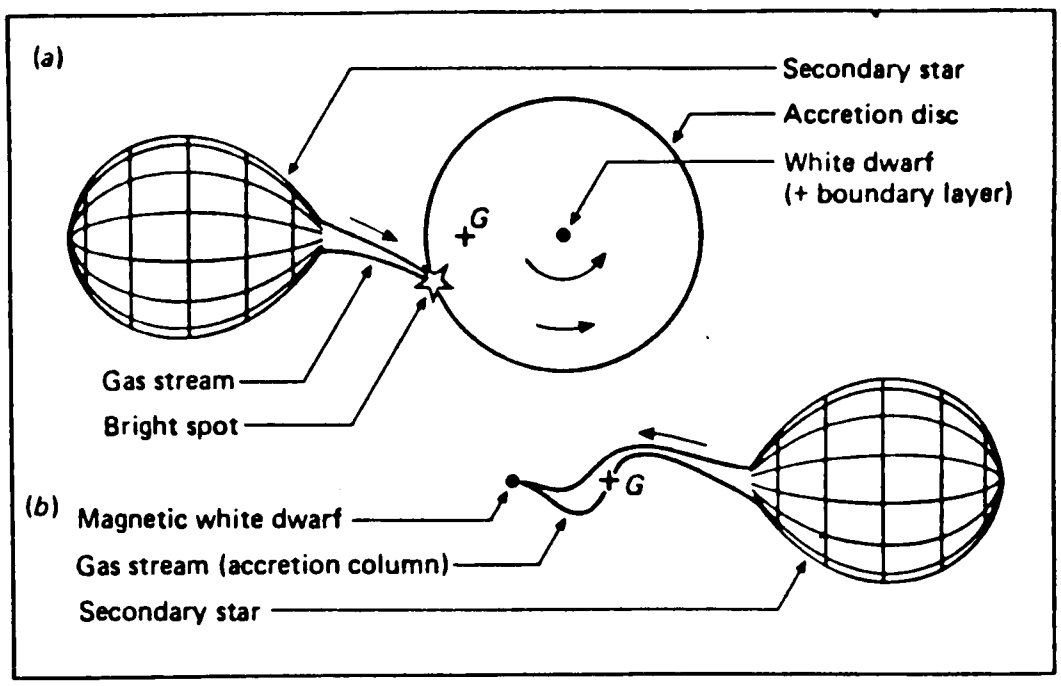

Figure 1.2.3: The two basic models for cataclysmic variable stars. A low magnetic field system in which the compact object accretes matter via an accretion disc (Figure 1.2.3(a)) and a high magnetic field system (Figure 1.2.3(b)) in which the compact object accretes matter via an accretion column onto its magnetic pole (Wade and Ward 1985). The main sources of electromagnetic radiation are indicated.

For example neutron stars have been observed orbiting early type O or B ($M \geq 10$ $M_{\odot}$) stars. In these cases the neutron star accretes matter from the stellar wind of the primary. These objects are known as massive X–ray binaries (MXBs). Most MXBs are X–ray pulsars, the pulsations being caused by the accreting matter being channeled onto the magnetic poles of the compact object by a strong ($B \geq 10^{12}$ G) magnetic field. This produces hot spots on the neutron stars surface. The rotation axes and the B field axes are misaligned producing the pulsations.

Orbital periods for the X–ray pulsars are relatively long (~few days) and relatively easy to find, either by X–ray eclipses or by observing the Doppler shift in the pulse arrival times. The ratio of $L_X/L_{opt} \ll 1$ for most of these systems shows that the optical companion dominates the radiation from MXBs.

1.3 Close Binary Systems

Introduction

In the previous section I have discussed the basic accretion process. I will now give descriptions of real systems in which accretion takes place. The material in this subsection is arranged as follows:

In Section 1.3a a review of non–magnetic Cataclysmic Variables (CVs) which consist of a low mass ($M \leq 1 M_{\odot}$) secondary and a white dwarf primary is given. This is followed by a brief description of magnetic CVs.

In Section 1.3b a review of Low Mass X–ray Binaries (LMXBs) which consist of a low mass ($M \leq 1 M_{\odot}$) secondary and a neutron star primary is given.

1.3a Cataclysmic Variables

Non–Magnetic Systems

The basic model for non magnetic CVs was given by Crawford and Kraft (1956). It is comprised of a white dwarf primary and a Roche lobe filling low mass ($\leq 1 M_{\odot}$) non degenerate secondary. The white dwarf accretes matter from the secondary via Roche lobe overflow, the accreting material forming a disc as described in the previous section. A typical accretion luminosity using equation 1.2.1 is $L_{acc} \sim 10^{33}$ erg s^{-1} assuming $R_{WD}=10^4$ km, $M_{WD}=1 M_{\odot}$ and $\dot{M}=10^{-10}$ $M_{\odot}$ yr^{-1}. This compares with the solar luminosity of $L_{\odot}=4 \times 10^{33}$ erg s^{-1} (Allen 1973). In a typical CV the luminosity of the secondary (usually a ZAMS dwarf with $M_{sec} \leq 1 M_{\odot}$ and $L_{sec} \leq 1 L_{\odot} \sim L_{acc}$) is comparable to or less than the accretion luminosity. Since the temperature of the accreting material is typically $\sim 10^4$ K

the emission from CVs peaks in the UV. The cool secondary can sometimes be observed in the near IR (Friend *et al.* 1988).

Another significant source of optical radiation is the bright spot where the accretion stream impacts the accretion disc. This is responsible for the presence of pronounced humps in the photometric light curves of some dwarf novae (for eg. U Gem; Warner and Nather 1971).

Only one half of the total available accretion energy is emitted by the disc. The rest is dissipated in a region very close the the white dwarfs surface. This region is known as the boundary layer. It is from the boundary layer that the soft and hard X–rays observed ($L_X < 10^{31}$ erg s^{-1}) from some CVs are thought to originate (Cordova and Mason 1983).

Non magnetic CVs are classified in terms of their outburst characteristics as classical novae, recurrent novae and dwarf novae. A classical nova outburst (Warner 1989) is thought to be caused by runaway thermonuclear fusion of hydrogen on the surface of the white dwarf. A typical energy release is $\geq 10^{44}$ erg, which leads to a brightening of 8–15 magnitudes. They are thought to be recurrent on timescales of $\sim 10^4$ yrs.

Recurrent novae are similar to classical novae but they have smaller eruptive events with changes in magnitude of ~4–9 and a recurrence time of 10–50 yrs. The origin of their outbursts is unclear being caused either by a thermonuclear event or by an episode of enhanced accretion (Cordova and Mason 1983).

Since DN are the only CVs studied in this thesis I will describe their properties in more detail.

The Outburst Mechanism of Dwarf Novae

Observations show that the enhanced luminosity observed for non–magnetic

DN in outburst comes from an enhanced accretion rate onto the white dwarf. Two different models have been proposed to explain the observed outburst behaviour. Both require the mass flux ($\dot{M}$) through the disc to increase but the mechanisms used to obtain this increase are different.

i) The disc instability model.

This model invokes a variation in the viscosity of the material in the disc which alters the transport time of material through the disc. Matter flows at a steady rate through the L1 point both in quiescence and during outburst. In quiescence the disc viscosity is low and the viscous timescale ($\tau \propto \text{viscosity}^{-1}$) is long. Matter accumulates in the disc and its surface density increases. When the density reaches a critical level the viscosity within the disc rises rapidly. This rapid rise in viscosity may be due to the ionization of hydrogen within the disc. This leads to a decrease in the viscous timescale and a corresponding increase in the flux of material through the disc. An outburst occurs. When the disc density decreases to a certain critical level the viscosity drops suddenly and the system becomes cool and faint. Mass then begins to build up in the disc again and the cycle repeats (Faulkner, Lin & Papaloizou 1983).

ii) The secondary instability model.

In this model the viscosity of the material in the disc remains approximately constant but the amount of material the secondary star transfers through the inner Lagrangian point (L1) varies. One possible way it can vary is if the photosphere of the red dwarf, local to the L1 point, is unstable. This instability may be driven by the recombination of hydrogen in the photosphere of the red dwarf though a rigorous quantitative analysis of this process has yet to be performed. An outburst then occurs when there is a large but temporary increase ($\sim$2–3 orders of magnitude) in the mass transfer rate through the L1 point. The nature

of the outburst then depends on the interplay between the viscous timescale and the timescale of matter being deposited into the disc (Bath, Clarke and Mantle 1986).

At present observations can be found to support either model. Two examples are given below, one supporting the disc instability model another supporting the secondary instability model.

The discs in DN are observed to be larger just after outburst than in quiescence (eg. U Gem; Smak 1984). This is predicted by the disc instability model. The outburst begins in the outer disc region. Matter moves rapidly through the disc but also rapidly moves outwards to conserve angular momentum. Hence the disc increases in size.

On the rise to outburst it is observed that the UV flux rises later than the optical flux. This supports the secondary instability model since for this model the temperature rises appreciably only after the increase in $\dot{M}$ has effected large parts of the disc (Verbunt 1986).

It may therefore be that a hybrid approach incorporating features of both models will need to be used if the outburst characteristics of DN are to be successfully reproduced. Such an approach has recently been taken by Duschl & Livio (1989).

The Classification of Dwarf Novae

Dwarf novae are subdivided into U Gem, Z Cam and SU UMa classes; these are described in more detail below. The name of each subclass was derived from the prototype object. The classification scheme is based on the morphology of the outburst light curves. Representative light curves for each subclass of DN

are shown in Figure 1.3.1(a)–(c).

U Gem

These are the "classical" dwarf novae. They brighten by a factor of 2–6 magnitudes and remain in the bright state for ~1–3 days. The outbursts recur on semi–regular timescales of ~weeks (Vogt 1989). There is some tendency for short and long outbursts to alternate (Cordova and Mason 1983), but the spread in total energy of these eruptions is less than a factor of 4. A typical light curve is shown in Figure 1.3.1(a).

Z Cam

The light curves of this subclass of DN are different from the U Gem type in that they occasionally have standstills in luminosity which interrupt the regular outburst quiescent cycle for extended periods (sometimes years). During standstill the luminosity remains constant at a value intermediate between outburst and quiescence. The end of standstill always comes with a decline to minimum. A typical light curve is shown in Figure 1.3.1(b).

SU UMa

These are classified by two very distinct outburst states. The "normal outburst" state which is identical to the U Gem outbursts and the "superoutburst" state which is much less frequent and recurs every 8–10 months, with $\delta m \geq 5$ and lasts

typically 12–18 days. The superoutburst recurs on a much more regular basis than the normal outbursts. Whilst in superoutburst their light curves display small scale variations which recur with a period slightly in excess of the orbital period. These are the so-called "superhumps". A typical light curve is shown in Figure 1.3.1(c).

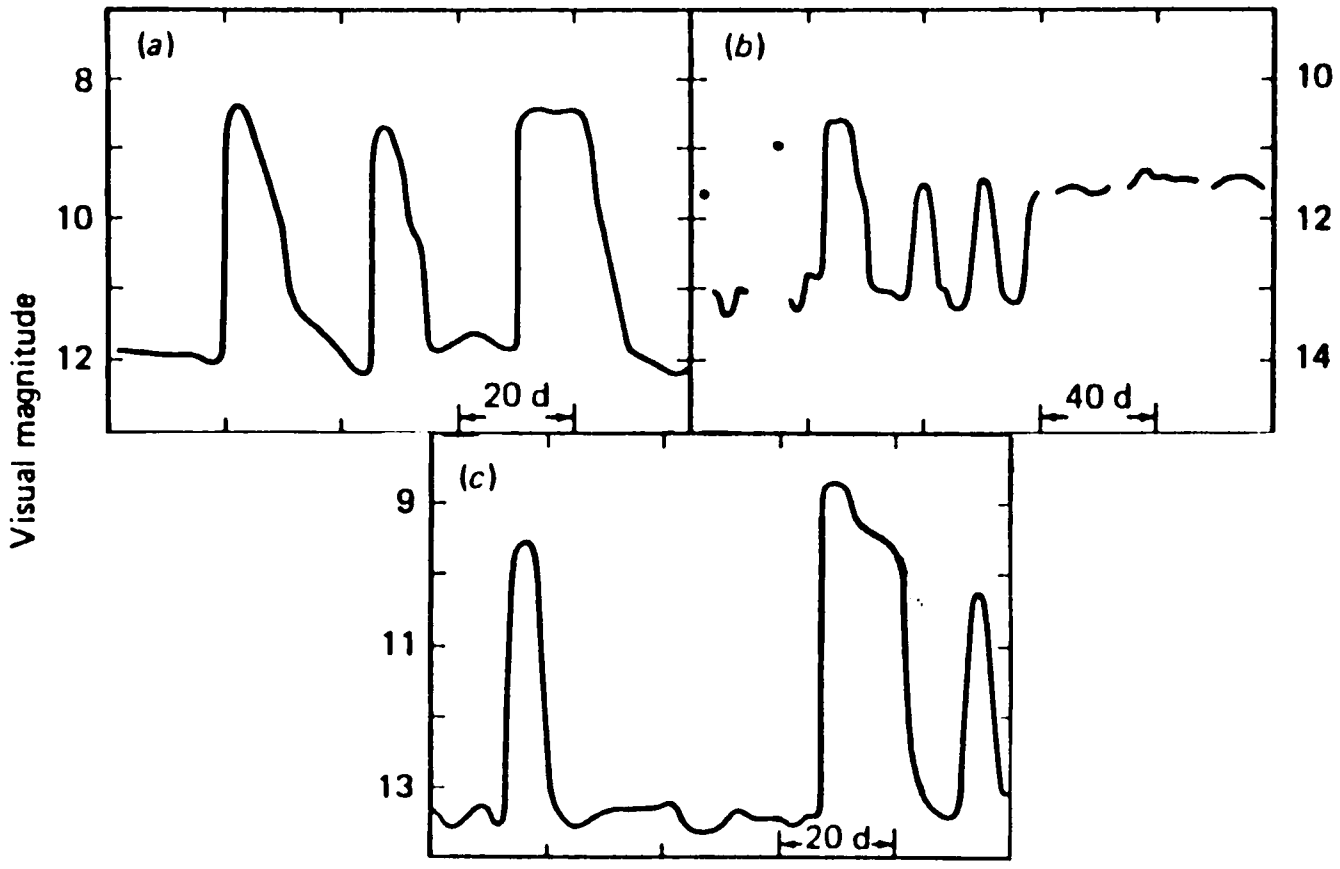

Figure 1.3.1: Typical light curves for the three classes of dwarf novae. Figure 1.3.1(a) U Gem type showing long and short outbursts. Figure 1.3.2(b) Z Cam displaying standstill behaviour. Figure 1.3.3(c) SU UMa type showing a normal outburst followed by a superoutburst (Wade and Ward 1985). These are described in more detail in the text.

The Optical Spectra of Dwarf Novae

Much of the optical emission from non–magnetic CVs comes from the accretion disc. In quiescence the continuum spectrum of a typical DN is flat. In outburst the spectrum is generally bluer. The appearance of the spectral lines varies markedly between the quiescent and outburst states (Figure 1.3.2).

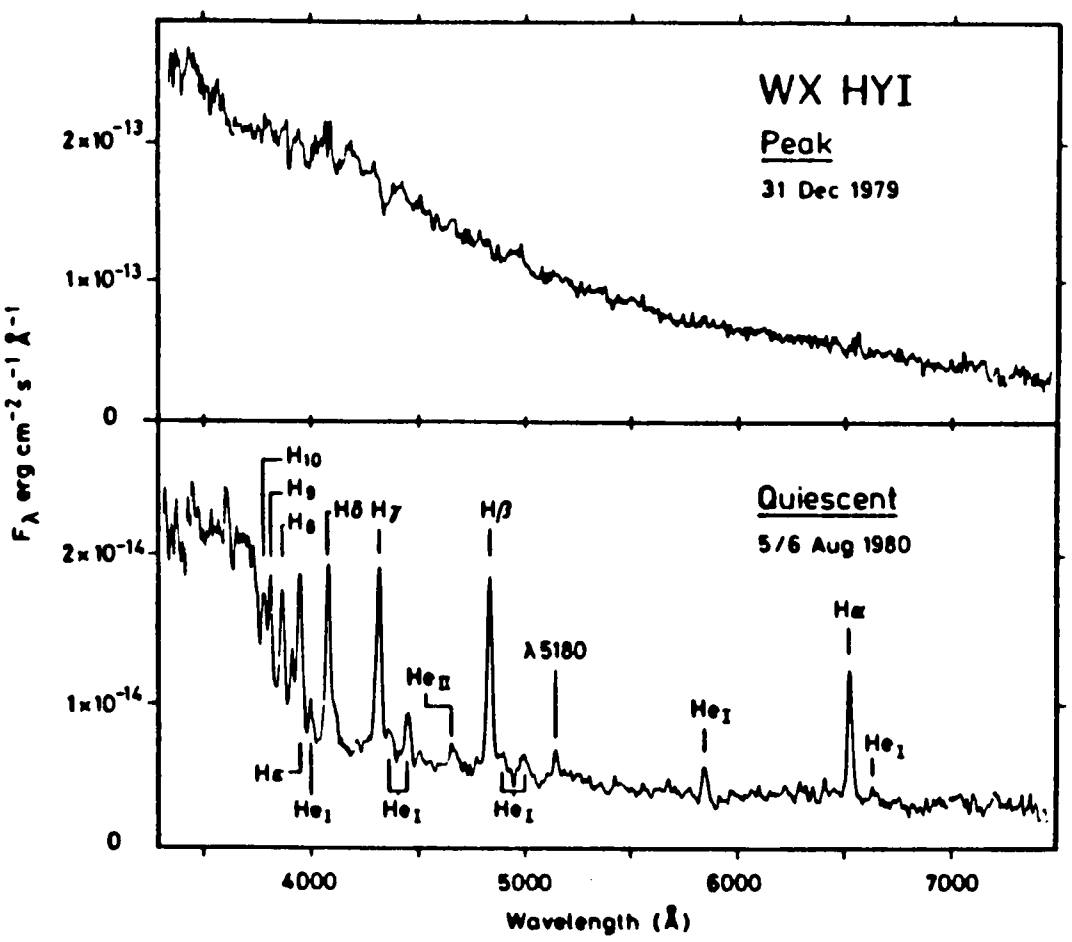

Figure 1.3.2: The spectrum of the dwarf nova WX Hydri in two distinct states: quiescence and outburst. The two states have very different spectra. In quiescence the spectrum is dominated by strong emission lines in outburst these lines are replaced by weak absorption features (Wade and Ward 1985).

In quiescence the optical spectrum is dominated by strong emission lines of hydrogen and neutral helium. Often He II is also present. The main line forming region is thought to be the accretion disc with additional contributions coming from the bright spot and the gas stream. The emission lines are double peaked in high inclination systems (Horne and Marsh 1986). In the UV emission lines of highly ionized species are present (eg. C IV).

On outburst the emission lines are replaced by broad shallow absorption lines usually of hydrogen and neutral helium. The UV lines often have P–Cygni profiles indicating the presence of a mass outflow (Szkody 1985). As the DN returns to quiescence the spectrum returns to an emission line state.

The optical emission can be modelled by assuming that it is possible to sub-

divide the disc into optically thick annuli each of which is characterised by a temperature T(R), with the highest temperature nearest to the white dwarf. This type of model generally reproduces the gross structure of the optical and UV emission, but other components need to be included such as emission from the secondary star (IR), the boundary layer (far UV and X–ray) and the bright spot (visual and near UV) to obtain a good representation of the overall spectral energy distribution for CVs (Cordova and Mason 1983).

Periodic Photometric Variations in Dwarf Novae

The optical light curves of dwarf novae are quite complex. Even the "simplest" show short term brightness variations known as flickering. Often, superimposed on these random photometric fluctuations are larger amplitude periodic variations. These periodic variations can be classified into three types, (i) a hump, (ii) a hump and an eclipse or (iii) a hump and two eclipses.

The hump is caused by the changing aspect of the bright spot around the orbital cycle. It persists for typically ~0.3–0.5 in phase. This type of non–eclipsing variation is observed only in low inclination DN. For higher inclination DN an eclipse is observed shortly after the hump maximum. This eclipse is caused by a partial obscuration of the bright spot by the red dwarf. For the highest inclination systems two eclipses occur shortly after hump maximum. The first is an eclipse of the white dwarf the second of the bright spot. Both these eclipses are caused by the red dwarf.

The orbital periods of DN can be determined from observations of this periodic structure.

Orbital Period Distribution

The orbital periods of DN are all short ($\leq$15 hrs) which from Keplers law means that the components have a typical separation of $\leq 3\times10^{11}$ cm (assuming $M_1+M_2=2M_\odot$). It is thought that systems with P$\geq$8 hrs probably have evolved secondaries so as to maintain Roche lobe overflow. When the orbital period versus the number of systems with these periods is plotted one gets the period distribution shown in Figure 1.3.3.

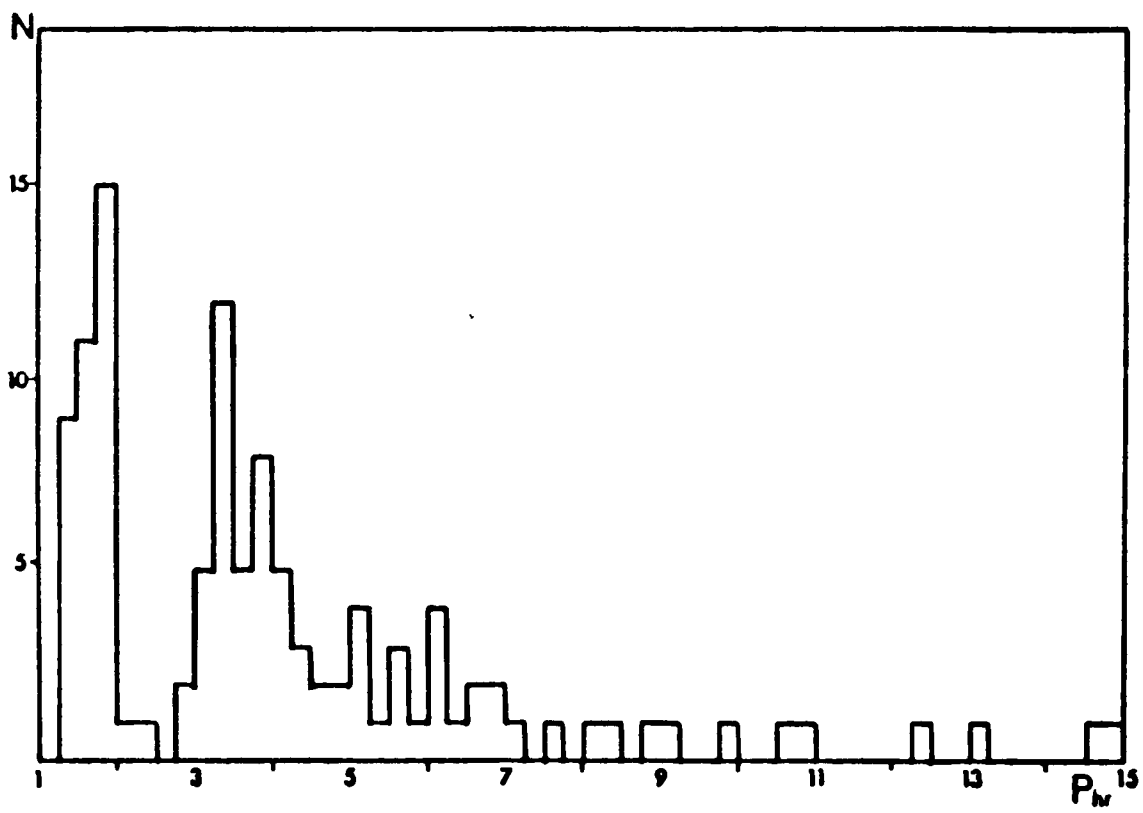

Figure 1.3.3: The orbital period distribution of CVs (P$\leq$15 hours). Note the period gap and the minimum period (King 1988).

It has two interesting features.

i) There are no CVs with orbital periods $\leq$80 minutes. This minimum period can be explained as follows. The orbital period of a semi-detached binary system is given by $P^2 \propto R^3_{sec}/M_{sec}$ (eg. King 1988). Initially the secondary is a lower main sequence star obeying the mass radius relation $M_{sec} \sim R_{sec}$. The mass of the secondary decreases via mass loss to the white dwarf, its radius

also decreases as it relaxes back into thermal equilibrium therefore the orbital period of the system begins to decrease. This continues until the secondary can no longer sustain thermonuclear burning ($M \leq 0.085\ M_{\odot}$), it then becomes degenerate. The radius of a degenerate star is inversely related to its mass and therefore as mass transfer continues the orbital period begins to increase. The radius of the secondary when it becomes degenerate corresponds to an orbital period of ~80 minutes (Paczyński 1981). It is possible for a system to have a shorter orbital period provided that the secondary is hydrogen depleted (Nelson *et al.* 1986).

ii) There is a period gap between 2 hours 10 minutes and 2 hours 50 minutes in which only a few systems are found. Generally SU UMa and AM Her stars are found below the period gap, whilst Z Cam and U Gem are found above the gap. The presence of the period gap can be explained as follows. Above the period gap the secondary, which rotates at the orbital period, loses angular momentum via magnetic braking in its wind and also by gravitational radiation. The orbital period decreases so rapidly that the secondary does not have time to relax back into thermal equilibrium. As the orbital period approaches three hours the secondary becomes fully convective and its magnetic field decreases to a low value. The rate of loss of angular momentum also decreases at this point and the secondary now has time to relax into thermal equilibrium. This causes it to contract inside its Roche lobe and the system becomes detached. Angular momentum continues to be lost via gravitational radiation and the orbital period continues to decrease, though at a slower rate than before. As the period decreases the Roche lobe reduces in size until it meets the secondary stars surface again (at an orbital period of ~2 hours). Mass transfer resumes and the CV is reborn (King 1988).

It has been found (Echevarria and Jones 1984) that the colour indices B–V and U–B for DN correlate strongly with orbital period. In particular the systems become redder (ie B–V becomes more positive) as the orbital period increases. This is due to the secondary star being larger and hence making a more important contribution to the total light output of the system.

Magnetic Systems

These are basically CVs whose white dwarf has a magnetic field that is strong enough to modify the accretion flow in some way.

Polars (AM Her type) have very strong magnetic fields with $B \geq 10^7$ G (Wade and Ward 1985). They do not form an accretion disc. Matter flowing through the L1 point is magnetically channelled directly onto the poles of the white dwarf star. The rotation period of the white dwarf is effectively the same as the orbital period of the system. The unique observational property of Polars is that the optical radiation is strongly polarized both linearly and circularly. Most of the gravitational energy is released in a standing shock near the pole. This includes much X–ray and optical radiation (Liebert and Stockman 1983). These systems also have low and high luminosity states.

The Intermediate Polars (DQ Hers) probably have weaker fields than Polars (typically $B \leq 10^7$ G). The magnetosphere of the white dwarf is within its Roche lobe and hence a partial disc is formed outside of the magnetospheric radius. They spectroscopically resemble other CVs but their defining feature is the presence of stable short period oscillations ranging from 33 seconds to 67 minutes (Wade and Ward 1985).

1.3b Low Mass X–ray Binaries (LMXBs)

Introduction

The basic model of a LMXB is very similar to that of a non–magnetic CV, only in the case of an LMXB the white dwarf is replaced by a neutron star with a low magnetic field. The accretion process is also very similar: ie. Roche lobe overflow of a red dwarf companion leading to accretion onto the compact object via an accretion disc. However the energy liberated in the LMXB case is ~1000 times more than in the CV case because the gravitational potential energy is $\propto 1/r$ and $r_{ns} \sim r_{wd}/1000$. Most of the radiation emitted from these systems is in the form of X–rays, some radiating at the maximum permissible luminosity, the Eddington luminosity (L_{edd}). At L_{edd} the outward radiation force per electron is balanced by the inward gravitational force on a proton hence inhibiting further accretion (for spherical accretion).

Observationally LMXBs fall into four non–exclusive categories, the bright bulge sources, the X–ray bursters, the globular cluster sources and the soft X–ray transients.

The general X–ray properties of LMXBs are characterised by a soft (kT~few keV) X–ray spectrum with many showing type I X–ray bursts (due to rapid thermonuclear burning in the surface layers of a neutron star surface, Lewin and Joss 1983) but with a marked absence of X–ray pulsations (which are common in MXBs) and eclipses (though dips are common, White 1989).

Most of the optical radiation from these sources comes from the reprocessing of a fraction of the X–rays into optical photons in the accretion disc.

For those systems for which optical counterparts have been found $L_X/L_{opt} \sim 10$–1000. This shows that most of the energy output by these systems is indeed

emitted in the form of X–rays.

In the following subsection I will review in detail the X–ray and optical properties of LMXBs.

X–ray Properties of LMXBs

LMXBs fall roughly into two categories when classified in terms of their X–ray luminosity. The very luminous ($\sim 10^{38}$ erg s^{-1}) bright bulge X–ray sources (including the two bright but non bulge sources Cyg X–2 and Sco X–1) and the less luminous ($\sim$few$\times 10^{37}$ erg s^{-1}) bursting X–ray sources (van Paradjis & Lewin 1986). Soft X–ray transients form a separate class of LMXB closely related to the X–ray burst sources.

The Bright Bulge Sources and QPO

Until very recently the bright non–bursting galactic bulge X–ray sources were almost a complete mystery. No optical counterparts could be found because of the high reddening of the bulge and no orbital modulations or X–ray pulsations were discovered. This situation has changed with the recent discovery that many of the brightest bulge sources display quasi–periodic oscillations (QPO) in their X–ray light curves (van der Klis 1989).

The timescales of the oscillations indicate that they are formed in the innermost regions of the LMXB accretion disc, close to the compact object. QPO peaks typically have the following characteristics:

i) centroid frequencies in the range 5–60 Hz

ii) a peak width ~1/2 the centroid frequency

iii) amplitudes ~1–10% of the total intensity

iv) recurrence

v) persistence for $\sim 10^5$ cycles.

QPO sources themselves fall into two distinct classes; Z type and Atoll type, the latter often displaying type I X–ray bursts (described in the next section). The Z type sources show three distinct X–ray spectral states in the X–ray colour – colour plane. These are the horizontal branch (HB), the normal branch (NB) and the flaring branch (FB). These sources do NOT jump between spectral states but move on the Z as they transit from one state to another. The mass accretion rate is thought to increase as the source moves from the HB, through the NB to the FB. Figure 1.3.4(a) shows an example of this behaviour. The power spectra of each of the states (Figure 1.3.4(b)) show several distinct features, the most important of which are the HB–QPO and the NB/FB–QPO. The HB–QPO frequency (typically ~15–55 Hz) is strongly correlated with X–ray intensity. The behaviour of the NB–QPO and the FB–QPO differ phenomenologically. The frequency of the former is not generally correlated with X–ray intensity and has a fixed frequency of ~5–7 Hz whilst the frequency of the latter is strongly correlated with intensity. The FB–QPO disappears into the noise as the source moves up the flaring branch. It is thought that the HB–QPO is produced by a different mechanism to that of the NB/FB–QPO.

The HB–QPO can be explained in terms of the modulated–accretion magnetospheric beat–frequency model of Lamb *et al.* (1985). In this model plasma clumps circulate at the inner edge of the accretion disc with a Keplerian frequency ν_K. These clumps enter the neutron stars magnetosphere (which rotates

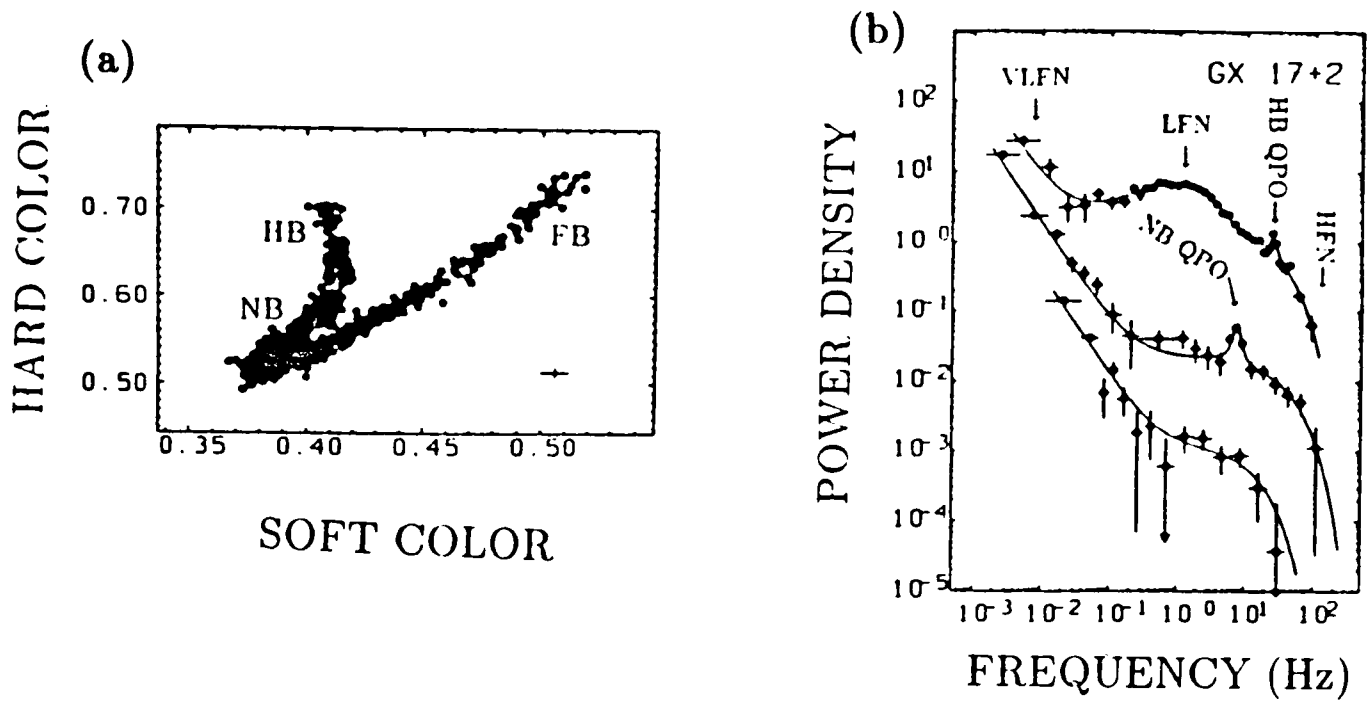

Figure 1.3.4: Figure 1.3.4(a) shows the locus that GX17+2 traces in the colour colour plane. The three states are known as Horizontal Branch (HB), Normal Branch (NB) and Flaring Branch (FB). Figure 1.3.4(b) shows the power spectra of GX17+2 in the three X–ray states (van der Klis 1989).

with the neutron star frequency ν_{ns}) more readily near the magnetic poles and therefore the accretion is modulated at the frequency $\nu_{QPO}=|\nu_{ns}-\nu_K|$. As the clump of plasma accretes the strength of the oscillation decreases. The observed correlation between the centroid frequency and the X–ray intensity can be explained as follows. As the accretion rate (and therefore the X–ray luminosity) increases the magnetosphere radius decreases and hence the Keplerian frequency of matter on the accretion disc edge increases. Since the rotation period of the magnetosphere is fixed the QPO frequency has to increase. For a more detailed review of this and other types of QPO see van der Klis (1989).

It has been suggested (van Paradjis and Lewin 1986) that the brightest bulge QPO sources (the Z sources) probably have evolved secondaries and hence $P_{orb}>10$ hours. The Roche lobe overflow is then driven by the secondary evolving off the main sequence onto the giant branch. This leads to a high $\dot{M}$ and hence high X–ray luminosity ($L_X \sim L_{Edd}$). The orbital periods of the bright

bulge sources have not been determined. However the two brightest non bulge QPO sources, Cyg X–2 and Sco X–1, both have P_{orb}>10 hours. This supports the suggestion that the Z sources have evolved secondaries. It has been found that P_{orb}<5 hrs for the Atoll sources. This implies that the accretion rates (and hence X–ray luminosities) will be lower for these sources than for the Z sources since their accretion rate is not governed by the evolution of the secondary. Also Atoll sources are thought to have a lower magnetic field than the Z sources since they do not display HB–QPO despite their lower accretion rate.

More work needs to be done before a coherent picture of the bright bulge sources and how they relate to the other LMXBs can be constructed.

Bursting Sources and Globular Cluster X–ray sources

These sources form a less luminous ($L_X \sim 10^{37}$ erg s^{-1}) population of LMXBs, most of which exhibit type I X–ray bursts. They are concentrated towards the galactic bulge (as are the previous sources) and are also found in globular clusters (see Section 1.4).

Type I X–ray bursts have rise times of ~1 s with decay times of ~3–100 s and typically recur on timescales of $\sim 10^4$–10^5 s. They are thought to be caused by thermonuclear helium flashes in the surface layers of weakly magnetic neutron stars (Aysali & Joss 1982). All but one of the bursting sources exhibit this type of X–ray burst. Type I and Type II X–ray bursts have been observed from the rapid burster MXB1730–335 in the globular cluster Liller 1 (Hoffman *et al.* 1978, Liller 1977). Type II bursts are thought to be caused by instabilities in the accretion flow around the neutron star (Joss 1977).

Extensive modelling of type I X–ray bursts has been performed by Aysali and

Joss (1982). They found that the thermonuclear flash model can satisfactorily explain their observed properties. Aysali & Joss (1982) found that for very high $\dot{M}$ there are no bursts and also that the presence of an intense magnetic field inhibits bursting. This could explain why the bright bulge sources are not X–ray bursters.

Until the advent of the EXOSAT satellite the orbital periods of only a few (mainly atypical) non–bursting X–ray sources were known. However EXOSAT discovered the presence of recurrent dips in the X–ray light curves of many bursting sources enabling their orbital periods to be determined (Parmar & White 1988). Dipping behaviour is caused by vertical structure on the accretion disc edge usually in the form of a bulge where the accretion stream impacts the edge of the accretion disc. There is also some evidence for a second smaller bulge $\sim$0.5 distant in phase from the first. Depending on the systems inclination then either dips ($i \geq 65°$), dips and possibly X–ray eclipses ($i \geq 80°$) or no orbitally related X–ray behaviour ($i \leq 65°$) is observed. Note that at very high inclinations the central X–ray source is permanently obscured by the vertical disc edge structure (Milgrom 1978). High inclination sources have low $L_X/L_{opt} \sim 10$ and the X–rays we observe are scattered into our line of sight by an accretion driven corona (ADC). A typical light curve of the dipping source X1822–371 is shown in Figure 1.3.5 (Mason 1986).

EXOSAT observations combined with some optical observations of low inclination sources and results from previous X–ray missions have established that X–ray bursters (and some other LMXBs) have short orbital periods <10 hours. This result implies that their secondaries are faint low mass dwarfs with mass transfer taking place by Roche lobe overflow.

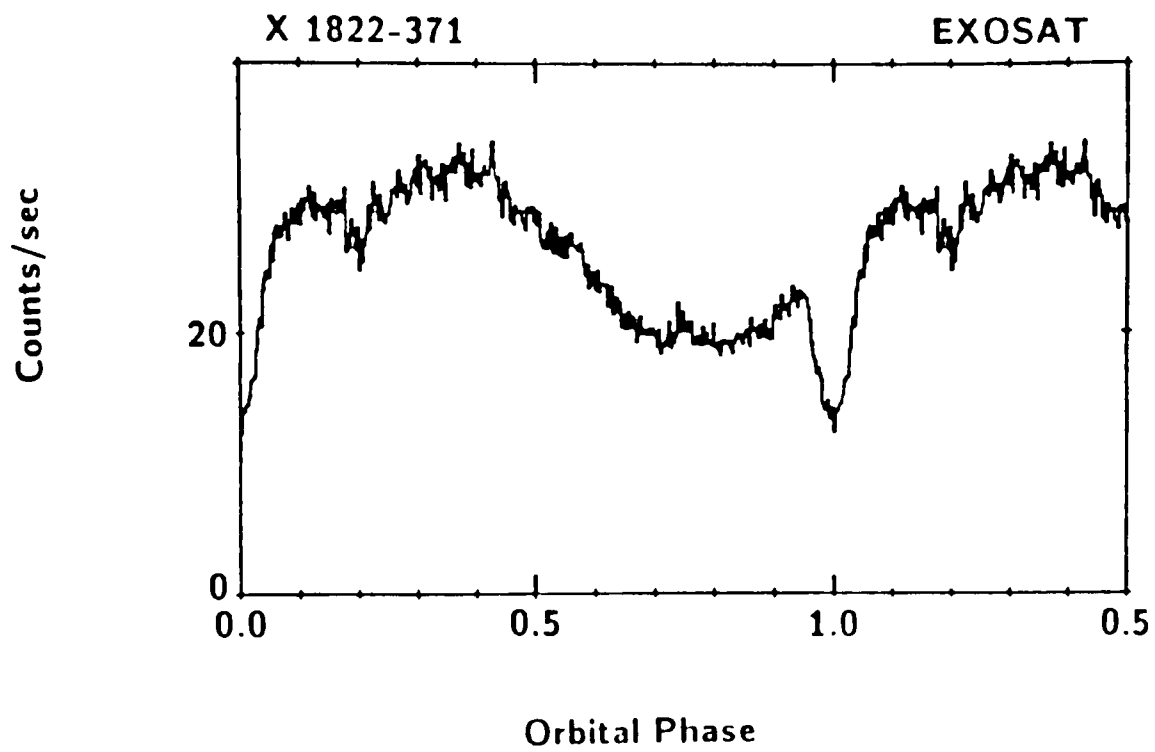

Figure 1.3.5: Dipping X–ray light curve of X1822–371 (Mason 1986)

Other modulations particularly X–ray pulsations, which are present in MXBs, have been searched for. These are not present in the X–ray light curves of any X–ray burster. Only the atypical non bursting sources Her X–1 and 4U1626–67 display X–ray pulsations (van Paradjis 1983). This is taken to indicate that bursting LMXB contain weakly magnetic neutron stars.

The Soft X–ray Transients

The X–ray behaviour of soft X–ray transients is different from the behaviour described above. They are invisible for most of the time but occasionally "turn on" reaching maximum X–ray brightness in a few days and then fading back into obscurity on timescales of weeks or months. Several have been observed to burst (eg. EXO0748–67 & MXB1659–29) during both outburst and quiescent phases (Cominsky & Wood 1984) indicating their similarity to bursting LMXB. The outburst mechanism for X–ray transients is not well understood. It has

been suggested that the outbursts are caused by a disc instability similar to that proposed to explain CV outbursts (Cannizzo *et al.* 1983). Alternatively Hameury *et al.* (1986) suggest that the illumination of the secondary by X–rays from the accreting neutron star enhances the mass transfer rate until the X–ray illumination is cut off by the disc edge. In the latter case the secondaries do not completely fill their Roche lobes.

The optical output of some X–ray transients in quiescence is dominated by their secondaries (usually K main sequence dwarfs eg. Murdin *et al.* 1980). However in outburst the optical output from the accretion disc dominates in these systems and their spectra resemble those of classical LMXB.

Optical Properties of LMXBs

Photometry and Optical Variations

LMXBs on average have a M_V=+1±1 with colours $(B-V)_o$=+0.0±0.3 and $(U-B)_o$=–0.9±0.2 (1σ errors, van Paradjis 1983). Most LMXBs have values close to these. There are however a few exceptions to this norm, these being the X–ray transients in quiescence and the very compact systems 4U1916–05 and 4U1905+00 (Chevalier and Ilovaisky 1990) which have faint discs $M_V \geq +4$.

Time resolved optical photometry of LMXBs has revealed the presence of orbital modulations in several systems. Optical photometry is especially important in studying low inclination ($i \leq 65°$) systems because orbital modulations are still present in the optical when they are absent in the X–ray.

Two common types of orbital modulation are observed: "single wave" (or sinusoidal) and "double wave" (or ellipsoidal) variations. Single wave variations are

usually seen in LMXBs where the optical brightness variation is due to X–ray heating of the companion star. This type of modulation is usually observed when LMXBs are in an optical high state (eg. Figure 1.3.6 from Corbet *et al.* 1986).

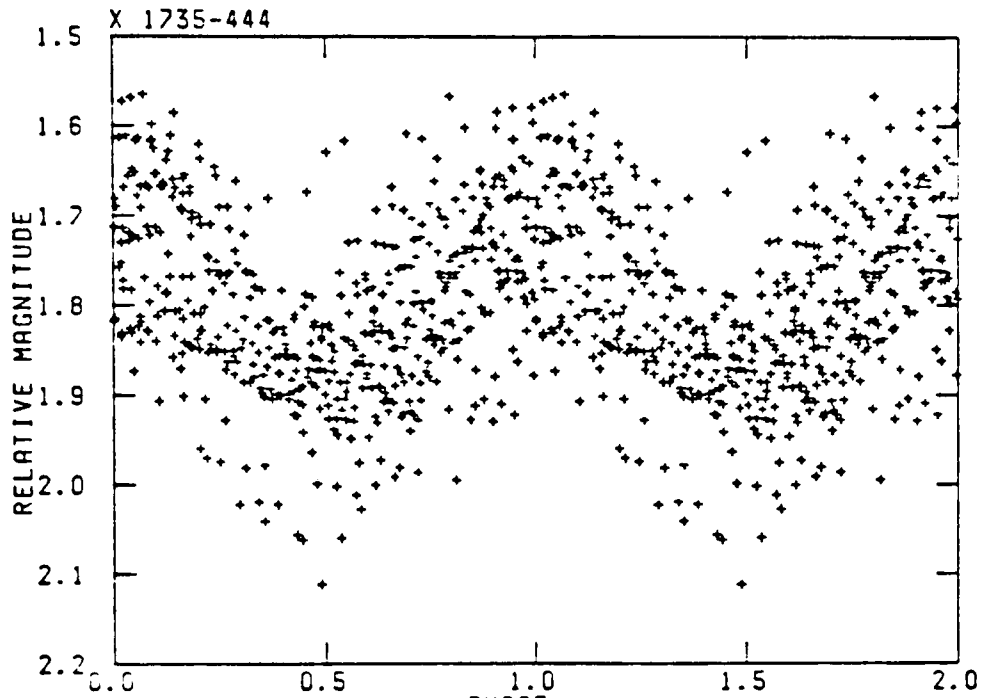

Figure 1.3.6: The light curve of 4U1735–444 (in bright state) displaying single wave variations (Corbet *et al.* 1986).

Ellipsoidal variations are caused by the varying aspect of the tidally distorted companion star. This gives two peaks per cycle indicating that the secondary is filling or close to filling its Roche lobe. Many LMXBs show this type of behaviour in quiescence (eg. Figure 1.3.7 from Chevalier *et al.* 1989). Ellipsoidal variations are usually at quite a low level ($\leq$0.2 magnitudes) and are easily masked by other larger photometric variations.

High inclination systems, for egs. X1822–371 (Mason 1986) and Cal 87 (Callanan *et al.* 1989), often show eclipses in their light curves. These are caused by eclipses of the accretion disc by the primary bulge on the outer edge of the disc

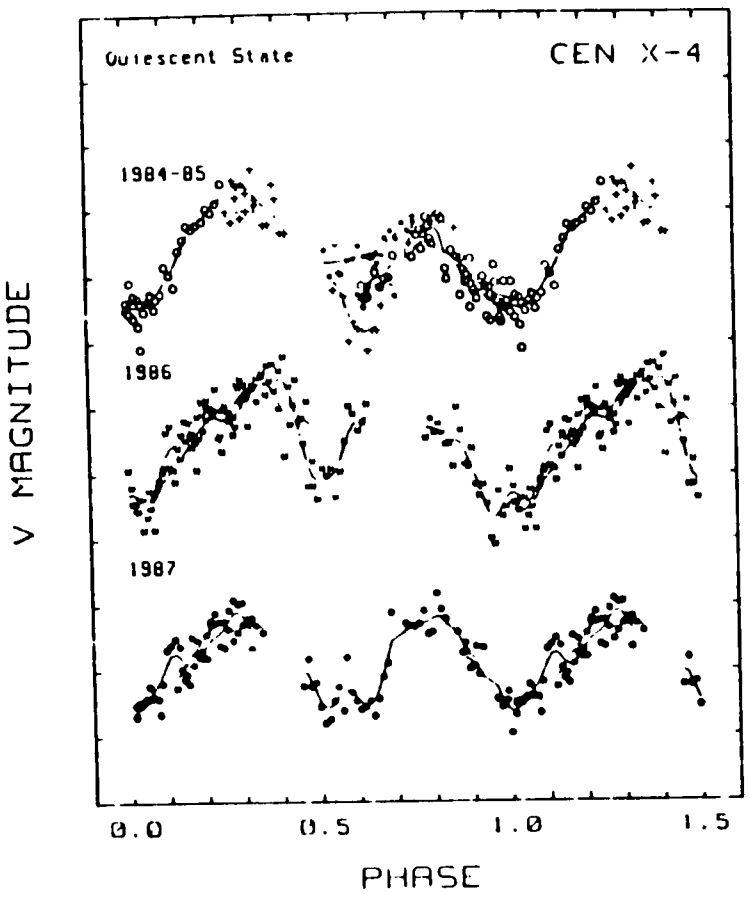

Figure 1.3.7: The light curve of Cen X–4 (a X–ray transient in quiescence) displaying ellipsoidal variations (Chevalier *et al.* 1989).

and also by the secondary star. The light curves often show other structure such as secondary dips which can be interpreted as a secondary bulge on the disc appearing ~0.5 in phase away from the first.

Several non orbital photometric variations are also observed in the light curves of LMXBs.

One such variation is optical bursts. These have been observed to occur quasi–simultaneously with X–ray bursts (eg. see Pedersen *et al.* 1982) but delayed by a few seconds with respect to the X–ray burst. The delay is due to the reprocessing of X–rays in the accretion disc.

Another variation is optical pulsations. These have been seen to emanate from Her X–1 and 4U1626–67 (both of which contain X–ray pulsars). These arise from the reprocessing of pulsed X–rays from the magnetized neutron star in the accretion disc and companion star.

Long term photometric variations on timescales of months have been observed

in the light curves of Her X–1 (Gerend and Boynton 1976) and LMC X–4 (Ilovaisky *et al.* 1984). A possible interpretation of these long term variations is the precession of an accretion disc about its orbital plane.

Spectroscopy of LMXBs

Spectroscopically LMXBs are observed to have flat or blue continua with strong emission lines, principally those of He II λ4686 Å and N III λ4640–4660 Å the latter feature being produced by the Bowen process. There are occasionally other lines present (such as Balmer lines) in emission or absorption.

The Bowen process is initiated by a chance coincidence of frequencies in the He II Lyα λ303.8 Å and O III λ303.8 Å . A fraction of the O III photons (the λ374 Å photons) which are created by a cascade through the O III energy ladder are absorbed again by N III and hence produce the N III emission lines including the blend at λ4640–4660 Å . Other fluorescence lines are also formed in this process, notably O III lines. McClintock, Canizares and Tarter (1975) have shown that this selective mechanism must be present to explain the observed relative strength of He II to N III.

A radial velocity study of most LMXBs is unfortunately not possible since they are too faint and their periods are too short to permit time resolved spectroscopy. However such a study has been possible for several of the more luminous X–ray binaries. Four examples of time resolved spectroscopy of LMXBs are described briefly below.

In the longer period systems, Cyg X–2 (Cowley *et al.* 1979) and 2S0921–63 (Cowley *et al.* 1982) the companion star is luminous enough to be detectable spectroscopically, the absorption lines (produced by the secondary star) being

modulated on the orbital period. The radial velocity curve derived from the absorption lines of the companion star to Her X–1 (HZ Her) is also modulated on the orbital period (Crampton 1975). Also the radial velocity of the *emission* lines in Sco X–1 were found to be modulated on the orbital period (0.79 days, Crampton *et al.* 1976); the emission line object in the latter case being the accretion disc.

Spectroscopy of soft X–ray transients in quiescence has been fruitful in establishing the nature of their secondary stars. The secondaries are usually K main sequence stars (egs. A0620–00, (Oke 1977) Aql X–1, (Thorstensen *et al.* 1978) and Cen X–4 (Chevalier *et al.* 1989)) though this need not be the case for all X–ray transients since EXO0748–67 probably has a M dwarf secondary (Crampton *et al.* 1986).

1.4 Globular Clusters

Introduction

Globular clusters are spherical gravitationally bound collections of $\sim 10^5$–10^6 stars. They are very old ($>10^{10}$ years $\sim$ the same age as the galaxy) with their stars all forming at around the same time out of the same primordial matter. Because of this globular clusters are excellent laboratories for testing the results of stellar evolutionary models. Note that most globular clusters are observed to be metal poor with respect to the galaxy.

A typical Hertzsprung Russell diagram for a globular cluster is shown in Figure 1.4.1. Most of the prominent features are marked. These are:

i) the main sequence (MS). These stars have not undergone significant nuclear

evolution during their lifetime (usually M<0.8 $M_\odot$)

ii) the turnoff point (TO). This is the point just before the stars begin hydrogen shell burning (usually occurring at M~0.8 $M_\odot$)

iii) the sub–giant branch (SGB). This is where hydrogen shell burning begins and the stars start to ascend the giant branch

iv) the red giant branch (RGB). These stars have a hydrogen burning shell and an inert helium core

v) the red horizontal branch (RHB) and the blue horizontal branch (BHB). The red giants evolve onto this part of the diagram when core helium burning begins with shell hydrogen burning continuing.

vi) The asymptotic giant branch (AGB). These stars have both helium and hydrogen burning shells with an inert C–O core.

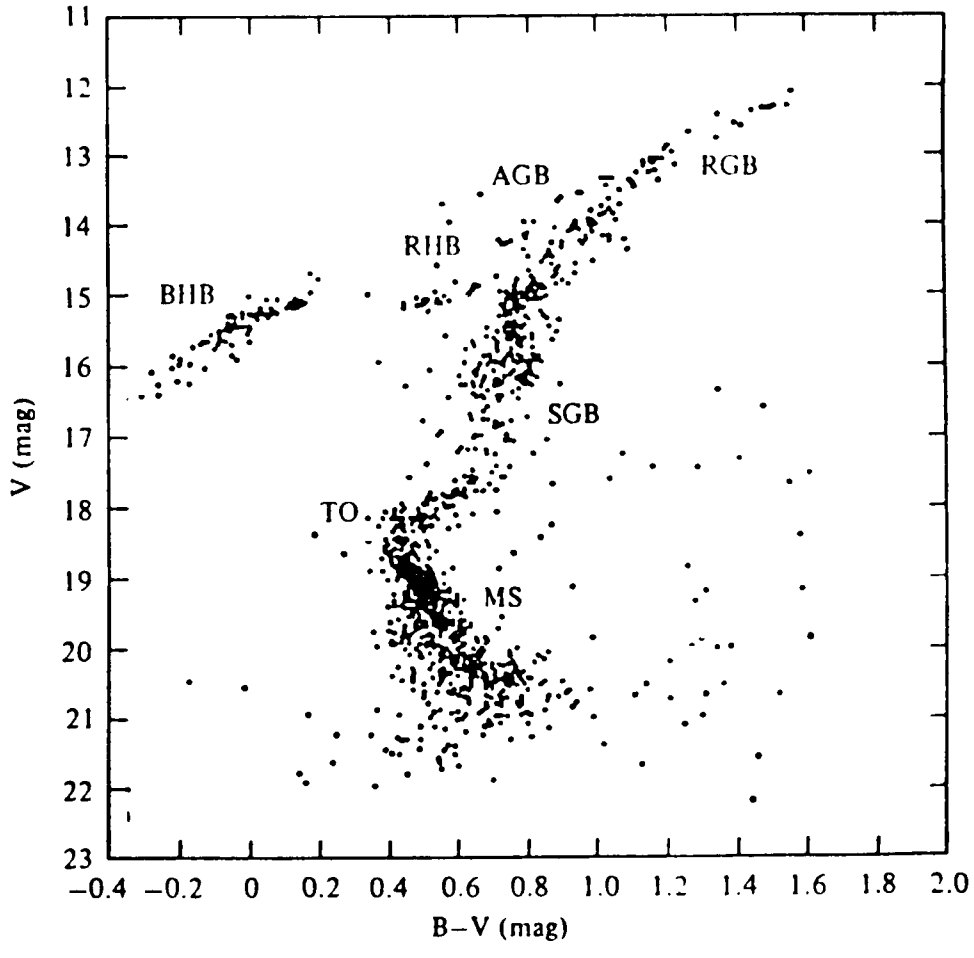

Figure 1.4.1: The colour magnitude diagram for a typical globular cluster (Madore 1980). The principal defining features are marked, see text.

Besides these there are two other significant stellar populations in globular clusters, both the remnants of stellar evolution, white dwarfs and neutron stars. Neutron stars have only been directly observed in globular clusters either as millisecond radio pulsars or as point X–ray sources.

The observed optical luminosity profile of a globular cluster can adequately be described in terms of a King model (King 1962). The function used to fit the profile has only three parameters, the central surface density, the core radius (r_c) and the tidal radius (r_t). The tidal radius is the radius beyond which the cluster cannot maintain bound orbits against the tidal field of the galaxy. The core radius specifies the region of almost constant surface density near the cluster centre. These models have proved invaluable in the study of the structural parameters of globular clusters. The comparison of such models with observations show that some clusters have an excess of luminosity at the core, an example of which is shown in Figure 1.4.2 (M15).

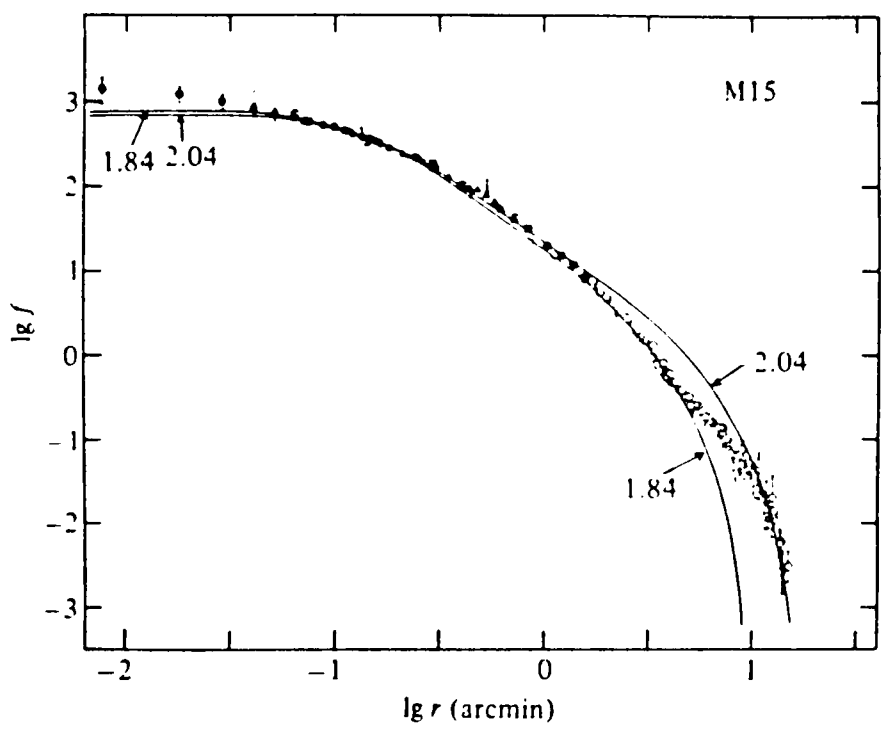

Figure 1.4.2: The surface brightness profile for the globular cluster M15 (Newell and O'Neil Jr 1978). The solid curves are two computed King model surface brightness distributions. The labelled parameter is $\log_{10}(r_t/r_c)$. At small radii there is a luminosity excess over the predicted surface brightness distribution.

This excess is generally taken to be evidence that core collapse (described below) has occurred in such clusters.

Globular Cluster Evolution

Globular clusters are not static entities. They are thought to have evolved (and are evolving) since their formation. The individual stars within the cluster core reach a pseudo–equilibrium relatively quickly ($\leq 10^8$ yrs) by two body relaxation. This means that the velocity distribution in the core is approximately Maxwellian; however the core never achieves true equilibrium since the high velocity tail of the distribution is always being torn out of the cluster by the tidal field of the Milky Way.

Two body encounters cause the outer "halo" of the cluster to expand whilst the inner parts collapse to ever increasing densities. The contraction of the core halts with the formation of one or several "hard" binary stars whose binding energy are greater than the Maxwellian equipartition energy within the core. LMXBs and CVs meet this criterion (Heggie 1980). These binaries give up their energy to the surrounding core stars thereby preventing further core collapse. In so doing they become more firmly bound. The binaries can be formed in one of two ways, tidal capture (Fabian *et al.* 1975) or three body interactions (Hills 1976). The former is thought to be the dominant mechanism in globular clusters, at least for neutron stars, because the rarity of ordinary binaries in globular clusters reduces the likelihood of three body encounters (Verbunt 1988). Also white dwarf binaries may under certain conditions undergo accretion induced collapse (AIC) increasing the number of neutron star binaries (Bailyn, Grindlay and Garcia 1990).

When hard binaries form the cluster begins to evaporate on large timescales ($\gg 10^{10}$ years), via the escape of weakly bound stars, mass loss through stellar evolution and mass loss through scattering events. This is known as the post core collapse phase (Elson, Hut & Inagaki 1987).

Interacting Binary Stars in Globular Clusters

There is some observational evidence for the presence of interacting (ie. "hard") binary stars in globular clusters. These fall into three categories, neutron star binaries, CVs and blue stragglers. They are discussed, in turn below.

It was found by Katz (1975) that globular clusters contain many more LMXBs per unit mass than a randomly selected part of the galaxy (by a factor of ~1000). Also the presence of at least 15 binary or single millisecond radio pulsars, which are thought to represent a later evolutionary stage of LMXBs, is further evidence that the formation of neutron star binaries in globular cluster cores is very common (Ray & Kluźniak 1990, Biggs *et al.* 1990). All the LMXB and most of the radio pulsars with measured positions lie within two core radii of the core indicating that they are more massive than the average cluster star. The X–ray properties of the globular cluster LMXBs are very similar to those of the field LMXBs; many burst, there is an X–ray transient (in NGC6440) and a bright non bursting source (in M15), (Callanan *et al.* 1987). However, optical studies of these objects are very difficult due to the crowded nature of the field and to date only one firm optical counterpart (AC211) to a globular cluster X–ray source (in M15) has been found and studied optically (Aurière *et al.* 1984). Possible optical counterparts to the X–ray sources in globular clusters 47 Tuc (Aurière *et al.* 1989) and NGC6712 (Cudworth 1988 and Neito *et*

al. 1990) have recently been discovered. These identifications need to be confirmed. However spectroscopy of Cudworths (1988) candidate failed to show any of the characteristic emission lines of a LMXB throwing its candidacy into doubt (Charles 1990).

Since the number of white dwarfs, formed in globular clusters as end products of the evolution of cluster members, is likely to be much larger than the number of neutron stars, one expects (Hut and Verbunt 1983; Verbunt 1988; Verbunt & Meylan 1988) that globular clusters contain a large number of cataclysmic variables (eg. Verbunt and Meylan (1988) predict that 36 CVs would be formed by tidal capture in 47 Tuc). These should be observable as faint, $M_V \geq +5$, blue $(B-V)_o \leq -1$ objects. However, in spite of much observational effort, these have remained difficult to find. So far, only two good candidate dwarf novae have been found in globular clusters, both identified on the basis of their variability (confirmed by subsequent spectroscopic data): V101 in M5 (Margon *et al.* 1981; see also Naylor *et al.* 1989 and Ch. 3), and V4 in M30 (Margon *et al.* 1983 and Ch. 2). Also, two novae are possible globular cluster members: T Sco in M80 and an anonymous nova in M14 (Webbink 1980). The latter was recently recovered by Shara, Moffat and Potter (1990).

The paucity of CVs in globular clusters remains one of the major unsolved puzzles in globular cluster evolution today. Bailyn, Grindlay and Garcia (1990) give a possible explanation for this dilemma. This relies on the fact that unstable mass transfer occurs in binaries when the mass of the main sequence secondary (m_2) is $\geq 0.8 m_1$ (where m_1 in this instance is the mass of the white dwarf). In globular clusters the main sequence turnoff is typically ~ 0.8 $M_\odot$, therefore for stable mass transfer the white dwarf mass m_1 must have a mass ≥ 1 $M_\odot$. All globular cluster tidal capture white dwarfs with $m_1 < 1$ $M_\odot$ therefore

do not form CVs. Instead the rapid unstable mass transfer produces a thick extended envelope around the white dwarf which ultimately leads to the merger of the two stars. Bailyn *et al.* (1990) perform calculations involving the mass function of the main sequence of globular clusters and conclude that the simple tidal capture calculations overestimate the number of CVs produced in globular clusters by at least a factor of 10. If Bailyn *et al.* (1990) are correct then the observed absence of CVs in globular cluster cores is explained.

Blue stragglers form a third class of close binary in globular clusters. These stars appear as an extension to the main sequence above the turnoff point in globular cluster HR diagrams. Several explanations have been put forward to explain their existence I will give a brief description of three of them.

The first is that blue stragglers are younger than the majority of cluster stars. This is unlikely since there is no evidence of recent star formation in globular clusters.

A second mechanism is the internal mixing of material within single stars, this has the effect of extending the stars main sequence lifetime. However no specific mechanism for mixing exists.

A third mechanism is that blue stragglers form through mass transfer in a close binary system, the binary possibly evolving from a primordial detached system. A consequence of this is that blue stragglers should be binary systems. Until recently no evidence for the binarity of blue stragglers had been found, throwing doubt on this mechanism. However four eclipsing blue stragglers have recently been discovered, one in ω Cen with $P_{orb} \sim 1.4$ days (Margon and Cannon 1989) and three in NGC5466 with $P_{orb} \leq 0.52$ days (Mateo *et al.* 1990). Two of the binaries discovered in NGC5466 display continuous periodic variability indicative of their being contact binaries (W UMa). These observations provide the first

evidence that mass exchange is occurring in blue stragglers and that the binary hypothesis can indeed explain the presence of at least some blue stragglers in globular clusters. Mateo *et al.* (1990) suggests that the contact binaries will merge to form single blue straggler stars and that this mechanism has produced most of the isolated blue stragglers observed.

1.5 Radio Emission from LMXBs and Globular Clusters

In this section I review the radio properties of galactic LMXBs and their radio emission mechanism. I also describe the results of radio observations of globular clusters.

Radio Emission from LMXBs

The discovery of stellar X–ray emission in the 1960s led to radio and optical observations of the same region of the sky. This led to radio counterparts being discovered for several X–ray objects. These included triple lobed (lobe separation 1′.2) radio emission (flux density ∼20 mJy) from Sco X–1 (Hjellming and Wade 1971a), unresolved radio emission from the galactic centre X–ray source GX17+2 and the black hole candidate Cyg X–1 (Hjellming and Wade 1971b). However it was realised that there was no simple correlation between the radio emission and the X–ray emission. In addition a simple extrapolation of the observed thermal X–ray emission to radio wavelengths underestimated the observed radio flux by a substantial amount. This implied that the emission regions were spatially distinct with the production of X–rays close to the compact object (by the thermal bremsstrahlung mechanism) and the radio emission coming from a more extended region. Radio measurements showed that

the spectral slope for Sco X–1 was $\alpha \sim 0.8$–1.2 (flux density $\propto \nu^{-\alpha}$) implying that the emission mechanism was non–thermal (Miyamoto and Matsuoka 1977).

More recently, high sensitivity radio surveys ($\sim$100–400 μJy beam^{-1}) have detected only 20–30% of LMXBs (Geldzahler 1983, 1987, Grindlay and Seaquist 1986 and Nelson and Spencer 1988). All these surveys failed to detect any more systems displaying extended structure. To date only a few X–ray emitting binaries display this structure. These are: the LMXBs Sco X–1 (Fomalont *et al.* 1983), Cyg X–3 (Strom *et al.* 1989) and GX17+2 (Gopal–Krishna and Steppe 1980) as well as the X–ray binary SS433 (Hjellming and Johnston 1981). This indicates that luminous large (>10″) scale extended radio emission is NOT a common phenomena for these systems.

As mentioned previously the emission mechanism has been shown to be non–thermal for the two well studied LMXBs Sco X–1 and Cyg X–3 and also for SS433. Hjellming and Johnston (1988) have recently put forward a model which can explain the observed emission from all X–ray emitting binaries (both extended and unresolved) in terms of synchrotron emission. In their model the observed radio emission is produced in adiabatically expanding conical jets emitting synchrotron radiation. Whether their model is physically reasonable or not the non–thermal radio emission must come from a region that has a relativistic electron population and that is threaded by a magnetic field.

Recently Penninx (1990) has compared the radio and X–ray properties of LMXBs. He found that the persistently bright Z–type X–ray sources were bright radio emitters and that their radio emission was directly related to their X–ray spectral state. In particular the brightest radio emission is produced when the objects accretion rate is lowest; ie. on the horizontal branch. He also found that the fainter, mainly bursting Atoll type X–ray sources were generally fainter

radio emitters than the Z–type sources. He suggested that this behaviour may be related to the mass accretion rate and the magnetic field (both thought to be higher in the Z–type sources) but does not give a detailed explanation as to why this might be the case.

Radio Emission from Globular Clusters

During the 1970s and early 1980s radio surveys of globular clusters were undertaken. Several radio sources were found in the fields of most of the clusters surveyed (Johnson 1976, Rood, Turner and Goldstein 1978 and Gopal–Krishna and Steppe 1980). This included some in the fields of the X–ray emitting clusters NGC6624 and NGC7078. However the radio sources in these latter fields were too far from the X–ray source positions for them to be related. The observed number of radio sources in the fields of globular clusters were consistent with extragalactic radio source counts (Birkinshaw and Downes 1982). Despite repeated attempts to discover radio counterparts to globular cluster LMXBs (Geldzahler 1983, Grindlay and Seaquist 1986, Nelson and Spencer 1988) no firm detections were reported.

Radio emission from globular clusters has been detected in the form of millisecond pulsars. The first of these to be discovered was the isolated pulsar in M28 (Lyne *et al.* 1987) followed by the binary millisecond pulsar in M4 (Lyne *et al.* 1988). From late 1986 onwards many (to date 15) millisecond radio pulsars have been found in globular clusters (Ray & Kluźniak 1990). This discovery is important for two reasons. Firstly it provides evidence for the formation of

compact binaries in globular clusters. Secondly it provides one of the missing links in the evolution of LMXBs (as do the few known galactic millisecond pulsars). Millisecond pulsars, both binary and *isolated*, are thought to form at a later stage in the evolution of LMXBs, the neutron star being spun up by accretion processes in the progenitor LMXB system (Lyne *et al.* 1988).

The discovery of these millisecond pulsars in globular clusters means that their average mass can be estimated by using their positional offset from the host cluster cores (Callanan 1989; Grindlay *et al.* 1984). This will be important in finding out whether the binary pulsars are significantly more massive than the isolated systems.

The observed radio emission from globular clusters is associated with neutron stars. Until the observations reported in Chapter 5 this had been exclusively limited to observations of millisecond radio pulsars.

1.6 References

Allen, C.W., 1973. *Astrophysical Quantities,* The Athlone Press, London.

Aurière, M., Le Fèvre, O. & Terzan, A., 1984. *Astron. Astrophys.,* **138,** 415.

Aurière, M., Koch-Miramond, L. & Ortolani, S., 1989. *Astron. Astrophys.* **214,** 113.

Aysali, S. & Joss, P.C., 1982. *Astrophys. J.,* **256,** 637.

Bailyn, C.D., Grindlay, J.E. & Garcia, M.R., 1990. *Astrophys. J.,* **357,** L35.

Bath, G.T., Clarke, C.J. & Mantle, V.J., 1986. *Mon. Not. R. astr. Soc.,* **221,** 269.

Batten, A.H., 1967. *Ann. Rev. Astron. Astrophys.,* **5,** 25.

Biggs, J.D., Lyne, A.G., Manchester, R.N. & Ashworth, M., 1990. *IAU Circ.* 4988.

Birkinshaw, M. & Downes, A.J.B., 1982. *Astrophys. J.,* **258,** 154.

Callanan, P., Fabian, A.C., Tennant, A.F., Redfern, R.M. & Shafer, R.A., 1987. *Mon. Not. R. astr. Soc.,* **224,** 781.

Callanan, P.J., Machin, G., Naylor, T. & Charles, P.A., 1989. *Mon. Not. R. astr. Soc.,* **241,** 37p.

Callanan, P., 1989. *Private Communication.*

Cannizzo, J.K., Wheeler, J.C. & Ghosh, P., 1983. In:*CVs and LMXBs,* ed. Patterson, J. & Lamb, D.Q., Reidel, Holland.

Charles, P.A., 1990. In:*Proceedings of the 23rd ESLAB Symposium,* Vol. 1, p. 129, eds. Hunt, J. & Buttrick, B., ESA Publications Division, ESTEC, Noordwijk, The Netherlands.

Chevalier, C., Ilovaisky, S.A., van Paradjis, J., Pedensen, H. & van der Klis, M., 1989. *Astron. Astrophys.,* **210,** 114.

Chevalier, C. & Ilovaisky, S.A., 1990. In:*Proceedings of the 23rd ESLAB Symposium,* Vol. 1, p. 345, eds. Hunt, J. & Buttrick, B., ESA Publications Division, ESTEC, Noordwijk, The Netherlands.

Cominsky, C.R. & Wood, K.S., 1984. *Astrophys. J.,* **283,** 765.

Corbet, R.H.D., Thorstensen, J.R., Charles, P.A., Menzies, J.W., Naylor, T. & Smale, A.P., 1986. *Mon. Not. R. astr. Soc.,* **222,** 15.

Cordova, F.A. & Mason, K.O., 1983. In:*Accretion Driven Stellar X-ray Sources, Ch. 4.,* eds. Lewin, W.H.G. & van den Heuvel, E.P.J., Cambridge University Press, Cambridge.

Cowley, A.P., Crampton, D. & Hutchings, J.B., 1979. *Astrophys. J.,* **231,** 539.

Cowley, A.P., Crampton, D. & Hutchings, J.B., 1982. *Astrophys. J.,* **256,** 605.

Crampton, D., 1975. *Astrophys. J.*, **187**, 345.

Crampton, D., Cowley, A.P., Hutchings, J.B. & Kaat, C., 1976. *Astrophys. J.*, **207**, 907.

Crampton, D., Cowley, A.P., Stauffer, J., Ianna, P. & Hutchings, J.B., 1986. *Astrophys. J.*, **306**, 599.

Crawford, J.A. & Kraft, R.P., 1956. *Astrophys. J.*, **123**, 44.

Cudworth, K.M., 1988. *Astron. J.*, **96**, 105.

Duschl, W.J. & Livio, M., 1989. *Astron. Astrophys.*, **209**, 183.

Echevarria, J. & Jones, D.H.P., 1984. *Mon. Not. R. astr. Soc.*, **206**, 919.

Elson, R., Hut, P. & Inagaki, S., 1987. *Ann. Rev. Astron. Astrophys.*, **25**, 565.

Fabian, A.C., Pringle, J.E. & Rees, M.J., 1975. *Mon. Not. R. astr. Soc.*, **172**, 15P

Faulkner, J., Lin, D.N.C. & Papaloizou, J., 1983. *Mon. Not. R. astr. Soc.*, **205**, 359.

Fomalont, E.B., Geldzahler, B.J., Hjellming, R.M. & Wade, C.M., 1983. *Astrophys. J.*, **275**, 802.

Frank, J., King, A.R. & Raine, D.J., 1985. In:*Accretion Power in Astrophysics.*, Cambridge University Press, Cambridge.

Friend, M.T., Martin, J.S., Smith, R.C. & Jones, D.H.P., 1988. *Mon. Not. R. astr. Soc.*, **233**, 451.

Geldzahler, B.J., 1983. *Astrophys. J.*, **264**, L49.

Geldzahler, B.J., 1987. *Publs. astr. Soc. Pacif.*, **99**, 1036.

Gerend, D. & Boynton, P.E., 1976. *Astrophys. J.*, **209**, 562.

Gopal-Krishna & Steppe, H., 1980. *Astr. Astrophys.*, **88**, 354.

Grindlay, J.E., Hertz, P., Steiner, J.E., Murray, S.S. & Lightman, A.P., 1984. *Astrophys. J.*, **282**, L13.

Grindlay, J.E. & Seaquist, E.R., 1986. *Astrophys. J.*, **310**, 172.

Hameury, J.M., King, A.R. & Lasota, J.P., 1986. *Astron. Astrophys.*, **162**, 71.

Heggie, D.C., 1980. In:*Globular Clusters*, p. 281, eds. Haines, D. & Madore, B., Cambridge University Press, Cambridge.

Hills, J.G., 1976. *Mon. Not. R. astr. Soc.*, **175**, 1p.

Hjellming, R.M. & Wade, C.M., 1971a. *Astrophys. J.*, **164**, L1.

Hjellming, R.M. & Wade, C.M., 1971b. *Astrophys. J.*, **168**, L21.

Hjellming, R.M. & Johnston, K.J., 1981. *Astrophys. J.*, **246**, L141.

Hjellming, R.M. & Johnston, K.J., 1988. *Astrophys. J.*, **328**, 600.

Hoffman, J.A., Marshall, H.L. & Lewin, W.H.G., 1978. *Nature,* **271,** 630.

Horne, K. & Marsh, T.R., 1986. *Mon. Not. R. astr. Soc.,* **218,** 761.

Hut, P. & Verbunt, F., 1983. *Nature* **301**, 587.

Ilovaisky, S.A., Chevalier, C., Motch, C., Pakull, M., van Paradjis, J. & Lub, J., 1984. *Astr. Astrophys.,* **140,** 251.

Johnson, H.M., 1976. *Astrophys. J.,* **208,** 706.

Joss, P.C., 1977. *Nature,* **270,** 310.

Katz, J.I., 1975. *Nature,* **253,** 698.

King, A.R., 1988. *Q. Jl. R. astr. Soc.,* **29,** 1.

King, I.R., 1962. *Astron J.,* **67,** 471.

Lamb, F.K., Shibazaki, N., Alpar, M.A. & Shaham, J., 1985. *Nature,* **317,** 681.

Lewin, W.H.G. & Joss, P.C., 1983. In:*Accretion Driven Stellar X-ray Sources.,* p. 41, eds. Lewin, W.H.G. & van den Heuvel, E.P.J., Cambridge University Press, Cambridge.

Liebert, J. & Stockman, H.S., 1983. In:*Cataclysmic Variables and Low Mass X-ray Binaries.,* p. 151, eds. Lamb, D.Q. & Patterson, J., D. Reidel Publishing Company, Dordrecht.

Liller, W., 1977. *Astrophys. J.,* **213,** L21.

Lyne, A.G., Brinklow, A., Middleditch, J., Kulkarni, S.R., Backer, D.C. & Clifton, T.R., 1987. *Nature,* **328,** 399.

Lyne, A.G., Biggs, J.D., Brinklow, A., Ashworth, M. & McKenna, J., 1988. *Nature,* **332,** 45.

Madore, B., 1980. In:*Globular Clusters,* p. 21, eds. Haines, D. & Madore, B., Cambridge University Press, Cambridge.

Margon, B. & Cannon, R., 1989. *Observatory,* **109,** 82.

Margon, B., Downes, R.A. & Gunn, J.E., 1981. *Astrophys. J.,* **247,** L89.

Margon, B. & Downes, R.A., 1983. *Astrophys. J.,* **274,** L31.

Mason, K.O., 1986. In:*The Physics of Accretion onto Compact Objects,* p. 46, eds Mason, K.O., Watson, M.G. & White, N.E., Springer–Verlag, Belin.

Mateo, M., Harris, H.C., Nemec, J. & Olszewski, E.W., 1990. *Astron. J.,* **100,** 469.

McClintock, J.E., Canizares, C.R. & Tarter, C.B., 1975. *Astrophys. J.,* **198,** 641.

Milgrom, M., 1978. *Astron. Astrophys.,* **67,** L25.

Miyamoto, S. & Matsuoka, M., 1977. *Space Sci. Rev.,* **20,** 687.

Murdin, P., Allen, D.A., Morton, D.C., Whelan, J.A.J. & Thomas, R.M., 1980. *Mon. Not. R. astr. Soc.,* **192,** 709.

Naylor, T., Allington-Smith, J., Callanan, P.J., Charles, P.A., Hassall, B.J.M., Machin, G., Mason, K.O., Smale, A.P. & van Paradjis, J. 1989. *Mon. Not. R. astr. Soc.*, **241**, 25p.

Nelson, L.A., Rappaport, S.A. & Joss, P.C., 1986. *Astrophys. J.*, **304**, 231.

Nelson, R.F. & Spencer, R.E., 1988. *Mon. Not. R. astr. Soc.*, **234**, 1105.

Neito, J.-L., Aurière, M., Sebag, J., Arnaul, J., Lelièvre, G, Blazit, A., Foy, R., Bonaldo, S. & Thouvenot, E. 1990. *Astron. Astrophys.*, In Press

Newell, B. & O'Neil, Jr, E.J., 1978. *Astrophys. J. Suppl.*, **37**, 27.

Oke, J.B., 1977., *Astrophys. J.*, **217**, L181.

Paczyński, B., 1981. *Acta. Astron.*, **31**, 1.

Parmar, A.N. & White, N.E., 1988. In:*X-ray Astronomy with EXOSAT*, eds. White, N.E. & Pallivicini, R., Memoria S.A.It., **59**, 147.

Pedersen, H, van Paradjis, J., Motch, C., Cominsky, L., Lawrence, A., Lewin, W.H.G., Oda, M., Ohashi, T. & Matsuoka, M., 1982. *Astrophys. J.*, **263**, 340.

Penninx, W., 1990. In:*Proceedings of the 23rd ESLAB Symposium*, Vol. 1, p. 185, eds. Hunt, J. & Buttrick, B., ESA Publications Division, ESTEC, Noordwijk, The Netherlands.

Ray, A. & Kluźniak, W., 1990. *Nature*, **344**, 415.

Rood, R.T., Turner, K.C. & Goldstein, S.J., 1978. *Astrophys. J.*, **225**, 804.

Shakura, N.J. & Sunyaev, R.A., 1973. *Astr. Astrophys.*, **24**, 337.

Shara, M., Moffat, A.F.J. & Potter, M., 1990. *Astron. J.*, **99**, 1858.

Smak, J., 1984. *Acta Astron.*, **34**, 93.

Strom, R.G., van Paradjis, J. & van der Klis, M., 1989. *Nature.*, **337**, 234.

Szkody, P., 1985. In:*Recent Results on CVs*, p. 39., ed. Burke, W.R., ESA Scientific and Technical Publications Branch, The Netherlands.

Thorstensen, J.R., Charles, P.A. & Bowyer, S., 1978. *Astrophys. J.*, **220**, L131.

van der Klis, M., 1989. *Ann. Rev. Astron. Astrophys.*, **27**, 517.

van Paradjis, J., 1983. In:*Accretion Driven Stellar X-ray Sources.*, p. 189, eds. Lewin, W.H.G. & van den Heuvel, E.P.J., Cambridge University Press, Cambridge.

van Paradjis, J. & Lewin, W.H.G., 1986. In:*The Evolution of Galactic X-ray Binaries*, 187. eds. Truemper, J., Lewin, W.H.G. & Brinkmann, W., D. Reidel, Dordrecht, Holland.

Verbunt F., 1986. In:*The Physics of Accretion onto Compact Objects.*, eds. Mason, K.O., Watson, M.G. & White, N.E., Springer-Verlag, Berlin. 59.

Verbunt F., 1988. *Adv. Space Res.*, **8**, 529.

Verbunt F. & Meylan, G., 1988. *Astr. Astrophys.*, **203**, 267.

Vogt, N., 1989. In:*Classical Novae, Ch. 12.*, eds. Bode, M.F. & Evans, A., John Wiley & Sons Ltd, Chichester.

Wade, R.A. & Ward, M.J., 1985. In:*Interacting Binary Stars, Ch. 4.1.*, eds. Pringle, J.E. & Wade, R.A., Cambridge University Press, Cambridge.

Warner, B., 1989. In:*Classical Novae, Ch. 1.*, eds. Bode, M.F. & Evans, A., John Wiley & Sons Ltd, Chichester.

Warner, B. & Nather, R.E., 1971. *Mon. Not. R. astr. Soc.*, **152**, 219.

Webbink, R.F., 1980. In:*Close Binary Stars: Observations and Interpretation, IAU Symp. 88,* p. 574, ed. Plavek, M.J., Popper, D.M. & Ulrich, R.K., Reidel, Dordrecht.

White, N., 1989. *Astron. Astrophys. Rev.*, **1**, 85.

Chapter 2

Observations of the Dwarf Nova V4 in M30

In Chapters 2, 3 and 4 I will describe the results of observations made of globular cluster cataclysmic variables. Section 1.4 gave a general description of close binary systems in globular clusters. Here I report the results of observations of the candidate globular cluster dwarf nova, V4 in M30. Photometry of the object was taken so as to determine its quiescent colours. Low resolution spectroscopy was performed to obtain the first good spectrum of the object and to try to establish its radial velocity and hence cluster membership.

I discuss the implications of the results of these observations. It is likely that V4 is a *foreground* object in the field of M30. This is based on an analysis of its quiescent magnitude, outburst magnitude and its radial velocity. In addition it is probably a short period system near the period gap.

2.1 Introduction

The large amplitude variable V4 was first discovered by Rosino (1949). He reported an outburst timescale of $\sim$2 weeks, with a M_{pg}(outburst)$\sim$16.4 and an amplitude of $\geq$2 magnitudes. He concluded that these properties were compatible with V4 being a DN.

V4 then remained unobserved for over 30 years until a resurgence in interest in globular cluster binaries prompted Margon and Downes (1983) to obtain a

spectrum of the object. The spectroscopy was performed at low (~15 Å) resolution on the 4-m reflector at the Cerro Tololo Inter-American Observatory. The spectrum they obtained resembled that of a DN in quiescence displaying the Balmer series in emission and possibly He II λ4686 and the C III/N III Bowen blend as well. From the quiescent magnitude of V4 (V~19.4) they argued that it is probably a cluster member, even though it is greater than 5′ (~50 r_c) from the cluster core! Their spectrum was of too low a resolution and too noisy to determine the objects radial velocity. This was unfortunate since M30 has a high radial velocity (–172 km s^{-1}, Harris & Racine 1979) and this measurement would have been an indicator of cluster membership. Shara, Moffat and Potter (1990) have recently obtained the first outburst spectrum of V4. This displays the classical spectrum of a DN in outburst ie. broad shallow Balmer absorption lines with a very blue continuum. However their spectral resolution was also too low to confirm cluster membership. From their spectrum it is possible to estimate an outburst magnitude of $\leq$16.8. This magnitude is consistent with the photometry of Rosino (1949).

2.2 Observations

All the observations described in this chapter were taken at the Observatorio del Roque de los Muchachos on the island of La Palma. The photometry and spectroscopy were performed on V4 using the 4.2-m WHT telescope. This section is split into two parts: subsection 2.2.1 describing the photometry and subsection 2.2.2 describing the spectroscopy.

There is no good finding chart of V4 in the literature. However the object appears anonymously, in outburst, on the plate of Alcaíno & Liller (1980). To

provide a good finding chart for V4 I reproduce the appropriate part of their chart with the object indicated (Figure 2.1). V4 forms part of a close ~4″ pair. Any observations of the system are severely hampered by the presence of the very bright (V~8.7) close by (~25″) star.

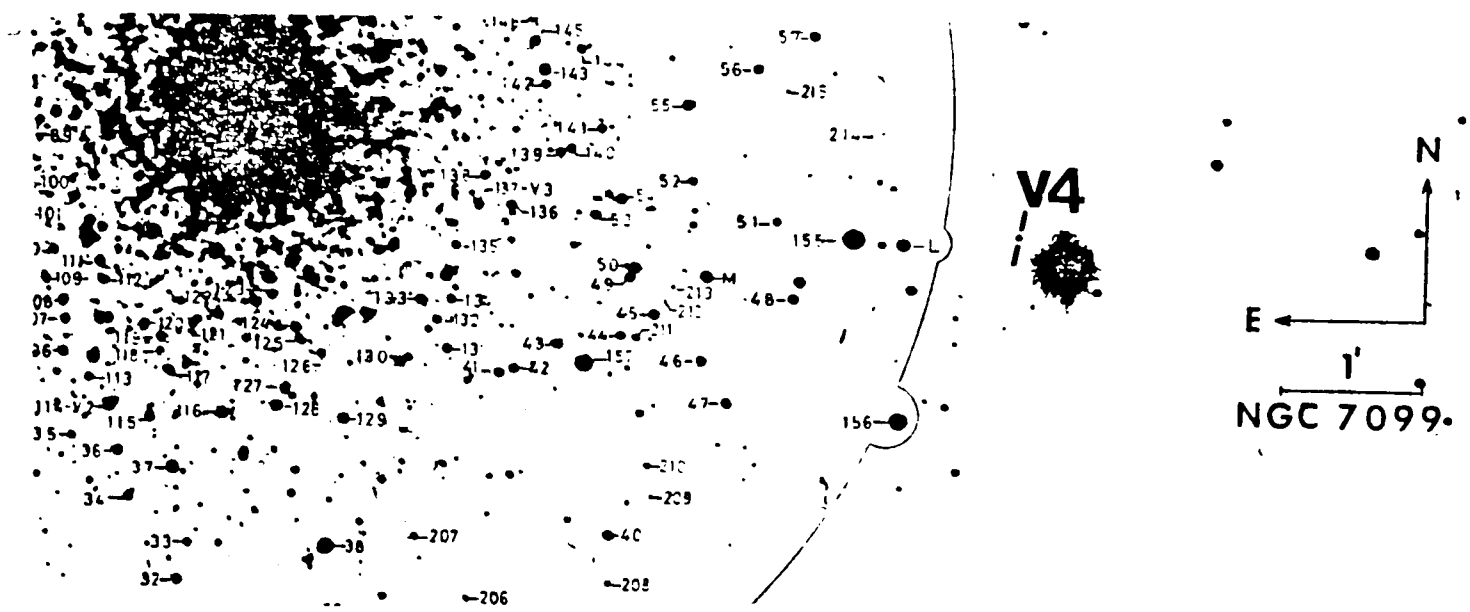

Figure 2.1: The Finding Chart of V4 in M30 (NGC7099) (adapted from Alcaino and Liller 1980). The circle, whose centre is the cluster core, has a radius of 5′.

2.2.1a Photometry of V4

These observations were taken in Johnson U, B, V and R band (Johnson 1965) with the WHT on June 24 1988. A CCD camera with a dye–coated GEC P8603 CCD chip was used. This chip has a read out noise of ~5 e pixel^{-1} and a pixel size of 22×22 μm. The camera was mounted at one of the Nasmyth foci. This gave an on chip plate scale of 0.1″ pixel^{-1}, or alternatively 4.51″ mm^{-1}.

Each frame was exposed for 100 s. The seeing was approximately 0.7″ and conditions photometric. Observations of standard stars G93z48 and 112z223 (Argyle *et al.* 1988, Landolt 1983) were performed so as to calibrate the data. Sky flat field frames were also taken. A log of the V4 and standard star observations is given in Table 2.1.

The CCD frames were reduced in the standard way. A mean bias level (from the overscan region) was subtracted from all the CCD frames. Normalised U, B, V

and R flat field frames were prepared and the appropriate image frames divided by them. The flat field frame is necessary to correct for sensitivity variations across the chip. These variations could be of three types: large scale, pixel to pixel or "black hole" (due to dust or grease on the CCD). Each of these sensitivity variations is corrected for efficiently by the use of a normalised flatfield frame.

Table 2.1 Photometry Observing Log for V4

Object –	Time of Observation (UT)	Filter –	Exposure Time (s)	Air Mass
M30/V4	04:59	U	100	1.63
M30/V4	05:11	B	100	1.64
M30/V4	05:19	V	100	1.65
M30/V4	05:21	R	100	1.66
G93z48	05:28–05:32	UBVR	50, 20, 10, 10	1.13×4
112z223	05:36–05:42	UBVR	50, 20, 20, 10	1.29, 1.30, 1.31×2

Aperture photometry was performed using DAOPHOT (Stetson 1987). An aperture was placed around the star, whose centroid was determined visually. Then an annulus was placed around the aperture so as to determine the sky brightness per pixel (taken as the modal pixel value within the annulus). Profile fitting photometry was inappropriate in this instance because there were insufficient stars (2) on the frame to determine the point spread function accurately.

2.2.1b Photometry Results

The instrumental magnitudes ($m_{ins\lambda}$) in a given band (λ) corrected for atmospheric extinction (a_λ) are obtained using the standard equation,

$m_{ins\lambda}=m_{dao\lambda}+2.5\log_{10}(t_{exp})-a_\lambda(1+\text{air mass})$, where $m_{dao\lambda}$ is the raw magnitude from DAOPHOT and t_{exp} the exposure time of the frame. The extinction coef-

ficients for a given wavelength band are a_U=0.4554, a_B=0.2079, a_V=0.1079 and a_R=0.0606 (Argyle *et al.* 1988). The transformation factors, $\gamma_\lambda = m_{real\lambda} - m_{ins\lambda}$ derived from the standard star observations (magnitude $m_{real\lambda}$) were consistent to within $\leq$0.05 magnitudes. They have values γ_U=–1.90, γ_B=–0.48, γ_V=–0.28 and γ_R=–0.09. In practice the correction for air mass only changes the final values by ~0.1 magnitudes.

The quiescent magnitudes of V4 are V=19.0, with U–B=–0.6, B–V=0.0 and V–R=+0.6. The error estimated by DAOPHOT in the aperture photometry was found to be unrepresentative of the real error in the measurement. This was probably due to problems in determining the sky background because of the presence of the nearby bright star. An estimate of the true error was obtained by repeatedly performing photometry on V4 with the centre of the aperture at different offsets from the stars centre (by up to 6 pixels, 0.6″). Provided the photometry aperture was large enough (in this case r_{ap}~20 pixels (~2″) was found to be optimum) then the instrumental magnitudes should all have had the same value. However these varied by about ~0.2–0.3 magnitudes for U,B and V and ~0.1 magnitudes for R. Hence a realistic error for these magnitudes is $\leq$0.3.

2.2.2a Low Resolution Spectroscopy of V4

The spectroscopic observations were carried out using the Faint Object Spectrograph (FOS–2, Allington–Smith *et al.* 1989), mounted at the Cassegrain focus of the WHT. The FOS–2 is a fixed format, high–throughput, collimator-less spectrograph. The detector is a cryogenically cooled GEC P8603 dye coated CCD chip. The detector has a read out noise of ~10 e pixel^{-1} rms, a gain of

2.1 e ADU^{-1} with pixels that are 22 μm square. The grating has a 150 lines mm^{-1}. The resulting spectrum is cross dispersed so as to be accommodated on the detectors surface. The FOS–2 covers a spectral range from 3600–5000 Å in the second and 5000–9000 Å in the first order, with dispersions 4.3 Å $pixel^{-1}$ and 8.7 Å $pixel^{-1}$ and a resolution of 1.5 pixels. The observations reported here were taken during the FOS–2 commissioning run prior to the integration of FOS–2 into ISIS (the Intermediate Dispersion Spectrograph).

The three sets of observations were taken on the consecutive nights 25, 26 and 27 June 1988. A summary of these can be found in Table 2.2.

Table 2.2 Spectroscopy Observing Log for V4

Object –	Date & Time of Observation (UT)	Exposure Time (s)	Air Mass	Parallactic Angle	Slit Angle
M30/V4	25th 04:36	500	1.62	358	354
M30/V4	25th 04:45	500	1.62	3	354
M30/V4	25th 04:54	500	1.63	5	354
EG139	25th 05:45	30	1.16	75	75
HZ44	25th 21:26	50	1.04	112	113
M30/V4	26th 04:59	300	1.64	8	354
M30/V4	26th 05:04	300	1.64	9	354
M30/V4	26th 05:10	300	1.65	11	354
M30/V4	27th 05:02	300	1.65	10	354
M30/V4	27th 05:07	300	1.65	11	354
EG139	27th 05:48	20	1.19	75	75

A 20″ long slit was used with a 1″ width on the first two nights and 0.75″ width on the last night. There was cloud present for some of the night of 26 June 1988 so the spectra are only calibrated for relative not absolute spectrophotometry. The spectra taken on the night of 27 June 1988 are of poorer quality than the previous two nights since the use of a narrow (0.75″) slit caused some light loss. Sahara dust was also present on this night causing additional extinction. Light

loss due to differential refraction should be small because the slit angle was approximately at the parallactic angle.

To calibrate the data flux standards EG139 and HZ44 were observed (Oke 1974).

Spectral Extraction

The data were extracted initially using the on–line facility at the WHT. The standard extraction procedure is described in detail in Allington–Smith *et al.* (1989). The slit image is first straightened using a predetermined polynomial. Since these observations were taken at a low zenith distance (ZD) and the default geometric correction factors (GCFs) were determined by observing stars at low ZD then the default GCFs are adequate. The actual extraction is then standard: ie. the sky derived from an uncontaminated region of the slit image is subtracted from the object then the object is summed along columns where the target is visible. Wavelength calibration and flux calibration are then performed automatically with default values set up. However because of the intrinsic faintness of the source and because there were at least two stars on the slit during any one exposure it was decided to use an optimal extraction algorithm to reprocess the data.

The limitation of the standard extraction technique is well known, namely that to preserve spectrophotometric accuracy pixels that contain little starlight must be included in the sum thereby increasing the statistical noise within the extracted spectrum. Horne's (1986) optimal extraction algorithm solves this problem by assigning non–uniform weights to each pixel in the sum that are related to their variances. This effectively maintains spectrophotometric accuracy whilst reducing the statistical noise. The limitation of this optimal technique is that the track the spectrum takes on the detector in the dispersion direction

must only vary slowly with wavelength. Since FOS–2 spectra are cross dispersed they exhibit severe curvature and therefore standard optimal extraction algorithms cannot be used on the unstraightened slit image. However no benefit is gained by using such algorithms on the straightened slit image either. This is because the old pixel grid is resampled onto a new pixel grid. The inevitable mismatches between the old and new grids introduces significant resampling noise especially if the object is vary faint. This resampling noise is not removed by standard optimal extraction algorithms and their use can actually degrade the signal to noise in the extracted spectrum (Allington–Smith *et al.* 1989).

The optimal CCD spectral extraction procedure followed was that of Horne (1986) as modified by Mukai (1990) so as to cope with the effect of a cross disperser. His algorithm avoids introducing resampling noise by extracting the spectrum without straightening the slit image. This is done by first splitting the columns into subcolumns (whilst preserving the total number of counts per wavelength) and then effectively finding polynomials that run parallel to the spectrum. This enables accurate weighting factors to be determined. This modification to Horne's (1986) algorithm is implemented in the DILEMMA package (Direct Image Linearization Method for Maximum Accuracy). It was found that optimal extraction gave a considerable improvement over the usual extraction procedure especially in the second order.

The spectra were then wavelength and flux calibrated whilst in DILEMMA. The wavelength calibration was obtained from observations of CuAr and Hg arc lamps.

The flux calibration was performed using observations of the flux standards HZ 44 and EG 139 and the spectrophotometric distribution for these stars given by Oke (1974). The instrument response function (IRF) was obtained by finding

the ratio of the tabulated to observed standard star data. The extracted spectra were then multiplied by the IRF to give the true flux distribution. Corrections for air mass were also made at this time.

Removal of telluric absorption features longward of 6500 Å is very important otherwise serious contamination of the reduced spectra would result. The removal was facilitated by the observation of featureless F stars in the vicinity of M30. A polynomial was fit through the F stars spectrum (ignoring the atmospheric bands), then a correction factor ($\tau(\lambda)$) was obtained by dividing the polynomial fit to the continuum. This was successful in removing most atmospheric features though remnants of the B-band ($\sim$ 6840 Å) remain. Note that the depths of the telluric absorption features do not increase linearly with airmass. At the resolution used here each pixel spans a few Angstroms which include clear continuum regions as well as one or more highly saturated telluric lines. CCD observations show that the strength of these lines scales as airmass$^{0.6}\equiv$secz$^{0.6}$, with the correction factor being applied in the following manner; (observed flux)=(incident flux)exp($-\tau(\lambda)\times$secz$^{0.6}$). When this correction is applied the the telluric bands are efficiently removed (Horne 1988, Wade and Horne 1988).

2.2.2b Spectroscopy Results

The individual spectra taken on a single night were added together to improve the signal to noise. The resultant summed spectra are called Night 1, Night 2 and Night 3 respectively and are displayed in Figures 2.2–2.4. A remnant of the atmospheric feature at λ6840 is present.

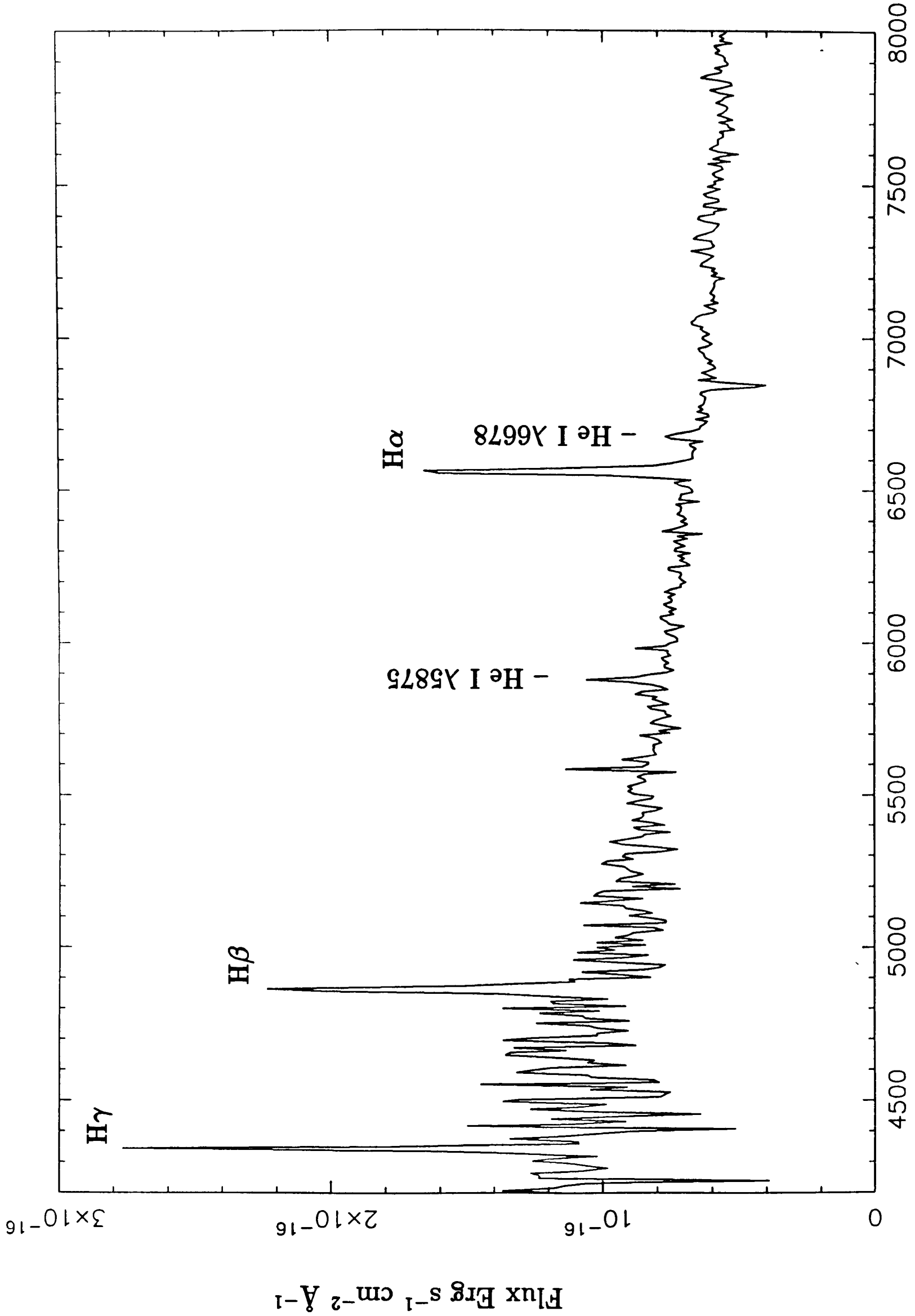

Figure 2.2: The spectrum of V4 taken on 24th June 1988

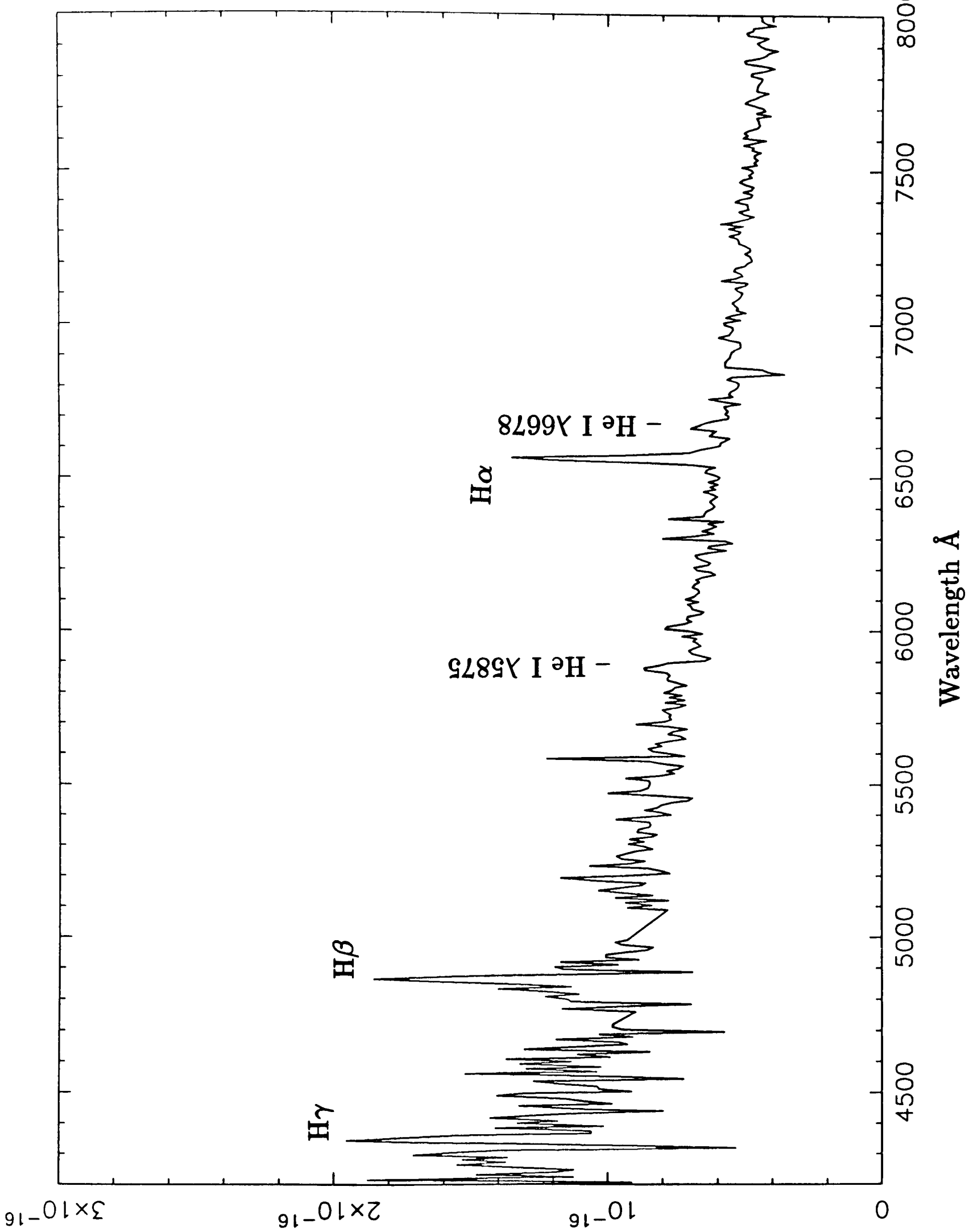

Figure 2.3: The spectrum of V4 taken on 25th June 1988

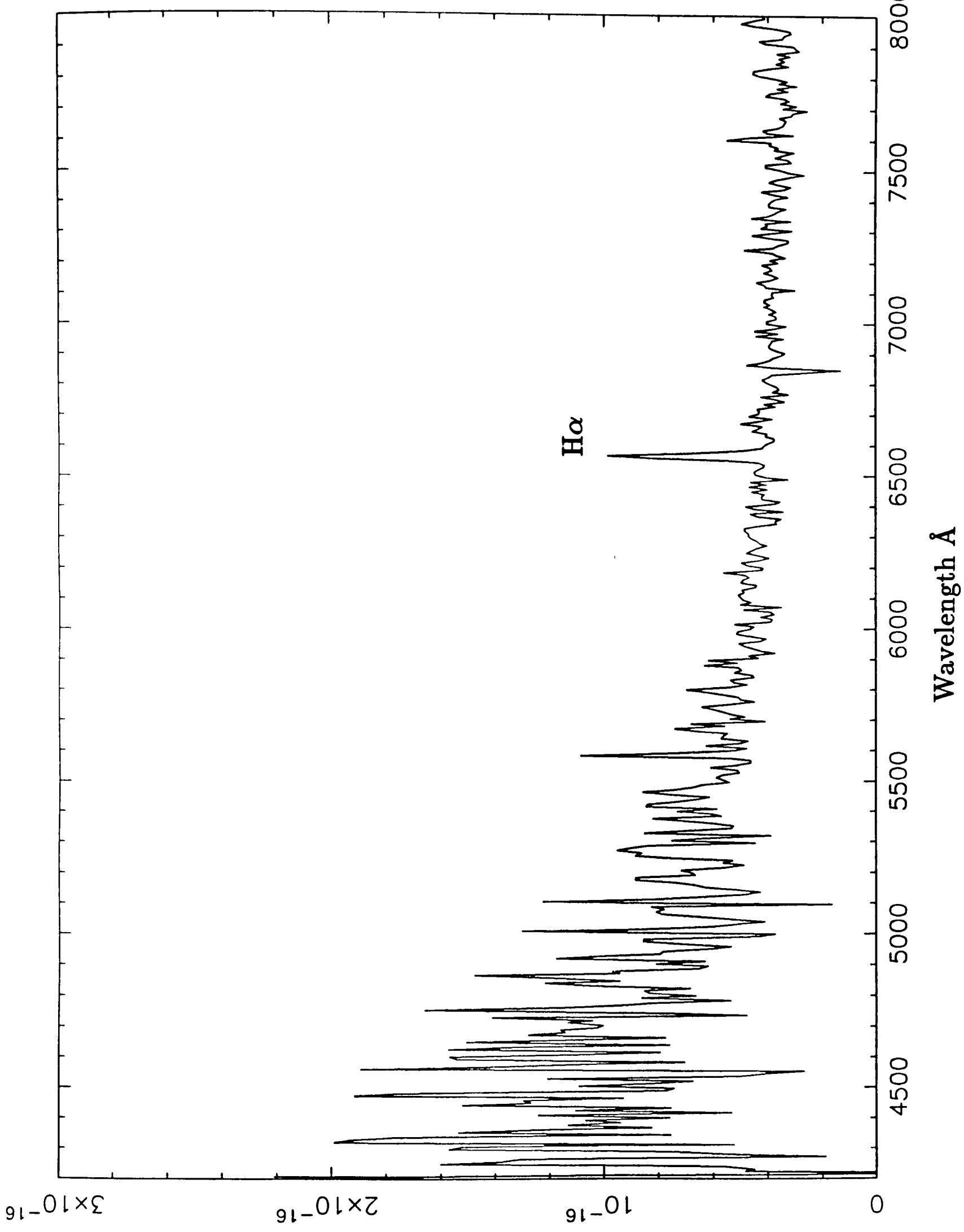

Figure 2.4: The spectrum of V4 taken on 26th June 1988

Before the addition was carried out I checked to make sure there were no radial velocity shifts within each nights data. The spectra obtained for each night were cross correlated with one another. Each spectrum was rectified by fitting it and then dividing it by a third order polynomial. The data were then normalised to zero. The end of the normalised spectra was masked with a cosine bell. This effectively resulted in a loss of 10% of the data at either end of the spectra. The mask width was chosen so as not to interfere with any spectral lines. No shift was detected within the groups of data to a level of $\sim$0.7 Å ($\sim$0.1 pixels in the first order). Therefore they could be added without loss of information.

The spectrum of Night 3 is very noisy when compared to those taken on Nights 1 and 2 (especially in the second order). This is due to significant light loss because of the use of the narrow slit. The spectra of Nights 1 and 2 are very similar. Night 1 displays Balmer emission lines Hα – Hϵ as well as He I λ6678 and λ5875. Night 2 displays fewer Balmer lines, probably because the second order of Night 2 is noisier than that of Night 1. Night 2 looks slightly bluer ($\sim$0.1 in synthetic magnitude terms, see below) than Night 1, though this is not a significant difference within the errors. Gaussian profiles were fitted to the Balmer emission lines for each night, using the QDP package (Tennant 1989). This makes use of a non–linear least squares fit to the data using the algorithm of Marquardt (Bevington 1969). The line free continuum was modelled with a constant and linear term. The results are given in Table 2.3, the errors in brackets are 2σ. The mean radial velocity of the Hα line is +130$\pm$30 km s^{-1}. When heliocentrically corrected this becomes +150$\pm$30 km s^{-1}. Although this differs markedly from the cluster radial velocity (–172 km s^{-1}, Harris and Racine 1979), the significance of this result is diminished for two reasons:

i) To obtain the best wavelength calibration both the optimal extraction and

the standard extraction (Allington–Smith *et al.* 1989) require "fine tuning" after the initial calibration. This is done by looking at the wavelength of the O I (5577) sky feature and forcing it to be at the correct wavelength.

This can cause shifts of ~0.3 pixels (or 2–3 Å) which is equivalent to ~150 km s^{-1} at Hα. The pixel shift was assumed to be linear and was applied to the second order also. This improves the wavelength calibration to about ~0.1 pixels (or ~50 km s^{-1} at Hα, Mukai 1989).

ii) The FOS–2 resolution in the first order is ~ 13 Å with about ~6 Å in the second order. The FWHM of the emission lines is typically ~20–30 Å . Thus any observations done at this resolution will mask any fine structure in the lines. This could have the effect of distorting the velocity measured.

However taking the above two points into account the consistency of the Hα radial velocity from one night to the next implies that the result is significant and provides some evidence for a difference in radial velocity between the object and the cluster.

Table 2.3 Line Centroids and Equivalent Widths for V4

Night –	Spectral Line	Measured Wavelength Å	Radial Velocity km s^{-1}	EW Å
1	Hα	6565.2 (0.2)	–109 (9)	36.9 (3)
2	Hα	6565.5 (0.8)	–123 (37)	30.0 (4)
3	Hα	6566.4 (1.0)	–164 (45)	29.6 (7)
1	Hβ	4861.5 (0.4)	–	30.8 (8)
2	Hβ	4862.5 (1.6)	–	19.2 (6)
1	Hγ	4344.1 (1.1)	–	21.3 (8)
1	Hδ	4103.8 (1.8)	–	–
1	He I λ6678	6680.4 (2.3)	–	3.7 (1)
1	He I λ5875	5879.5 (1.5)	–	5.9 (2)

The equivalent width of each line was measured, the errors in brackets are 2σ.

These are given in Table 2.3. A first order polynomial was fitted to the line free continuum to aid this measurement. There are no significant changes in the equivalent width of the lines from night to night.

Each spectrum was folded through Johnson B, V and R band filter response curves (Johnson 1965). Night 3 showed a half a magnitude drop in V and R when compared to Nights 1 and 2. This was probably due to the use of a very narrow slit. The B magnitude of Night 3 is not physical because the flux dips below zero at some points in this band. The folded magnitudes are shown in Table 2.4. The error (in parentheses) is the total spread in synthetic magnitudes.

Table 2.4 Folded Magnitudes for V4

Band	Night 1	Night 2	Night 3
B	19.24 (0.2)	19.11 (0.3)	–
V	19.08 (0.04)	19.08 (0.1)	19.47 (0.02)
R	18.60 (0.1)	18.71 (0.1)	19.02 (0.1)
B–V	0.16 (0.1)	0.03 (0.1)	–
V–R	0.48 (0.07)	0.37 (0.05)	0.45 (0.1)

The mean of Night 1 and Night 2 are V=19.1±0.1, B–V=0.1±0.1 and V–R=0.4±0.1. Since the folded magnitudes of Night 1 and Night 2 are essentially the same then the atmospheric conditions were probably spectrophotometric during the time of the observations taken on Night 2 as well as on Night 1. Note that these values are the same (within the errors) as those of the photometry.

The analysis of the spectral data presented here (except for the gaussian fits) was performed using the STARLINK DIPSO package (Howarth and Murray 1988).

2.3 Discussion

All these observations indicate that V4 is not a member of M30. Not only is V4 far from the cluster core (~50 r_c) but its (1) radial velocity, (2) outburst magnitude, (3) quiescent colour and magnitude and (4) distance derived from the Hβ equivalent width are all in conflict with cluster membership. I will discuss each numbered point below in more detail.

2.3.1 The Radial Velocity

For these measurements the mean heliocentrically corrected radial velocity of V4 is ~150±30 km s^{-1} (Hα). This differs significantly from the cluster radial velocity of –172 km s^{-1}. Although the measured radial velocity of V4 is subject to large systematic errors these observations provide the first evidence for a significant radial velocity difference between this object and M30. Provided the objects mean radial velocity is representative of its γ velocity then this result implies that V4 is not a cluster member.

2.3.2 The Outburst and Quiescent Magnitudes

The outburst magnitude of V4 is ~16.4 – 16.8 (Rosino 1949, Shara, Moffat and Potter 1990). Assuming that V4 is a member of M30, then using E_{B-V}=0.06 and d=7.2 kpc (Webbink 1985) the absolute outburst magnitude of V4 is M_V(outburst)~2.1. Patterson (1984) groups dwarf nova into "low $\dot{M}$" which have M_V(outburst)~+5.7 and spend >90% of their time in quiescence, and "high $\dot{M}$" with M_V(outburst)~+4.3 and spend <80% of their time in qui-

escence. Hence V4 is not a "low $\dot{M}$" system since it is too bright. Even if V4 were a "high $\dot{M}$" system it is still 2 magnitudes brighter in outburst than the mean for this type of system. Therefore it is clear that if V4 is a cluster member then it is a highly luminous dwarf nova.

However assuming that V4 is a "high $\dot{M}$" system, not in M30, then from the mean absolute outburst magnitude of "high $\dot{M}$" systems I estimate its distance to be $\sim$2.7 kpc. Clearly this is much closer than the cluster. If it were a "low $\dot{M}$" system it would be at a distance of 1.4 kpc, making the cluster membership problem worse. Using the mean quiescent magnitudes of "high $\dot{M}$" ($M_V \sim +7.8$) and "low $\dot{M}$" ($M_V \sim +9.2$) systems and comparing them with the quiescent magnitude of V4 ($V \simeq 19$) gives a similarly anomalous result.

Note that the quiescent and outburst spectra rule out the possibility that V4 is a magnetic system (see Wade and Ward 1985 for a sample spectrum of a magnetic variable).

Another inconsistency arises when one tries to interpret the outburst magnitude using the outburst magnitude – period relation found by Warner (1987). He showed that there was a tight correlation between the absolute magnitude of dwarf novae in outburst (corrected for effects of inclination) and the orbital period of the system. Leaving aside inclination effects for the moment, if one assumes M_V(outburst)$\sim$2.1 *is* the maximum outburst magnitude of V4 then one finds that the orbital period of the system is $\sim$13.7 hours. This is a very long period for a dwarf nova with only BV Cen (P_{orb}=15 hrs) being longer. To apply Warners relation correctly inclination effects need to be taken into account. Lower inclination (ie higher projected disc area) dwarf nova are visually brighter (by up to one magnitude) than their higher inclination cousins. By assuming the most extreme possibility ie i$\sim$0° then M_V(corr)$\sim$3.1. This mag-

nitude implies that $P_{orb} \geq 10.0$ hours, which is still long for dwarf novae.

Echevarria and Jones (1984) find that there is a close relation between the *quiescent* colour of a dwarf nova and its orbital period. In particular they find that if $P_{orb} > 5$ hours then $(B-V) > 0.6$ but if $P_{orb} < 5$ hours then $(B-V) < 0.3$. The quiescent state spectroscopy and photometry give $(B-V)_o \sim 0.0 - 0.1$ for V4. This result implies that the orbital period of V4 must be ≤ 5 hours in conflict with that inferred from the relation of Warner (1987).

It is possible to consider the above period problem in another way. This is best done by comparing the quiescent magnitude of V4 and the implied magnitude of a secondary star in a long period system. The latter can be estimated using the relation found by Echevarria (1983) relating the absolute magnitude and the orbital period of main sequence binaries. Note that his relation is only approximately valid for long period systems since the secondaries in dwarf nova with $P_{orb} > 6$–8 hours may be somewhat evolved (Patterson 1984). Assuming for the moment that V4 has an orbital period of ~ 10.0 hours (and therefore in the cluster) then using the relation of Echevarria (1983), $M_V(\mathrm{sec}) \sim +4.5$; the same as the quiescent magnitude of V4, $M_V \simeq 4.5$. Therefore if the period was long the secondary would contribute significantly to the spectrum in quiescence as observed for dwarf nova with $P_{orb} > 6$ hours (Oke and Wade 1982). This is clearly not the case: an inspection of the spectra (Figures 2.2–2.4) does not indicate the presence of a secondary star. However if $P_{orb} < 5$ hours as inferred from the quiescent colours then $M_V(\mathrm{sec}) > 8$ consistent with the appearance of the quiescent spectrum.

The quiescent colours and the general appearance of the spectrum of V4 infer a short orbital period for the system. However the the outburst magnitude implies a long orbital period. This discrepancy is best resolved if V4 is a field object.

2.3.3 The Equivalent Width of Hβ

It is possible to make a crude estimate of the distance to V4 using the equivalent width of the Hβ line. The equivalent width of this line $\sim$30 Å . Using the empirical relation derived by Patterson (1984) relating absolute disc magnitude, (M_V(disc)) and $H\beta$ equivalent width then M_V(disc)$\sim$8$\pm$1.5. Since the contribution of the secondary star to the overall luminosity is small (see above) then $V_{quies}\sim$19 can be used to estimate a distance to V4 of at least 1.6 kpc. Although only a lower limit, the derived distance is much closer than the cluster, implying that V4 is in the foreground to M30.

2.4 Conclusions

In this chapter I have argued that these observations of V4 are inconsistent with it being a cluster member but are consistent with it being a field DN. I predict that the object has a short orbital period (P<5 hours) and a probable distance of 2–3 kpc.

Obviously more observations are necessary, both photometry to establish its orbital period (if possible) and higher resolution spectroscopy to obtain a definitive radial velocity.

2.5 References

Alcaíno, G. & Liller, W., 1980. *Astron. J.*, **85**, 1330.

Allington-Smith, J.R., Breare, J.M., Carrasco, B.E., Ellis, R.S., Parry, I.R., Webster, J., Gellatly, D.W., Gribbin, F.J., Ingle, M., Jorden, P.R., Lowne, C.M., Powell, J.R., Thorne, D.J., Taylor, C., van Breda, I.G., Waltham, N.R., Worswick, S.P. & Wynne, C.G., 1989. *Mon. Not. R. astr. Soc.*, **238**, 603.

Argyle, R.W., Mayer, C.J., Pike, C.D. & Jorden,P.R. 1988. In:*I.N.G. User Manual – No. XVIII. A User Guide to the JKT CCD Camera (Version 1)*

Bevington, P.R., 1969. *Data Reduction and Error Analysis for the Physical Sciences.*, McGraw-Hill, New York.

Echevarria, J., 1983. *Rev. Mex. astr. Astrophys.*, **8**, 109.

Echevarria, J. & Jones, D.H.P., 1984. *Mon. Not. R. astr.Soc.*, **206**, 919.

Harris, W.E. & Racine, R., 1979. *Ann. Rev. Astron. Astrophys.*, **17**, 241.

Horne, K.D., 1986. *Publs. astr. Soc. Pacif.*, **98**, 609.

Horne, K.D., 1988. In:*New Directions in Spectrophotometry.*, eds. Davis Philip, A.G., Hayes, D.S. & Adelman, S.J., L. Davis Press, Schenectady, N.Y., USA.

Howarth, I.D. & Murray, J., 1988. *Science and Engineering Research Council, Rutherford Appleton Laboratory, Space and Astronomy Division, Starlink Project, Starlink User Note* **50.1**

Johnson, H.L. 1965. *Astrophys. J.*, **141**, 923.

Landolt, A.U. 1983. *Astron. J.*, **88**, 439.

Margon, B. & Downes, R.A., 1983. *Astrophys. J.*, **274**, L31.

Mukai, K., 1989. *Private Communication.*

Mukai, K., 1990. *Publis. Astron. Soc. Pacif.*, **102**, 183.

Oke, J.B., 1974. *Astrophys. J. Suppl.*, **27**, 21.

Oke, J.B. & Wade, R.A., 1982. *Astron. J.*, **87**, 670.

Patterson, J., 1984. *Astrophys. J. Suppl.*, **54**, 443.

Rosino, L., 1949 *Mem. Italian Astr. Soc.*, **20**, 63.

Shara, M., Moffat, A.F.J. & Potter, M., 1990. *Astron. J.*, **99**, 1858.

Stetson, P.B., 1987. *Publs. astr. Soc. Pacif.*, **99**, 191.

Tennant, A.F., 1989. *The QDP/PLT User's Guide,* NASA, USA.

Wade, R.A. & Ward, M.J., 1985. In:*Interacting Binary Stars,* eds. Pringle, J.E. & Wade, R.A., Cambridge University Press.

Wade, R.A. & Horne, K., 1988. *Astrophys. J.*, **324**, 411.

Warner, B., 1987. *Mon. Not. R. astr. Soc.*, **227**, 23.

Webbink, R.F. 1985. In:*Dynamics of Star Clusters IAU Symp. No. 113*, p. 541, eds. J. Goodman and P. Hut, Reidel, Dordrecht.

Chapter 3

Observations of the Dwarf Nova V101 in M5

In this chapter I report the results of the first time resolved photometry of the globular cluster DN V101. I also describe the results of low resolution spectroscopy of the object in three distinct states. From these observations I conclude:

i) That the overall observed properties of V101 are consistent with it being a member of M5.

ii) From the quiescent colours, the photometry and the spectroscopy that the period of V101 is >5 hours and that it will be possible to determine the systems orbital period photometrically.

iii) That the secondary star is probably evolved and of spectral type G.

3.1 Introduction

The large amplitude variable V101 (Hogg 1973) in the field of M5 was first discovered by Oosterhoff (1941). He reported that the object had an outburst magnitude of $m_{pg}\sim17.5$ and quiescent magnitude of $m_{pg}>19.5$, with a recurrence time of ~60 days. These observations lead him to suggest that the object was probably a dwarf nova.

The object then remained unobserved for over forty years until spectroscopy

of the object was performed by Margon, Downes and Gunn (1981). The 5-m Hale reflector CCD spectrograph was used to obtain a low resolution (~25 Å) spectrum of V101 in quiescence. The spectrum displayed strong Hα and He I λ5876 in emission, characteristic features of DN spectra in quiescence (Section 1.3a). The objects spectrum was quite red providing evidence for the presence of a large cool secondary. As the heliocentrically corrected radial velocity of M5 is only 59 km s^{-1} (Harris & Racine 1979) the resolution of Margon, Downes and Gunn (1981) was too low to determine the radial velocity of V101 and so confirm or exclude cluster membership.

Photometry of V101 was undertaken by Shara, Moffat and Potter (1987). They obtained one frame per night in B for ~14 nights during 1985 and 1986. Two of these frames are reproduced in their paper and form excellent finding charts. During the 1985 observations the object underwent an outburst (M_B=+4.3) which had a rise time of ~4 days. V101 then slowly declined to quiescence (M_B=+7.6) over the next ~10 days. Using empirical relationships between rise / decline times and orbital periods for known DN they were able to estimate that P_{orb}~11 hours. A long orbital period is consistent with the red spectrum observed by Margon, Downes and Gunn (1981). Note however that the relationships they use may not be applicable to all DN (la Dous 1990). More recently Shara, Moffat and Potter (1990) report spectroscopy obtained with the CTIO 4-m (7th June 1988) and the CFHT 3.6-m (14th and 15th June 1988) obtained concurrently with the spectral observations described later in this chapter. Their results are in broad agreement with those discussed below but the Hβ (EW=–20±5 Å) and Hγ (EW=–32±5 Å) emission lines in their spectra show hints of structure. They suggest that this structure, if real implies that V101 is a high inclination system and the orbital period can be measured by monitoring its light variations.

3.2 Observations

All the observations described in this chapter were taken at the Observatorio del Roque de los Muchachos on the island of La Palma. The photometry was performed on V101 using the 2.5-m Isaac Newton telescope (hereafter INT). The spectroscopy was taken using the FOS–2 low resolution spectrograph on the WHT. This section is split into subsection 3.2.1 where the photometric observations and results are described and subsection 3.2.2 spectroscopic observations and results are reported.

3.2.1a Photometry of V101

These observations were taken at the 2.5-m INT telescope using the prime focus camera. The camera is equipped with a dye coated GEC CCD which has similar characteristics to the CCD described in Section 2.2.1a. The pixel size in this instance was 0.54″ (22μm square) and the CCD had a gain of 4 e ADU^{-1}. There were two sets of observations. On the 31 March 1990 a colour sequence of V101 was taken in U, B, V, R and I. The standard stars 121968 and 99z6 (1 April 1990) were observed to obtain an absolute calibration of the CCD frames (Argyle *et al.* 1988, Landolt 1983). On the 1 April 1990 54 images of V101 were taken in R band; the first had an exposure time of 400 s, the rest 300 s. The observations were taken between 00:34 UT and 05:55 UT. The seeing was 1.5″$\sim$2″ throughout the night except for the last $\sim$20 minutes when the seeing worsened to 3–4″, the observing conditions were photometric. Both bias and flat field frames were taken (the latter in all the filters used). A summary of these observations are shown in Table 3.1.

The data were reduced as in Section 2.2.1a except this time a normalised bias

frame was used in conjunction with the mean level in the overscan region. This enabled the pixel to pixel bias variation across the frame to be removed as well as the mean level. The normalised bias frame was the cumulative mean of twenty separate zero second exposures.

Table 3.1 The Photometry Observing Log of V101

Object –	Date (1990) & Time of Observation (UT)	Filter –	Exposure Time (s)	Air Mass
M5/V101	31st Mar. 04:53	U	1000	1.158
M5/V101	31st Mar. 04:12	B	600	1.123
M5/V101	31st Mar. 04:24	V	400	1.129
M5/V101	31st Mar. 04:33	R	400	1.137
M5/V101	31st Mar. 04:50	I	500	1.154
121968	31st Mar. 01:53–02:23	B, U, V, R, I	2, 5, 2×3	~1.18
99z6	1st Apl. 20:38–20:48	R, B, V, U, I	2, 4, 10, 60, 5	~1.15
M5/V101	1st Apl. 00:34, 00:44–05:55	R	400, 300×53	–

Profile fitting photometry was performed on four stars in the frame as well as V101 by DAOPHOT (Stetson 1987). Four bright stars in relatively uncrowded parts of the CCD frame were used to define the point spread function (PSF) ie. the two dimensional intensity profile of the star as recorded by the CCD. These stars (2–5) along with V101 (star 1) are marked on the image of the field shown in Figure 3.1. Aperture photometry was used on the standard stars.

3.2.1b Photometry Results

The instrumental magnitudes are calculated using the method described in Section 2.2.1b. The transformation factors (γ_λ) derived from the observations of the two standard stars were consistent to <0.05 magnitudes. They have values of γ_U=–1.76, γ_B=–0.64, γ_V=–0.43, γ_R=–0.10 and γ_I=–0.90. The latter (γ_I) was calculated using a_λ=0.014 (Argyle *et al.* 1988).

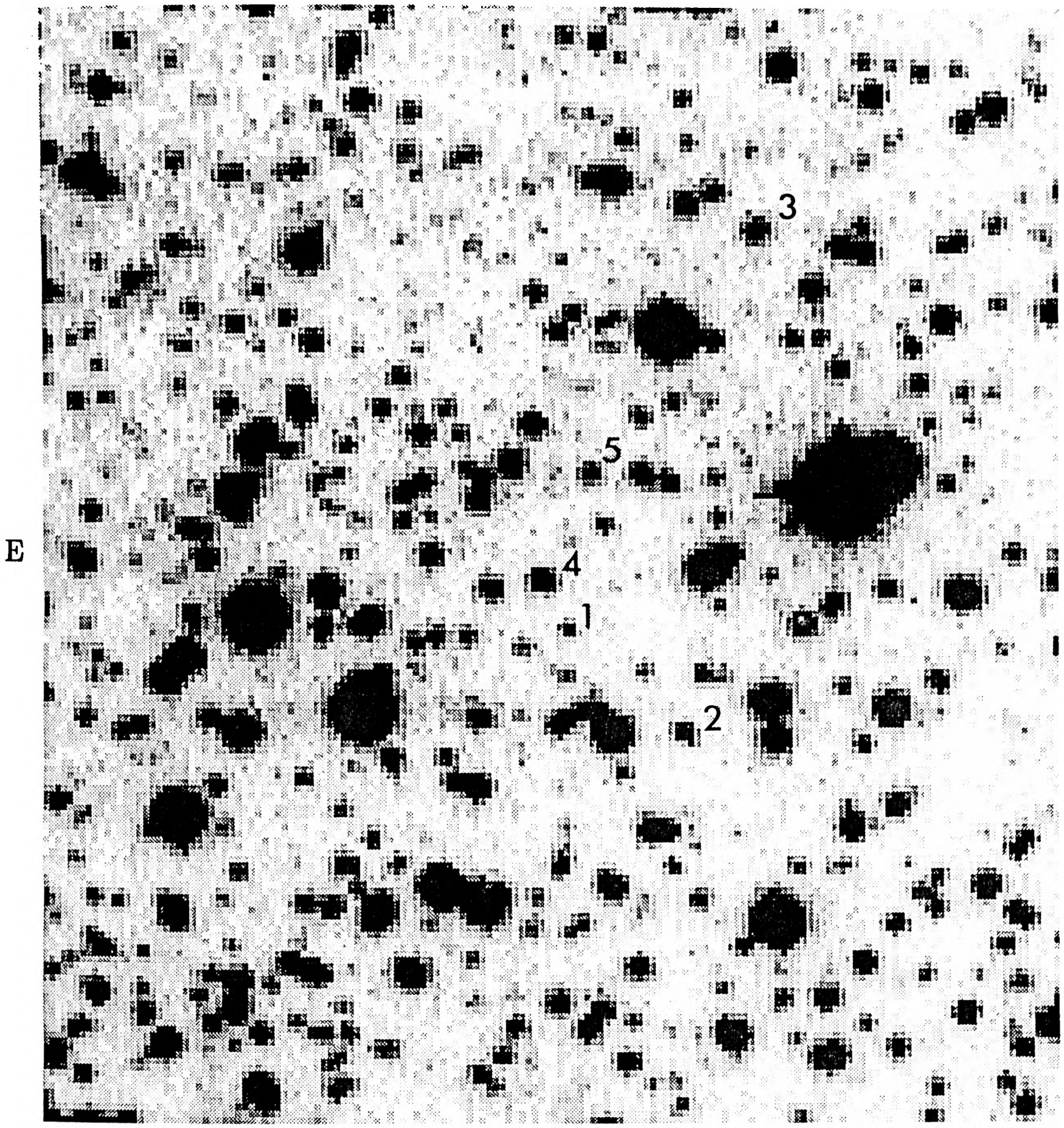

Figure 3.1: The star field around V101. V101 is marked as "star 1", the other stars (2–5) define the PSF of the CCD frame. The scale is 5.1″ cm^{-1}. North is at the top and East to the left.

The correction of the magnitudes for the effect of airmass changes their final values by <0.05 magnitudes.

The object was in quiescence during both nights. From the observations taken on the 31 March the quiescent magnitude and colours of V101 are V=21.7±0.1, U–B=–0.25±0.18, B–V=0.6±0.1, V–R=0.7±0.1 and R–I=0.3±0.1. The quoted errors are 1σ. Since reddening is low in the column to M5 with E_{B-V}=0.02 (Richer and Fahlman 1987) these colours and magnitudes are effectively the same as the dereddened values.

The time resolved photometry data taken on 1 April 1990 are shown in Figure 3.2. The x–axis is in fractions of a day (after 0:00 am 1 April 1990) and each point is plotted at mid integration. The y–axis shows the calibrated magnitude of star 5 and V101. These were calibrated using a "bootstrap" technique. Light curves of star 5 and V101 were generated by subtracting their instrumental magnitudes from that of star 4, a bright field star. The calibrated magnitude of star 4 was V=19.4, the difference generated in the first step was then subtracted from this magnitude yielding the calibrated light curve. The error bars are those derived from the profile fitting photometry. The photometry run lasted for about five hours and during that time the light curve shows a hump. The hump in the light curve persists for at least two and a half hours.

3.2.2a Low Resolution Spectroscopy of V101

These observations were performed with the FOS–2 as described in Section 2.2.2a. They were taken on eight separate nights separated by fourteen days. A 20″ long slit with a 1″ width was used throughout except on the nights of 19 and 20 June 1988 where additional spectra were taken using a 2″ wide slit. This was done to obtain accurate spectrophotometry.

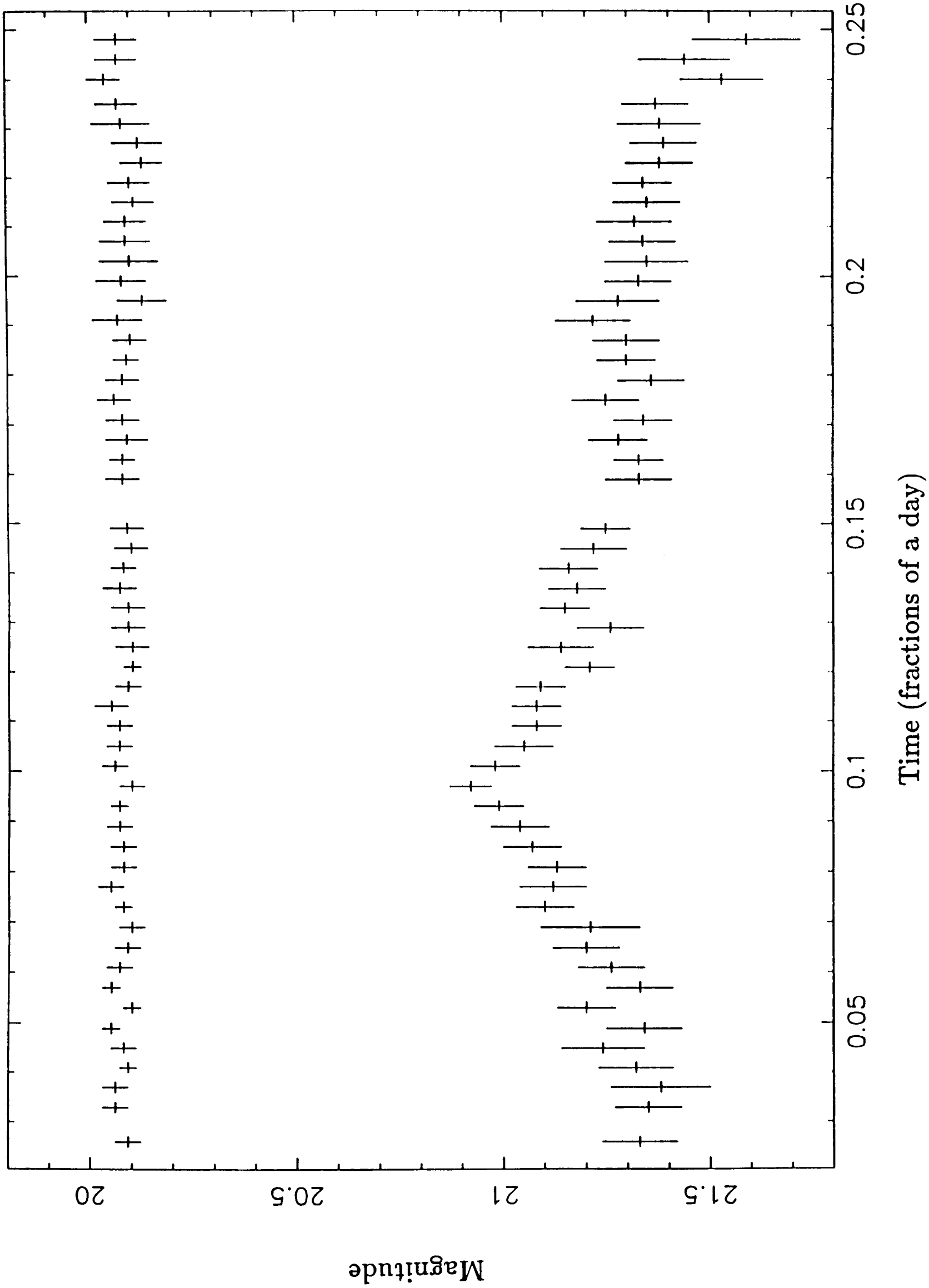

Figure 3.2: The light curve of V101 (lower curve) and that of a comparison star, star 5 (upper curve)

Conditions remained spectrophotometric throughout the observations of V101 and the seeing was generally subarcsecond. All of the observations were taken at the parallactic angle so light loss due to differential refraction was insignificant. A summary of these observations can be found in Table 3.2.

Table 3.2 The Spectroscopy Observing Log of V101

Date –	Time UT	Exposure (s)	Air Mass –	Slit Angle	Parallactic Angle
7 June 1988	00:10–01:56	1000	1.14–1.40	32	26–50
14 June 1988	00:15–00:33	500×2, 1000	1.19–1.22	26	34–38
15 June 1988	00:24	1000	1.203	29	40
16 June 1988	00:12–00:31	1000	1.19–1.23	24	34–40
17 June 1988	00:00	1000	1.21	–	–
17/18 June 1988	23:49	600	1.16	28	30
19 June 1988	00:09	600	1.21	35	37
19 June 1988	01:19	100	1.46	50	51
20 June 1988	00:07	600	1.22	36	38
20 June 1988	00:18	100	1.24	36	40
21 June 1988	00:57	600	1.41	48	51

All the spectra were extracted using the standard package (Allington–Smith *et al.* 1989) as described in Section 2.2.2a. In addition the first order of the spectra taken on the night of the 7th June 1988 were optimally extracted and wavelength calibrated (Mukai 1990) as described in Section 2.2.2a. This was done because the object was very faint V$\sim$21.3 on 7th June and optimal extraction provides the highest possible signal to noise. No spectrophotometric standard was observed on the 7th June so the data could not be flux calibrated hence the intensity was left as counts.

3.2.2b Spectroscopy Results

The object was found to be in three states during these observations. A qui-

escent state, an outburst state and a "bright" outburst state. The latter only occurred on the night of 17/18 June 1988 and was about one magnitude brighter than the normal outburst state. Figure 3.3 shows the sum of all the quiescent state spectra, Figure 3.4 an outburst spectrum and Figure 3.5 the "bright" outburst spectrum. The quiescent spectrum clearly shows Hα, Hβ and He I λ5876 in emission, also possibly Hγ. In outburst the emission lines diminish in strength with only Hα being visible in emission. Also the spectra become bluer. However on the night of the "bright" outburst the spectrum was very red and Hα becomes a weak absorption feature. The spectra on either side of the bright outburst were like those of "normal" outburst. Note that V101 may have been mis–identified with a field star during the "bright" outburst state. This would explain both the objects redness and the anomalous occurrence of the "bright" outburst during an otherwise normal outburst.

The wavelength calibration of the optimally extracted (June 7th) spectra were checked against the position of the O I λ5577 line and a shift based on this applied to the first order spectra. The maximum shift applied was 0.7 Å .

For each optimally extracted spectrum the Hα line was fitted with a gaussian, the line free continuum being defined by a constant and linear term (Tennant 1989). The gaussian centroids of the fits are shown in Table 3.3. The radial velocity of the Hα line varies systematically during the 1.75 hours observation on the night of 7 th June 1988. This is shown in Figure 3.6, the points are plotted at the mid integration point of each spectrum. As can be seen from Table 3.3 the actual wavelength shifts are much greater than the shift derived from the OI 5577 line. The total spread in the Hα line radial velocity variations for all these observations is 600 km s^{-1}. These results are the same as those derived from the standard extraction.

The equivalent width of the Hα line was measured for each night. A linear

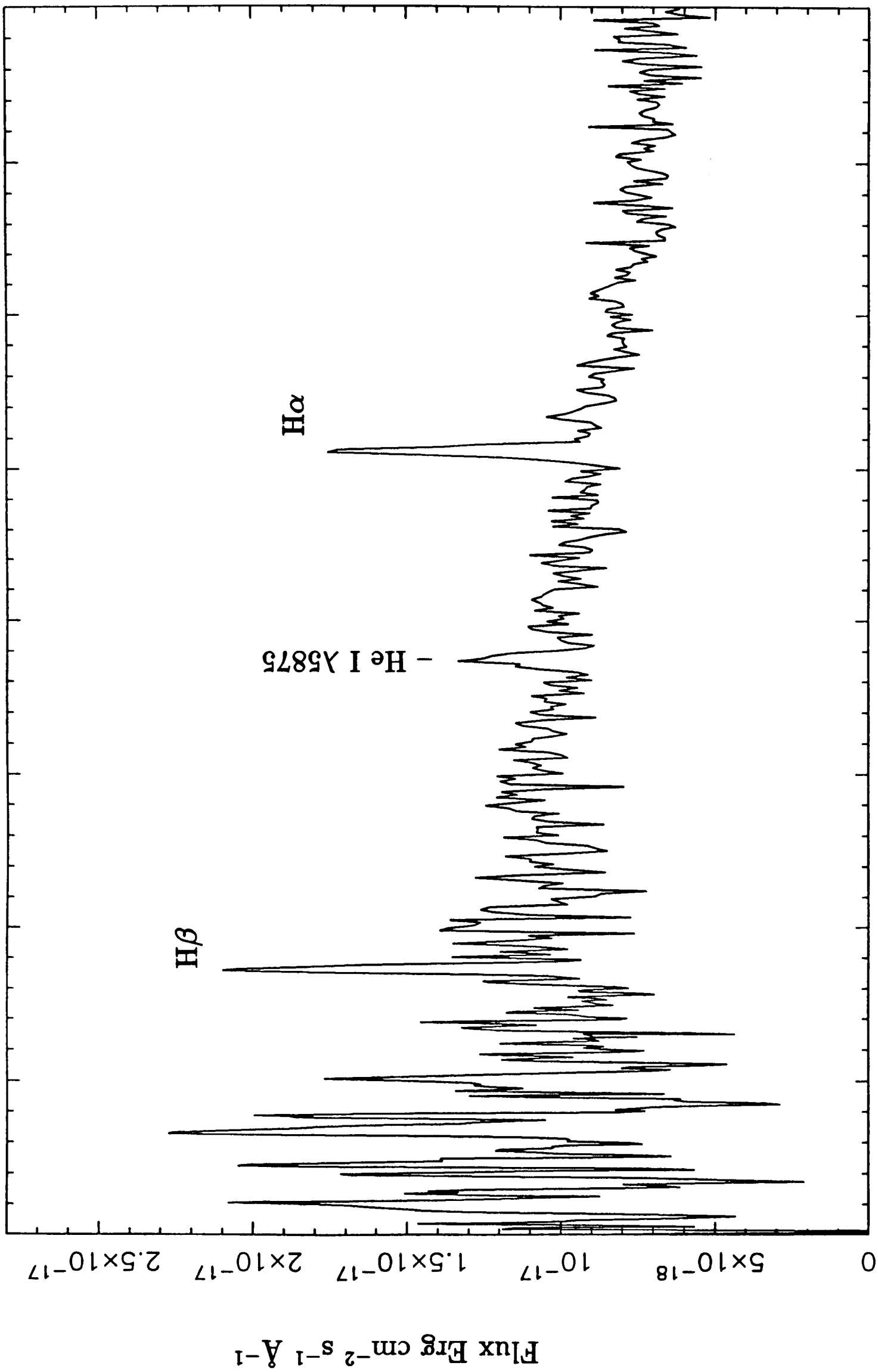

Figure 3.3: The quiescent spectrum of V101 (6/7 June 1988)

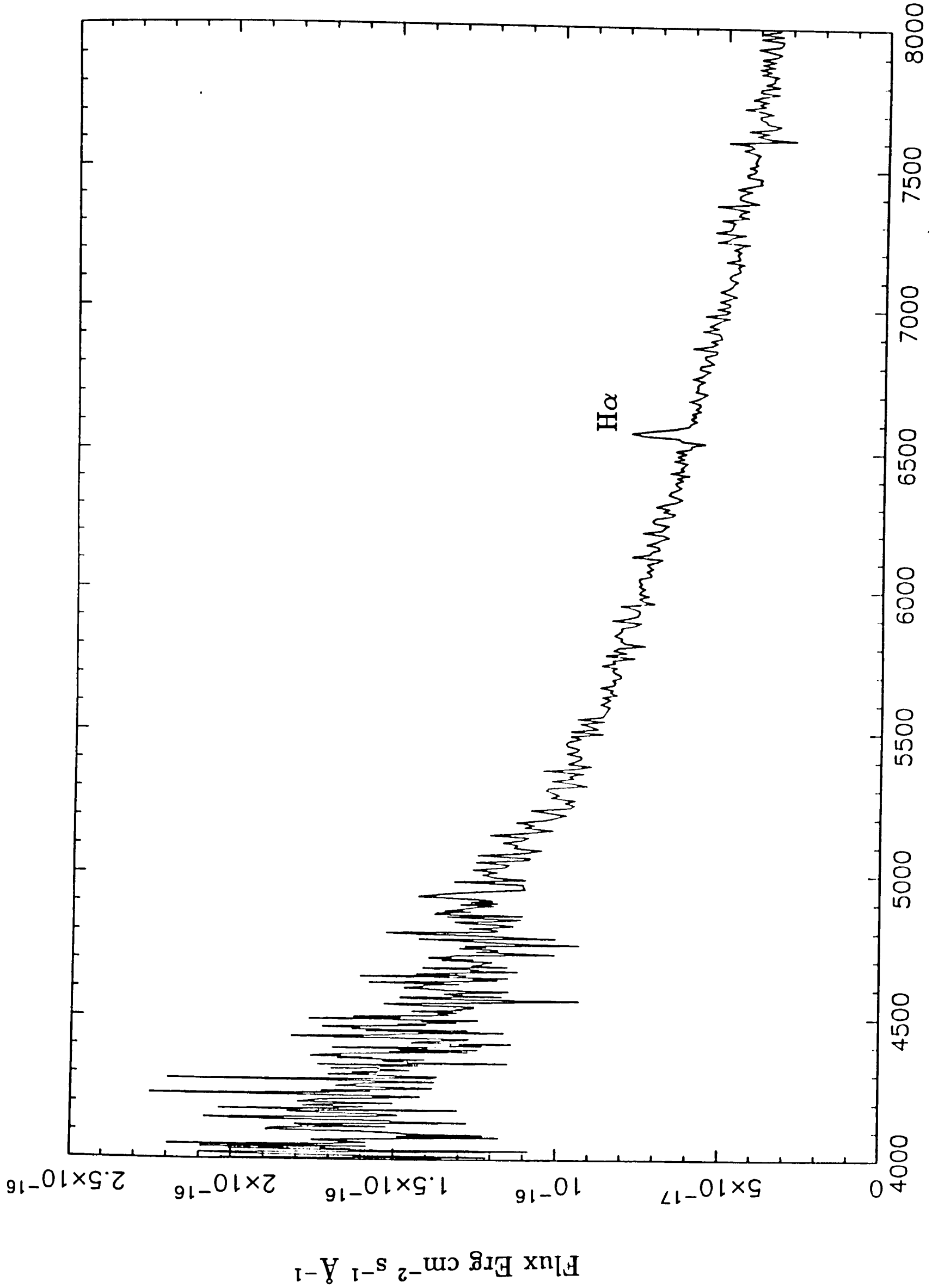

Figure 3.4: The outburst spectrum of V101 (16 June 1988)

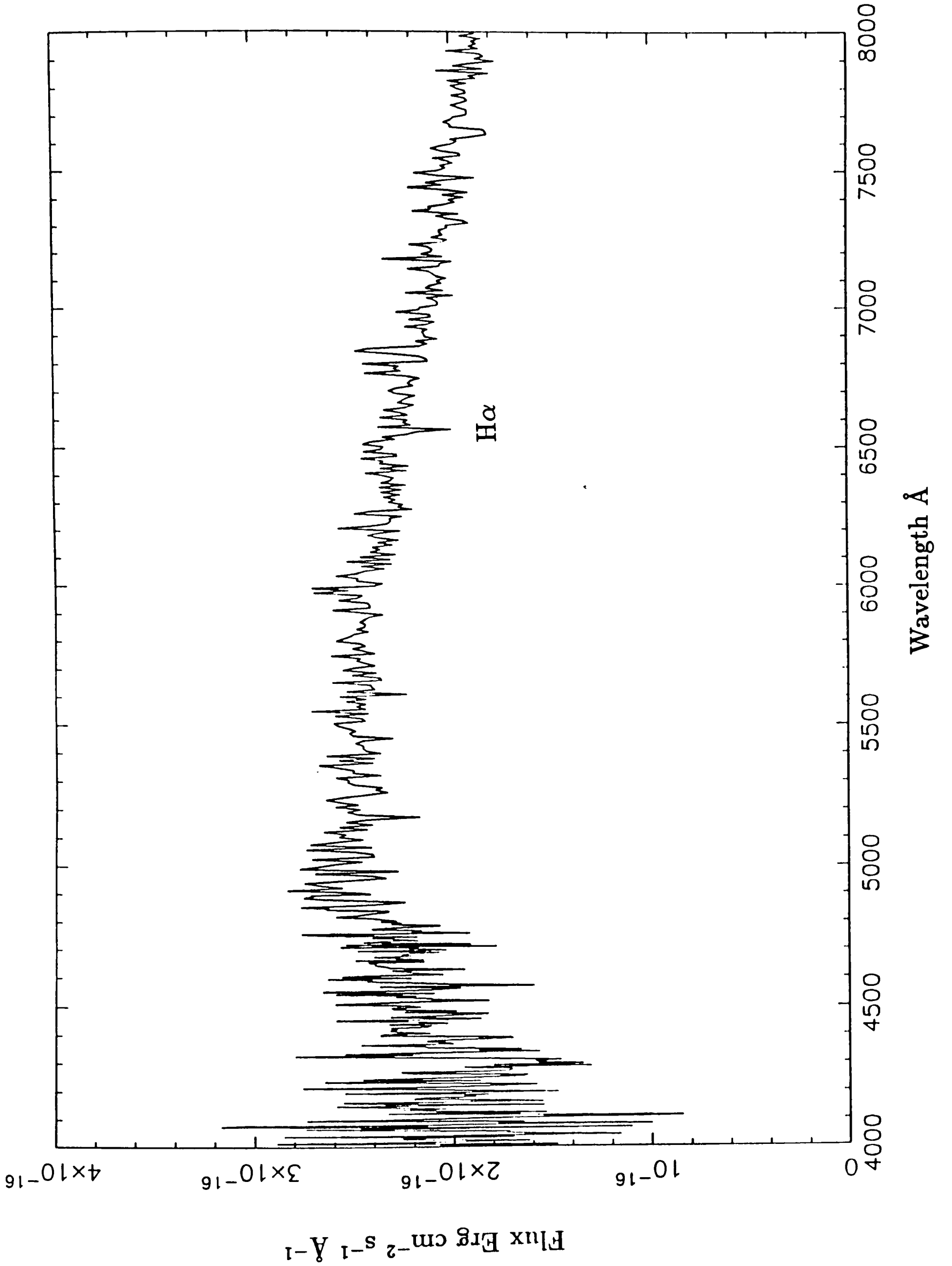

Figure 3.5: The "bright outburst" spectrum of V101 (17/18 June 1988)

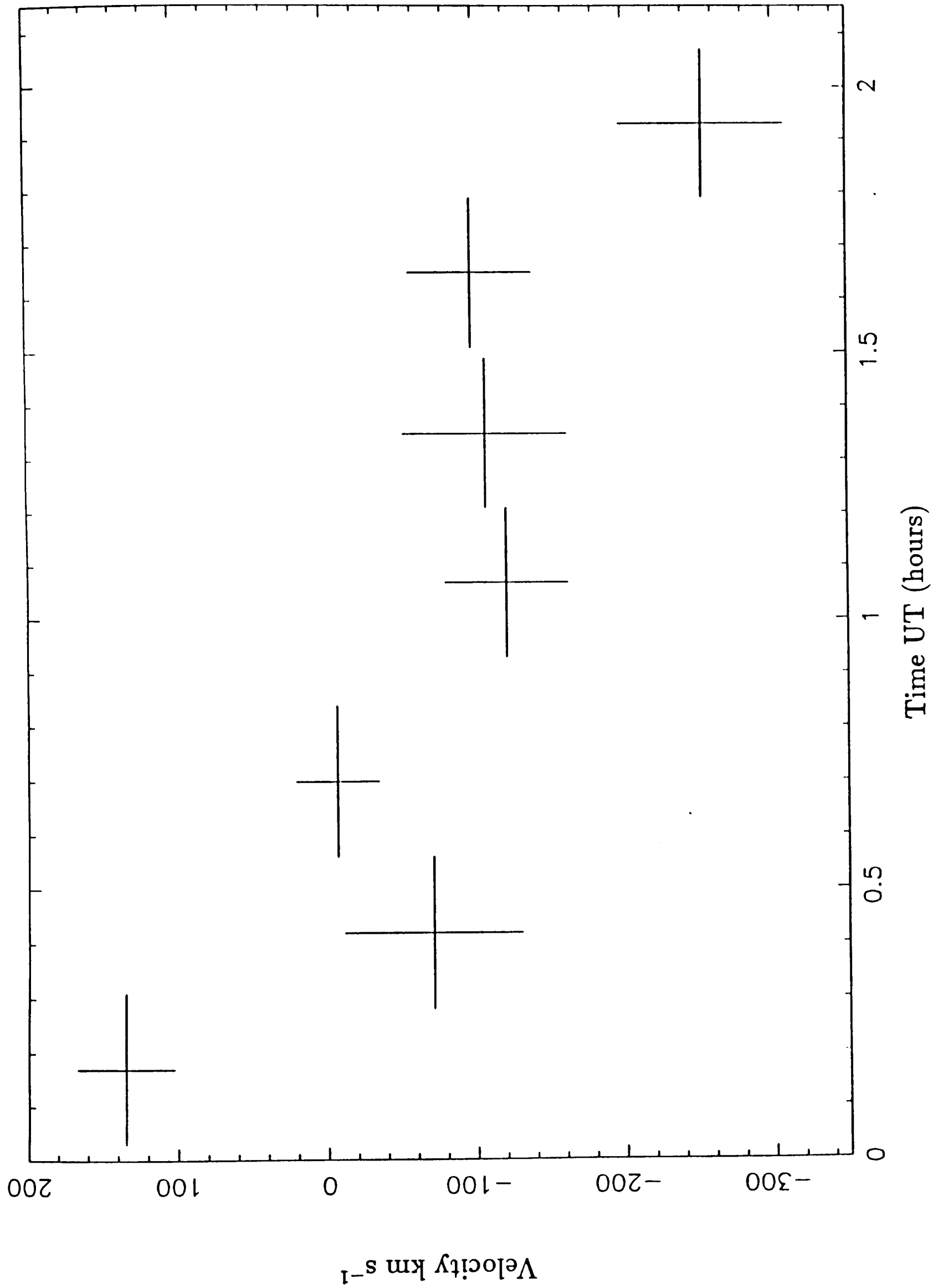

Figure 3.6: The radial velocity variation of the Hα line on June 6/7 1988

continuum was fitted to the line free region of the spectrum to aid the EW measurement. The results are shown in Table 3.3.

Table 3.3 The Equivalent Widths and Gaussian Centroids of Hα

Date –	Time UT	Equivalent Width Å	Gaussian Centroid Å
7 June 1988	00:10	–36.4 (7.0)	6565.8 (1.5)
7 June 1988	00:25	–43.8 (13.3)	6561.3 (3.6)
7 June 1988	00:42	–33.5 (10.2)	6562.7 (1.7)
7 June 1988	01:04	–38.9 (7.7)	6560.2 (1.7)
7 June 1988	01:21	–29.6 (8.4)	6560.5 (2.4)
7 June 1988	01:39	–31.5 (8.5)	6560.7 (1.8)
7 June 1988	01:56	–28.7 (8.7)	6557.3 (2.3)
14 June 1988	00:24	–6.6 (1.0)	6572.2 (2.1)
15 June 1988	00:24	–4.6 (2.4)	6566.0 (3.0)
16 June 1988	00:21	–8.2 (0.6)	6567.4 (2.7)
17 June 1988	00:00	–4.9 (3.2)	6564.6 (6.1)
17/18 June 1988	23:49	+1.5 (1.4)	6564.3 ( )
19 June 1988	00:09	–8.3 (3.1)	6569.6 (4.2)
20 June 1988	00:07	–14.1 (3.4)	6569.1 (2.2)
21 June 1988	00:57	–17.4 (7.0)	6564.8 (3.5)

As can be seen the equivalent width of the Hα line is large ($\sim$33 Å) in quiescence and small in outburst ($\sim$10 Å). The errors quoted are 2σ. After the second 17/18 June 1988 observation the EW of the Hα line begins to increase signalling a return to quiescence.

Finally the summed spectrum for each night was folded through Johnson B, V and R filter response curves (Johnson 1965, Tritton 1989). The results of these folds are shown in Table 3.4. There are two things of note:

i) Light loss due to the use of a narrow slit was probably uniform along the slit because the observations were performed at the parallactic angle. The colours obtained here are therefore probably correct. The object was red in quiescence (B–V=0.7) and blue in outburst (B–V=0.2). The quiescent colour is in good agreement with that obtained by the photometry in subsection 3.2.1b.

ii) The wide slit (2″) observations on the 19th and 20th June 1988 are found to be ~0.5 magnitudes higher than their narrow slit (1″) counterparts. This could be taken to represent a typical value for the light lost during narrow slit observations. However this need not be the case since the observations of V4 in M30 show that the light loss can be minimal even when a narrow slit is used. Obviously the exact amount of light loss depends on the seeing.

Table 3.4 The Folded Magnitudes of the Merged Spectra

Date	B	V	R	B–V	V–R	Object State†
7 June 1988	22.0	21.3	20.7	0.7	0.6	Q
14 June 1988	19.4	19.2	19.0	0.2	0.2	O
15 June 1988	19.0	18.9	18.7	0.1	0.2	O
16 June 1988	19.1	18.9	18.6	0.2	0.3	O
17 June 1988	19.4	19.4	19.1	0.0	0.3	O
17/18 June 1988	18.8	17.9	17.2	0.9	0.7	B
19 June 1988	19.8	19.5	19.2	0.3	0.3	O
19 June 1988	–	18.9	18.5	–	0.4	WS
20 June 1988	19.9	19.4	19.1	0.5	0.3	O
20 June 1988	–	19.0	18.5	–	0.5	WS
21 June 1988	20.8	21.0	20.5	–0.2	0.5	O

†Q=Quiescence, O=Outburst, B=Bright Outburst, WS=Wide Slit.

3.3 Discussion

In subsection 3.3.1 I will discuss the implications of the photometric observations whilst in 3.3.2 those of the spectroscopic observations.

3.3.1 The Photometry of V101

3.3.1a Time Resolved Photometry

The "hump" phenomena seen in the light curves of dwarf nova, caused by verti-

cal structure on the edge of the accretion disc, is a powerful tool for determining the orbital periods of non eclipsing DN (Warner 1976, la Dous 1990). This is because humps appear in the light curves of DN even if their inclination is too low to permit eclipses of the primary star or the accretion disc by the larger secondary star. The discovery of hump like phenomena in the light curve of V101 would be particularly exciting because it would then be possible to determine the orbital period of the system.

If the bump in the light curve is indeed a "hump" then, since no eclipse follows maximum light (which they always do for eclipsing DN) the inclination of the system is probably <65°, in conflict with the predictions of Shara, Moffat and Potter (1990). This result implies that the structure in the Hβ and Hγ emission lines they observe is just noise and not due to the high inclination of the system. Since in general the humps persist for ~0.5 in orbital phase (la Dous 1990) the duration of the hump implies P_{orb}~5–7.5 hours. Unfortunately the length of this observation prevents a recurrence of the hump being observed.

3.3.1b The Quiescent Colours and Magnitude

Dwarf nova have quiescent state magnitudes that vary by ~0.5 magnitudes. V101 is no exception and has a quiescent V magnitude of <21.3 during the 1988 FOS–2 observation and 21.7 during the 1990 photometry. Using the known distance to M5 (d=7.6 kpc, Webbink 1985) the quiescent V magnitude implies an M_V~7.1. Patterson (1984) finds that the average absolute quiescent magnitude, for "high $\dot{M}$" systems (Section 2.3.2) is M_V~7.8, with a spread of about 2 magnitudes. Hence the quiescent magnitude of V101 is consistent with it being a "high $\dot{M}$" system and a cluster member.

The colours from both the FOS–2 and the photometric observations are similar ie: B–V$\sim$0.6 and V–R$\sim$0.6. From the intrinsic redness of the object one infers an orbital period of $\geq$6 hours (Echevarria and Jones 1984). This is in agreement with the result of the time resolved photometry. Using the relationship relating orbital period and absolute magnitude for main sequence binaries derived by Echevarria (1983) one can infer a magnitude of M_V(sec)$\leq$4.7 for the secondary and a spectral type of G2 or earlier. Thus there are two things to conclude from this result:

i) the secondary is too bright to be a ZAMS and could be evolved since the turnoff point for M5 is $\sim$3.9–4.7 (Richer and Fahlman 1987). Note that one would expect the secondary to have undergone some evolution if the period was >6 hours (la Dous 1990).

ii) The secondary would make a substantial contribution to the light output of the system in quiescence (M_V(quiescence)$\sim$7.1), but probably not in outburst (M_V(outburst)$\sim$3.1). The red colour of V101 in quiescence (the average DN has B–V$\sim$0 in quiescence) implies that the secondary is indeed making a substantial contribution to the light output. If the light from the secondary dominates V101 in quiescence then from B–V one estimates a $T_{eff}\sim$6000 K and a spectral type G from its B–V and V–R (Allen 1973). The nature of the secondary is discussed further in the spectral observations.

3.3.1c The Outburst Magnitude

The object twice appeared in outburst on the plates of Oosterhoff (1941) at $m_{pg}\sim$17.5. Assuming B–V$\sim$0 for DN in outburst then V$\sim$17.6 since B=m_{pg}+0.1 (Allen 1973). This implies an absolute magnitude for V101 in outburst of $M_V\sim$3.1. This is consistent with the mean absolute outburst magnitude of

"high $\dot{M}$" systems ($M_V \sim 4.3$) and therefore cluster membership.

If the "bright" outburst is a real feature of the system then from it one can infer a maximum outburst magnitude of ≤ 17.9. This is consistent with the value obtained by Oosterhoff (1941).

An estimate of the orbital period for the system can be obtained from the relationship found by Warner (1987) between accretion disc luminosity at maximum (when inclination effects had been corrected for) and orbital period. By assuming that i=0° and then correcting for the inclination effect the absolute visual magnitude of V101 becomes ≤ 4.1. Warners relation then infers $P_{orb} \geq 5.9$ hours. This is consistent with the results of the time resolved photometry since the presence of a hump in the light curve implies that i>0° and hence P_{orb} must be greater than 5.9 hours.

3.3.2 The Spectroscopy of V101

An accurate determination of the γ velocity of V101 would provide the most direct confirmation of cluster membership. However to find this it is necessary to obtain the objects radial velocity curve around an orbital cycle: for example as has recently been done for the eclipsing blue straggler NJL5 in the globular cluster ω Cen (Margon and Cannon 1989). Unfortunately neither these results nor those of Shara, Moffat and Potter (1990) cover a long enough time base to obtain a full radial velocity curve and hence I am unable to use this method for establishing cluster membership. Note that this technique may not be a foolproof way of establishing cluster membership since the optical counterpart to the X–ray source in M15, AC211, is known to have a variable γ velocity (Ilovaisky 1990).

However several things are clear. The Hα emission line in the quiescent spectrum does exhibit a large and systematic variation (Figure 3.6). If this variation is symmetric and periodic then the orbital period must be $\geq$3.5 hours. This is rather short when compared to the above period estimates and that of Shara, Moffat and Potter (1987) but does confirm that V101 lies above the period gap. The redness of the quiescent spectrum indicates that the secondary makes a significant contribution to the total light output of the system. This is consistent with the conclusions reached from the photometry results and is a general result for long period (>6 hours) dwarf novae.

The secondary must be earlier than M dwarf. This is because a main sequence M dwarf in M5 will have V>23 (Allen 1973) whereas V101 has V$\leq$22 in quiescence and hence the dwarf would be insufficiently luminous to redden the spectrum. Also the distinctive M dwarf TiO bands seen in the spectrum of other long period (P$\sim$6–7 hours) DN (eg. U Gem, Wade 1979) are absent. Since V101 has a red spectrum in quiescence in common with the longer period DN such as RU Peg (9 hours, Warner 1976) and BV Cen (15 hours, Vogt and Breysacher 1980) this indicates that the secondary is of G or possibly K type, not necessarily main sequence. Any of the spectral absorption lines associated with a secondary star of this type such as Fe I or Mg I are unresolved or lost in the general noisiness of the quiescent spectrum. Also these features would be weaker is this system because of its low metallicity. From the photometry and spectroscopy I conclude that the secondary is probably of evolved G type and that it dominates the optical flux from the system in quiescence.

The object became bluer (B–V$\sim$0.2) in outburst. This indicates that in common with other DN the accretion disc is now the dominant light source (la Dous 1990). All the emission lines disappear except Hα. The presence of any

emission lines is unusual for a dwarf nova in outburst since the disc is generally optically thick at this time with the spectral lines usually being in absorption (Wade and Ward 1985).

Another unusual aspect of this system is the presence of the "bright" outburst state. In this state the Hα line became an absorption feature and the system turned very red (B–V$\sim$0.9). A possible interpretation of this behaviour could be that a second burst of mass transfer had just taken place prior to the observations of 17/18 June 1988. This would cause the system to redden as cool material is dumped onto the disc edge from the secondary star. Since the Hα line becomes an absorption feature at this time it is possible that the residual Hα emission seen in outburst is produced in the outer portion of the disc. However as mentioned previously the 'bright" outburst may not be a real feature of V101 and more observations are needed to confirm this behaviour. An alternative explanation is that the object was mis–identified, possibly with a field K dwarf, during this observation.

After the "bright" outburst the system begins its decline from outburst becoming first bluer and then slowly fainter and redder with the EW of the Hα emission line increasing in the three subsequent observations. The observed behaviour of V101 on decline from outburst is typical for a DN returning to quiescence (Wade and Ward 1985).

The overall spread in radial velocity is $\sim$600 km s^{-1}. This large spread is probably caused by the "S–wave" effect seen in several DN such as U Gem and WZ Sge (Wade and Ward 1985). This effect is produced by an extra source of emission, usually the accretion stream or bright spot, distorting the observed line profiles. A study of this shift can still be used to obtain the orbital period of V101 but a proper dynamical study of the system will be difficult since the "S–wave" will mask the underlying motion of the white dwarf.

3.4 Conclusions

Clearly V101 has unusual properties for a dwarf nova, especially its outburst behaviour.

However V101 is a very important system since it is the only DN to date whose photometric properties are consistent with it being a member of M5. Also the system has a long orbital period, almost certainly between five and eight hours with an evolved secondary of spectral type G.

The two most important observations that are now needed are time resolved photometry over several nights to establish the orbital period of V101 and then time resolved, high resolution spectroscopy so as to establish the systems radial velocity curve and γ velocity.

The "bright" outburst, if real, is clearly most interesting. However, further spectroscopy is required before this behaviour is accepted as intrinsic to V101.

3.5 References

Allen, C.W., 1973. *Astrophysical Quantities,* The Athlone Press, London.

Allington-Smith, J.R., Breare, J.M., Carrasco, B.E., Ellis, R.S., Parry, I.R., Webster, J., Gellatly, D.W., Gribbin, F.J., Ingle, M., Jorden, P.R., Lowne, C.M., Powell, J.R., Thorne, D.J., Taylor, C., van Breda, I.G., Waltham, N.R., Worswick, S.P. & Wynne, C.G., 1989. *Mon. Not. R. astr. Soc.,* **238,** 603.

Argyle, R.W., Mayer, C.J., Pike, C.D. & Jorden,P.R. 1988. In:*I.N.G. User Manual - No. XVIII. A User Guide to the JKT CCD Camera (Version 1)*

Echevarria, J., 1983. *Rev. Mex. astr. Astrophys.,* **8,** 109.

Echevarria, J. & Jones, D.H.P., 1984. *Mon. Not. R. astr.Soc.,* **206,** 919.

Harris, W.E. & Racine, R., 1979. *Ann. Rev. Astron. Astrophys.,* **17,** 241.

Hogg, H.S., 1973. In:*Pub. David Dunlap Obs.,* **3,** 1.

Ilovasiky S.A., 1990. In:*Proceedings of the 23rd ESLAB Symposium,* Vol. 1, p. 145, eds. Hunt, J. & Buttrick, B., ESA Publications Division, ESTEC, Noordwijk, The Netherlands.

Johnson, H.L., 1965. *Astrophys. J.,* **141,** 923.

Landolt, A.U., 1983. *Astron. J.,* **88,** 439.

la Dous, C. 1990. In:*Cataclysmic Variables and Related Objects,* in press, ed. Hack, M., NASA/CNRS Monograph Series on Non–Thermal Phenomena in Stellar Atmospheres.

Margon, B., Downes, R.A. & Gunn, J.E., 1981. *Astrophys. J.,* **247,** L89.

Margon, B. & Cannon, R., 1989. In:*The Observatory,* **109,** 82.

Mukai, K., 1990. *Publis. Astron. Soc. Pacif.,* **102,** 183.

Oosterhoff, P. Th., 1941. *Ann. Sterrwacht Leiden,* **17,** part 4.

Patterson, J., 1984. *Astrophys. J. Suppl.,* **54,** 443.

Richer, H.B. & Fahlman, G.G., 1987 *Astrophys. J.,* **316,** 189.

Shara, M., Moffat, A.F.J. & Potter, M., 1987. *Astron. J.,* **94,** 357.

Shara, M., Moffat, A.F.J. & Potter, M., 1990. *Astron. J.,* **99,** 1858.

Stetson, P.B., 1987. *Publs. astr. Soc. Pacif.,* **99,** 191.

Tennant, A.F., 1989. *The QDP/PLT User's Guide,* NASA, U.S.A.

Tritton, K. 1989. *Private Communication.*

Vogt, N. & Breysacher, J., 1980. *Astrophys. J.,* **235,** 945.

Wade, R.A., 1979. *Astron. J.,* **84,** 562.

Wade, R.A. & Ward, M.J., 1985. In:*Interacting Binary Stars* eds. Pringle, J.E., & Wade, R.A., Cambridge University Press.

Warner, B., 1976. In:*The Structure and Evolution of Close Binary Systems, IAU Symp. No. 73*, p. 85, eds Eggleton, P., Mitton, S. & Wheland, J.A.J., Reidel, Dordrecht, Holland.

Warner, B., 1987. *Mon. Not. R. astr. Soc.*, **227**, 23.

Webbink, R.F., 1985, In:*Dynamics of Star Clusters IAU Symp. No. 113,* p. 541, eds. J. Goodman and P. Hut, Reidel, Dordrecht.

Chapter 4

Observations of Cataclysmic Variable Candidates in M71

Richer and Fahlman (1988) proposed that the six UV–excess objects they detected in the globular cluster M71 were candidate CVs. In this chapter I present the results of photometry and low resolution spectroscopy of several of these candidates. The results reported here show that the two brightest candidates are hot subdwarfs probably in M71. I argue that it is unlikely that many (if any) of the remaining candidates could be CVs or sdBs (subdwarf B stars) in the cluster. Although the nature of the remaining candidates is still to be determined, I use space density arguments to suggest that they could be field white dwarfs as opposed to field sdB, sdO or CVs.

4.1 Introduction

On theoretical grounds one expects that many interacting binary stars with a compact component (a neutron star or a white dwarf) will be formed in globular clusters (Section 1.4). Many neutron star binaries have been found in globular clusters either in the form of LMXBs (Hertz and Grindlay 1983) or binary and single millisecond pulsars (Ray & Kluźniak 1990). Until recently there was no effective way of searching for CVs in globular clusters. However with the advent of CCD detectors this situation has changed and a way is now available for a systematic search for globular cluster CVs. This is done most efficiently by con-

structing a deep colour magnitude diagram of the cluster core, then identifying all objects with the following photometric properties; $M_V \geq +5$ and $(U-B) \leq -1$. Single stars with these photometric properties do not occur in globular clusters in large numbers. It is therefore relatively simple to ascertain whether the candidate stars have other properties (eg. an emission line spectrum and/or large ($\delta V \geq 2$) variability) consistent with being CVs.

Using CCD photometry Richer and Fahlman (1988) constructed such a diagram for the globular cluster M71. On this they identify six objects whose magnitudes and colours are consistent with those of CVs.

4.2 Observations

All the observations described in this chapter were taken at the Observatorio del Roque de los Muchachos on the island of La Palma, using the 4.2-m William Herschel Telescope (WHT).

For convenience the candidate CV stars have been numbered 1 through 6.

4.2.1 Photometry

These observations were made in R band with the WHT on June 5 1988. The CCD camera described in Section 2.2.1 performed these observations. The exposure times varied between 100–400 s. Of necessity these had to be kept short because the camera rotator was not enabled and longer exposures would have resulted in very badly trailed images.

The observing conditions themselves were quite poor; high cirrus and a bright moon meant that the resulting images were not of photometric quality. However

they do make a fine series of finding charts for the six candidate CVs. These are reproduced in Plate 4.1(a–e). Only stars 3, 5 and 6 were detected, the other fields are presented for completeness. The position of each candidate is marked on the plate.

The size of each field is 40×60″, Table 4.1 gives a summary of the plate details along with the approximate centre of each field (with an accuracy of ∼20″).

Table 4.1: Central Positions of the Finding Charts

Star No	Plate No.	RA (1950)	Dec (1950)
1	1(a)	19 51.58	18 38.0
2	1(b)	19 51.53	18 38.8
3	1(c)	19 51.46	18 37.8
4&5	1(d)	19 51.70	18 39.3
5&6	1(e)	19 51.69	18 39.9

4.2.2a Low Resolution Spectroscopy

The spectroscopic observations were carried out using the Faint Object Spectrograph (FOS–2, Allington–Smith *et al.* 1989), mounted at the Cassegrain focus of the WHT. A brief description of this instrument is to be found in Section 2.2.2a. Good seeing enabled the width of the 20″ long slit to be set to 1″.

The three brightest CV candidate stars proposed by Richer & Fahlman (1988) were observed on the nights of 12 June 1988, (between 02:59 and 04:15 UT) and 20 June 1988 (between 03:09 and 04:41 UT). Table 4.2 gives a summary of the spectral observations. In addition to the candidate stars two flux standards (HZ44 and EG139) were observed.

The data were optimally extracted using the DILEMMA package (Mukai 1990, Section 2.2.2a).

Plate 4.1(a–e)

Finding charts for the six candidate CVs in M71. From top left to bottom right: (a) star 1; (b) star 2; (c) star 3; (d) stars 4 & 5; (e) stars 5 & 6.

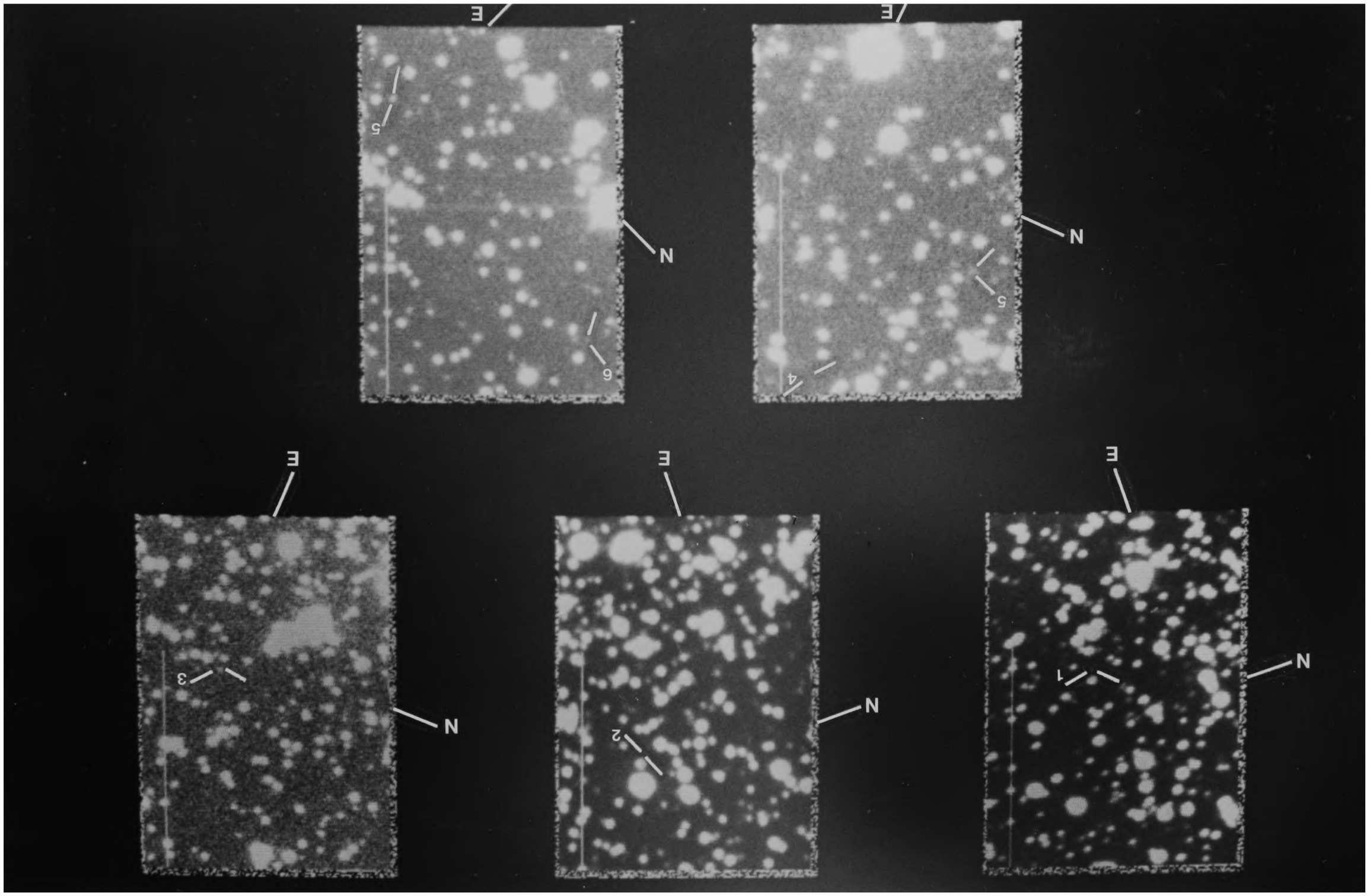
E
N
1
E
N
2
E
N
3
E
N
4
E
N
5
E
N
6

The wavelength calibration obtained from a CuAr arc was refined by defining a shift that forced the OI 5577 Å night sky line to be at 5577 Å. This shift never amounted to more than 0.2–0.3 pixels thus giving an absolute wavelength calibration accurate to ~50 km s^{-1}. This method of fine tuning the wavelength calibration is the same as that described by Allington–Smith *et al.* (1989). The pixel shift was assumed to be linear and was applied to the second order also.

Table 4.2: FOS Observing Log for the M71 CV Candidates

Star no.	Date (1988) & Start Time (UT)	Air Mass	PA of Slit	Parallactic Angle	Exposure time (s)
HZ44	11 Jun. 21:20	1.008	0	172	60
5	12 Jun. 02:59&03:32	1.03/1.02	313/313	320/351	2000×2
6	12 Jun. 04:15	1.03	313	37	2000
3	20 Jun. 04:41	1.09	89	60	1000
5	20 Jun. 03:09&03:26	1.01/1.02	78/57	16/21	1000×2
6	20 Jun. 03:53&04:12	1.03/1.05	347/347	43/52	1000×2
EG139	20 Jun. 05:29	1.08	75	91	30

4.2.2b Spectroscopy Results

The spectrum of star 3 was too faint to be successfully extracted from the CCD. The individual spectra of star 5 were added together to increase the effective integration time and the first and second orders merged. This was also done for star 6. The spectrum of star 6 was then smoothed with a Gaussian filter (FWHM=7 Å) to reduce the high frequency noise. The merged spectra of stars 5 and 6 are shown in Figures 4.1 and 4.2. A full discussion of the spectra is left until the next section but note that the second order of star 6 is particularly noisy and the identifications of the spectral lines marked somewhat uncertain. The spectra of star 5 from the night 12 June 1988 were added together as were its spectra from night 20 June 1988.

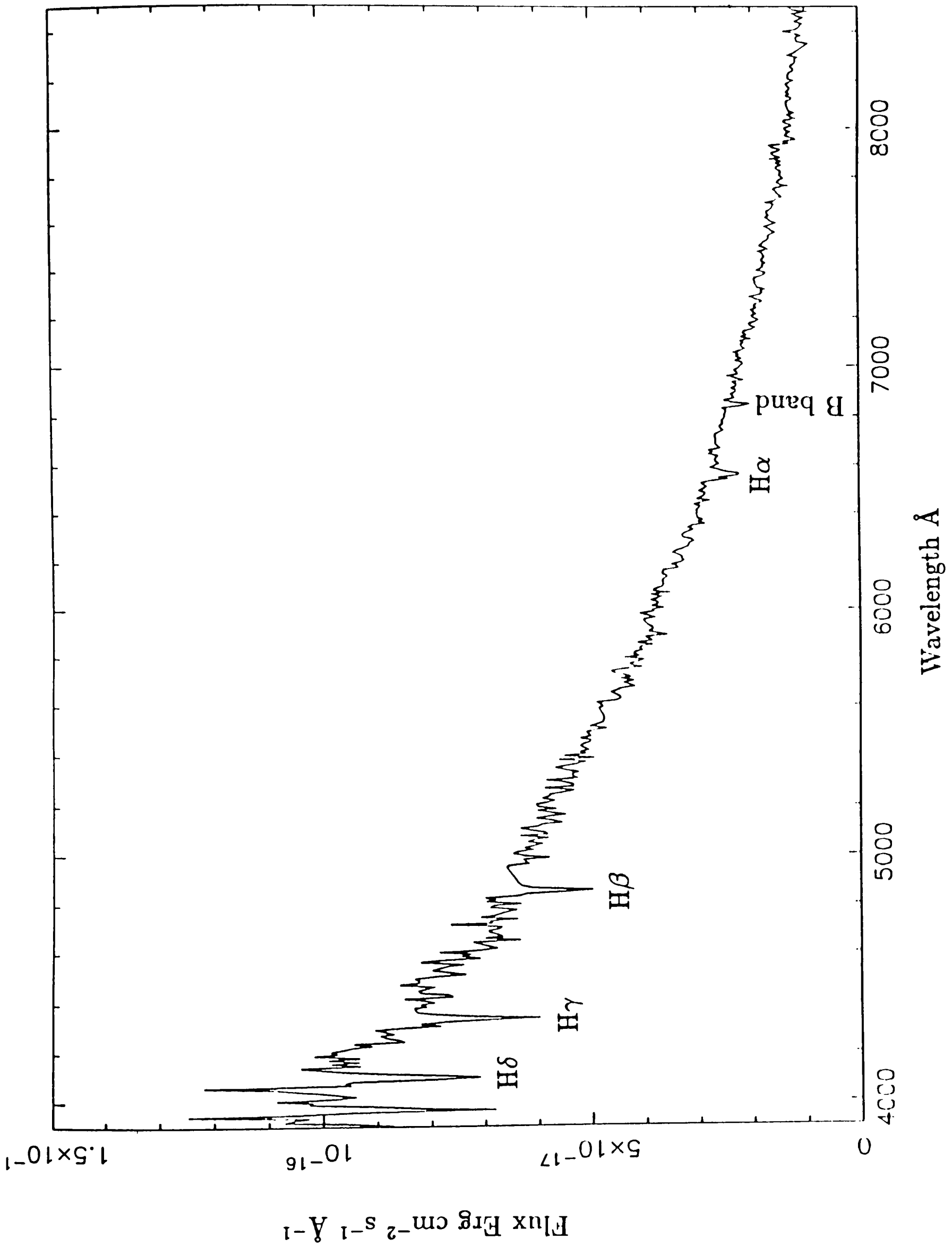

Figure 4.1: The merged FOS spectrum of star 5 in M71

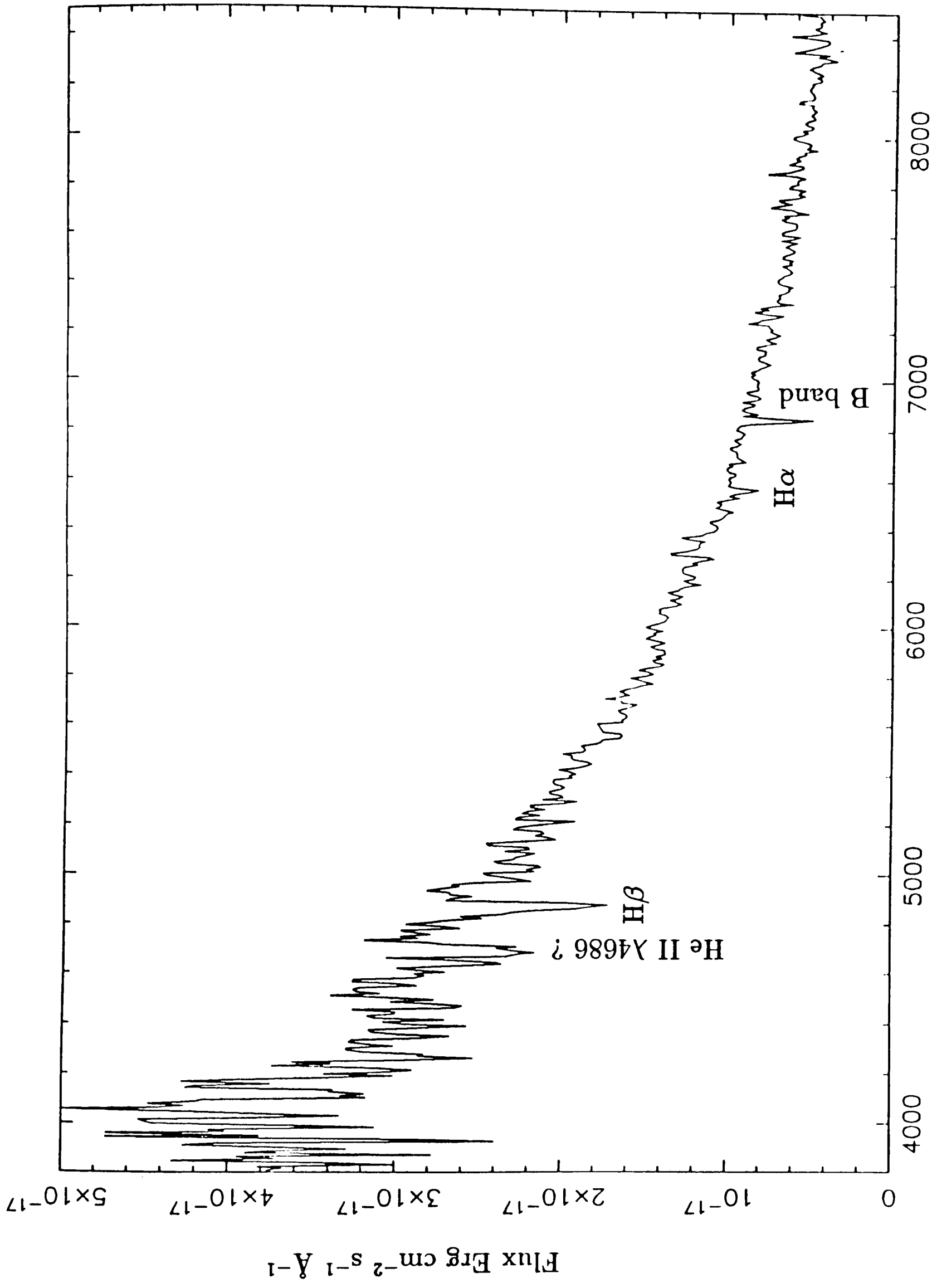

Figure 4.2: The merged FOS spectrum of star 6 in M71

These will be referred to as "Night 1" and "Night 2" respectively. These additions were done so as to improve the S/N in the spectra. Gaussian profiles were fitted to the Hα, Hβ and Hγ lines for these two nights, using the QDP package (Tennant 1989). This makes use of a non–linear least squares fit to the data using the algorithm of Marquardt (Bevington 1969). The results of these fits are shown in Table 4.3. The errors quoted are 2σ.

Table 4.3: Centroid Wavelengths and Equivalent Widths of Star 5 for Night 1 and Night 2, in Angstroms

Night	Hα		Hβ		Hγ	
-	Wavelength	EW	Wavelength	EW	Wavelength	EW
Night 1	6563.4±4.4	6.0±1.2	4862.2±2.2	4.7±2.2	4342.7±3.7	6.9±2.2
Night 2	6561.8±3.8	7.2±1.5	4856.6±4.6	6.2±2.7	4338.2±5.2	7.3±2.8

The fits are not of high precision (2σ error 2–6 Å) but within the errors there is no evidence for a systemic radial velocity shift from one night to the next which suggests that star 5 is not a binary system. Within the errors the measured line positions are consistent with the object being at rest. For instance, the mean radial velocity of the Hα line is -10 ± 100 km s^{-1}. The radial velocity of M71 is -19 ± 1 km s^{-1} (Webbink 1981) and hence the radial velocity of star 5 is consistent with it being a cluster member. Even if the heliocentric correction is taken into account the radial velocity of star 5 would only increase by $\sim$14 km s^{-1}, which would still be consistent with cluster membership. However, although the radial velocity of star 5 *is* consistent with cluster membership the uncertainty of the fits to the spectral lines (due to the FOS resolution) is too large to draw a firm conclusion.

The equivalent widths of the Hα, Hβ and Hγ lines were measured for both

nights and were, within the 2σ errors, found to be the same (see Table 4.3). Star 6 was too faint to do a similar analysis. Only Hα is definitely present, the other lines are, at best, only tentative identifications. However the Hα line of star 6 could not be fitted with a Gaussian profile because there were insufficient data points for it to be defined.

Synthetic B, V and R magnitudes were obtained for the spectra by folding the Johnson filter response curves (Johnson 1965, Tritton 1989) through each of the extracted spectra. The mean of these synthetic magnitudes and an error estimated from the scatter about the mean value were derived. These are shown in Table 4.4.

Table 4.4: Magnitudes for Stars 5 and 6

Star no.	Apparent Magnitude			Statistical Error			Dereddened Magnitudes			M_V –
-	B	V	R	B	V	R	B	V	R	-
5	19.9	19.8	19.6	0.10	0.10	0.13	18.6	18.9	19.0	5.6
6	20.9	20.9	20.7	0.15	0.10	0.22	19.7	20.0	20.1	6.7

The values derived by this technique may be subject to some systematic light loss due to (a) the slit being narrow and (b) the slit not being at the parallactic angle. The latter was necessary to avoid having numerous cluster stars on the slit. Since the seeing was sub–arcsecond for both these observations the light loss was probably small. This is confirmed by the fact that these absolute magnitudes agree with those of Fahlman and Richer (1989). The derived magnitudes were then corrected for the foreground reddening to M71, E_{B-V}=0.28 (Richer and Fahlman 1988) with A_V=3.3E_{B-V}, A_B=1.32A_V and A_R=0.74A_V respectively (Allen 1973). This gave B–V=+0.08±0.12 ((B–V)$_o$=–0.22±0.12)

and B–V=+0.01±0.15 ((B–V)$_o$=–0.30±0.15) for stars 5 and 6 respectively. Assuming that the stars are members of M71 and hence at a corresponding distance of 4.4 kpc (Webbink 1985) I obtain the objects absolute visual magnitudes (M_V) given in Table 4.4. These values have an estimated uncertainty of ±0.3 magnitudes. This is mainly due to the uncertainty of the distance to M71. The analysis of the spectral data was performed using the STARLINK DIPSO package (Howarth & Murray 1988).

4.3 Discussion

In subsection 4.3.1 I will discuss the nature of the two spectroscopically observed candidates (stars 5 and 6). In subsection 4.3.2 I estimate how many CVs one might expect to observe in M71. I then go on to discuss the nature of the remaining four candidates in terms of stellar populations and reach a conclusion as to their nature.

4.3.1 The Nature of the Two Spectroscopically Observed Candidates

The spectrum of star 5 shown in Figure 4.1 is dominated by strong Balmer lines in absorption but shows no other readily identifiable features. The spectrum of star 6 also has strong Hα and probably Hβ. It could also show the helium line λ4686 in absorption. However, this identification is uncertain because of the noisy nature of the spectrum shortward of λ5000. In any event these spectra do not look like those of cataclysmic variables, which are characterized by emission lines, particularly in the Balmer series. Only during the initial stages

of dwarf-nova outbursts do their spectra show very broad and shallow Balmer absorption lines. These, however, disappear after a few days (see e.g. Hessman 1986). Apart from the fact that the chance of encountering both stars just after the start of a dwarf-nova outburst is extremely small, the separation of these observations (see Table 4.2) by several days exclude the possibility that these stars are dwarf novae in the initial stage of an outburst. Furthermore the spectra of cataclysmic variables with persistently high mass transfer rates show the Balmer lines in emission (although their equivalent width is anti-correlated with the mass transfer rate, e.g. Patterson 1984) I therefore conclude that stars 5 and 6 are not cataclysmic variables and I next consider what they might be.

The shape of the continuum of star 5 (see Figure 4.1), and the equivalent width of the Balmer absorption lines in its spectrum are similar to the results found for sdB stars (see e.g., Wagner *et al.* 1988). The spectrum of star 6 has a continuum shape similar to that of star 5, and in addition to the Balmer lines shows possible He II absorption at 4686 Å . Thus it is likely that these stars are similar objects. The colours of stars 5 and 6 [$(B-V)_o = -0.22 \pm 0.12$, and -0.30 ± 0.15, respectively] are consistent with those of sdB stars (Green *et al.* 1986), and with the values of $(U-V)_o$ obtained for stars 5 and 6 by Fahlman and Richer (1989). These colours yield a very approximate effective temperature of ~30,000 K (Allen 1973). However if the He II 4686 Å line is a real feature in the spectrum of star 6 then the object is more likely to be a sdOB or even a sdO rather than a sdB star, but since the reality of this feature is questionable I assume that the object is a sdB star.

A recent survey of underluminous blue stars by Downes (1986), which includes forty sdB stars, gives a mean absolute visual magnitude $M_V = +5.0 \pm 1.4$ for sdB stars, with a range $+2.4 \leq M_V \leq +8.4$. The absolute magnitudes obtained for

stars 5 and 6 therefore are consistent with their being sdB stars and members of M71. A summary of sdB star properties is given in Appendix I.

4.3.2 The Nature of the Remaining Candidates

Although it was not possible to obtain a spectrum for the third brightest star (see above) Druiker, Fahlman & Richer (1989) have managed to do this and find that it may also be a blue subdwarf.

Assuming cluster membership Fahlman & Richer (1989) find that the remaining three blue stars have $M_V \geq +8.7$. The faintest sdB (out of 40 sdBs) in the survey of UV–excess objects by Downes (1986) has an $M_V=8.4$. It is therefore unlikely that there would be three sdB stars fainter than this in M71. It is always possible that globular cluster sdB stars are different to field sdB stars though the observations of Heber *et al.* (1986) make this conclusion unlikely. Heber *et al.* (1986) compares the observational properties of sdB stars in the galactic disk with those of possible globular cluster sdB stars. They showed that the characteristics of the sdB stars in NGC6752 (a low-metallicity globular cluster with [Fe/H]=–1.64, see Webbink 1985) were the same as those of the field sdB stars. This indicates that metallicity is not an important factor governing the luminosities or colours of sdB stars. Since the metallicity of M71 ([Fe/H]=–0.45, Webbink 1985) is close to that expected for galactic–disk objects, one would expect its sdB stars to be similar to the sdB stars found in the field.

Bailyn and Iben (1989) suggest that some globular clusters contain a large number of sdB stars. These are thought to be produced by mergers of low mass white dwarf pairs that are formed from primordial main–sequence binaries. Although the three brightest stars could belong to this "merger" sdB population

the remaining three candidates probably do not because they are very faint when compared to field sdBs. It is therefore unlikely that the three remaining UV–excess objects are sdB stars in M71. As far as their colours are concerned, $(U–V)_o \sim -0.7$ to -1.0 (Richer and Fahlman 1988) these objects could be sdB, sdO, CV, or white dwarf (WD) stars outside M71, or perhaps globular cluster CVs. I consider these possibilities in turn.

4.3.2a The Expected Number of CVs in M71

I consider the possibility that some of the faint CV candidate stars proposed by Richer and Fahlman (1988) are quiescent CVs in M71. To do this I will make an estimate of the actual number of CVs expected to produced in the core of M71.

Verbunt and Meylan (1988) have calculated the number of CVs produced in ω Cen and 47 Tuc. They assume that tidal capture is the dominant mechanism for the formation of white dwarf binaries. Because of the low number density of globular cluster binaries they justifiably neglect three body interactions as a rival (or complimentary) binary formation mechanism. They predict that 7 and 36 white dwarf binaries form in ω Cen and 47 Tuc respectively. I have scaled their results to M71 by assuming that the number of white dwarf binaries produced in the core of a globular cluster scales as the number of collisions (n_{coll}). Verbunt and Hut (1987) find that $n_{coll} \propto \rho^2 r_c^3 / v_o$ where ρ is the number density of stars within the core, r_c is the core radius and v_o is the velocity dispersion. Table 4.5 gives these various parameters for M71, ω Cen and 47 Tuc taken from Webbink (1985) as well as a scale factor S for each cluster defined as $S = \rho^2 r_c^3 / v_o$.

It is assumed that the mean stellar mass of the main sequence for each cluster

Table 4.5 The Observed Parameters for ω Cen, 47 Tuc and M71

Cluster	R_c	log(n)	v_0	Scale Factor (S)
-	pc	$M_\odot$ pc^{-3}	km s^{-1}	$\times 10^6$
M71	1.06	3.242	3.27	4.44
ω Cen	3.96	3.347	13.79	89.0
47 Tuc	0.52	5.024	13.15	477.7

is the same. The number of white dwarf binaries produced in M71 can then be estimated using $n_{M71}=(S_{M71}/S_{\omega Cen})\times n_{\omega Cen}$. This gives a value of only 0.3 for the number of white dwarf binaries in M71. Using S_{47Tuc} and n_{47Tuc} gives the same results. Hence one would not expect to observe any white dwarf binaries or more particularly CVs in the core of M71.

4.3.2b Space Density Considerations

In this subsection I use space density arguments to try to decide whether the three remaining unclassified UV–excess objects identified by Richer and Fahlman (1988) are field sdB, sdO, CV or WD stars.

To calculate the total number of objects in a given stellar population one needs to know three quantities (1) the space density, ρ_o, (objects pc^{-3}), (2) the scale height, z_o (pc) of the object concerned and (3) the solid angle of space surveyed Ω (steradians). The total number N is then obtained by evaluating the integral, equation 4.1,

$$N = \rho_o \Omega \int_o^{r_{max}} r^2 exp(-\frac{h}{z_o}) dr \qquad 4.1$$

along the line of sight. The area of space surveyed Ω by Richer & Fahlman (1988) was $(24')^2$ (or alternatively $4\pi\times 24/(4\pi\times(57.3^2)\times(60^2)) = 2.03\times10^{-6}$ steradians. The quantity h is the height above the galactic plane (see Figure 4.3).

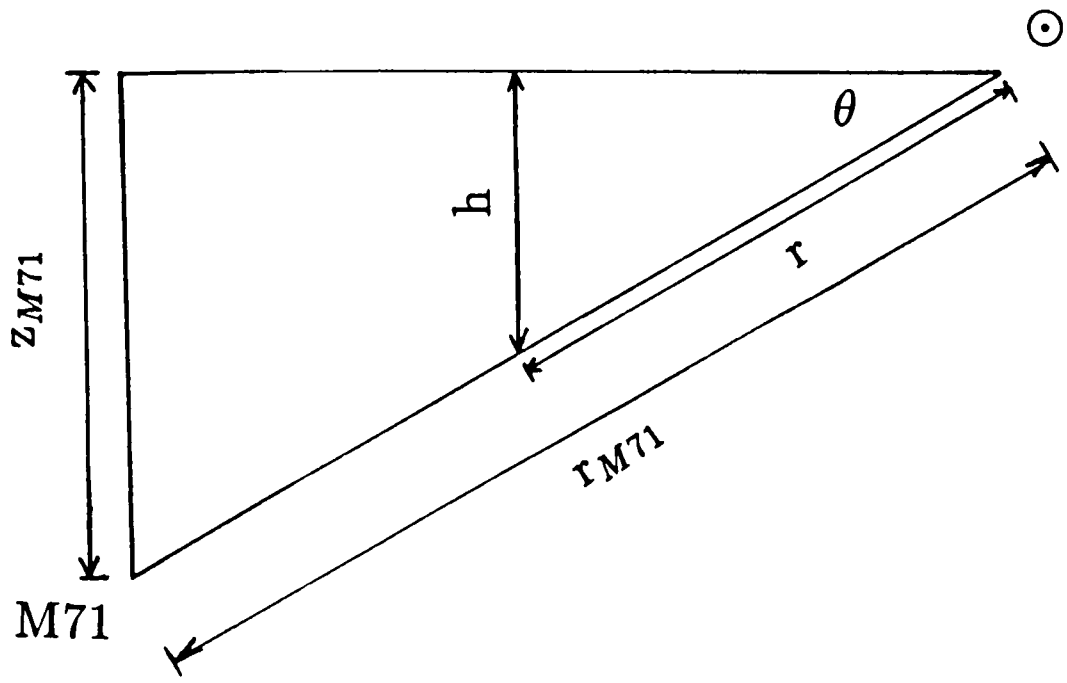

Figure 4.3: The relationship between h and r. M71 is at a distance of r_{M71} from the sun (⊙) and z_{M71} below the galactic plane.

This equation can be calibrated by considering the geometry shown in Figure 4.3. Obviously $h=r\sin\theta$. Since the integration is performed along the column to M71 $\sin\theta=z_{M71}/r_{M71}$ and hence $h=rz_{M71}/r_{M71}$. Now if we set $z_{M71}/r_{M71}\times 1/z_o=\alpha$ then using a standard integral‡ equation 4.1 becomes in integrated form equation 4.2,

$$N = \rho_o\Omega[-\frac{exp(-r\alpha)}{\alpha}(r^2+\frac{2r}{\alpha}+\frac{2}{\alpha^2})]_{r=0}^{r=r_{max}} \qquad 4.2$$

which is the total number of any particular object at a distance of r_{max}. Finally an estimate of r_{max} can be made using Pogsons law $5\log_{10}(r_{max})=V_{lim}-M_{V_o}-A_V+5$. In this case a nominal value of $A_V=0.84$ is assumed, that is three times the reddening to M71. $V_{lim}\sim 24$ is taken from the magnitude limit of Richer and Fahlmans (1988) survey of M71 and M_{V_o} is the mean absolute magnitude of the stellar population concerned.

The space densities and the scale heights of sdB, sdO and CV stars are poorly

‡ $\int x^m exp(ax)dx = (1/a \times x^m exp(ax)) - m/a \times \int x^{m-1} exp(ax)dx$, (Gradshteyn & Ryzhik 1980).

constrained (Downes 1986, Patterson 1984). However they are known well enough to calculate the approximate number of objects in the field of M71. The results of these calculation are reported in Table 4.6.

Table 4.6 The Results of Space Density Considerations for Various Galactic Stellar Populations

Object -	Space Density ρ no. pc^{-3}	Scale Height pc	M_{Vo} -	Magnitude Range M_V	r_{max} kpc	N§ -
sdB	$\sim 2\times10^{-6}$ [1]	325 [2]	5 [1]	2.9–9.6 [1]	42.9	0.05 (0.25)
sdO	$\sim 7\times10^{-7}$ [1]	175 [1]	5.3 [1]	3.2–10.1 [1]	37.3	0.01 (0.03)
CV[3]	$\sim 5\times10^{-6}$	150	7.5	4.3–9.2	13.6	0.06 (0.13)
WD	$\sim 0.72\times10^{-3}$ [1]	270 [1]	11 [1]	10–12	2.7	5.4 (-)

§The number in brackets is derived for a distance of 10 kpc, the unbracketed number is for 4.4 kpc (to the cluster) for sdB, sdO and CVs and at its magnitude limit for WDs.
[1]Downes (1986)
[2]Green, Schmidt & Liebert (1986)
[3]The CV parameters are taken from Patterson (1984)

It is very unlikely that sdB, sdO or CV stars are present in the foreground or the background of M71. Even if r_{max} is taken to be 10 kpc then the *total number* of all of these objects in the 10 kpc column to M71 is <0.5. On the other hand the number of white dwarfs in the *field* of M71 is ~5. *It is therefore likely that the three remaining UV-excess objects to M71 are nothing more mysterious than field white dwarfs.*

The space densities and scale heights used here are consistent with those derived from surveys of these objects by other authors; for sd stars: Green, Schmidt & Liebert (1986) and for white dwarfs: Fleming, Liebert & Green (1986) and Boyle (1989).

This calculation only gives order of magnitude estimates for the numbers of ob-

jects in the field to M71. A more sophisticated approach would be to integrate equation 4.1 over the luminosity function of the stellar population concerned. These luminosity functions are unfortunately poorly constrained for all of these objects except white dwarfs. I use the three luminosity functions derived by Downes (1986), Boyle (1989) and Fleming, Liebert & Green (1986) for white dwarfs to obtain the number of white dwarfs in the field to M71 more accurately. This new calculation provides a useful check on the crude calculation of ~5 white dwarfs in the field. The various luminosity functions and the number of white dwarfs in each luminosity bin are given in Table 4.7.

Table 4.7 The Luminosity Functions of White Dwarfs and the Number of Each in Each Luminosity Bin

M_V	-	8.5	9.5	10.0	10.5	11.0	11.5	12.0	12.5
$^1\rho$	$\times 10^{-6} pc^{-3}$	-	-	39	56	53	265	305	-
r_{max}	kpc	-	-	4.29	3.40	2.70	2.15	1.71	-
N†	-	-	-	0.8	0.7	0.4	1.1	0.7	-
$^2\rho$	$\times 10^{-6} pc^{-3}$	3.74	15.0	-	84.8	-	210.0	-	312.0
r_{max}	kpc	8.55	5.40	-	3.40	-	2.15	-	1.35
N†	-	0.4	0.6	-	1.2	-	1.0	-	0.4
$^3\rho$	$\times 10^{-6} pc^{-3}$	0.39	3.99	-	65.3	-	180.0	-	234.0
r_{max}	kpc	8.55	5.40	-	3.40	-	2.15	-	1.35
N†	-	0.04	0.2	-	1.0	-	0.8	-	0.3

†Assuming a scale height of z=270 pc
[1]The White Dwarf luminosity function of Downes (1986)
[2]The White Dwarf luminosity function of Boyle (1989)
[3]The White Dwarf luminosity function of Fleming *et al.* (1986)

The expected number of white dwarfs derived from these luminosity functions in the foreground or background to M71 are 3.7, 3.6 and 2.3 respectively. These results agree with the crude estimate above and reinforce the view that

the other UV–excess objects are field white dwarfs and unassociated with the cluster.

4.4 Conclusions

These observations show that the two brightest CV candidates in M71 (Richer and Fahlman 1988), for which spectra have been taken are almost certainly sdB stars in M71. Although some of the remaining fainter candidates may be globular cluster CVs, it is more likely that they are field white dwarfs.

4.5 References

Allen, C.W., 1973. *Astrophysical Quantities,* The Athlone Press, London.

Allington-Smith, J.R., Breare, J.M., Carrasco, B.E., Ellis, R.S., Parry, I.R., Webster, J., Gellatly, D.W., Gribbin, F.J., Ingle, M., Jorden, P.R., Lowne, C.M., Powell, J.R., Thorne, D.J., Taylor, C., van Breda, I.G., Waltham, N.R., Worswick, S.P. & Wynne, C.G., 1989. *Mon. Not. R. astr. Soc.,* **238,** 603.

Bailyn, C.D. & Iben Jr, I., 1989. *Astrophys. J.,* **347,** L21.

Bevington, P.R., 1969. *Data Reduction and Error Analysis for the Physical Sciences,* McGraw Hill, USA.

Boyle, B.J., 1989. *Mon. Not. R. astr. Soc.,* **240,** 533.

Downes, R.A., 1986. *Astrophys. J. Suppl.,* **61,** 569.

Druiker G.A., Fahlman G.G. & Richer B.H., 1989 *Astrophys. J.,* **342,** L27.

Fahlman, G.G. & Richer, H.B., 1989. In:*White dwarfs, IAU Colloqium,* **114,** p. 416, ed. G. Wegner., Springer-Verlag, Berlin Heidelberg.

Fleming, T.A., Liebert, J. & Green R.F., 1986. *Astrophys. J.,* **308,** 176.

Gradshteyn, I.S. & Ryzhik, I.M., 1980. In:*Tables of Integrals, Series and Products, Corrected and Enlarged Edition,* p. 92, Academic Press, New York.

Green, R.F., Schmidt, M. & Liebert, J., 1986. *Astrophys. J. Suppl.,* **61.** 305.

Heber, U., Kudritzki, R.P., Caloi, V., Castellani, V., Danziger, J. & Gilmozzi, R., 1986. *Astr. Astrophys.,* **162,** 171.

Hertz, P. & Grindlay, J.E., 1983. *Astrophys. J.,* **267,** L83.

Hessman, F.V., 1986. *Astrophys. J.* **300,** 794.

Howarth, I.D. & Murray, J., 1988. *Science and Engineering Research Council, Rutherford Appleton Laboratory, Space and Astronomy Division, Starlink Project, Starlink User Note* **50.1**

Johnson, H.L., 1965. *Astrophys. J.,* **141,** 923.

Mukai, K., 1990. *Publis. Astron. Soc. Pacif.,* **102,** 183.

Patterson, J., 1984. *Astrophys. J. Suppl.,* **54,** 443.

Ray, A. & Kluźniak, W., 1990. *Nature,* **344,** 415.

Richer, H.B. & Fahlman, G.G., 1988 *Astrophys. J.,* **325,** 218.

Tennant, A.F., 1989. *The QDP/PLT User's Guide,* NASA, U.S.A.

Tritton, K. 1989. *Private Communication.*

Verbunt, F. & Hut, P., 1987. In:*The Origin and Evolution of Neutron Stars, IAU Symp. 125,* p. 187, eds. Helfand, D.J. & Huang, J.H., D. Reidel, Dordrecht, Holland.

Verbunt, F. & Meylan, G., 1988. *Astr. Astrophys.*, **203**, 267.

Wagner, R.M., Sion, E.M., Liebert, J. & Starrfield, S.G., 1987. *Astrophys. J.*, **328**, 213.

Webbink, R.F., 1981. *Astrophys. J. Suppl.*, **45**, 259.

Webbink, R.F., 1985. In:*Dynamics of Star Clusters, IAU Symp. 113*, p. 541, eds. J. Goodman and P. Hut, Reidel, Dordrecht.

Chapter 5

Very Large Array Observations of Low Mass X–ray Binaries

In this chapter I report the results of deep Very Large Array (VLA) imaging of the cores of four globular clusters. These observations were made at 6 cm in hybrid A/B configuration. Selection of the clusters was made on the basis that they contained a luminous ($\geq 10^{36}$ erg s^{-1}) X–ray source. Radio counterparts were found for the X–ray sources in NGC7078 (M15) and NGC6712. They are both slightly extended and have integrated flux densities of 481±28 and 195±23 μJy respectively. Both coincide ($\leq 0.6''$) with previously suggested optical counterparts. The observed radio emission is interpreted as synchrotron radiation, though bremsstrahlung radiation cannot be ruled out as an alternative. 3σ upper limits for the radio emission from the globular clusters NGC1851 and NGC6624 were $\sim$63 μJy beam^{-1} and $\sim$87 μJy beam^{-1} respectively.

A "snapshot" observation of the galactic LMXB 4U2129+47 was also obtained. A 3σ upper limit for the radio emission from this object is $\leq$140 μJy beam^{-1}.

5.1 Introduction

There are 8 known persistently bright ($L_X \geq 10^{36}$ erg s^{-1}) point X–ray sources in globular clusters (eg. see Charles 1990). Seven of the eight exhibit type I X–ray bursts (thought to be thermonuclear flashes in the surface layers of an accreting neutron star) and none show X–ray eclipses or X–ray pulsations (Lewin and Joss 1983). The similarity of their X–ray properties to those of the galactic Low

Mass X–ray Binaries (LMXBs) indicate that they are probably a similar class of object. This type of object is described at length in Section 1.3b. The number of bright X–ray sources per unit stellar mass in globular clusters exceeds by $\sim 10^3$ that of X–ray binaries in the galaxy (Katz 1975). Also 15 millisecond radio pulsars whose progenitors are thought to be LMXBs (Lyne *et al.* 1987) or CVs (Grindlay and Bailyn 1988) have been found in globular cluster cores (Ray and Kluźniak 1990). Such a high binary generation rate can be explained by their formation in the dense globular cluster cores by two body (Fabian *et al.* 1975) or three body (Hills 1976) interactions. A review of binaries in globular clusters is given in Section 1.4.

The optical identification of galactic LMXBs has played an essential part in the study of these systems (eg van Paradjis 1983). However such identification in globular clusters is very difficult because the best X–ray positions derived from *Einstein* HRI observations have a typical 3σ error radius of $\sim 2.5''$ (Grindlay *et al.* 1984) and hence large numbers of stars exist in the X–ray error circles. The large error reflects systematic uncertainties associated with the *Einstein* attitude solution.

Faint radio emission ($\sim$1 mJy at 6 cm) has already been detected for about one third of LMXBs outside of globular clusters (Geldzahler 1983, 1987). This implies that faint radio emission might also be detectable from the bright globular cluster X–ray sources. As radio positions can be very accurate ($\leq 0.3''$ at 6 cm in hybrid A/B configuration for the VLA), the possibility of obtaining an optical identification is increased. In an attempt to detect radio emission from these objects it was decided to embark upon a deep radio mapping programme of globular clusters.

The galactic field LMXB 4U2129+47 has been previously observed and detected

in the radio with a flux density of 1.12±0.07 mJy at 6 cm (Geldzahler 1987). An observation of this object was taken so as to compare the radio properties of galactic field LMXBs with any discovered radio counterparts of globular cluster LMXBs.

5.2 Observations and Data Reduction

The VLA is an earth rotation aperture synthesis radio telescope. A description of radio telescopes and aperture synthesis is given in Appendix II. The observations were carried out at 6 cm with a bandwidth ($\Delta\nu$) of 50 MHz per intermediate frequency (IF) using both AC and BD IFs (Thompson *et al.* 1980). Since the sensitivity is $\propto\sqrt{(\Delta\nu)}$ and because this was primarily a detection experiment, the maximum bandwidth was selected. The primary targets were near the centre of the observing beam (the phase tracking centre) and hence the reduction in amplitude due to bandwidth smearing is negligible (Bridle 1989). The X–ray sources in the globular clusters NGC6624, NGC6712 and NGC7078 and the galactic X–ray source 4U2129+47 were observed between 11:13–18:12 UT on 19 February 1989. The X–ray source in the globular cluster NGC1851 was observed between 01:08–04:07 UT on 20 February 1989. Table 5.1 gives a summary of the observations.

Table 5.1: Observing Log of the LMXB X-ray Sources

Object	Calibrator	Date	Exposure time (hr)
NGC6712 (4U1850–08)	1829–106	19 Feb. 1989	1.40
NGC6624 (4U1820–28)	1808–209	19 Feb. 1989	1.15
NGC7078 (4U2127+11)	2128+048	19 Feb. 1989	0.98
4U2129+47	2146+608	19 Feb. 1989	0.13
NGC1851 (4U0512–40)	0537–441	20 Feb. 1989	1.83

The VLA was in hybrid A/B configuration (Figure 5.1), that is with a long North arm. The North arm was in A array configuration (furthest antenna ~19 km) and the East West arms were in B array configuration (furthest antenna ~6 km). This configuration was chosen as two of the sources (NGC6624 and NGC1851) have $\delta<-15°$ where the North–South extent of the u–v coverage (see Appendix II) is seriously foreshortened by projection (Bridle 1989). This is important since the "u–v plane", defined as the locus of points traced out on the ground by various projected baselines, represents how effectively the Fourier components (the visibilities), necessary for image reconstruction, have been sampled. Poor sampling in this plane leads to poor imaging. The choice of this configuration leads to the synthesised beam being more circular (or equivalently the u–v plane being covered more extensively) than it would be in the standard B configuration (all arms having ~6 km length). It would not have been as effective to use the higher resolution A array configuration for detection experiments since it could resolve "away" faint extended sources. Observations of 3C286 (7.41 Jy at 4885 MHz) and 3C48 (5.60 Jy at 4885 MHz) were made to establish the flux density scale (Baars *et al.* 1977).

To monitor the performance of the instrument and the atmospheric conditions, that is to determine the complex antennae gains; secondary calibrators (one per target) chosen from the VLA Calibrator List were observed. Good calibrators have the following properties; they are bright, have a small diameter, have accurately measured positions and are not significantly variable over the timescale of an observation. Those chosen from the VLA Calibrator list fulfil all these requirements. They were close ($\leq 5°$, except for 4U2129+47 see Table 5.1) to the target objects. The sequence of observations was chosen so as to obtain the best calibration of the data. This was a compromise between maximising the

ID	Radius(in Km)
1	.97
2	18.94
3	2.97
4	3.19
5	.44
6	9.44
7	6.39
8	15.47
9	.48
10	6.39
11	4.15
12	2.33
13	1.43
14	4.15
15	12.30
16	.97
17	6.91
18	.15
19	5.22
20	.00
21	1.59
22	1.59
23	.48
24	3.19
25	5.22
26	2.33
27	4.71
28	.15

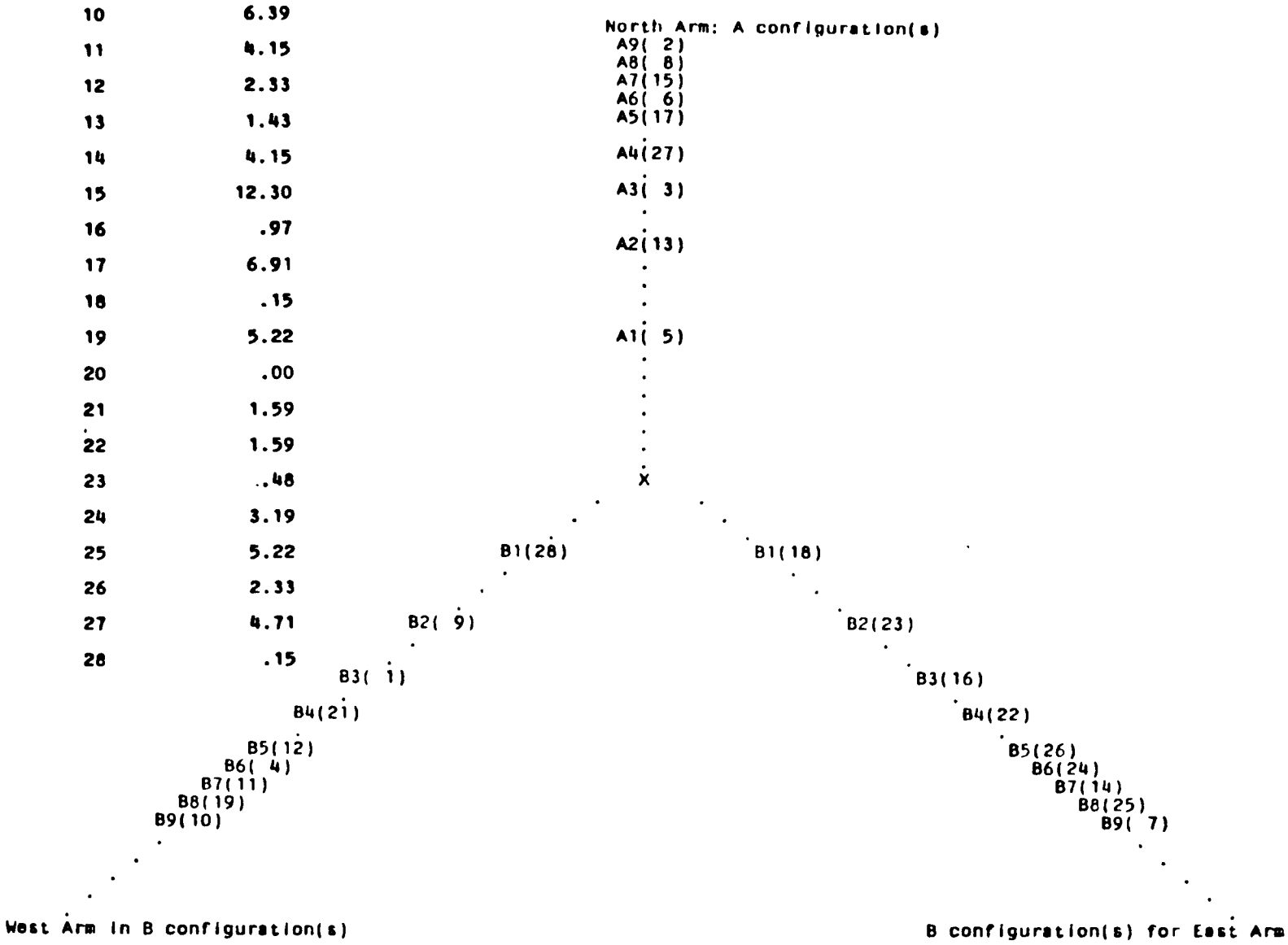

Figure 5.1: The hybrid A/B configuration of the VLA. The table gives the antenna ID number (in brackets on the figure) and the distance from the array centre in kms.

integration time and adequately monitoring the atmospheric and instrumental variations. The compromise reached was a ~15 minute target observation sandwiched between two ~4 minute secondary calibrator observations. The weather was calm and the phases of the calibrators remained stable during both runs. All 27 antenna were operative. The observations were arranged to provide the greatest possible u–v plane coverage for each source. This meant that the observations of any particular source were spaced out approximately uniformly throughout the observing period.

The data were edited and calibrated using the DEC-10 computer at the VLA site (this computer is no longer operative). Bad data was identified from printouts of the correlator outputs. Since the true visibility (see Appendix II) is known for the secondary calibrators their observed visibilities are used to derive a a set of calibration factors. These factors are then used to calibrate the data for instrumental gain and phase variations. The secondary calibrators are variable in intensity on monthly or yearly timescales, so it is not possible to maintain accurate lists of their flux densities. Observations of the primary flux calibrators 3C286 and 3C48, whose flux densities are known accurately and which do not vary, were therefore used to derive the true flux densities of the secondary calibrators. The calibration factors derived from individual measurements of the secondary calibrators were averaged over an approximately 40 minute timestep, these were then applied to the appropriate targets.

The absolute accuracy of the astrometry is limited by the precision of the positions of the secondary calibrators. All the secondary calibrators had a quoted 1σ positional error of $\leq 0.15''$. This represents the error in the astrometry of these observations.

The radio maps were made using the US National Radio Astronomical Obser-

vatory (NRAO) Astronomical Image Processing System (AIPS) as installed on the Jodrell Bank Alliant computer and on the Oxford University Astrophysics Department VAX3800 computer. The various stages of data analysis are described in Appendix II. An outline of the main steps is given below.

Natural weighting of the u–v points was used since this gives the best signal to noise ratio for detecting weak sources. Also a u–v taper was applied to the visibilities so as to reduce the significance of the outlying points in the u–v plane. Its extent (FWHM) is given in Table 5.2. The parameters used in map reconstruction are also given in Table 5.2 (i.e. the half power beam width (HPBW) and position angle of the beam and the peak map flux density beam^{-1}).

Table 5.2: Beam Parameters

Object	Beam $''$	Position angle $^\circ$	uv-taper kλ	Cell Size $''$	Peak map flux mJy beam^{-1}
NGC6712	2.00×2.00	0.0	200×200	0.20	0.16
NGC6624	1.95×1.73	−34.8	100×150	0.25	8.28
NGC7078	2.59×2.31	−54.1	100×150	0.25	11.80
NGC1851	2.62×1.81	+15.5	100×100	0.20	0.11
4U2129+47	1.76×1.58	+72.1	100×200	0.20	0.24

Dirty maps (Appendix II) were produced for each source. These were then CLEANed (Högbom 1974).

The sidelobes of a few bright sources (~few mJy) in the fields of NGC6624 and NGC7078 caused substantial contamination of the field. However their presence permitted self calibration, resulting in a drastic improvement in the quality of the maps with noise levels close to their theoretical values (Bridle 1986).

Bright sources were not present in the fields of NGC6712, NGC1851 and 4U2129+47 and CLEANing produced maps with noise levels close to their theoretical limits.

5.3 Results

Nine radio sources, six of which had not been previously detected, were found in the fields of the four globular clusters observed. Radio counterparts were found for the X–ray sources in the globular clusters NGC7078 and NGC6712, both of which appear extended. No radio counterparts were found for the X–ray sources in the globular clusters NGC6624 and NGC1851 nor to the galactic X–ray source 4U2129+47. Table 5.3 summarises the results of these observations for the globular clusters. The values in Table 5.3 were derived as follows.

Columns 1 and 2 the cluster and object names. The objects are named following the nomenclature of Johnson (1976).

Columns 3 and 4 give the right ascension and declination of all the radio objects. These values were found by fitting a two dimensional Gaussian profile to the data (using JMFIT in AIPS). The formal error given by JMFIT for the centroid of the Gaussian is very small $\leq 0.1''$. However the true astrometric error is larger than this because it relies on the positions of the secondary calibrators which are only known to $1\sigma \sim 0.2''$. This represents the absolute error on the astrometry of the observation.

Columns 5 and 6 give both the peak and integrated flux densities, (as derived from the Gaussian fits) for the sources. Where necessary the integrated flux density is corrected for bandwidth smearing (Bridle 1986). The correction factors are derived from Figure 16–6 in Synthesis Imaging (Bridle 1986). The error bars on this figure are used to derive the errors in the corrected flux densities. Note that the target objects are close to the centre of the field and are not subject to significant bandwidth smearing.

Column 7 gives the measured and theoretical rms noise for the maps. The observed rms is the mean pixel value from a source free region of the map.

Table 5.3 Results of 6 cm Observations of the Four Globular Clusters

Object	Name	RA (1950)	Dec (1950)	Peak Flux μJy/beam	Integrated/Corrected Flux Density μJy	Map rms μJy/beam	core offset	Distance† kpc	Luminosity‡ 10^{18}erg s^{-1} Hz^{-1}
NGC7078	4U2127+11	21 27 33.28	+11 56 50.9	195	481/481	30/27	0.48	9.7[1]	54.5
NGC7078	K648	21 27 34.36	+11 57 14.6	3505	4024/4064	30/27	5.33	9.7[1]	461.9
NGC7078	M15A	21 27 35.02	+11 52 58.0	11858	13832/25149	30/27	42.20	–	–
NGC7078	M15B	21 27 26.88	+11 57 05.7	5978	6077/6985	30/27	17.66	–	–
NGC6712	4U1850–08	18 50 21.08	–08 46 04.2	163	195/195	24/22	0.10	6.5[2]	9.95
NGC6624	4U1820–30	–	–	<87	–/<87	29/25	–	8.0[1]	<6.72
NGC6624	NGC6624A	18 20 42.70	–30 24 48.1	7980	9810/17210	29/25	41.93	–	–
NGC6624	NGC6624B	18 20 42.30	–30 21 41.0	630	800/1356	29/25	41.20	–	–
NGC6624	NGC6624C	18 20 46.01	–30 22 36.6	340	805/1519	29/25	46.87	–	–
NGC6624	NGC6624D1	18 20 23.10	–30 16 29.2	226	703/2130	29/25	78.95	–	–
NGC6624	NGC6624D2	18 20 23.34	–30 16 28.2	133	766/2321	29/25	79.06	–	–
NGC1851	4U0513–40	–	–	<63	–/<63	21/20	–	12.0[1]	<11.0

†Distances from [1]Webbink 1985, [2]Cudworth 1988.
‡Assuming 1mJy$\equiv 10^{-29}$ W m^{-2} Hz^{-1}

column (1) gives the name of the globular cluster observed,
column (2) the source name,
columns (3) and (4) the right ascension and declination of each source (equinox 1950),
column (5) the observed peak flux density.
Where no radio counterpart was found 3σ upper limits to the flux density are given,
column (6) the integrated and corrected flux densities. The corrected flux densities are the integrated flux densities corrected for bandwidth smearing (Bridle 1986)
columns (7) the measured/theoretical map rms (Bridle 1986),
column (8) the distance of the radio source from the optical centre of the globular cluster as a fraction of core radius (following Grindlay *et al.* 1984),
column (9) the assumed distance to the globular cluster,
column (10) the luminosity of each source known to be a globular cluster member.

The theoretical rms, or alternatively the minimum signal the radio telescope can detect, is estimated by considering the thermal fluctuations that are present in the receiver output. These fluctuations are equivalent to the thermal noise power per unit bandwidth one observes in a resistor, $w=k_BT$, where k_B is Boltzmanns constant (1.38×10^{-23} J K^{-1}). It has been shown that the theoretical noise limit of the VLA (μJy beam^{-1}) is given by, $S/(N\times\sqrt{(T_{int}\times\Delta\nu)})$ where the sensitivity is S=7.4 mJy at 6 cm using two IFs. As four IFs are used (A, B, C and D), this value must be divided by $\sqrt{2}$. N=27 is the number of antenna, T_{int} (hr) is the integration time of the observation (Table 5.1) and $\Delta\nu$=50 (MHz) is the bandwidth (NRAO Newsletter 37). The sensitivity of a large synthesis array is similar to that of a single antenna with the same total (synthetic) area. This is because the fraction of information lost by a large array due to incomplete sampling of the radio sky brightness distribution is negligible. The synthesis array has the additional advantage that all points in its field are sampled with this sensitivity. An equivalent single antenna would have to observe each point on the sky for time T_{int} (Crane and Napier 1989).

Column 8 gives the distance of the radio source from the centre of the globular cluster as a fraction of its core radius. The core radii for NGC7078, NGC6712, NGC6624 and NGC1851 are 5.5″, 49.0″, 5.2″ and 5.9″ respectively. These, and the positions for the optical centres of the globular clusters are taken from Grindlay *et al.* (1984). The angular offset $\Delta\theta$, is obtained using spherical trigonometry, can be found using the equation $\mathrm{Cos}(\Delta\theta)=\mathrm{Sin}(\delta_1)\mathrm{Sin}(\delta_2)-\mathrm{Cos}(\delta_1)\mathrm{Cos}(\delta_2)\times\ \mathrm{Cos}(\alpha_1-\alpha_2)$ where α_1, δ_1 and α_2, δ_2 are the right ascension and declination of the core and radio object respectively. This result is then converted into arcseconds (206265″ per radian) and divided by the core radii. This gives a direct indication of the objects distance from the globular clusters

core. As can be seen from Table 5.3 most of the detected radio sources are distant from the globular cluster core.

Columns 9 and 10 gives the distance to the globular cluster (9) and the luminosity, or luminosity limit, of the radio sources known to be cluster members (10). The luminosity (L) per unit bandwidth is $L=4\pi d^2$ multiplied by the integrated flux density (F). This can be expressed as $\equiv 1.208\times10^{18}D^2F$ where F is measured in mJy and D is the distance to the globular cluster in kpc.

The X–ray source 4U2129+47 was not detected. The map had a measured rms of $\sim$50 μJy beam^{-1}.

5.4 Discussion

5.4.1 NGC7078

The X–ray source in NGC7078 (4U2127+11) has an X–ray luminosity in the 2–11 keV band of $L_X\sim8\times10^{36}$ erg s^{-1} (Callanan *et al.* 1987). It is the only globular cluster X–ray source from which a classical type I X–ray burst has not been observed. Also it is unique among these sources in that it has a firmly established optical counterpart (AC211; Aurière *et al.* 1984) which is blue and variable with V$\sim$15. Spectroscopy (Naylor *et al.* 1988) showed that the orbital period of the system was $\sim$9 hrs whilst photometry refined the orbital period to be 8.54 hrs (Ilovaisky *et al.* 1987). The position of the optical counterpart (AC211) has been determined to a 3σ accuracy of 0.6″ (Geffert *et al.* 1989). This differs from the position derived from observations with the *Einstein* HRI by $\sim$2.4″ (Grindlay *et al.* 1984).

A previous attempt to detect a radio counterpart to the X–ray source (Grindlay

and Seaquist 1986) placed an upper limit on the radio flux density of $\leq$500 μJy (3σ) at 6 cm.

Four radio sources were detected in the field of NGC7078. A radio map of the region is given in Figure 5.2a. Two were already known, the planetary nebula K648 (Gathier *et al.* 1983) and a bright, possibly extragalactic, source M15A (Birkinshaw and Downes 1982; Gopal-Krishna and Steppe 1980). The flux densities of K648 (4.1$\pm$0.2 mJy) and M15A (25.1$\pm$2.8 mJy) are in agreement with previous measurements. Of the newly discovered sources, one is 97″ from the centre of the globular cluster and has a flux density of 7.0 mJy. It is probably unrelated to the cluster. The second is a 6.7σ detection centered on 21h 27m 33.28s, +11° 56′ 50.9″ (1950) with a peak flux density of 195 μJy beam^{-1} and integrated flux density of 481$\pm$28 μJy (Figure 5.2b). This is almost certainly the radio counterpart of the X–ray source since the peak of the radio emission is coincident to within 0.2″ with the position of the optical counterpart as determined by Geffert *et al.* (1989). Also the likelihood of finding a serendipitous radio source within the X–ray error circle is small (Fomalont *et al.* 1984): see also Section 5.4.6. The optical position, along with that derived from *Einstein* HRI observations (Grindlay *et al.* 1984), is marked on the map of the radio source shown in Figure 5.2b.

It is very unlikely that this radio source is a millisecond pulsar. The three known millisecond pulsars in NGC7078 have flux densities of $\leq$12 μJy at 4885 MHz[†]; twenty five times less than the flux density of the object observed here. Therefore, if it had been a pulsar it would have been detected in the surveys of Anderson *et al.* (1989A & B) and Wolszczan *et al.* (1989A).

[†]Anderson *et al.* (1989A&B) and Wolszczan *et al.* (1989A) report flux densities of ~1.6 mJy at 430 MHz for the millisecond pulsars in NGC7078. Typical globular cluster pulsars have power law spectra with spectral slopes of $\leq$–2 (Kulkarni, Narayan & Romani 1990). Scaling the flux density at 430 MHz to the observing frequency of 4885 MHz gives ~12 μJy.

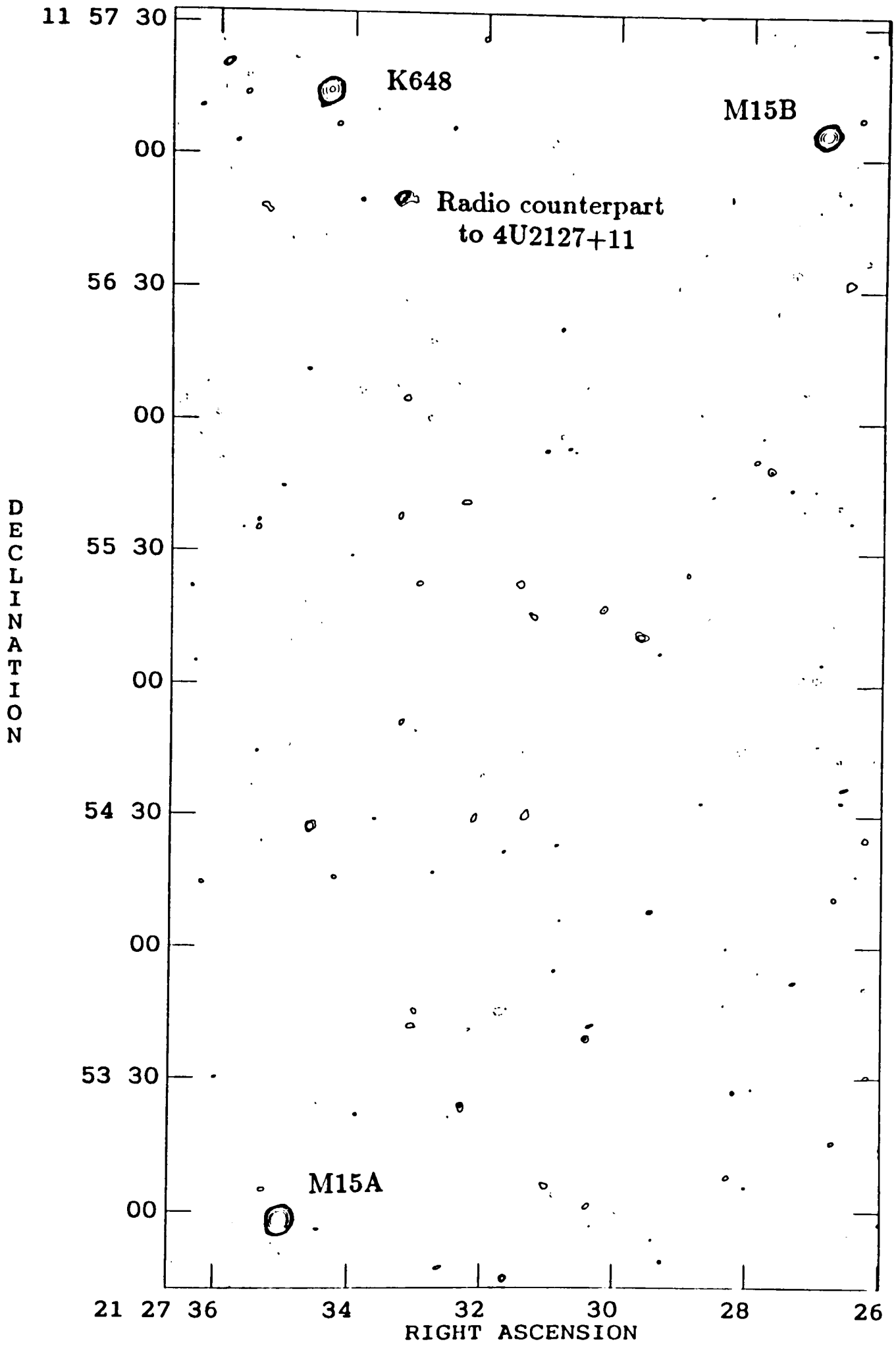

Figure 5.2(a): Radio map of NGC7078. The contours shown are –3, 3, 4, 5, 6, 7, 10, 20, 50 and 100 times 30 μJy beam^{-1}, the rms level of the map.

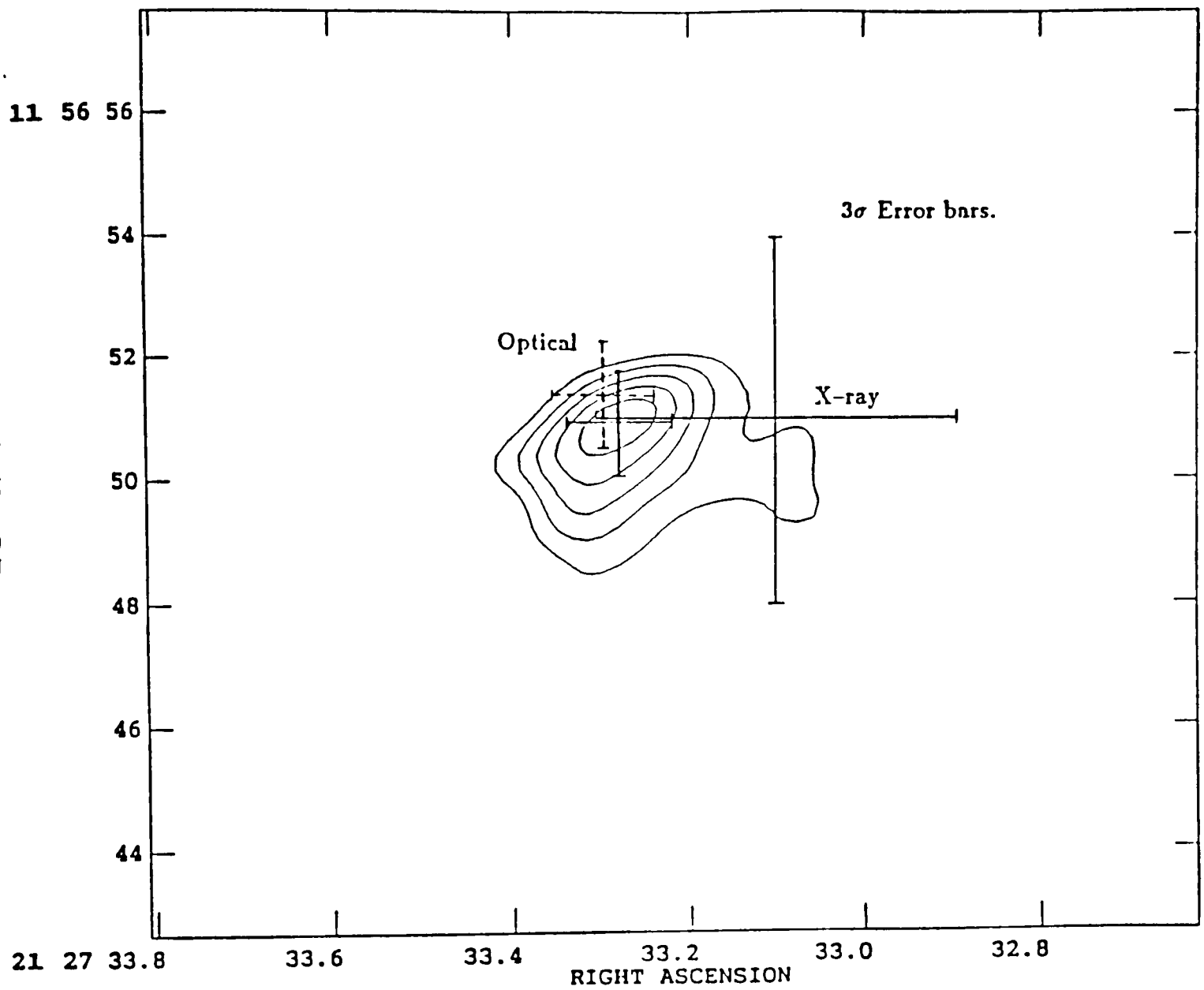

Figure 5.2(b): The radio counterpart to the X-ray source 4U2127+11. The contours shown are -3, 3, 4, 5, 6 and 7 times 30 μJy beam^{-1}, the rms level of the map. The points marked are the peak of the radio emission, the X-ray source (Grindlay *et al.* 1984) and the optical counterpart (Geffert *et al.* 1989).

The emission region appears to be elongated by ~3″ with position angle 95° and to have a width of ~1″ perpendicular to this direction. The brightness temperature of the object is ~10 K. This represents the equivalent temperature the object would have if the observed radio emission was due to blackbody emission. This is estimated from the Rayleigh–Jeans approximation to the blackbody distribution ie. $I_\nu = 2k_B T_b/\lambda^2$ W m^{-2} Hz^{-1} sr^{-1}. $I_\nu = S_\nu/\Omega$, the solid angle subtended is $\Omega \sim (1'' \times 3'')/(206265)^2$ and the measured flux density is $S_\nu = S_{6cm} = 0.481$ mJy. There is also a possible extension of the radio emission to the west of the main emission region but further observations are needed to confirm this.

Taking the distance to NGC7078 to be 9.7 kpc (Webbink 1985) the emission region has dimensions ~0.14×0.047 pc. If it is assumed that the angle to the line of sight is ~30° the estimated volume of the emitting region is $(1'' \times 1'' \times 3'') \times (1/\mathrm{Cos}(30°) \equiv 1.82 \times 10^{52}$ cm^3. As this is only a monochromatic intensity measurement the spectral slope is unconstrained and it is impossible to decide between emission mechanisms. However, synchrotron emission has been shown to be the most likely explanation for radio emission from galactic LMXBs (Hjellming and Johnston 1988). It is reasonable to assume that this mechanism is also operative for globular cluster LMXBs. For the radio counterpart to the X–ray source in NGC7078 it is assumed that a power law with the functional form $S(\nu) \propto \nu^\alpha$ with $\alpha = -0.8$ (which is a typical value for LMXBs, Strom *et al.* 1989) between $\nu_1 = 10$ MHz and $\nu_2 = 100$ GHz is a good approximation to its spectrum. From the observed integrated flux density, S_0, and a distance of 9.7 kpc, one obtains a luminosity, $L = 4\pi d^2 \int_{\nu_1}^{\nu_2} S_0 \nu^\alpha \, d\nu$, which becomes $L = 4\pi d^2 4885 \times 10^6 \int_{0.01}^{100} S_0 \nu'^\alpha \, d\nu'$ with the parameterization $\nu' = \nu/4885$ MHz, implying a luminosity of 2.82×10^{30} erg s^{-1}. Pacholczyk (1970) gives expressions

for the equipartition magnetic field and the minimum total energy stored within the source in the form of relativistic particles and a magnetic field. These give an equipartition magnetic field of B_{min}=860$f^{-2/7}$ μG and a value for the minimum total energy of $E_{min}\sim1.27\times10^{45}f^{3/7}$ erg (Pacholczyk 1970). The filling factor, f, represents the fraction of the source volume which is occupied by the magnetic field and the relativistic particles. The magnetic field, and hence the minimum total energy, is dependent upon the ratio (k) of the proton energy to electron energy. This in turn is dependent upon the mechanism that generates the relativistic particles. This ratio has a wide range of values. I have used $k=\frac{\epsilon_p}{\epsilon_e}=100$. The results are not sensitive to the value of k since it has a low power law dependence (2/7) in the equations given by Pacholczyk (1970). The lifetime of the source to synchrotron emission given by the ratio of the total electron energy (ϵ_e) to the observed source luminosity is $\tau=2.56\times10^{12}$ s. This is much greater than the light crossing time ($\sim5.45\times10^6$ s) of the source indicating that synchrotron radiation can easily explain the observed emission.

5.4.2 NGC6712

The globular cluster NGC6712 contains a bright bursting X–ray source with $L_X\sim5\times10^{37}$ erg s^{-1} in the 2–11 keV band (Bradt and McClintock 1983). The X–ray source is very close ($\sim5''\equiv0.1r_c$) to the optical centre of the globular cluster (Grindlay *et al.* 1984). Cudworth (1988) proposed that a V$\sim$20 blue star could be the optical counterpart to the X–ray source. However recent high resolution images (FWHM 0.4–0.6″) by Neito *et al.* (1990) have thrown some doubt on Cudworth's candidate. They report the detection of two faint (V$\sim$21) stars (one of which is very blue) $\sim$0.6″ from Cudworth's candidate and suggest

that one of these is the optical counterpart. Charles (1990) reports that spectra taken of Cudworths object did not show any of the characteristic spectral features of LMXB (He II and Bowen blend emission). This has thrown further doubt on the candidacy of this object.

A 6.7σ source centred on 18h 50m 21.08s, –08° 46′ 04.2″ (1950) with a peak flux density of 163 μJy beam^{-1} and an integrated flux density of 195±23 μJy was detected. Figure 5.3 shows a map of the radio source. The peak of the emission is within the *Einstein* HRI X–ray error circle given by Grindlay *et al.* (1984) and is in close positional agreement with the suggested optical counterparts of both Cudworth (1988) and Neito *et al.* (1990). This source is probably the radio counterpart to the X–ray source in NGC6712. However, it is possible (though unlikely) that the detected radio source is a bright millisecond pulsar. Only 2 of the 13 globular cluster millisecond pulsars have flux densities comparable to that of the object found here (when their flux densities are scaled to the distance of NGC6712 with an assumed spectral slope of $\simeq$–2; see Table 5.5 below). Thus it is unlikely that NGC6712 would contain a radio pulsar of this brightness which coincided with the X–ray position.

Furthermore, Biggs, Lyne and Johnston (1990) have placed an 8σ upper limit on the pulsed emission (10 – 500 ms) from a millisecond pulsar in NGC6712 of 1.6 mJy (1420 MHz). Taking the 3σ upper limit as being 0.6 mJy and scaling to 4885 MHz (spectral index $\sim$–2) any pulsar in the cluster would have a flux density of <50 μJy ie. undetectable in this survey. Alternatively the spectral slope implied from this limit is flatter than –0.9. Since globular cluster millisecond pulsars have a spectral slope of about –2.0 to –2.4 (Kulkarni, Narayan and Romani 1990) it would be an extremely unusual pulsar if its spectral slope was so flat. *The positional coincidence of the radio object, X–ray object and possible*

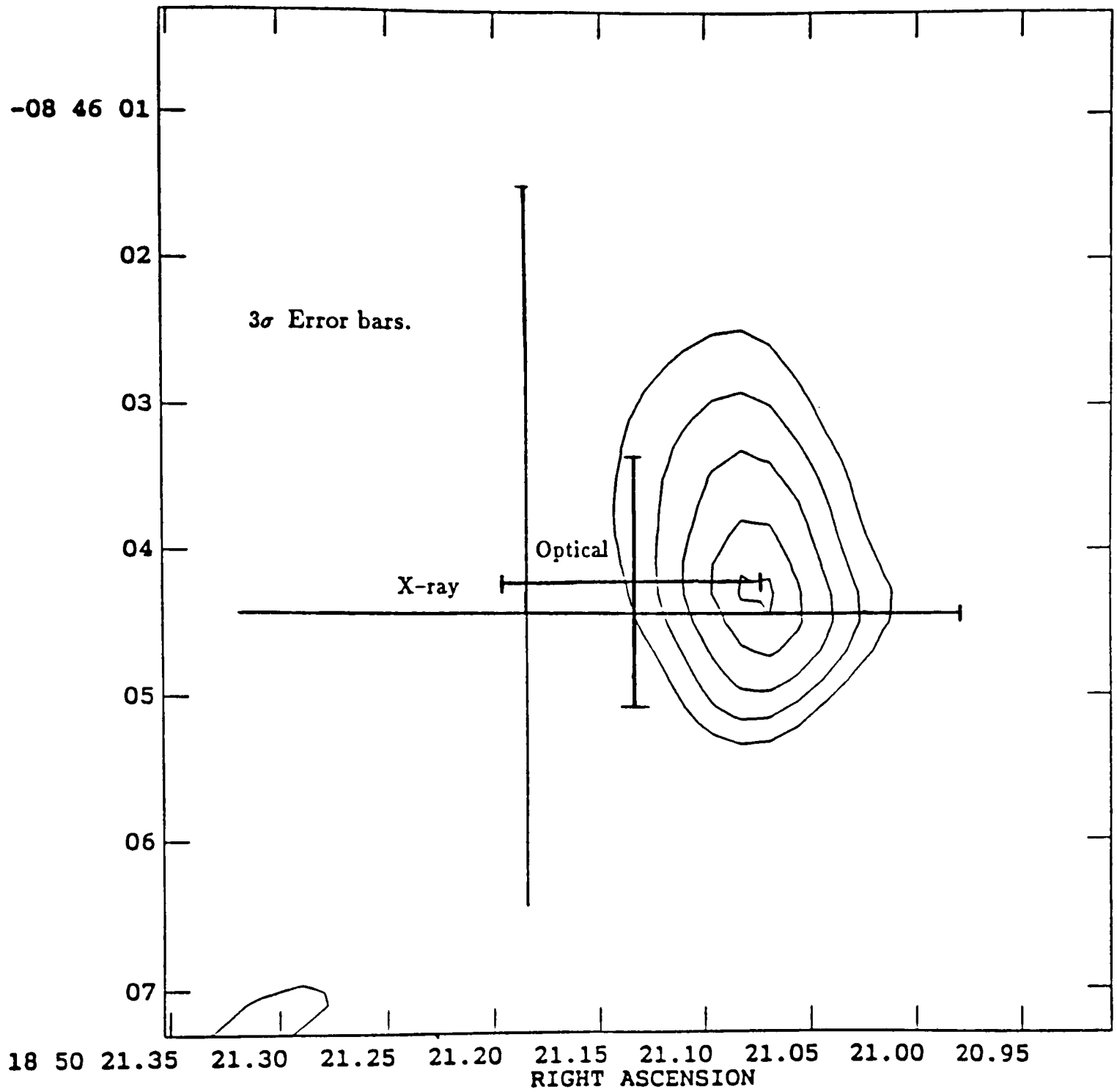

Figure 5.3: The radio counterpart to the X–ray source 4U1850-08. The contours shown are –3, 3, 4, 5, 6 and 7 times 24 μJy beam^{-1}, the rms level of the map. The points marked are the X–ray source (Grindlay *et al.* 1984) and the possible optical counterpart (Cudworth 1988).

optical counterparts coupled with the flux density/spectral slope arguments lead one to conclude that this object is not a millisecond pulsar in NGC6712.

The object appears elongated by $\sim$2.1″ in the direction of PA=–11° and unresolved ($\leq$0.3″) in the perpendicular direction (79°). Assuming that the synchrotron analysis applied in Section 5.4.2 is valid here then the emitting volume of gas ($\leq 3.3\times10^{50}$ cm^3) has a luminosity of $\sim 5.09\times10^{29}$ erg s^{-1}. From this an equipartition B field of $\sim 1.7 f^{-2/7}$ mG and a minimum total energy of $\sim 8.8\times10^{43} f^{3/7}$ erg can be inferred. The lifetime of the source to synchrotron emission is $\tau\sim 9.6\times10^{11}$ s as this is much greater than the light crossing time of the source (τ=1.4$\times10^6$ s) synchrotron emission can explain the observed emission, as was the case for NGC7078.

5.4.3 NGC6624

Of all the globular clusters NGC6624 contains the brightest X–ray source, with a luminosity of $L_X\sim 8\times10^{37}$ erg s^{-1} in the 2–11 keV band (Bradt and McClintock 1983). It has an orbital period of 685 s (Stella *et al.* 1987) which is the shortest known orbital period of any X–ray burster (White 1986).

Two previous attempts (both at the VLA) have been made to detect this source. Grindlay and Seaquist (1986) report a 4σ detection with a flux density level of 490 μJy at 1400 MHz. Their radio source was 2.4″ distant from the X–ray source. Geldzahler (1983) reports the 6σ detection of a 2.4 mJy source (at 1465 MHz) $\sim$5.3″ from the X–ray position but only 1.6″ from the optical centre of the globular cluster. His 1σ positional accuracy was $\sim$0.4″. This radio source is sufficiently far from the X–ray position to make any association unlikely. Neither of these sources are detected here to a 3σ flux density level of 87 μJy.

Four radio sources are detected in the field of NGC6624 (Figure 5.4). All these sources are located a long way ($\geq$214″) from the optical centre of NGC6624. Maps of the four serendipitous sources are shown in Figure 5.5(a–d). The object NGC6624A had a previously reported flux density of 12±2 mJy at 2695 MHz (Johnson 1976) which is consistent with that estimated here. The other objects have provisionally been named using the nomenclature of Johnson (1976). It is found that NGC6624D is a double radio source; the separate components have been labelled NGC6624D1 and NGC6624D2 in Table 5.3.

No radio counterpart was found to the X–ray source. The 3σ upper limit on emission at 6 cm is $\sim$87 μJy beam^{-1} from a circle (radius $\sim$120″) surrounding the X–ray position.

If the source found by Grindlay and Seaquist (1986) is real and non variable then its spectral index is $\alpha<-1.4$. If the object is variable and has $\alpha=-0.8$ then it must have been fainter by a factor of $\sim$2 during these observations. Grindlay and Seaquist (1986) did not detect Geldzahlers' (1983) source in their survey of the cluster implying that the source is variable by a factor of $\geq$8.

If a source as luminous as either of the the radio counterparts to the X–ray sources in NGC6712 or NGC7078 existed in NGC6624, it would have been detected in this survey (Table 5.3).

5.4.4 NGC1851

The X–ray source in NGC1851 is a typical member of its class, exhibiting bursts and an X–ray luminosity in quiescence in the 2–11 keV band of $\sim5\times10^{36}$ erg s^{-1} (Bradt and McClintock 1983). The optical counterpart to this source has not been identified (Da Costa 1982) despite the distance of the X–ray source from the globular cluster core ($\sim$12″) (Grindlay *et al.* 1984).

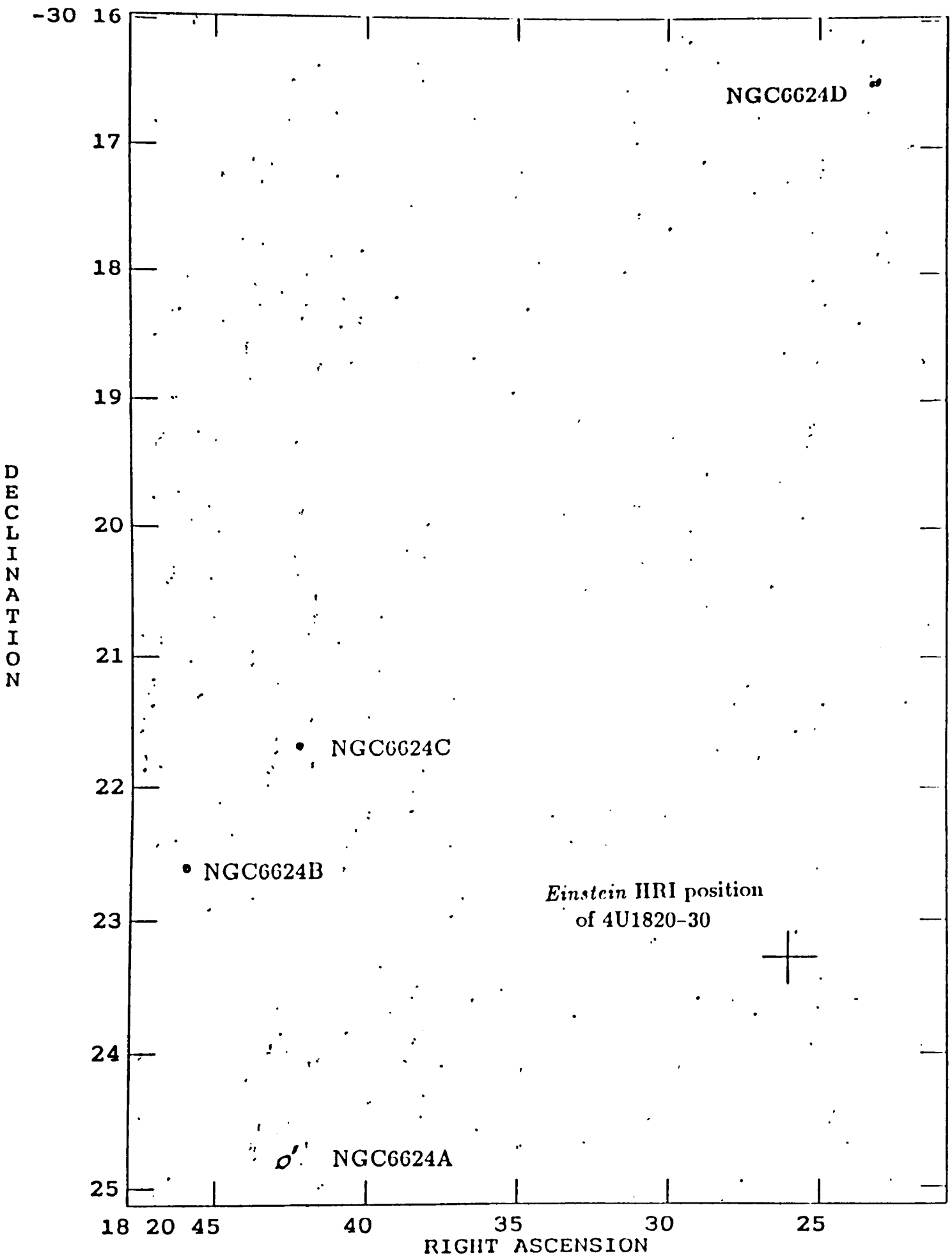

Figure 5.4: Radio map of NGC6624. The contours shown are –3, 4, 5, 6, 7, 10 and 20 times 29 μJy beam^{-1}, the rms level of the map. The position of the X–ray source is marked (Grindlay *et al.* 1984).

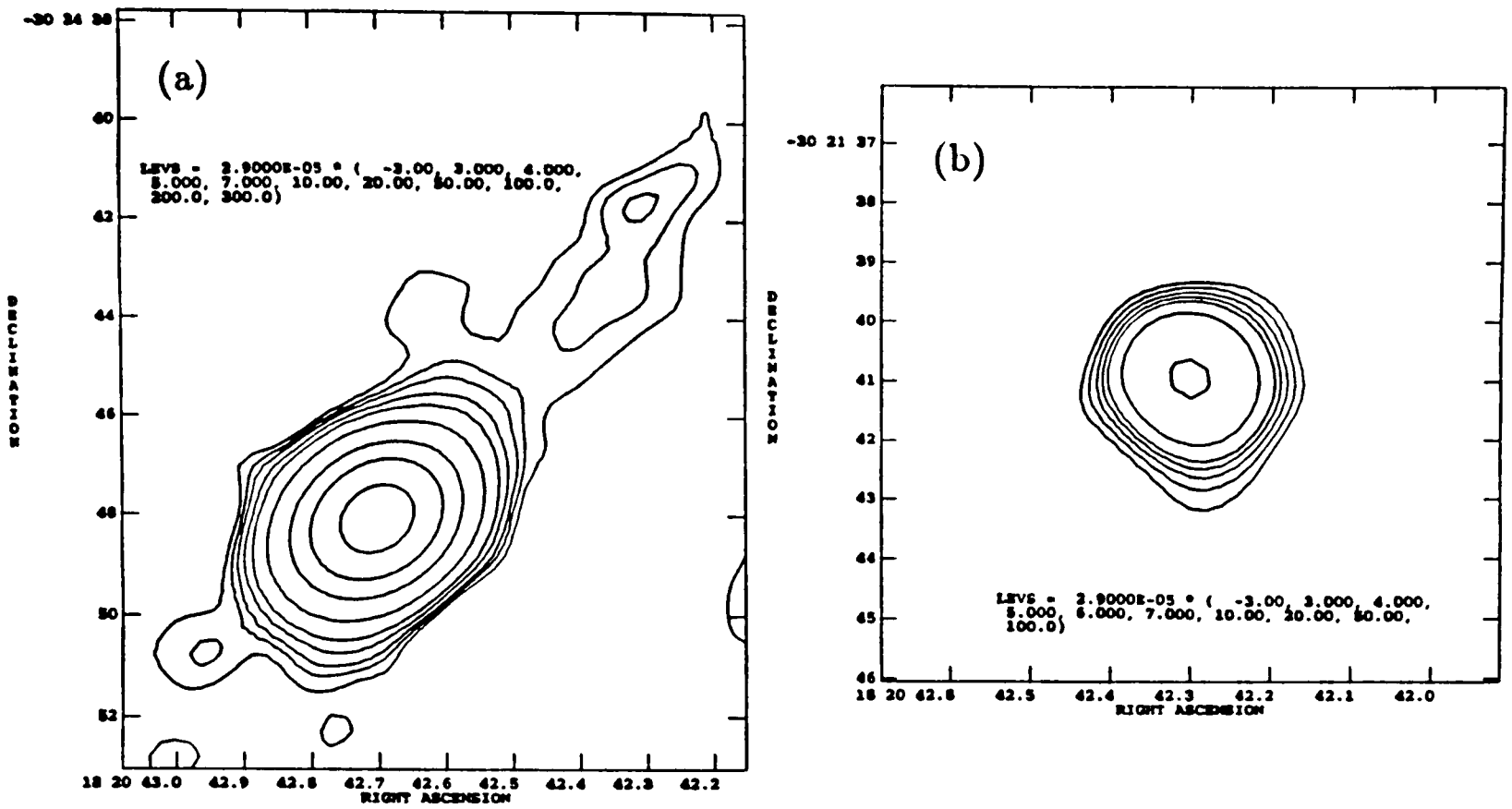

Figure 5.5(a–d): Maps of the four serendipitous radio sources in the field of NGC6624. From top left to bottom right: (a) NGC6624A; (b) NGC6624B; (c) NGC6624C and (d) the double radio source NGC6624D. The contour levels used are indicated on each map.

These radio observations have not revealed any point source radio emission from a circle (radius ~45″) around the X–ray position to a 3σ limit of 63 μJy. If there is a radio counterpart to the X–ray source in NGC1851 then it must have been less luminous than that in NGC7078 during these observations (Table 5.3).

5.4.5 4U2129+47

The galactic LMXB 4U2129+47 has been observed in both "high" and "low" X–ray (and optical) states.

In the high state (pre 1983) the object had been detected as a highly variable 1–37 μJy (5 keV), low luminosity (2–10 keV, $L_X \sim 5\times10^{35}$ erg s^{-1}) X–ray source (Bradt and McClintock 1983). The object was also optically bright (B~17), with its optical light curve displaying large (ΔB~1.5 mag) amplitude, periodic (P_{orb}=5.2 hour) single wave modulations (Thorstensen *et al.* 1979). A single wave light curve is due to the changing aspect of an X–ray heated secondary. The similarity of this light curve to that of Her X–1 led Thorstensen *et al.* (1979) to suggest that these two systems were similar. Spectroscopy taken in 1981 by Horne, Verbunt and Schneider (1986) showed that the object displayed strong He II λ4686 and the Bowen blend (λ4640–4660) in emission similar to the optical counterparts to other LMXBs (van Paradjis 1983).

Observations reported by Pietsch *et al.* (1986) indicated that the object was no longer emitting X–rays, and that the optical counterpart had faded to B~18.6. Also the large amplitude variations seen in the light curve by Thorstensen *et al.* (1979) were no longer present. This led them to suggest that the X–ray emission had switched off. This explained both the absence of X–rays and the absence of any single wave photometric variation. Thorstensen *et al.* (1988) performed photometry on the low state optical counterpart. They expected to

find ellipsoidal variations in the light curve similar to those observed in other LMXBs in low state (eg. the X–ray transient Cen X–4, Chevalier *et al.* 1989). However no such modulations were present, to a limit of 1%, which is much lower than the expected value. A spectrum of the object taken in the low state no longer showed the emission lines found by Horne, Verbunt and Schneider (1986) but rather that of a late F main sequence star. Recently Garcia *et al.* (1989) using the results of extensive low state spectroscopy (spectra taken from June 1987 to October 1988) argue that 4U2127+49 is in fact a hierarchical triple system. The inner binary, forming the LMXB, dominates the systems radiative output in the X–ray high state. A F7 V star in a larger orbit (P_{orb}~30 days) dominates the optical output in the X–ray low state.

4U2129+47 was observed at 6 cm by Geldzhaler (1987) using the VLA. He detected an unresolved point source with a flux density of 1.12±0.07 mJy. He suggested that this was the radio counterpart to the X–ray source. The observations reported here do not show any 6 cm emission from this object to a 3σ flux density limit of 150 μJy. These two observations indicate that the object is variable by at least a factor of 8, in its "off" state. Radio emitting LMXBs undergo larger flux density variations often on shorter timescales (eg. Hjellming and Wade (1971) report that Sco X–1 varied by a factor of 60 in 25 hours!). Hence the variation reported here for 4U2129+47 is not remarkable for this type of object.

4U2129+47 may be interesting for another reason. Callanan (1989) has suggested that LMXBs in low state (eg. X–ray transients in quiescence) might contain radio pulsars. The neutron stars in LMXBs are thought to be spun up during the accretion process (Sections 1.4 and 1.5) but radio emission is suppressed because of the density of the material surrounding the source. Once

accretion has stopped the radio pulsar may turn on. Biggs, Lyne and Johnston (1990) have followed up this suggestion by searching 4U2129+47 for periodic pulsations at 610 MHz. They find $\sim 8\sigma$ upper limits (10 - 500 ms) for the flux density of any pulsations of 6.8 and 4.0 mJy for two separate observations. Two deductions can be made from this result.

Firstly the flux density limit obtained here does not rule out the possibility that a pulsar may be present at very low flux densities. At 4885 MHz the 4.0 mJy (610 MHz) upper limit becomes only ~ 62 μJy (α=–2). Hence no emission would have been detected in this survey.

Secondly and more seriously, apart from interstellar scintillation (that can cause the flux density from pulsars to change by up to an order of magnitude on short timescales) (Biggs, Lyne and Johnston 1990) pulsars are reasonably stable radio emitters. If Geldzahlers' (1987) 1.12 mJy (4885 MHz) source had been a pulsar then one would not expect its flux density to have changed significantly over two years. If its flux density had not changed then the expected flux density of the pulsar at 610 MHz would be ~ 72 mJy and easily detectable in the survey of Biggs, Lyne and Johnston (1990). Interstellar scintillation cannot explain the absence of radio emission and therefore the emission detected by Geldzahler (1987) was probably not a pulsar but normal LMXB radio emission.

5.4.6 General Discussion

This is the deepest radio survey yet of globular clusters and indeed is the deepest search to date performed for the radio counterparts of any LMXB. Previous radio surveys have only been undertaken to at best a 1σ rms noise level of $\sim$100–400 μJy beam^{-1} (Duldig *et al.* 1979, Geldzahler 1983, 1987, Grindlay

and Seaquist 1986 and Nelson and Spencer 1988). These observations have improved on the results of the previous surveys by an order of magnitude and have produced maps close to their theoretical noise limits. These results constitute the only firm detections so far of radio counterparts to any globular cluster X–ray sources.

It is possible to estimate how many serendipitous radio sources one would expect to observe in the X–ray error circle and in the area of the fields surveyed. This can be done by using the results of source count studies at 6 cm, for example that of Fomalont *et al.* (1984). The distribution law they obtain for radio sources with flux densities between 100 μJy and 10 Jy is, in integrated form,

$n(100\ \mu Jy \leq S \leq 10\ Jy) = (\int_{10^{-4}}^{10^{-1}} 500 \times S^{-1.75}\ dS + \int_{10^{-1}}^{10^{1}} 90 \times S^{-2.5}\ dS)\Omega = 664813.2\Omega$

where $\Omega = \delta A / r^2 \simeq \pi (r\theta^c)^2 / r^2 = \pi(\theta^c)^2$ is the solid angle subtended and $\theta^c \simeq$(radius of area surveyed in arcsec)/(206265). From this it is found that there should be $\leq 4.4 \times 10^{-4}$ sources in the error circle (radius $\sim 3'' \equiv 6.6 \times 10^{-10}$ sr) of a X–ray source. This implies that the total number of serendipitous radio sources which should have been observed in the X–ray error boxes of all four globular cluster LMXBs is $\leq 1.8 \times 10^{-3}$. Thus the detection of two sources within the 3σ X–ray error circles implies that the association with the X–ray sources is extremely likely.

The number of extragalactic sources in the mapped areas surrounding the globular cluster fields can be predicted using the above distribution law. Table 5.4 contains the results of this calculation. These show that the observed number of sources in the globular cluster fields are compatible with the source count results.

The two LMXB radio counterparts discovered with these observations have similar peak flux density levels of $\sim$160–200 μJy but the NGC7078 radio source

Table 5.4 The Predicted Number of Serendipitous Radio Sources in the Globular Cluster Fields

Globular Cluster	Box Surveyed† (arcsec) RA (θ_1)	Dec (θ_2)	$\Omega \simeq \theta_1{}^c \theta_2{}^c$ $\times 10^{-7}$ sr	n_{pred} –	n_{obs} –
NGC7078	139	290	9.47	0.6	2
NGC6712	104	100	2.44	0.2	0
NGC6624	362	539	45.9	3.0	4
NGC1851	102	102	2.45	0.2	0

†The RA and Dec dimensions are calculated using the spherical trigonometry formula given in Section 5.4.1.

appears more extended than the NGC6712 source. The radio emission seems to come from an extended region surrounding each X–ray source with dimensions $\sim 0.066 \times < 0.02$ pc for the NGC6712 radio counterpart and $\sim 0.14 \times 0.047$ pc for the NGC7078 radio counterpart. This is large when compared to the orbital sizes of these systems, which is $\sim 6 \times 10^{-8}$ pc for a LMXB similar to that in NGC7078. The bulk of the radio emission therefore does not arise from the very dense hot X–ray emitting gas surrounding the neutron star.

Several X–ray binaries display synchrotron powered double radio lobes (Sco X–1, Cyg X–3 and SS433; Strom *et al.* 1989 and references therein) though the majority of the LMXBs detected are unresolved to a limit of $<1''$ (Geldzahler, 1983, 1987). Both the radio counterparts detected here are extended. The counterpart in NGC7078 is of similar size to SS433, but significantly smaller than the double lobes of Sco X–1 (Fomalont *et al.* 1983) or Cyg X–3 (Strom *et al.* 1989). However, on the assumption of synchrotron emission, the derived magnetic field strengths are similar in all cases ($\sim$1 mG). Further support to the synchrotron hypothesis is given by the general X–ray similarity between globu-

lar cluster X–ray sources and the galactic bulge LMXBs whose radio properties have been shown by Hjellming and Johnston (1988) to be well explained by synchrotron emission. However with one intensity measurement at one frequency bremsstrahlung as an alternative source of the emission cannot be ruled out. Only further observations at different frequencies would allow differentiation between the two mechanisms.

I now consider why radio counterparts were found for the X–ray sources in only two of the four globular clusters observed. The detected radio sources have luminosities 54.5×10^{18} erg s^{-1} Hz^{-1} in NGC7078 and 9.95×10^{18} erg s^{-1} Hz^{-1} in NGC6712 respectively. A similar luminosity source would have been detected in NGC6624 with a peak flux density of $\geq$108 μJy beam^{-1}. However only a source as luminous as that in NGC7078 would have been detected in NGC1851 with a peak flux density of $\geq$124 μJy beam^{-1}. Since NGC6624 contains the most luminous globular cluster X–ray source, it does not appear that there is a simple correlation between L_X and L_R. Variability is always a possible explanation for missing correlations, but at present these observations do not permit further speculation about the possible relationship between L_X and L_R. Since galactic LMXBs are known to vary (Hjellming and Johnston 1986) the absence of a radio counterpart does not preclude the possibility that the X–ray sources in NGC6624 and NGC1851 are variable radio sources, that were, at the time of these observations, too faint to be detected.

Many radio pulsars have recently been detected in globular clusters. A summary of most of the known detections can be found in the table given in Ray & Kluźniak (1990) with a more up to date list given in Table 5.5. The spectral index for globular cluster millisecond radio pulsars is $\sim$–2 to –2.4 (Kulkarni, Narayan and Romani 1990). Using this spectral index and the flux density of

Table 5.5 The Flux Densities of the Globular Cluster Millisecond Pulsars Scaled to 4885 MHz and the Distance of the Surveyed Globular Clusters

Globular Cluster	Flux Density mJy	Frequency in MHz	Distance kpc	Flux Density (4885 MHz) μJy	Flux Density (μJy) of Pulsar in 7078[1]	6712	6624	1851	Reference -
M4	15.0	408.0	2.2	104.6	5.4	13.2	7.9	3.5	(1)
NGC6539	0.8	1500.0	3.1	75.4	7.7	18.9	11.3	5.0	(2)
47Tuc	0.6	1500.0	4.6	56.6	12.7	25.4	18.7	8.3	(3)
M28†	1.1	1465.0	5.8	61.1	21.8	48.6	32.0	14.3	(4)
Ter5	2.0	1500.0	7.1	188.6	101.0	247.3	148.5	66.0	(5)
NGC6440	1.3	1500.0	7.1	122.6	65.7	160.7	96.5	42.9	(6)
M5A	0.5	430.0	7.6	3.9	2.4	5.8	3.5	1.6	(7)
M5B	0.5	430.0	7.6	3.9	2.4	5.8	3.5	1.6	(7)
NGC6624A	2.0	620.0	8.0	32.2	21.9	53.6	32.2	14.3	(8)
NGC6624B	2.0	620.0	8.0	32.2	21.9	53.6	32.2	14.3	(8)
NGC7078A	1.6	430.0	9.7	12.4	12.4	30.3	18.2	8.1	(9)
NGC7078B	0.7	430.0	9.7	5.4	5.4	13.3	8.0	3.5	(10)
NGC7078C	1.7	430.0	9.7	13.2	13.2	32.2	19.4	8.6	(11)

[1]Distances are NGC7078 (9.7 kpc), NGC6712 (6.5 kpc), NGC6624 (8.0 kpc) and NGC1851 (12.0 kpc)
†Using the known spectral index of –2.4, (Lyne *et al.* 1987)

(1) Lyne *et al.* (1988), (2) D'Amico *et al.* (1990), (3) Manchester *et al.* (1990), (4) Lyne *et al.* (1987), (5) Lyne *et al.* (1990), (6) Manchester *et al.* (1989), (7) Wolszczan *et al.* (1989B), (8) Biggs *et al.* (1990), (9) Wolszczan *et al.* (1989A), (10) Anderson *et al.* (1989A), (11) Anderson *et al.* (1989B)

the known globular cluster millisecond pulsars it is possible to estimate their flux densities *had they been present* in the globular clusters surveyed. From the results shown in Table 5.5 it can be seen that most of the pulsars would be too faint to have been detected with these observations. Only the observed pulsars in Ter5 and NGC6440 have flux densities comparable to the flux density limits found here. However, as no peaks at these flux densities (except the radio counterparts) are found it can be concluded that no radio pulsars have been detected in this survey.

Grindlay *et al.* (1984) use the *Einstein* HRI positions of 8 bright globular cluster X–ray sources relative to their host cluster cores to derive the average mass of the bright X–ray sources. It should be possible to improve on this value as more radio counterparts to globular cluster X–ray sources are found since the positions derived by radio synthesis mapping represent a substantial improvement over those derived from the *Einstein* HRI .

5.5 Conclusions

By discovering the radio counterparts of two bright globular cluster X–ray sources the feasibility of deep radio mapping such sources as a technique for refining their X–ray positions has been demonstrated. Both the radio counterparts detected have extended emission regions which I have interpreted as synchrotron emission.

5.6 References

Anderson, S., Gorham, P., Kulkarni, S. & Prince, T., 1989A. *IAU Circ. No.* 4762.

Anderson, S., Gorham, P., Kulkarni, S. & Prince, T., 1989B. *IAU Circ. No.* 4772.

Aurière, M., Le Fèvre, O. & Terzan, A., 1984. *Astr. Astrophys.*, **138**, 415.

Baars, J.W.M., Genzel, R., Pauliny-Toth, I.I.K. & Witzel, A., 1977. *Astr. Astrophys.*, **61**, 99.

Biggs, J.D., Lyne, A.G. & Johnston, , 1990. In:*Proceedings of the 23rd ESLAB Symposium,* Vol. 1, p. 293, eds. Hunt, J. & Buttrick, B., ESA Publications Division, ESTEC, Noordwijk, The Netherlands.

Biggs, J.D., Lyne, A.G., Manchester, R.N. & Ashworth, M., 1990. *IAU Circ. No.* 4988.

Birkinshaw, M. & Downes, A.J.B., 1982. *Astrophys. J.*, **258**, 154.

Bradt, H.V.D. & McClintock, J.E., 1983. *Ann. Rev. Astr. Astrophys.*, **21**, 13.

Bridle, A.H., 1986. In:*Synthesis Imaging.*, Ch. 16, eds. Perley, R.A., Schwab, F.R. & Bridle, A.H., National Radio Astronomy Observatory, Green Bank, USA.

Bridle, A.H., 1989. In:*Synthesis Imaging in Radio Astronomy.*, Ch. 24., eds. Perley, R.A., Schwab, F.R. & Bridle, A.H., Bringham Young University Print Services, Provo, Utah, USA.

Callanan, P.J., Fabian, A.C., Tennant, A.F., Redfern, R.M. & Shafer, R.A., 1987. *Mon. Not. R. astr. Soc.*, **224**, 781.

Callanan, P.J., 1989. *Private Communication.*

Charles, P.A., 1990. In:*Proceedings of the 23rd ESLAB Symposium,* Vol. 1, p. 345, eds. Hunt, J. & Buttrick, B., ESA Publications Division, ESTEC, Noordwijk, The Netherlands.

Chevalier, C., Ilovaisky, S.A., van Paradjis, J., Pedensen, H. & van der Klis, M., 1989. *Astron. Astrophys.*, **210**, 114.

Crane, P.C. & Napier, P.J., 1989. In:*Synthesis Imaging in Radio Astronomy.*, Ch. 7, eds. Perley, R.A., Schwab, F.R. & Bridle, A.H., Bringham Young University Print Services, Provo, Utah, USA.

Cudworth, K., 1988. *Astron. J.*, **96**, 105.

Da Costa, G.S., 1982. *Publs astr. Soc. Pacif.*, **94**, 769.

D'Amico, N, Lyne, A.G., Bailes, M, Johnston, S., Manchester, R.N., Staveley–Smith, L, Lim, J., Fruchter, A.S. & Goss, W.M., 1990. *IAU Circ. No.* 5013.

Duldig, M.L., Greenhill, J.G., Thomas, R.M., Haynes, R.F., Simons, L.W.J. & Murdin, P.G., 1979. *Mon. Not. R. astr. Soc.*, **187**, 567.

Fabian, A.C., Pringle, J.E. & Rees M.J., 1975. *Mon. Not. R. astr. Soc.*, **172**, 15p.

Fomalont, E.B., Geldzahler, B.J., Hjellming, R.M. & Wade, C.M., 1983. *Astrophys. J.*, **275**, 802.

Fomalont, E.B., Kellermann, K.I., Wall, J.V. & Weistrop, D., 1984. *Science*, **225**, 23.

Garcia, M., Bailyn, C.D., Grindlay, J.E. & Molnar, L.A., 1989. *Astrophys. J.*, **341**, L75.

Gathier, R., Pottasch, S.R. & Goss, W.M., 1983. *Astr. Astrophys.*, **127**, 320.

Geffert, M., Aurière, M., Ilovaisky, S.A. & Terzan, A., 1989. *Astr. Astrophys.*, **209**, 423.

Geldzahler, B.J., 1983. *Astrophys. J.*, **264**, L49.

Geldzahler, B.J., 1987. *Publs. astr. Soc. Pacif.*, **99**, 1036.

Gopal-Krishna & Steppe, H., 1980. *Astr. Astrophys.*, **88**, 354.

Grindlay, J.E. & Bailyn, C.D., 1988. *Nature*, **336**, 48.

Grindlay, J.E., Hertz, P., Steiner, J.E., Murray, S.S. & Lightman, A.P., 1984. *Astrophys. J.*, **282**, L13.

Grindlay, J.E. & Seaquist, E.R., 1986. *Astrophys. J.*, **310**, 172.

Hills, J.G., 1976. *Mon. Not. R. astr. Soc.*, **175**, 1p.

Hjellming, R.M., & Wade, C.M., 1971. *Astrophys. J.*, **164**, L1.

Hjellming, R.M. & Johnston, K.J., 1986. In:*The Physics of Accretion onto Compact Objects*, p. 287, eds. Mason, K.O., Watson, M.G. & White, N.E., Springer–Verlag, Berlin, Germany.

Hjellming, R.M. & Johnston, K.J., 1988. *Astrophys. J.*, **328**, 600.

Horne, K., Verbunt, F. & Schneider, D.P., 1986. *Mon. Not. R. astr. Soc.*, **218**, 63.

Högbom, J., 1974. *Astrophys. J. Suppl.*, **15**, 417.

Ilovaisky, S.A., Aurière, M., Chevalier, C., Koch–Miramond, L., Cordoni, J.P. & Angbault, L.P., 1987. *Astr. Astrophys.*, **179**, L1.

Johnson, H.M., 1976. *Astrophys. J.*, **208**, 706.

Katz, J.I., 1975. *Nature*, **253**, 698.

Kulkarni, S.R., Narayan, R. & Romani, R.W., 1990. *Astrophys. J.*, **356**, 174.

Lewin, W.H.G. & Joss, P.C., 1983. In:*Accretion Driven Stellar X-ray Sources.*, p. 41, eds. Lewin, W.H.G., & van den Heuvel, E.P.J., Cambridge University Press, Cambridge.

Lyne, A.G., Brinklow, A., Middleditch, J., Kulkarni, S.R., Backer, D.C. & Clifton, T.R., 1987. *Nature,* **328,** 399.

Lyne, A.G., Biggs, J.D., Brinklow, A., Ashworth, M. & McKenna, J., 1988. *Nature,* **332,** 45.

Lyne, A.G., Johnston, S., Manchester, R.N., Staveley–Smith, L, D'Amico, N, Lim, J., Fruchter, A.S. & Goss, W.M., 1990. *IAU Circ. No.* 4974.

Manchester, R.N., Lyne, A.G., Johnston, S., D'Amico, N., Lim, J., Kniffen, D.A., Fruchter, A.S. & Goss, W.M., 1989. *IAU Circ. No.* 4905.

Manchester, R.N., Lyne, A.G., D'Amico, N., Johnston, S., Lim, J. & Kniffen, D.A., 1990. *Nature,* **345,** 598.

Naylor, T., Charles, P.A., Drew, J.E. & Hassall, B.J.M., 1988. *Mon. Not. R. astr. Soc.,* **233,** 285.

Nelson, R.F. & Spencer, R.E., 1988. *Mon. Not. R. astr. Soc.,* **234,** 1105.

Nieto, J.-L., Aurière, M., Thouvenot, E., Sebag, J., Lelièvre, G., Foy, R. & Arnaud, J., 1990. *IAU Circ. No.* 4944.

Pietsch, W., Steinle, H., Gottwald, M. & Graser, U., 1986. *Astron. Astrophys.,* **157,** 23.

Pacholczyk, A.G., 1970. In:*Radio Astrophysics,* W. F. Freeman & Co., San Fransisco.

Ray, A. & Kluźniak, W., 1990. *Nature,* **344,** 415.

Stella, L., Priedhorsky, W. & White, N.E., 1987. *Astrophys. J.,* **312,** L17.

Strom, R.G., van Paradjis, J. & van der Klis, M., 1989. *Nature.,* **337,** 234.

Thompson, A.R., Clark, B.G., Wade, C.M. & Napier, P.J., 1980. *Astrophys. J. Suppl.,* **44,** 151.

Thorstensen, J.R., Charles, P.A., Bowyer, S., Briel, U.G., Doxey, R.E., Griffiths, R.E. & Schwartz, D.A., 1979. *Astrophys. J.,* **233,** L57.

Thorstensen, J.R., Brownsberger, K.R., Mook, D.E., Remilliard, R.A., McClintock, J.E., Koo, D.C. & Charles, P.A., 1988. *Astrophys. J.,* **334,** 430.

van Paradijs, J., 1983. In:*Accretion Driven Stellar X-ray Sources.,* p. 189, eds. Lewin, W.H.G., & van den Heuvel, E.P.J., Cambridge University Press, Cambridge.

Wolszczan, A., Kulkarni, S.R., Middleditch, J., Backer, D.C., Fruchter, A.S. & Dewey, R.J., 1989A. *Nature.* **337,** 531.

Wolszczan, A., Anderson, S., Kulkarni, S.R. & Prince, T., 1989B. *IAU Circ. No.* 4880.

Webbink, R.F., 1985. In:*Dynamics of Star Clusters, IAU Symp. No. 113,* p. 541, eds. Goodman, J. & Hut P., Reidel, Dordrecht.

White, N.E., 1986. In: *The Evolution of Galactic X-ray Binaries.* p. 227, eds. Truemper, J., Lewin, W.H.G. & Brinkmann, W., Reidel, Dordrecht.

Chapter 6

Optical and X–ray Observations of the LMXB 4U0614+09

In this chapter I will describe the results of photometry, spectroscopy and simultaneous X–ray (with EXOSAT) and optical photometry of the galactic LMXB 4U0614+09.

Extensive CCD photometry (1986, 1987–88 and 1989) indicates that the object is variable on two characteristic timescales; ~10 days and ~1 hour. The former is discussed in terms of precession of an accretion disc whilst the latter may indicate a short orbital period for the system.

The X–ray and optical fluxes were found to be anticorrelated; several possible mechanisms to explain this behaviour are discussed.

Low resolution spectroscopy shows that 4U0614+09 is unusual in that it displays the Bowen blend λ4640–4660 in emission but *not* He II λ4686. I discuss several possible mechanisms that could explain this behaviour.

6.1 Introduction

The X–ray source 4U0614+09 (Forman *et al.* 1978) was optically identified by Murdin *et al.* (1974) with a faint (V~18), blue, variable star (V1055 Ori). It is located in the galactic plane.

Observations by the *Copernicus* (Davidsen *et al.* 1974), *Uhuru* (Forman *et al.* 1978) and *Ariel V* (Mason *et al.* 1976) X–ray observatories established that the

object is variable by a factor of ~2 on a timescale of hours and a factor of ~5 on longer timescales. A possible type I X–ray burst was observed by Swank *et al.* (1978). The most extensive set of X–ray observations were those obtained by *Ariel V*, comprising six separate observations each ~10–20 days long. Marshall & Millit (1981) found that the X–ray flux in three of these data sets was strongly modulated on a 5 day timescale. Davidsen *et al.* (1974) estimate the distance of 4U0614+09 to be ~4–8 kpc from a comparison of its peak X–ray flux to that of Sco X–1.

Most of the optical properties of 4U0614+09 are similar to those of other Low Mass X–ray Binaries (LMXBs). The ratio of its X–ray to optical luminosity, L_x/L_{opt} is >1000 (eg. Bradt & McClintock 1983). Its optical spectrum (Davidsen *et al.* 1974) is flat and fairly featureless except for the presence of C III/N III λ4640–50 in emission. Also its colours (B–V=0.26±0.10, U–B=–0.5±0.3,) are consistent with those of a lightly reddened (E_{B-V}~0.3) member of this class of object at a distance of ~4 kpc (Davidsen *et al.* 1974).

There are however some anomalies in this picture. Firstly Marshall & Millit (1981) point out that a ~5 day orbital period is unlikely. They argue that from the optical appearance of 4U0614+09 the optical counterpart must be intrinsically faint with $M_{opt} \leq 1 M_\odot$ and $R_{opt} \leq 1 R_\odot$. Assuming a period of 5 days they calculate that the Roche lobe of the optical star would be ~$10 R_\odot$ showing that the X–ray flux could not be fueled by Roche lobe overflow. Hence the P_{orb} must be substantially less than 5 days. Secondly it is very unusual for a LMXB to have only the Bowen blend in emission – He II λ4686 should also be present since it is a coincidence of the He II Lα line with O III λ303.8 which eventually produces the Bowen blend at λ4640–50 (McClintock, Canizares & Tarter 1975). Here I present extensive CCD photometry and William Herschel Telescope

(WHT) low resolution spectroscopy (FOS) of 4U0614+09 acquired in an attempt to determine the orbital period and to study the spectral characteristics of 4U0614+09. I also describe the results of a ~14 hour simultaneous optical and X–ray observation.

6.2 Observations

Several observations were obtained of 4U0614+09; these included four sets of photometry, thirteen spectra obtained over six nights and a short stretch of simultaneous optical and X–ray photometry. These are described below.

6.2.1 CCD Photometry: Observations and Results

Four campaigns of CCD photometry on 4U0614+09 were undertaken, these are outlined in Table 6.1 below. Also brief details of the simultaneous EXOSAT observation are given (see also Section 6.2.2).

Table 6.1 : CCD and X–ray Observing Log for 4U0614+09

Date	JD–2440000.0	Telescope
11–17 Feb. 1986	6473.6–6478.7	McGraw Hill 1.3-m
12–13 Feb. 1986	6474.4–6474.6	JKT 1.0-m
12–13 Feb. 1986	6474.4–6475.1	EXOSAT ME
19 Nov.–1 Dec. 1986	6754.9–6766.0	McGraw Hill 1.3-m
15 Dec. 1987–25 Jan. 1988	7144.8–7185.8	McGraw Hill 1.3-m
15 Dec.–23 Dec. 1987	7144.6–7152.6	JKT 1.0-m
19 Dec.–21 Dec. 1989	7879.5–7881.7	INT 2.5-m

The February 1986 and the December 1987 data were taken from two sites separated by several hours in longitude. This was done so as to obtain better time

coverage than could be obtained from just one site. Each campaign is described below.

(i) Between 11–17 February 1986 4U0614+09 was observed in the V band with the 1.3-m McGraw Hill reflector at the Michigan-Dartmouth-MIT (MDM) Observatory on Kitt Peak. The detector used was a thinned RCA CCD. It had a readout noise of ~60 e pixel^{-1} and a pixel size of 30 μm square. The prime focus plate scale was 0.62″ pixel^{-1}. The exposure time was 600 s. A short span of contemporaneous V band data was taken with the 1.0-m Jacobus Kapteyn telescope (JKT) at the Observatorio del Roque de los Muchachos on La Palma, simultaneously with a ~14 hour EXOSAT observation (12–13 February 1986, see Section 6.2.2). The JKT was equipped with an uncoated GEC P8603 detector. It had a readout noise of ~5–10 e pixel^{-1} and a pixel size of 22 μm square. The prime focus plate scale was 0.30″ pixel^{-1}. The exposure time for these frames was 500 s.

(ii) A 12 day observing run was undertaken in V band at MDM between 19 November–1 December 1986. The same detector and exposure time was used for this run as for February 1986.

(iii) Contiguous MDM–JKT observations were taken between 15–23 December 1987, with MDM observations continuing sporadically thereafter until 25 January 1988. The MDM observations were performed with a thinned RCA CCD chip similar to that described above. Each frame was exposed for 600 s. The JKT observations were cycled through U, B, V and R, these had exposure times 720, 500, 200 and 150 s respectively. The detector used at the JKT was a dye coated CCD similar to that described in Section 2.2.1a, the camera was mounted at the prime focus which gave an on-chip plate scale of 0.30″ pixel^{-1}.

(iv) Finally the 2.5-m Isaac Newton telescope (INT) prime focus camera was

used to perform B band photometry on 4U0614+09 on three consecutive nights in December 1989. These data sets are named Nights 1, 2 and 3 respectively. The detector was a thinned RCA chip. This had a readout noise of ~55 e pixel^{-1} and a pixel size of 30 μm square. This gave a prime focus plate scale of 0.74″ pixel^{-1}. The frames taken on Nights 1 and 2 had an exposure time of 100 s whereas those taken on Night 3 had an exposure time of 60 s. About 520 individual observations were taken during these three nights.

All the CCD frames were debiased and flatfielded using the method described in Section 2.2.1a. Aperture photometry was performed on 4U0614+09 and several other stars in the frame. Aperture photometry is appropriate in this instance because the field is not crowded (Davidsen *et al.* 1974). Aperture and profile fitting photometry using DAOPHOT (Stetson 1987) was performed on the December 1989 data. Figure 6.1 shows the field of 4U0614+09 with the target (star 1), comparison stars (2, 3, 4 and 8) and PSF stars (5, 7 and 8; used for the December 1989 data) indicated. Star 6 was found to be saturated and hence not used. The photometric light curves resulting from the entire data set are plotted in Figures 6.2–6.5. Each data point is plotted at the mid–integration point of the frame it was obtained from. The y–axis is relative photometry with respect to star 4 (Figure 6.1), the x–axis is time in JD–2440000.0. The curves are plotted so that an apparent rise on the y–axis corresponds to an increase in the luminosity of the source. Figure 6.5 is slightly different from the others since the frames were taken in B not V and star 1 – star 4 is plotted (hence the positive numbers), not the other way around as with the other curves. The object was found to be at the same mean magnitude and therefore in the same optical state during all these observations.

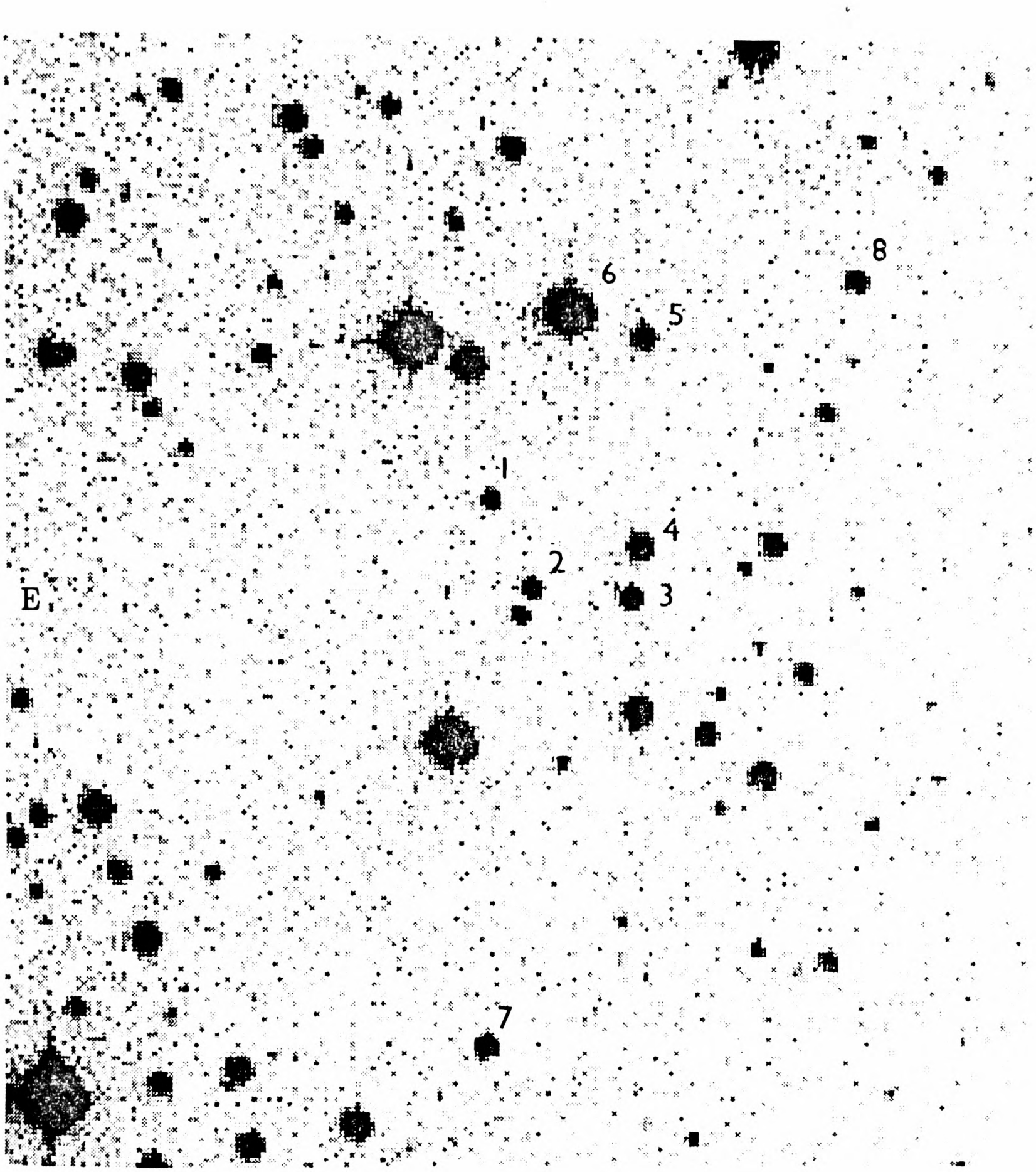

Figure 6.1: The star field around 4U0614+09. 4U0614+09 is marked as "star 1" the other stars (2–8) are either comparision stars or stars that are used to define the PSF of the frame (or both). The scale (on this Figure) is 9.3″ cm^{-1} (or 0.74″ $pixel^{-1}$). North is at the top and east to the left.

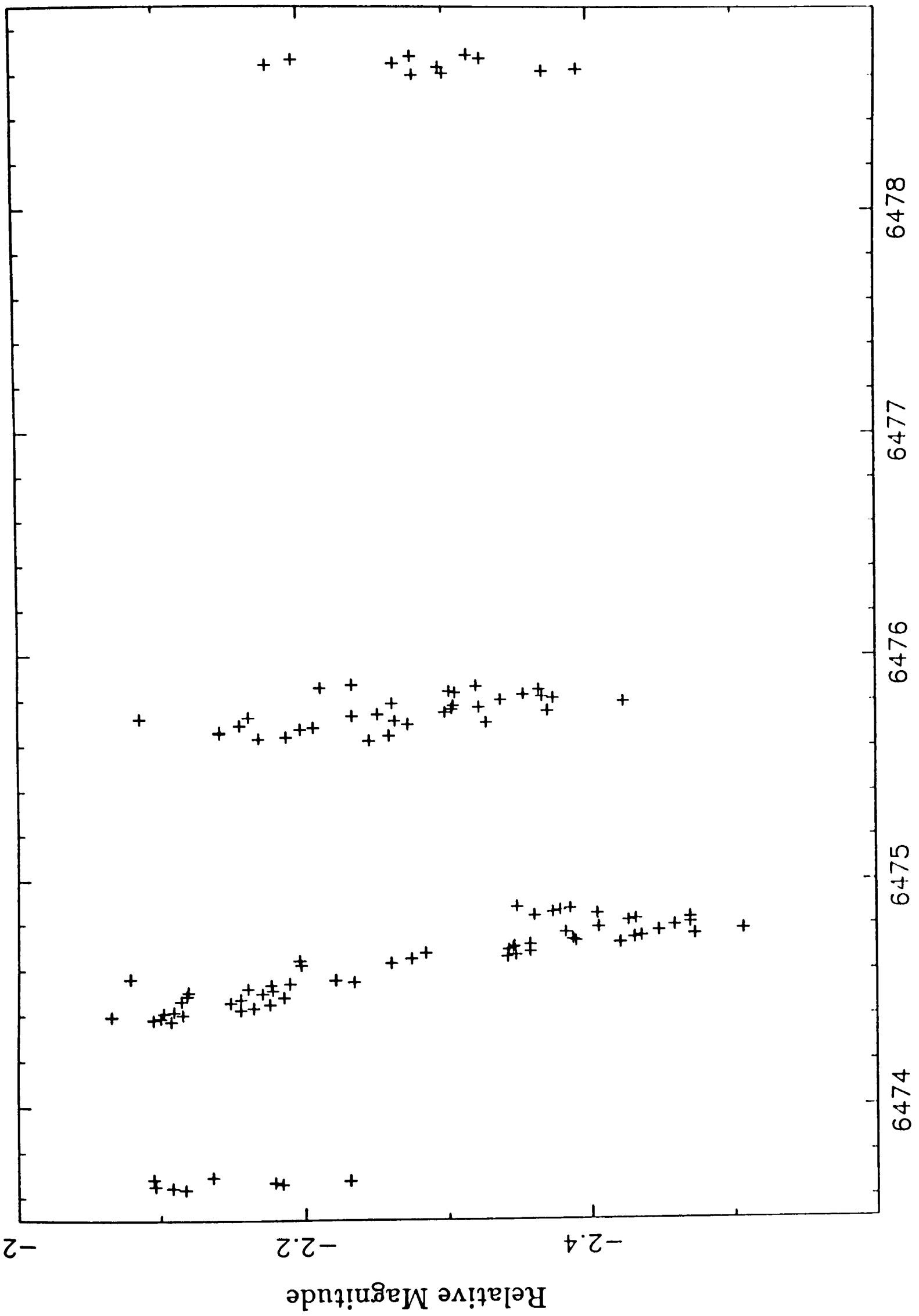

Figure 6.2: The February 1986 light curve of 4U0614+09

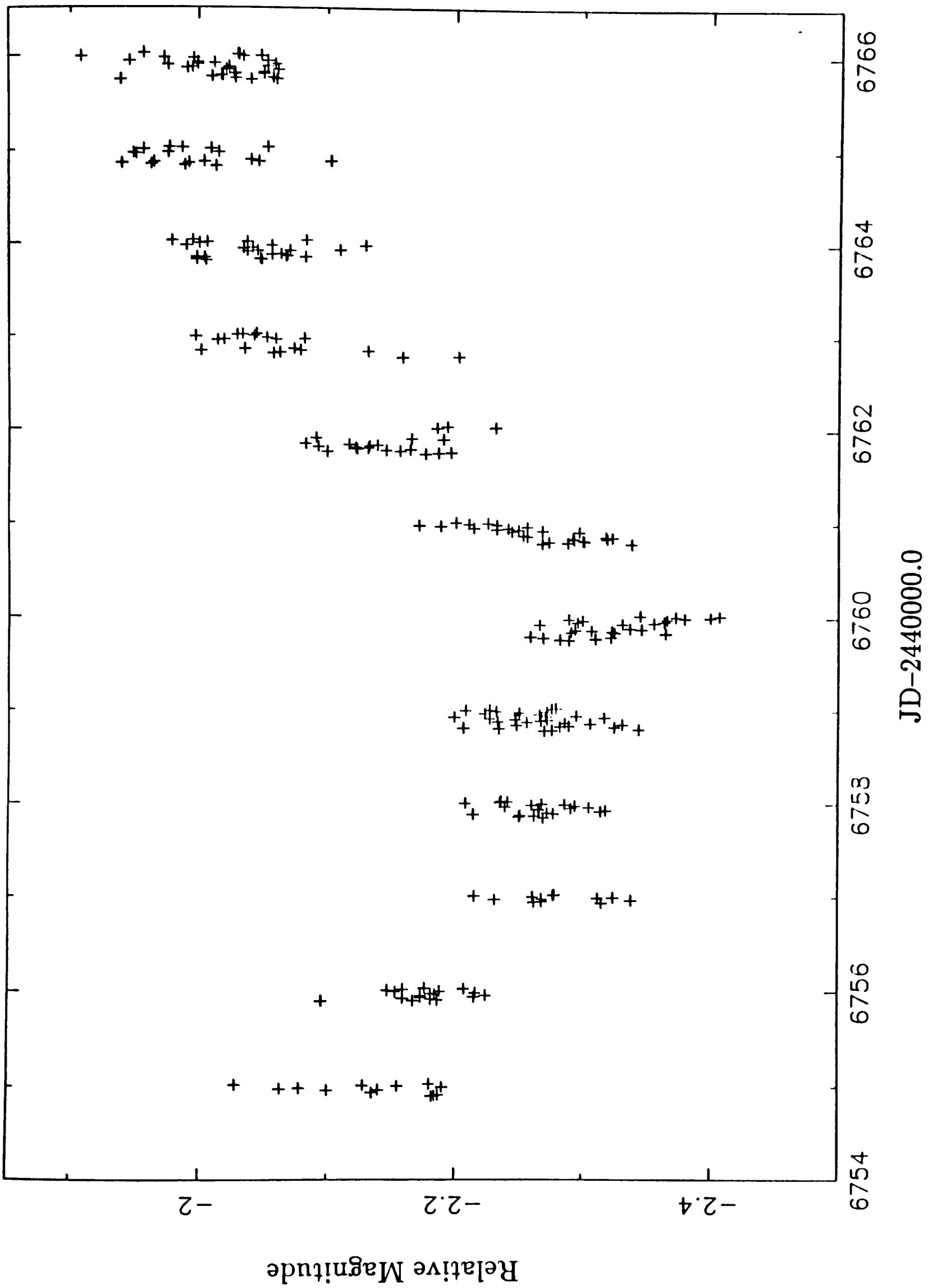

Figure 6.3: The November 1986 light curve of 4U0614+09. A smooth ~10 day variation is present.

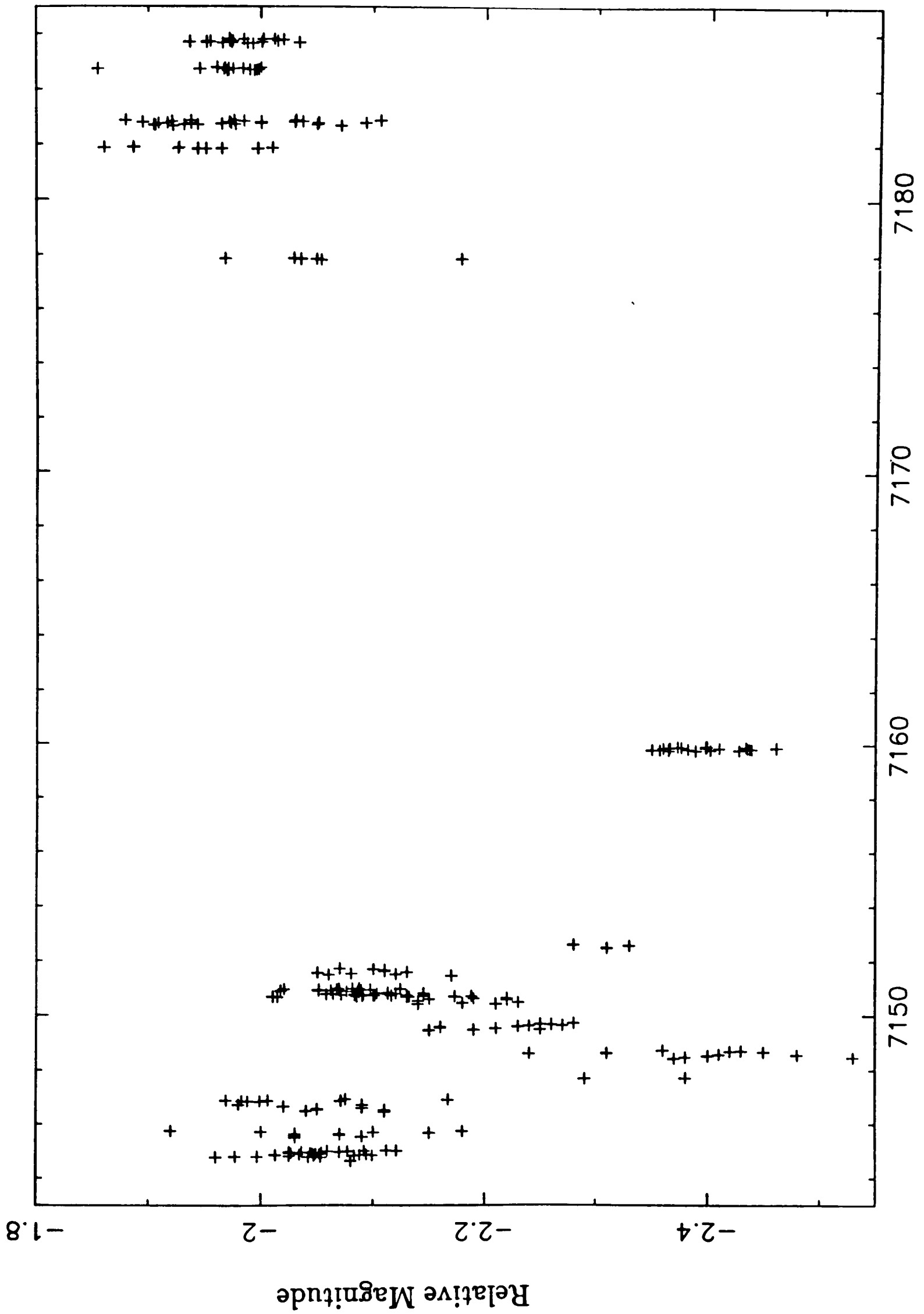

Figure 6.4: The December 1987 merged light curve of 4U0614+09, note the dips separated by ~10 days.

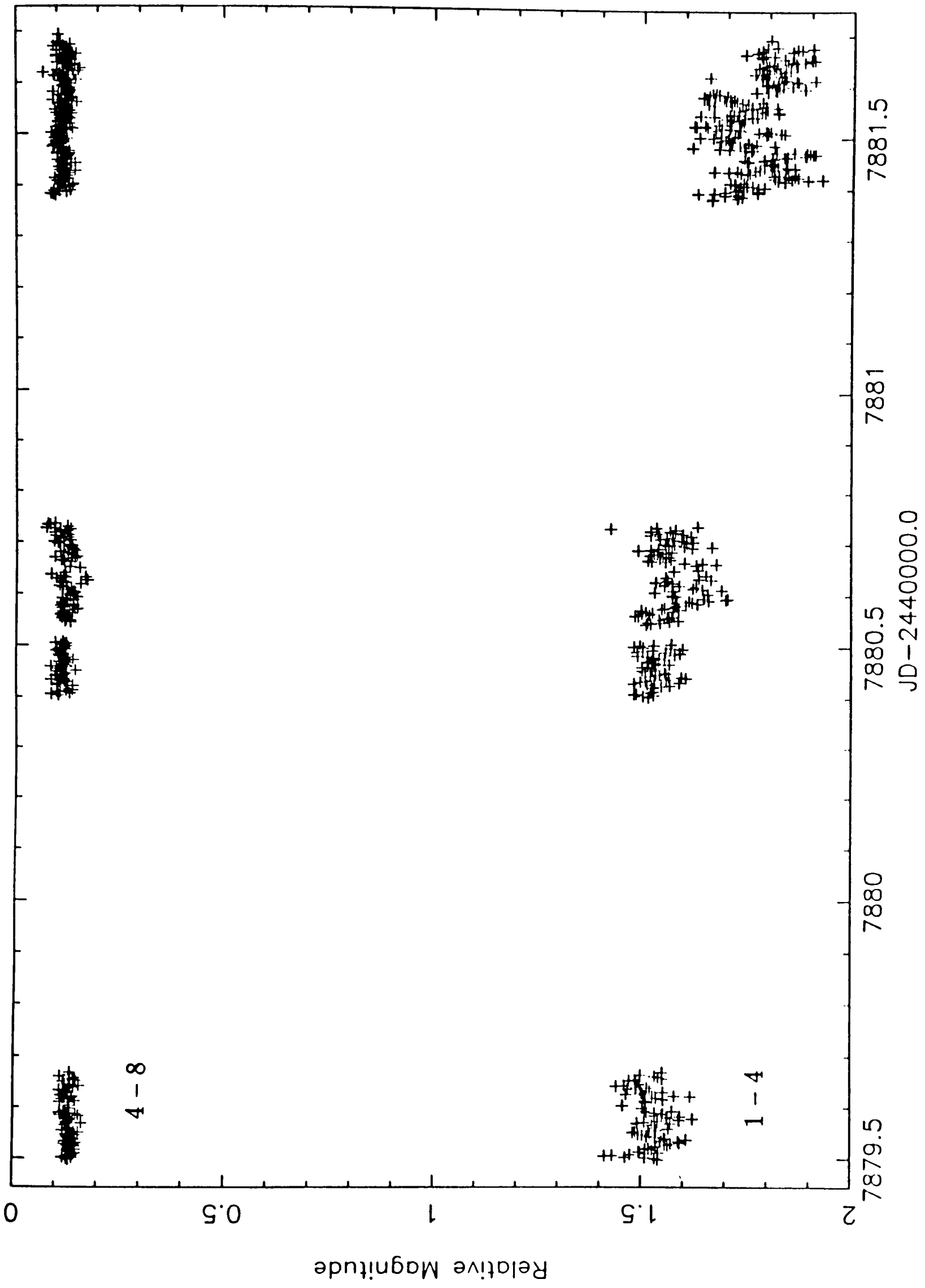

Figure 6.5: The December 1989 light curve of 4U0614+09. The object (curve labelled 1–4) displays ~1 hour timescale variability in the first (~JD2447879.6) and third (~JD2447881.5) nights data. The curve labelled 4–8 is the difference between two comparison stars.

As a check on the accuracy of the aperture photometry performed on the 1986 and 1987 data, profile fitting photometry was performed using DAOPHOT (Stetson 1987) on a subset of the JKT December 1987 data (the U and V band frames) and compared with the results of the aperture photometry. The light curves obtained by profile fitting and aperture photometry were essentially identical, confirming the accuracy of the latter.

The results of these observations are described in the next two subsections.

6.2.1a The 1986–1987 Optical Photometry Results

The colours of 4U0614+09 were obtained from the December 1987 JKT observations. This data was calibrated using observations of the standard stars 92–263 and Feige 24 (Landolt 1983, Argyle *et al.* 1988). The calibrated mean magnitude and colours of 4U0614+09 are V=+18.87±0.08, U–B=–0.86±0.11, B–V=0.26±0.11 and V–R=0.21±0.12. These values represent the mean of about fifteen data points taken over two photometric nights (JD 2447148.43–2447149.72, 0% humidity). The colour of 4U0614+09 did not vary during the December 1987 run. The difference between star 2 (V∼18.5) and star 4 (V∼16.5) was found to be stable to within ∼0.06 magnitudes (peak to peak). This represents the error in the relative photometry of 4U0614+09. The individual light curves are discussed in detail below.

The light curve observed in February 1986 is shown in Figure 6.2. There are two points to note here: (1) 4U0614+09 displayed intrinsic variability of ∼0.2–0.3 magnitudes during each night and (2) the JKT–MDM contemporaneous data (JD 2446474–2446475) exhibited a smooth decline followed by the beginning of a rise reminiscent of variability seen in other LMXBs on a timescale of ∼hours.

The MDM November 1986 results are shown in Figure 6.3. This light curve does not show any hint of a dip similar to that of Figure 6.2, although the ~0.2 magnitude variations are still present. However, the observations do show a smooth ~10 day variation. A periodogram of the data, plotted in Figure 6.6a (y–axis, $(mag/2)^2$; x–axis, frequency in day^{-1}), shows peaks around 1.08 days and 0.93 days. These peaks are significant but because of the 1-cycle-per-day alias problem (Thorstensen and Freed 1985) neither of them probably represent the real orbital period of the system.

The December 1987 – January 1988 JKT and MDM V band photometry was merged and is displayed in Figure 6.4. The most prominent features are the two ~0.4 magnitude dips occurring on a timescale of ~10 days. The periodogram (Figure 6.7a) shows peaks at 9.8 days, 1.02 days and 0.94 days, but the peaks that appeared in the November 1986 data were not present. The lack of coherence in the periodicities at ~1 day between the November 1986 and the December 1987 data argues strongly against their reality. However, since the 0.93 day (November 1986) and the 0.94 day (December 1987) periods are close to one another a case *could* be made that they are the same period. To test this hypothesis I applied a more sophisticated FT algorithm to the data, that is the one based on the one dimensional version of the CLEAN deconvolution algorithm (Lehto 1989, Roberts, Lehár and Dreher 1987). The power in the 0.93 day and 0.94 day peaks reduces significantly. This algorithm proceeds in a similar way to the two dimensional CLEAN used in the previous chapter (and described in Appendix II) for improving radio images. The window function, created by the unequal sampling of the data, is deconvolved in the following way. The highest peak in the periodogram is found and some fraction of its contribution to the power spectrum, both peak and sidelobes, is subtracted.

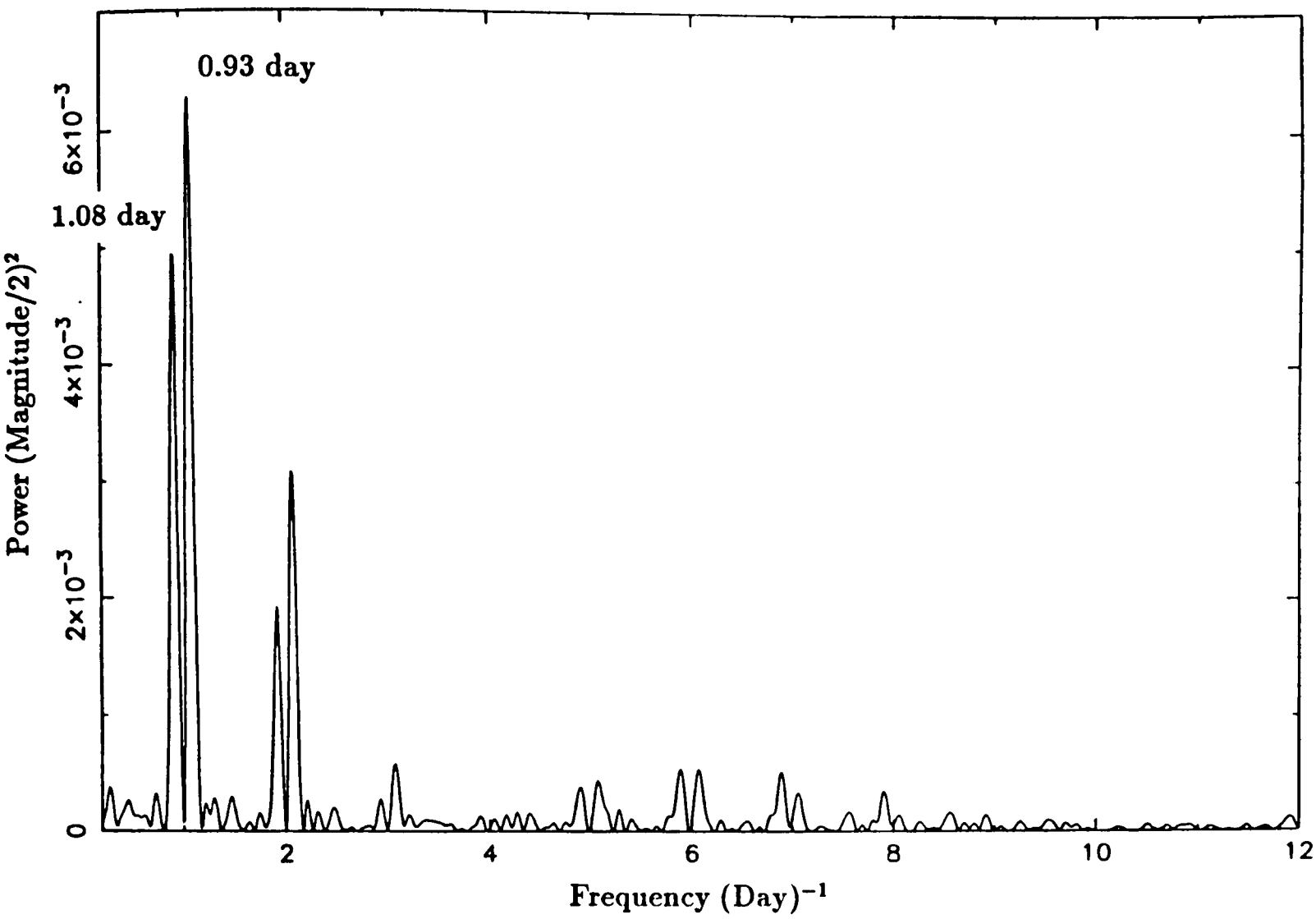

Figure 6.6a: The periodogram of the November 1986 data

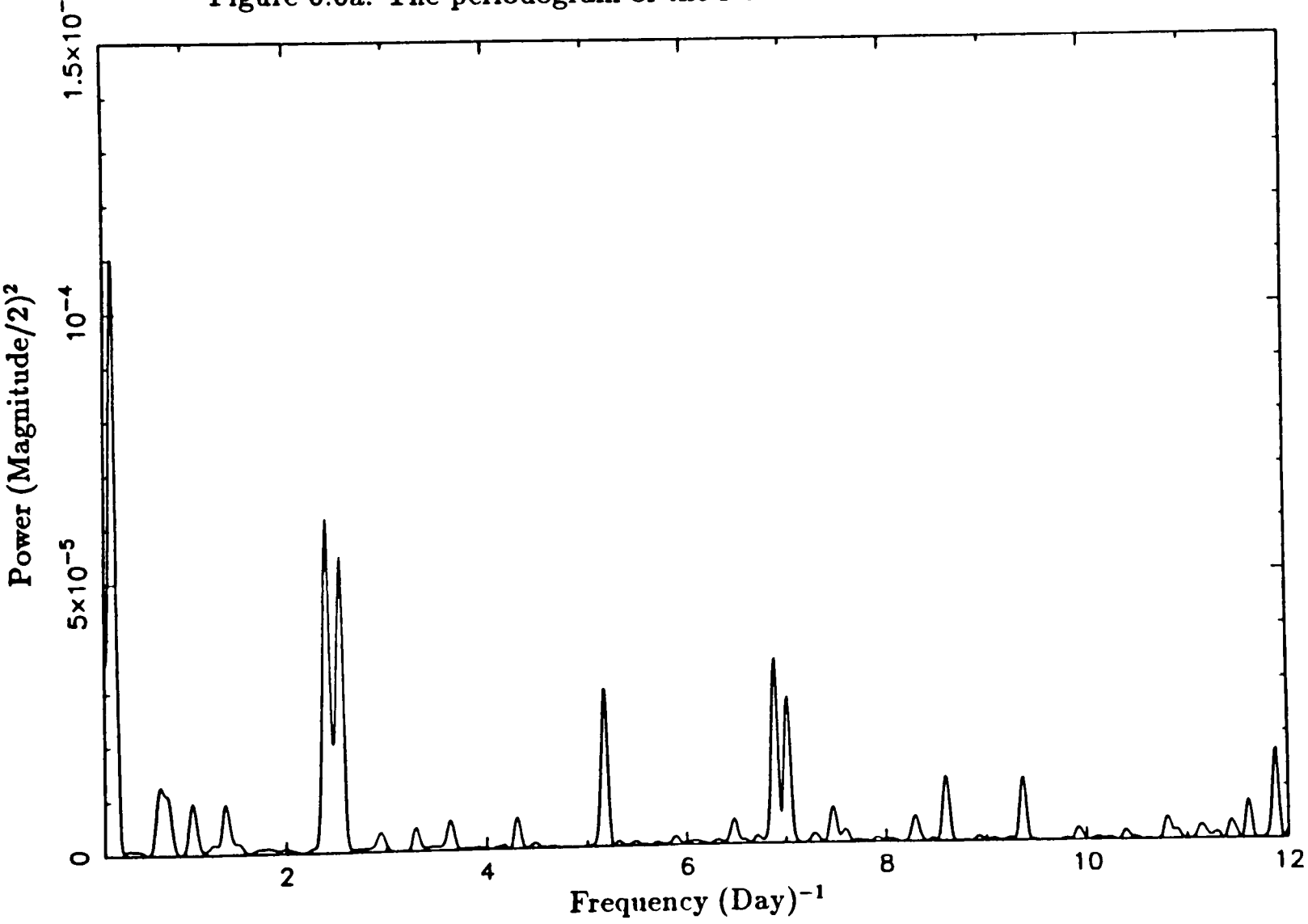

Figure 6.6b: The CLEAN periodogram of the November 1986 data

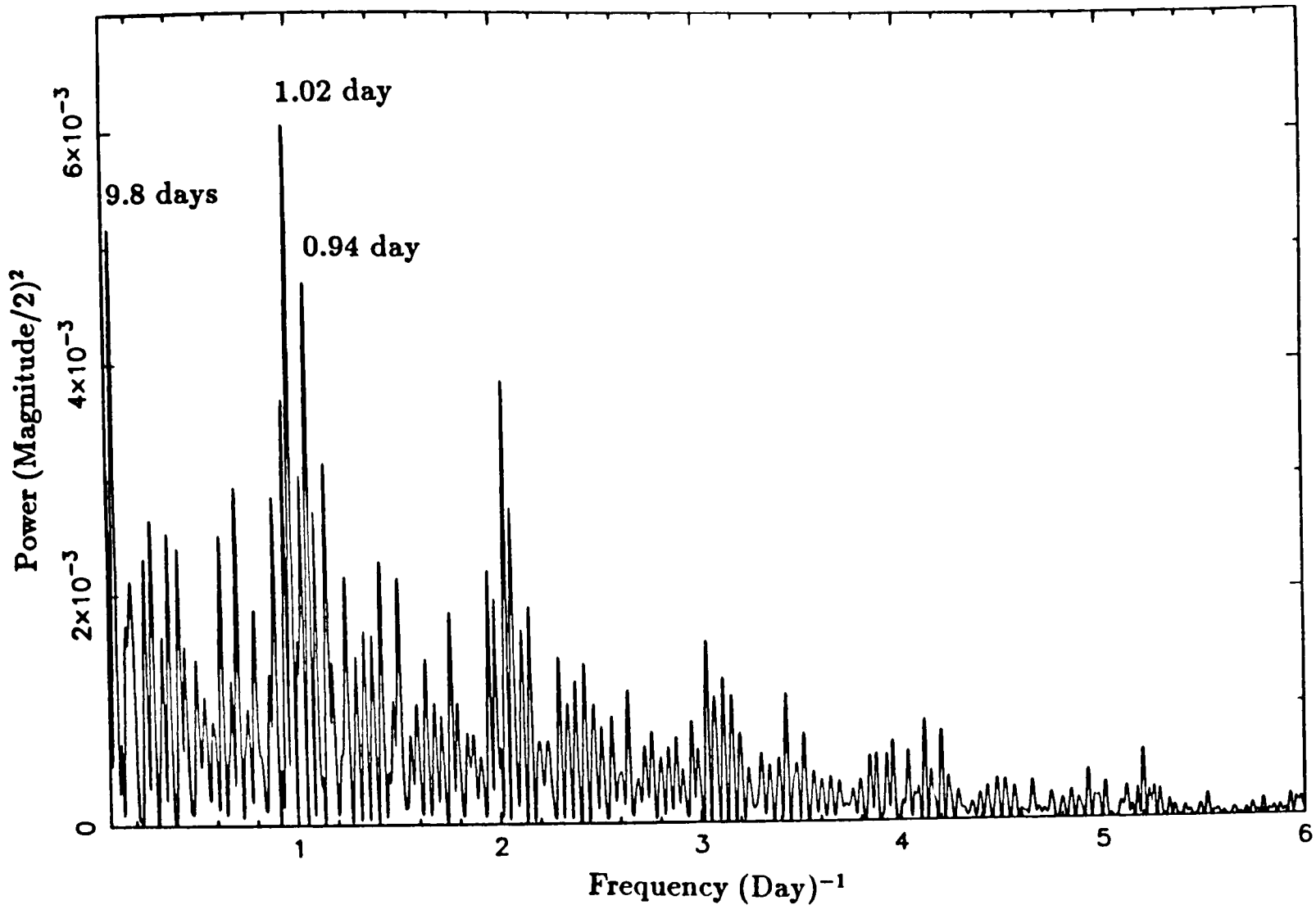

Figure 6.7a: The periodogram of the December 1987 data

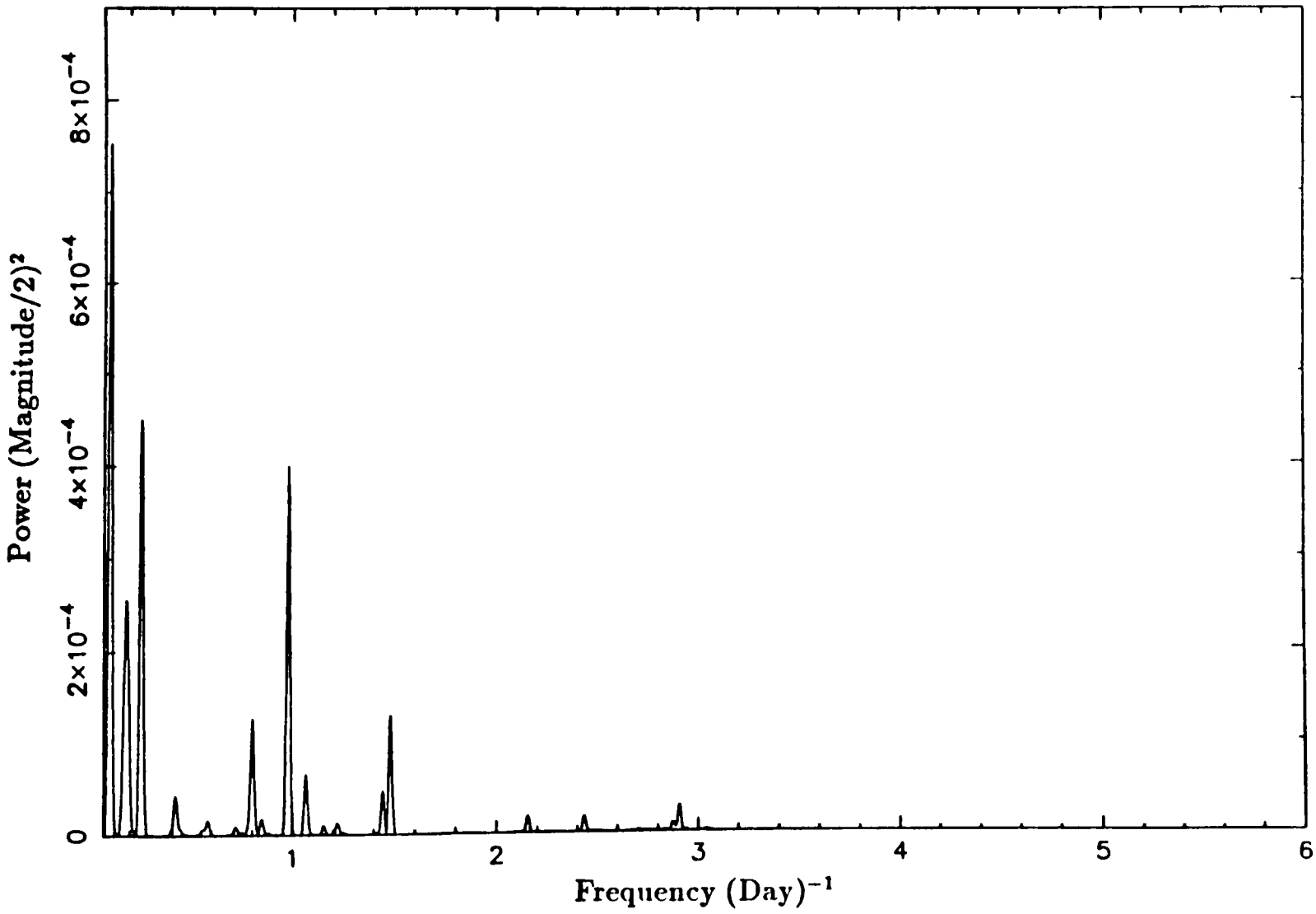

Figure 6.7b: The CLEAN periodogram of the December 1987 data

This process continues until a specified noise level is reached. The peaks found ("the clean components") are then convolved with a clean Gaussian beam whose width is ~1/(total observation span). These convolved peaks are then added back into the residual periodogram so as to preserve the noise level. The CLEANed power spectra of these two data sets are shown in Figures 6.6b and 6.7b respectively. The November 1986 variability at 0.93 days (and also 1.08 days) decreases to $\leq$0.007 magnitudes, whilst the December 1987 variability at 0.94 days decreases to $\leq$0.02 magnitudes. The effective disappearance of these periodicities when the one dimensional CLEAN algorithm is used confirms that their presence is due to incomplete data sampling and that they do not represent real periods in these data. However if the orbital period *is* ~1 day, then several days of continuous monitoring from different longitudes would be necessary to determine this unambiguously.

By examining the normal Fourier transform at periods between ~1–10 hours it was possible to place a limit of $\leq$0.1 magnitudes on the peak sinusoidal and hence orbital modulation.

No periodic modulations (~1 hr – 5 days) are present in any of these three data sets. However two of the three (November 1986, December 1987) do show modulation on a ~10 day timescale. This probably reflects a long term periodicity in the system. A light curve of the JKT–MDM 1987/1988 data folded on the 9.8 day periodogram peak is shown in Figure 6.8. The implications, for the system, of long timescale periodic variations are discussed in Section 6.3.3.

6.2.1b The 1989 Optical Photometry Results

The B band light curve of 4U0614+09 is shown in Figure 6.5. The relative

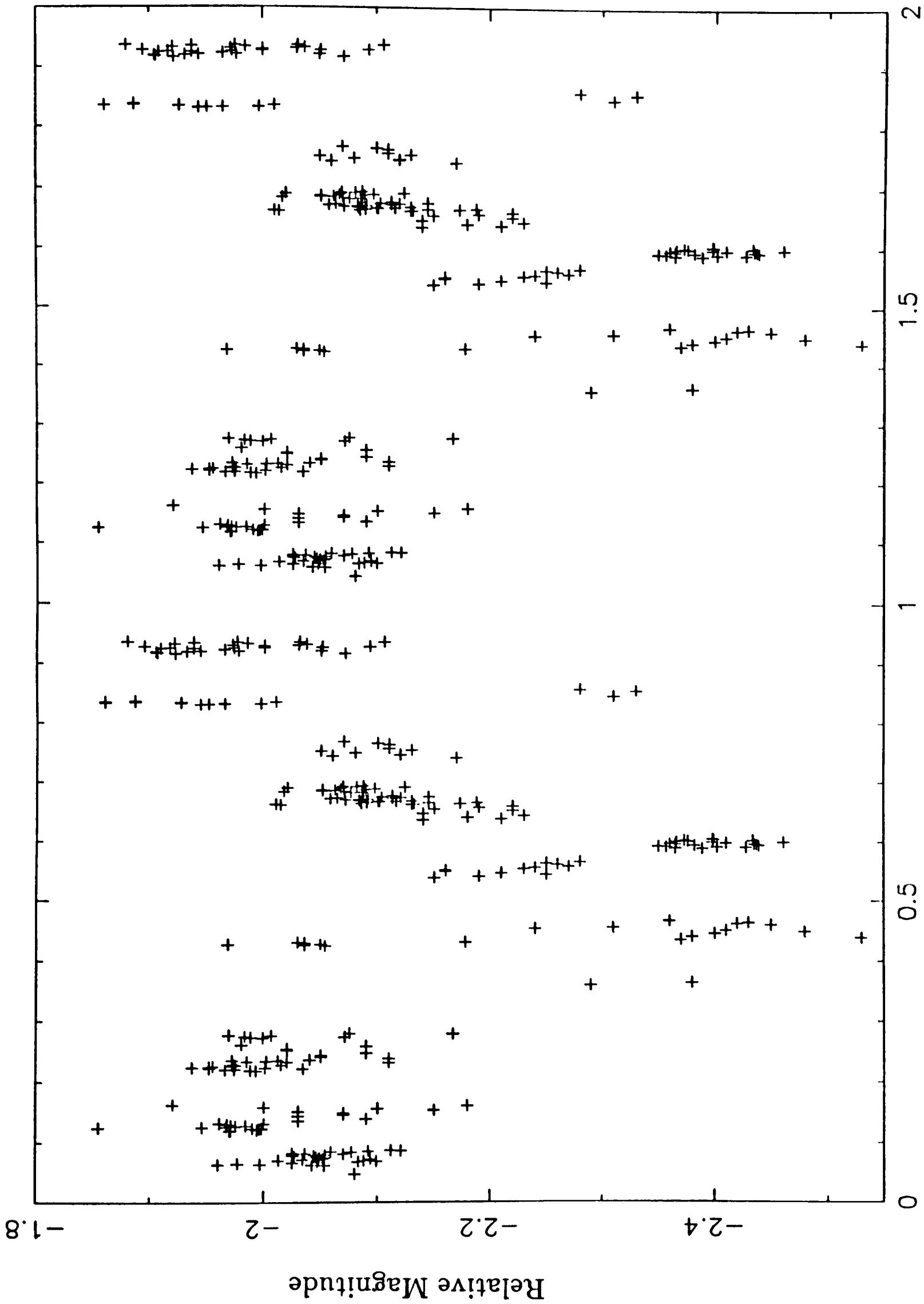

Figure 6.8: The December 1987 data folded on 9.8 days

difference between star 4 and star 8 is also shown. To obtain the best possible light curve any data points with errors (obtained from the DAOPHOT profile fitting photometry, Stetson1987) in excess of 0.03 magnitudes are neither plotted nor included in this analysis. The data from each night is plotted separately in Figures 6.9a–c. As can be seen from these plots the data from Nights 1 and 3 have dips that recur with ~1 hour periodicity. Periodograms of the data reveal the presence of significant power at ~65.1±5.8 minutes in the Night 1 and ~65.7±5.8 minutes in the Night 3 data sets. These periods are the same within the errors (derived from the FWHM of the periodogram peaks). The periodogram of the Night 2 data set does not show any power at this period, to a limit of ~0.008 magnitudes. Night 3 also shows peaks at ~0.2 days and ~30.2 minutes. Since the Night 3 data set is only ~0.35 days long and also because the ~0.2 day periodicity is not observed in the Night 1 or 2 data sets then the ~0.2 day variability observed on Night 3 is NOT periodic but is instead due to the intrinsic random variability of the source. A more sophisticated Fourier analysis was performed on each nights data using the one dimensional version of the CLEAN deconvolution algorithm (Roberts, Lehár and Dreher 1987). Each data set was prewhitened by subtracting a low order polynomial. The Night 3 data set was further prewhitened by subtracting a ~0.2 d sine wave. The results of these Fourier transforms are plotted in Figures 6.10a–c. The use of the more sophisticated FT algorithm confirms the results stated above. The peaks at ~65.3 minutes in the Night 1 and Night 3 periodograms overlap almost completely with the individual periods being the same to within 1% (<0.6 minutes). The fact that ~1 hour variability appears in two of the three data sets confirms its reality. Figures 6.11a and b shows the prewhitened data from Night 1 and Night 3 folded on the best period and binned into 10 equal phase

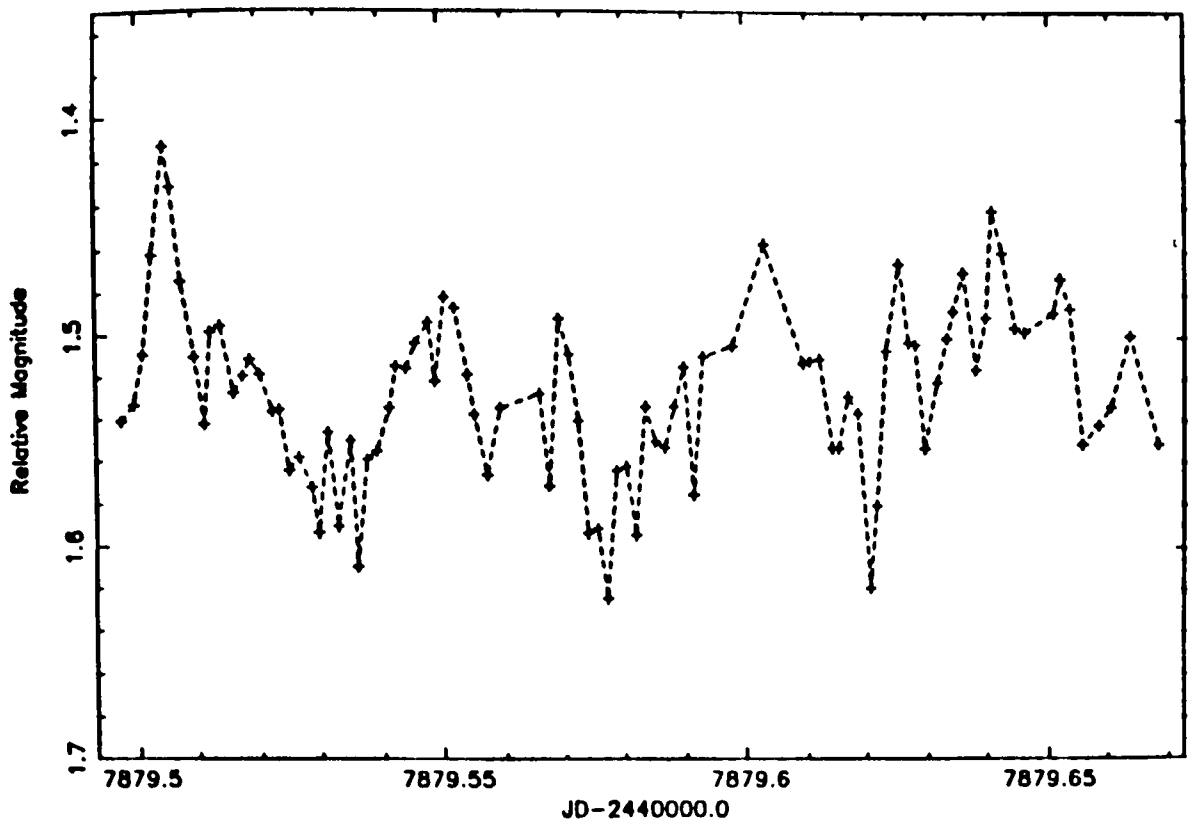

Figure 6.9a: Night 1: December 1989 optical photometry data

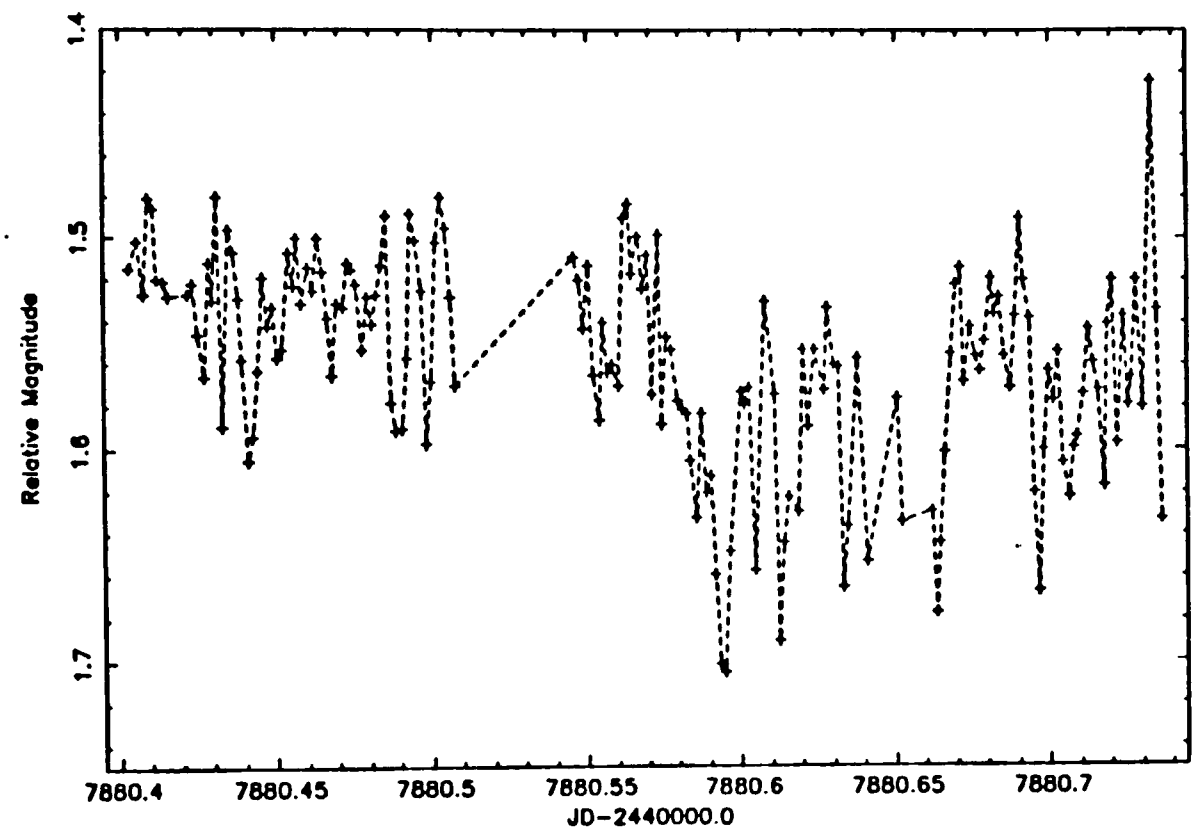

Figure 6.9b: Night 2: December 1989 optical photometry data

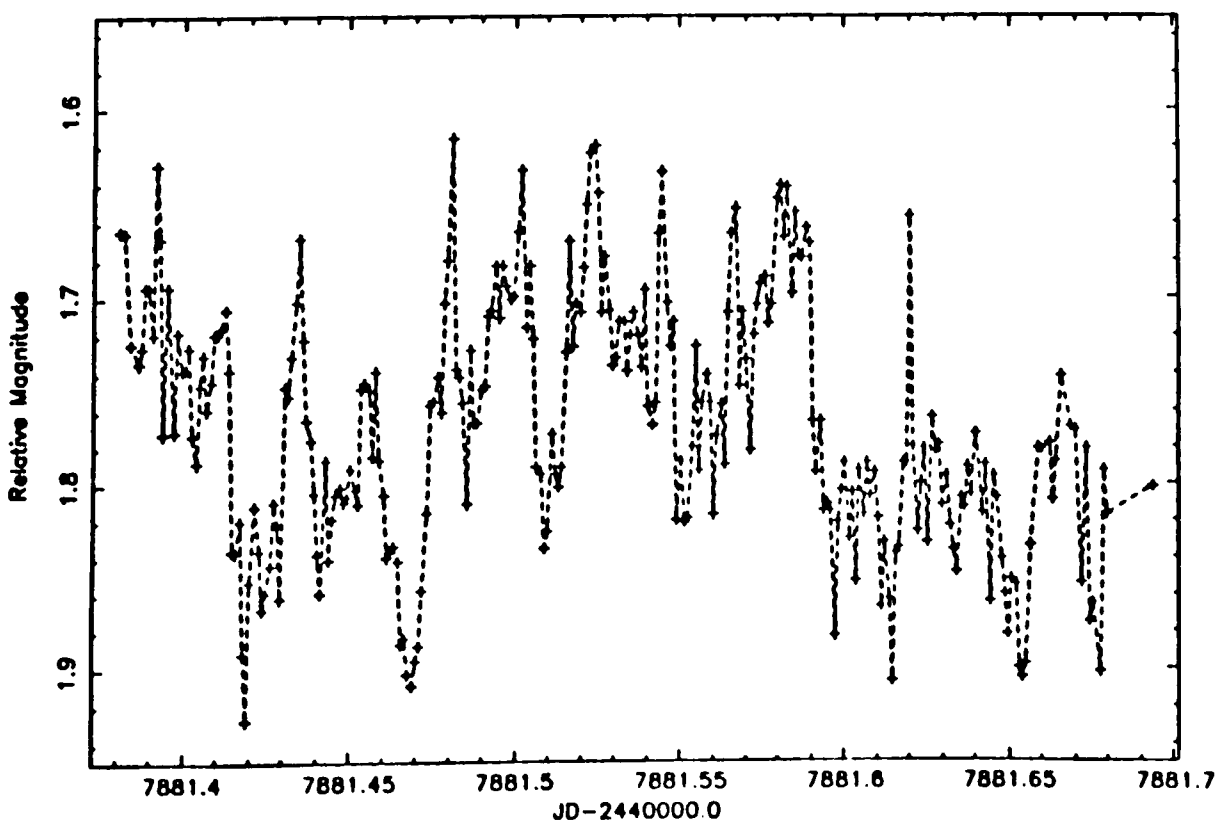

Figure 6.9c: Night 3: December 1989 optical photometry data

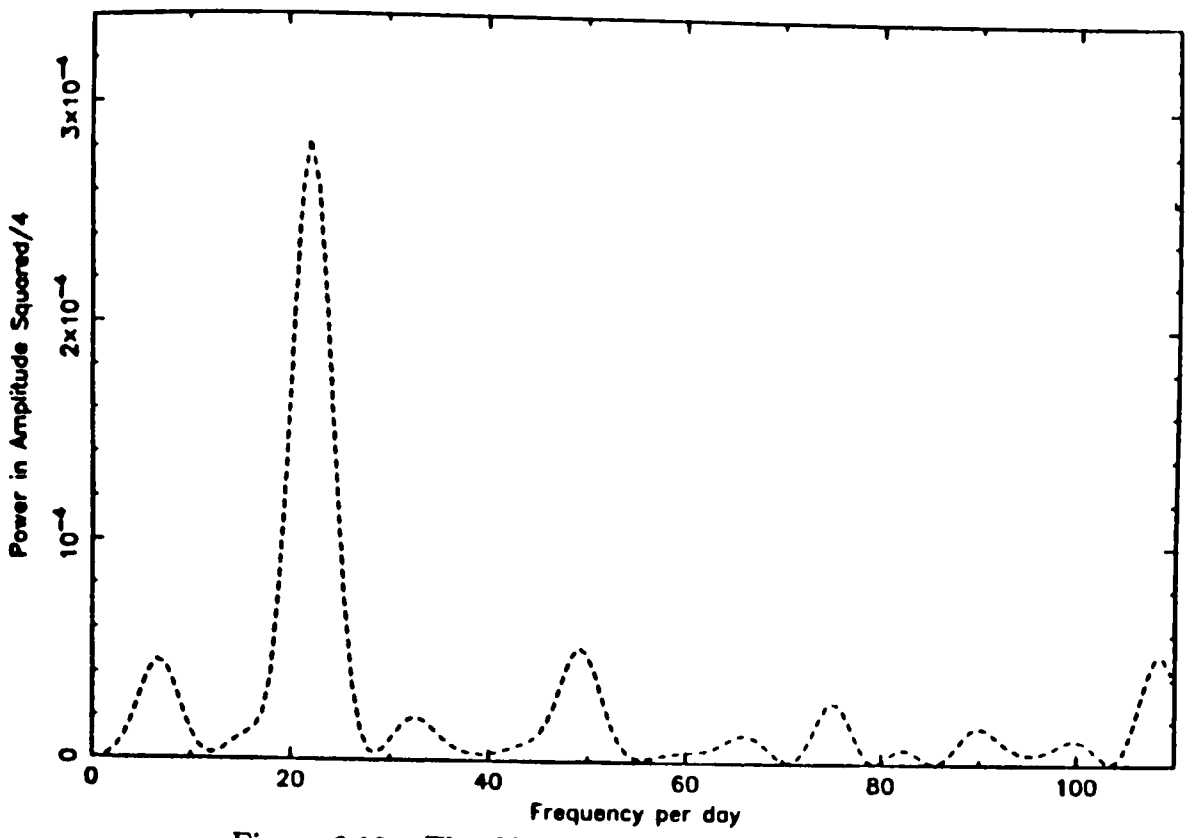

Figure 6.10a: The CLEAN power spectrum of Night 1

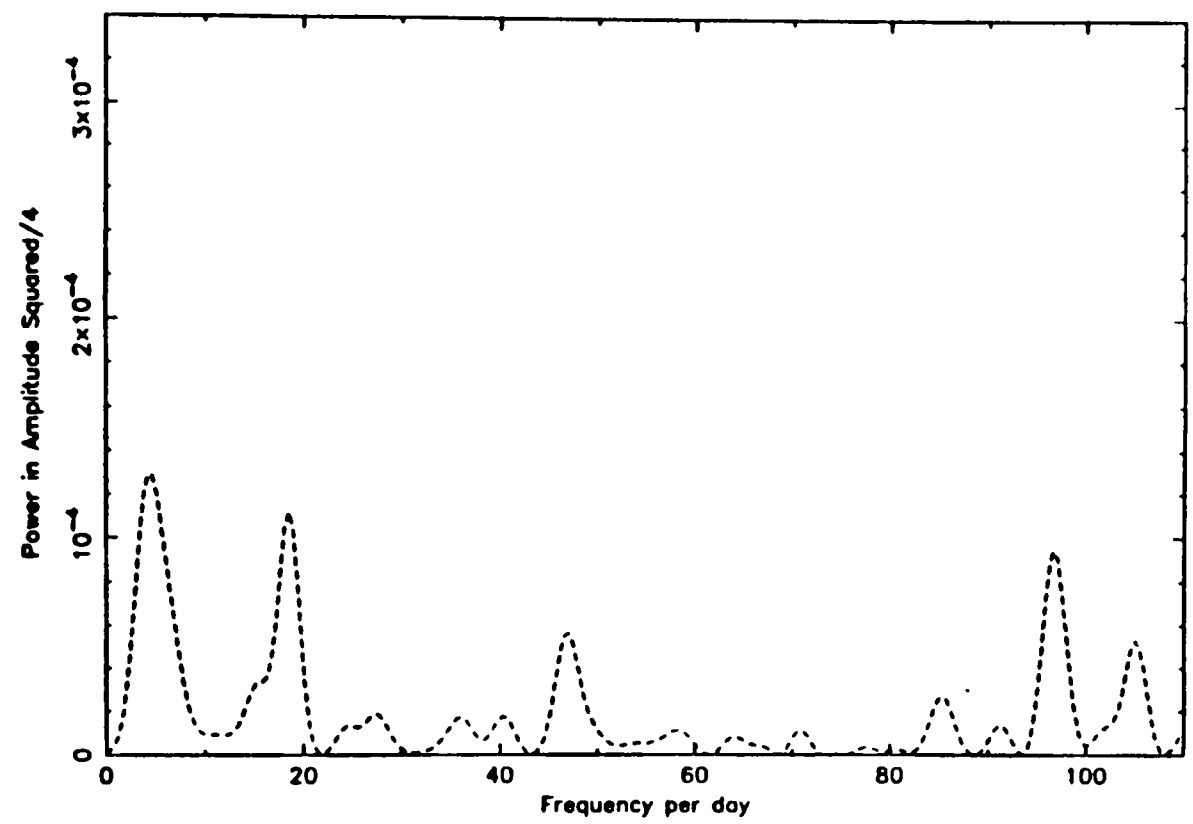

Figure 6.10b: The CLEAN power spectrum of Night 2

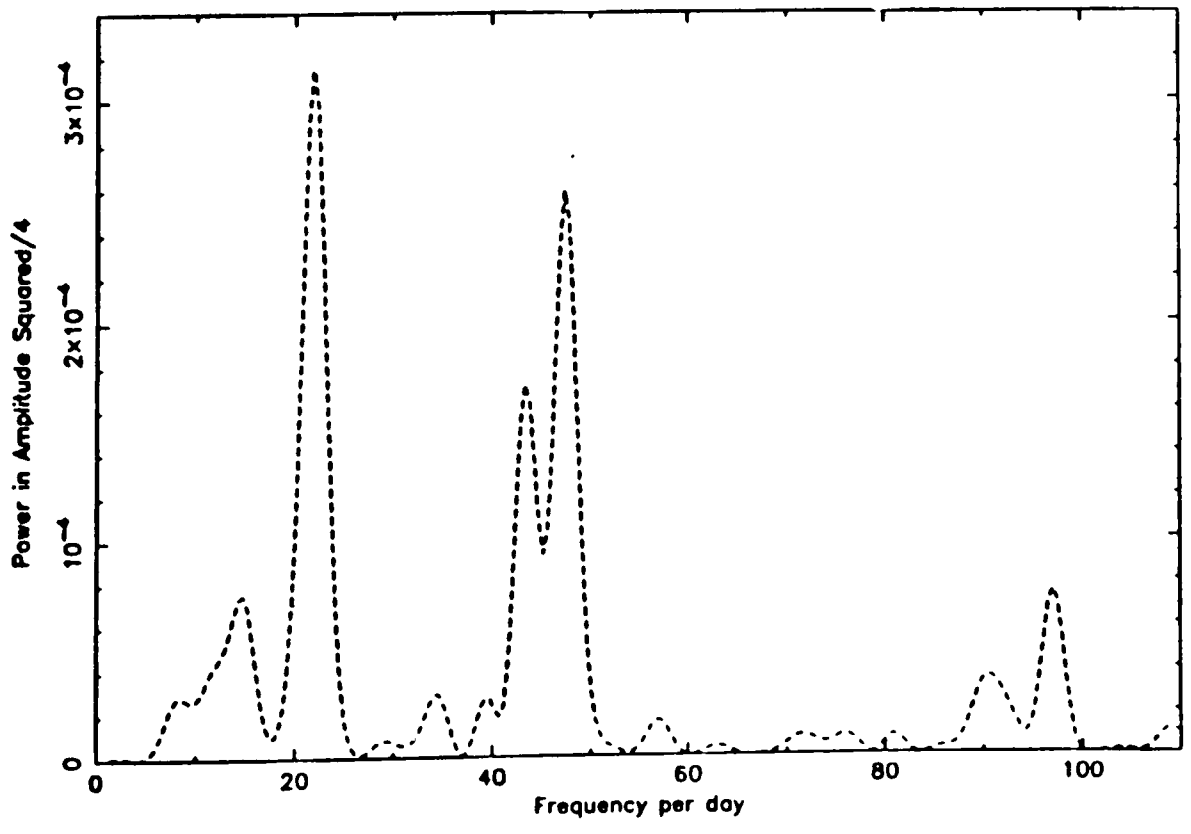

Figure 6.10c: The CLEAN power spectrum of Night 3

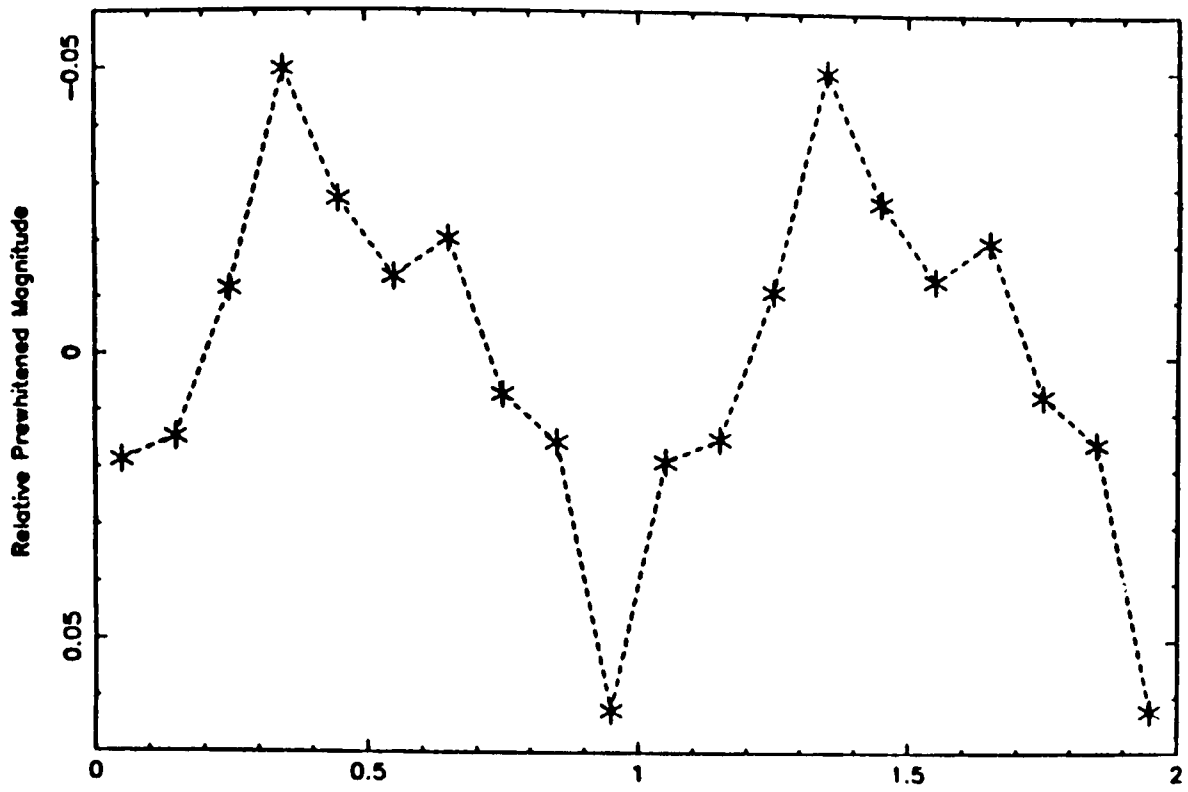

Figure 6.11a: Night 1 data, folded on 65.1 minutes,
binned into 10 equal phase bins

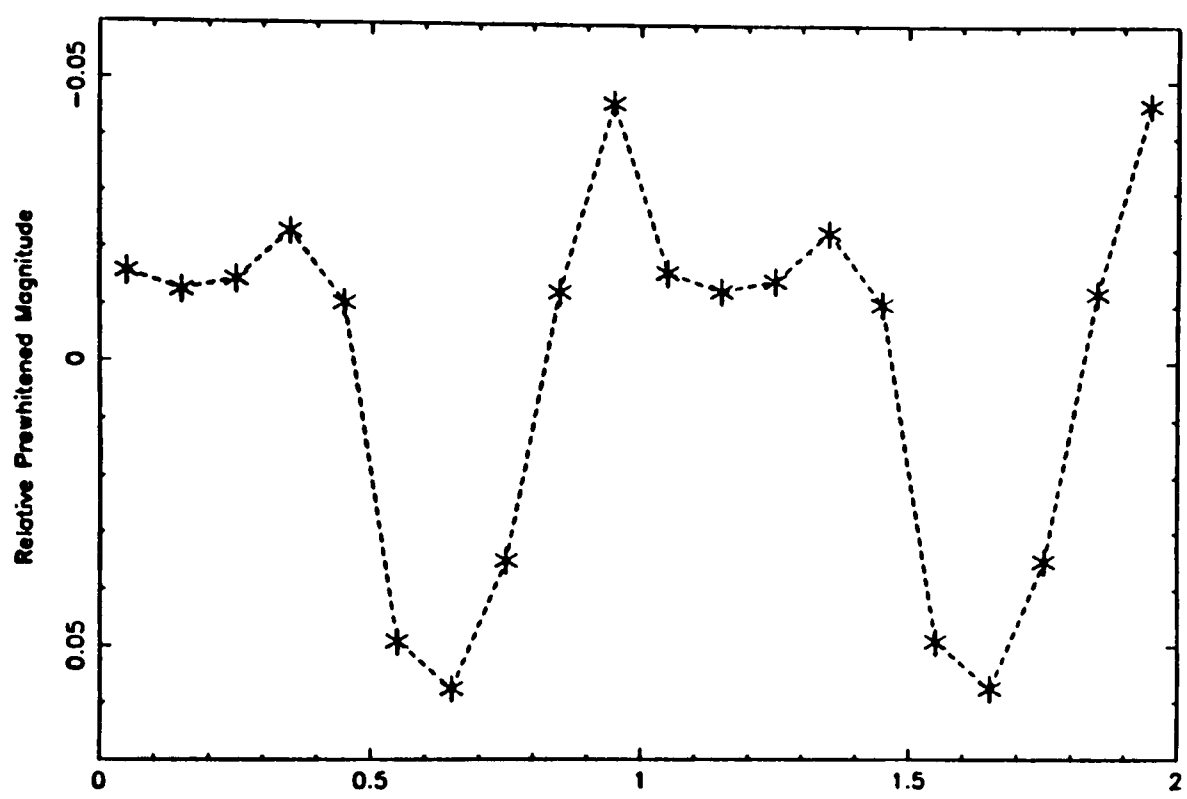

Figure 6.11b: Night 3 data, folded on 65.7 minutes,
binned into 10 equal phase bins

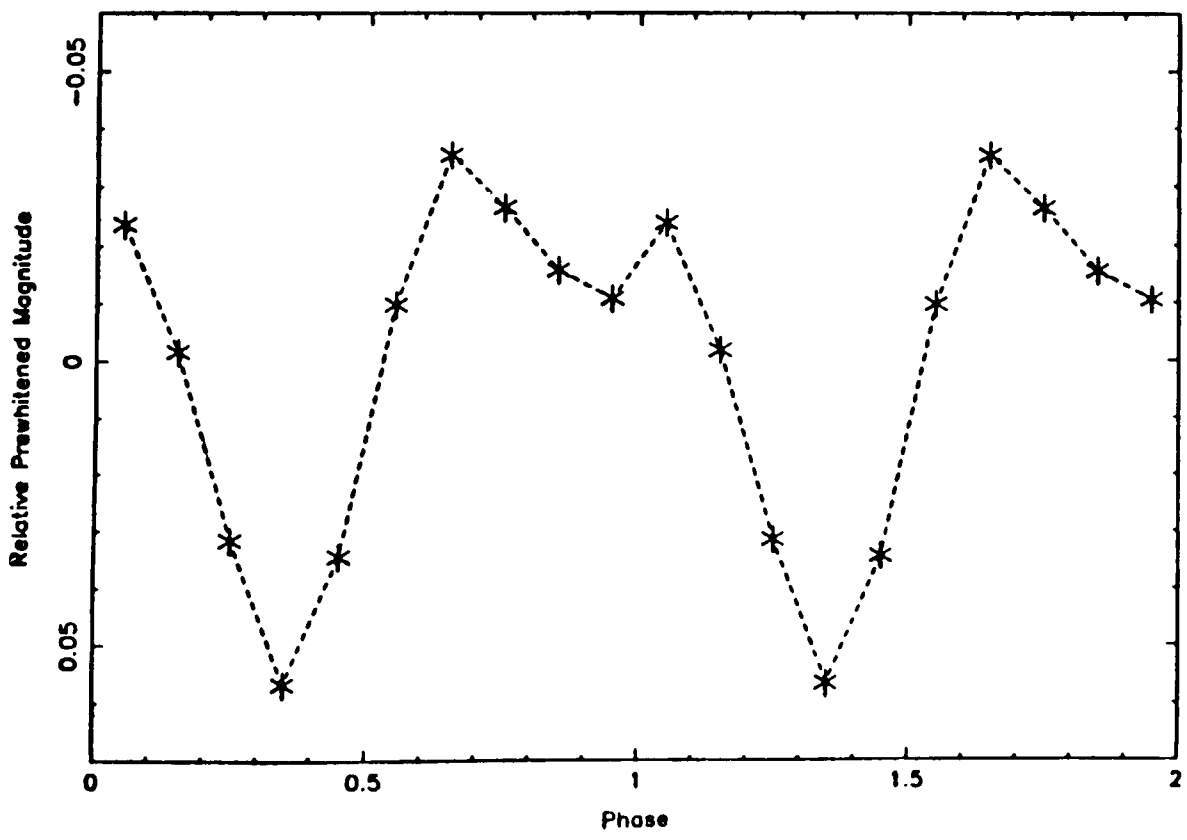

Figure 6.11c: Night 1 and Night 3 data, folded on 66.1 minutes,
binned into 10 equal phase bins

bins. Figure 6.11c shows the combined prewhitened data set (Night 1 and Night 3) folded on a period of ~66.1 minutes. Besides a dip of ~0.06 magnitudes these light curves seem to show two maxima per cycle, separated by ~20 minutes, with an "interdip" at the ~0.015 magnitude level. However, the reality of this feature must be questionable until its presence is confirmed by more observations.

The periodic variability could be the orbital period of the system or possibly some form of long period quasi–periodic oscillation (QPO).

6.2.2 Simultaneous EXOSAT and CCD photometry: Observations and Results

Simultaneous optical CCD photometry and EXOSAT Medium Energy Instrument (ME; Turner, Smith & Zimmermann 1981) observations were taken for ~14 hours on 12–13 February 1986 (Table 6.1). The optical observations are described in Section 6.2.1. During the observation half the array of proportional counters comprising the ME was offset by 2° to monitor the background. To allow for systematic differences, the detector halves viewing the source and background were alternated twice. The mean background spectrum was subtracted from the "on source" spectrum. The time resolution of the X–ray data was 1 s. The background–subtracted data was binned into 10 s intervals so as to improve its signal to noise. The background subtracted light curve is shown in Figure 6.12 along with the simultaneous optical photometry. The X–ray flux (1.2–3.8 keV) shows a gradual rise to maximum and is anticorrelated with the optical flux. The hardness ratio, defined as the ratio of the 3.9–7.7 keV to 1.2–3.8 keV flux, is shown in Figure 6.13 and is correlated with intensity.

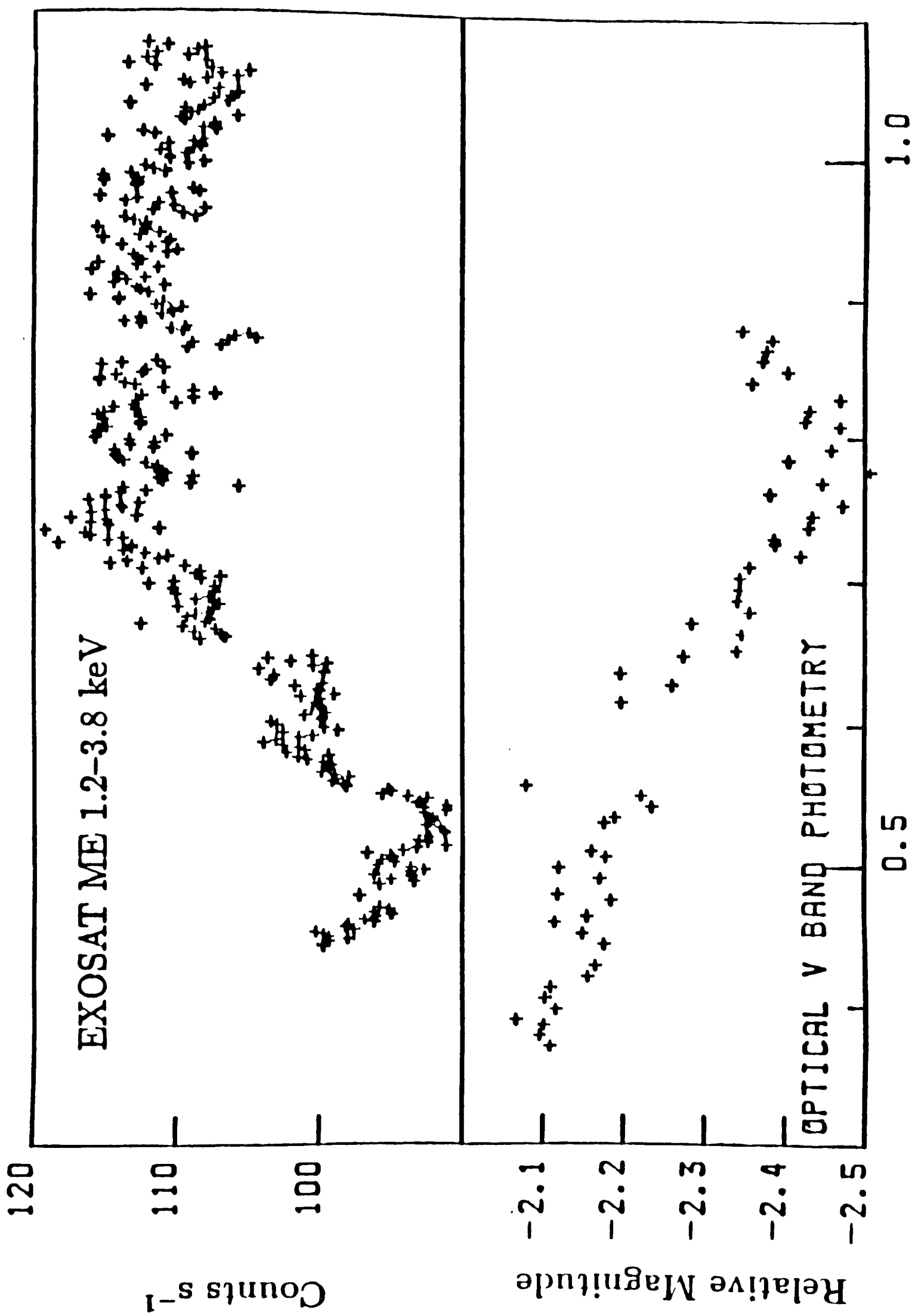

Figure 6.12: The February 1986 simultaneous EXOSAT ME and JKT observations

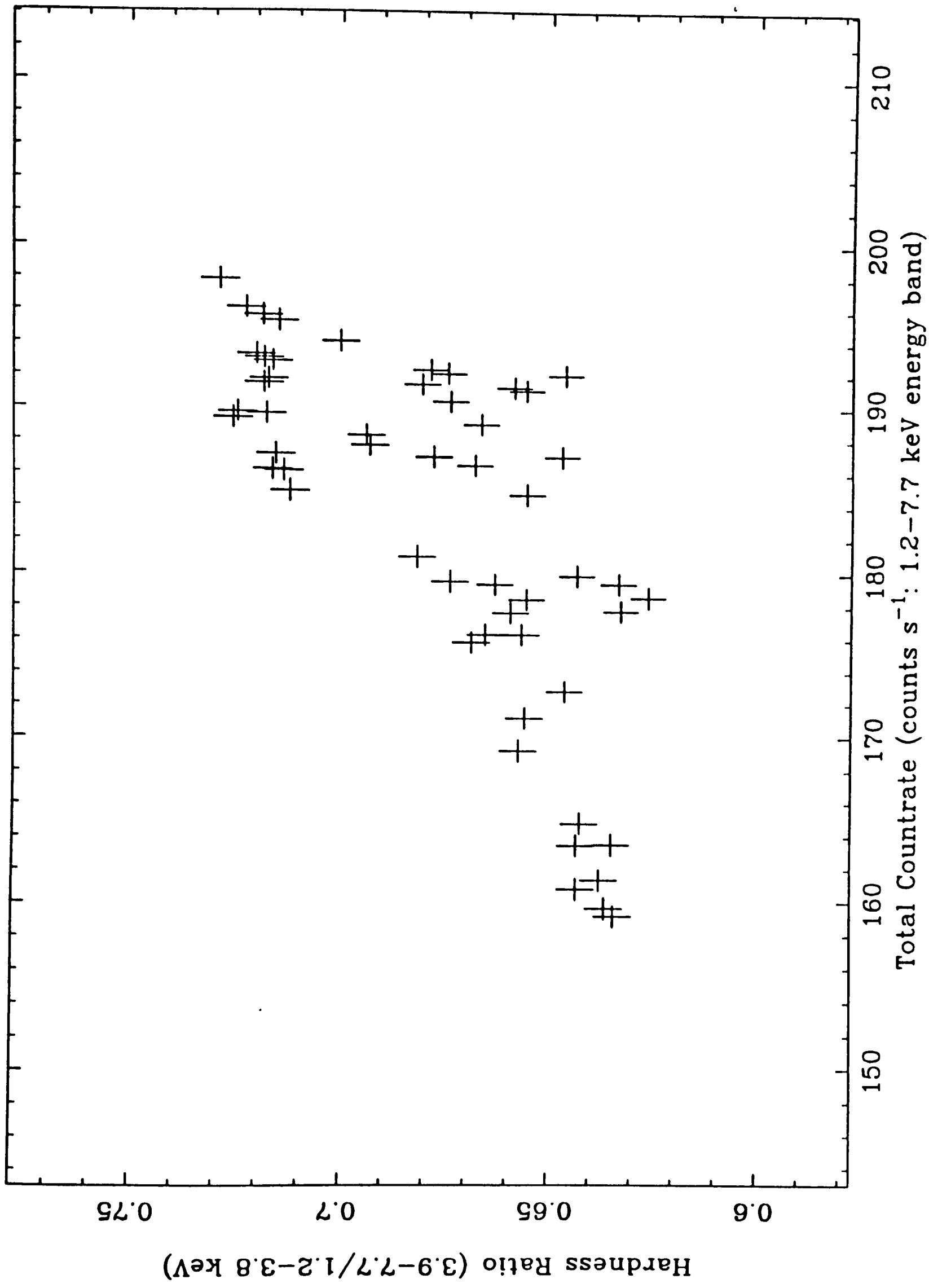

Figure 6.13: 4U0614+09 EXOSAT ME hardness ratio versus intensity

6.2.3 Optical Spectroscopy: Observations and Results

Spectroscopic observations of 4U0614+09 were carried out during February 1988 using the Faint Object Spectrograph (FOS, see Allington-Smith *et al.* 1989 and Section 2.2.2a for a description of the instrument) mounted at the Cassegrain focus of the 4.2-m WHT. Weather conditions were rarely photometric, often with variable cloud and poor seeing (>2″), therefore the absolute flux calibration is not reliable. All the observations were taken at low airmass (1.08–1.3). A 20″ long slit with a width of 1.5″ was used throughout. A log of the observations is given in Table 6.2.

Table 6.2 The Spectroscopy Observing log for 4U0614+09

Star	Date	Start times	Exposure	Magnitude†‡
–	1988	UT	times (s)	V
4U0614+09	08 Feb.	22:50 & 23:15 & 23:31	3×1000	19.4 (f)
4U0614+09	09 Feb.	23:00 & 23:45	2×2000	19.1 (f)
4U0614+09	10–11 Feb.	23:53 & 00:28	2×2000	19.3 (f)
4U0614+09	11 Feb.	22:47 & 23:19	2×2000	18.7 (b)
4U0614+09	13 Feb.	23:24 & 23:59	2×2000	18.3 (b)
4U0614+09	16 Feb.	22:55 & 23:30	2×2000	18.0 (b)

†Typical error ~0.2 magnitudes
‡f=faint state, b=bright state

The spectra were reduced using the optimal CCD spectral-extraction procedure of Horne (1986), as modified by Mukai (1990) described in Section 2.2.2a. The data were flux calibrated (for relative, not absolute fluxes) using observations of the flux standard HZ44 (Oke 1974).

6.2.3a Spectroscopy Results

Figure 6.14 shows the summed spectra of 4U0614+09. The only prominent feature that is visible in the spectrum is at ~λ4640–4660. The equivalent width of the feature is 4.3±0.6 Å (1σ error). No He II λ4686 emission is detected; the upper limit on the equivalent width is ≤0.9 Å (1σ error). The continuum is ill–defined in this region of the spectrum leading to difficulty in establishing an accurate upper limit on He II emission. Also the Balmer lines are absent with an upper limit for Hα emission being 1.5±0.8 Å equivalent width (1σ error). No ordinary stellar features were seen in the combined spectrum. An upper limit on the equivalent width of the interstellar line at λ4430 (Herbig 1975) is EW(4430)≤1.3±1.0 Å indicating that the object suffers only light reddening (E_{B-V}≤0.3±0.2, Allen 1973). This is consistent with the reddening given by FitzGerald (1968), with a colour excess in this region out to 1.5 kpc of 0.3 to 0.6. 4U0614+09 is at galactic longitude and latitude l=200.9° and b=–3.4° respectively. It breaks out of the 100 pc thick dust layer at about this distance and thereafter would not incur any further reddening. Also van Paradjis (1981) finds that the average $(B-V)_o$=0.0±0.3 for LMXBs and this is consistent with 4U0614+09 only being moderately reddened (E_{B-V}=0.3).

The spectra were grouped into *faint* and *bright* states; see Table 6.2. This grouping is fairly arbitrary because of the night to night variation in observing conditions. The equivalent width of the λ4640 feature was measured in the combined spectra for both states; in the *bright* state it was 4.0±1.5 Å and in the *faint* state 4.8±0.9 Å which to within the measurement errors are the same. No normal stellar features of any kind were found in either of the summed spectra.

Synthetic B and V magnitudes were obtained from each spectrum by folding

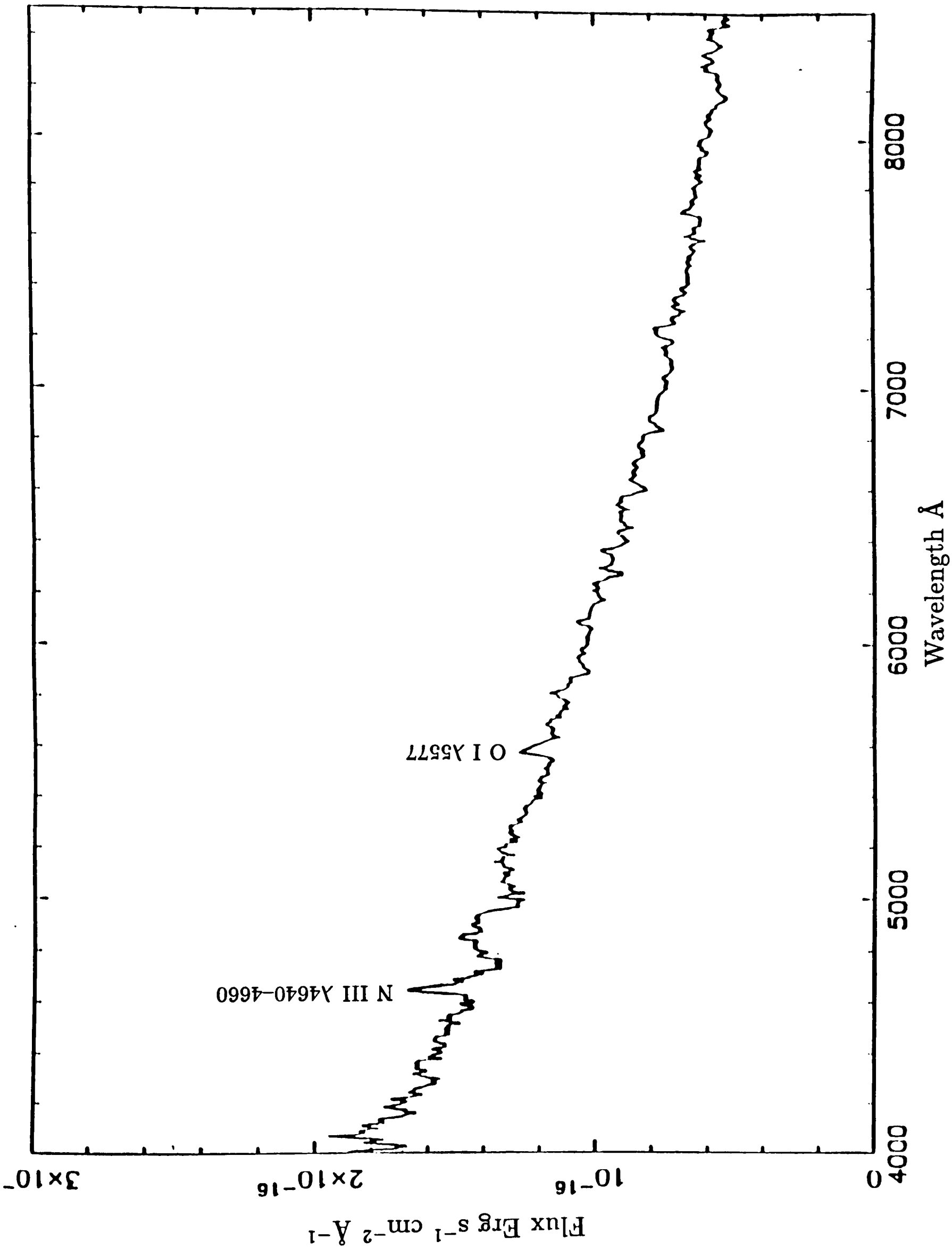

Figure 6.14: The summed spectrum of 4U0614+09

the Johnson filter response curves through each extracted spectrum (Johnson 1965, Tritton 1989). Because of the poor observing conditions the individual values differ by ~0.2 magnitudes. This represents the error in the value of V quoted in the last column of Table 6.2. However the B–V values are reliable and I have used the thirteen individual spectra to derive a mean B–V=0.32±0.02. This is consistent with the colour obtained from the JKT CCD Photometry. The analysis of the spectral data was performed using the Starlink FIGARO (Fuller 1989) and DIPSO (Howarth & Murray 1987) packages.

6.3 Discussion

6.3.1 X–ray Observations and Anticorrelated Optical Behaviour

The EXOSAT observation shows a broad minimum with a rise to an extended maximum. The flux variation is probably not dipping or eclipsing behaviour since the hardness ratio is well correlated with intensity. An anticorrelation would have been expected if the flux changes were produced by photoelectric absorption since soft X–rays are preferentially absorbed with respect to hard X–rays (eg. White and Swank 1982). Irregular flux changes on timescales of ~1 hour and correlated intensity/hardness ratio behaviour is a characteristic feature of some LMXBs (Mason *et al.* 1976). Provided the orbital period of 4U0614+09 is less than the duration of the EXOSAT observation one can infer from the absence of dipping or eclipsing behaviour that the inclination is $\leq 70°$, since systems with $i \geq 70°$ often show dipping behaviour caused by accretion disc structure at the disc edge occulting the central X–ray source (White 1989 and Section 1.3b).

The anticorrelated optical and X–ray behaviour is most unusual. One would expect the observed X–ray and optical fluxes to be correlated since most of the optical radiation is thought to be produced by the reprocessing of X–rays in an accretion disc. Anticorrelated X–ray/optical flux behaviour has been observed previously only in three systems, 4U1735–444 (Smale *et al.* 1986), Sco X–1 in the normal branch (Priedhorsky *et al.* 1986) and GX339–4 (Motch *et al.* 1983).

A possible way of explaining the anticorrelation is if the reprocessing area is anticorrelated in some way with the X–ray luminosity, and indeed Priedhorsky (1986) found that it is possible for the mass accretion rate (and hence the reprocessing area) to be anticorrelated with the X–ray luminosity. Smale *et al.* (1986) use this argument to explain the anticorrelation they observed between the X–ray and optical fluxes in 4U1735–444. However more extensive observations by Corbet *et al.* (1989) of 4U1735–444 showed that a large proportion of the optical modulation seen by Smale *et al.* (1986) could be accounted for by orbital variations. They suggest that the observed anticorrelation was probably due to the intrinsic chaotic variability of the X–ray flux.

Another alternative is if the optical emission and the X–ray emission originate from different but physically connected regions. Fabian *et al.* (1982) explain the short timescale (~20 s) anticorrelation seen in the optical and X–ray fluxes of GX339–4 (Motch *et al.* 1983) in terms of a model that has two emission regions, the optical radiation being due to optically thick cyclotron emission produced by hot clouds (kT~100 keV) near to the neutron star, whilst the X–ray emission is produced in cooler regions (kT~few keV).

However there exists at the moment no fully satisfactory explanation of the observed anticorrelated behaviour between the X–ray and optical fluxes.

6.3.2 The Absence of He II λ4686

The spectrum of 4U0614+09 is dominated by an emission feature at λ4640–4660. Various authors have attributed the presence of this feature in other LMXBs to the Bowen process (McClintock, Canizares & Tarter 1975; Deguchi 1985). The Bowen process is initiated by a chance coincidence of frequencies in the He II Lyα λ303.8 and O III λ303.8 line. A fraction of the O III photons (at λ374) which are created by the cascade through the O III energy ladder are absorbed again by N III and produce N III emission lines (including the blend at λ4640–4660). Other fluorescence lines are also formed in this process, notably O III lines. These lines have been observed in other LMXBs: e.g. 4U1735–444, 4U1636–53 and MXB1659–29 (Canizares, McClintock & Grindlay 1979) confirming that the Bowen process is active in at least these cases.

4U0614+09 is unusual in that it only shows λ4640–4660 and not He II λ4686. This is curious because in the Bowen blend process these spectral line formation regions are believed to be coincident. The presence of He II is necessary to produce Bowen blend emission. The He II λ4686 and He II Lyα are formed by the same physical process, electron recombination. Motch & Pakull (1989) find that all LMXB that have been studied spectroscopically show both the Bowen blend and the He II λ4686 line, in contrast to what is observed for 4U0614+09. They also find that the ratio of N $III_{4640-4660}$ to He II_{4686} (hereafter ζ) was >1 for some LMXBs (up to a maximum value of 1.5 for Sco X–1); for 4U0614+09 this ratio is >2.5 (90% confidence limit). Deguchi (1985) found that in his models of Bowen fluorescence the maximum allowable value for ζ is 0.4 if formed by the standard Bowen process. The anomalously large value of ζ observed for 4U0614+09 and for other LMXBs has at least 2 possible causes.

i) A metallicity effect. Motch & Pakull (1989) suggest that ζ is a metallicity

indicator. They point out that the optically identified LMC sources have very weak or no N III λ4640–4660 even though the metallicity of the LMC is only a factor of 2–4 less than the galactic metallicity (Westerlund 1990). Also AC211, the optical counterpart to the M15 X–ray source (Aurière *et al.* 1984), displays strong He II λ4686 but the N III λ4640–4660 blend is absent (for sample spectra see Figure 3 of Naylor *et al.* 1988). The latter case is almost certainly a metallicity effect since M15 has [Fe/H]=–2.1 (Webbink 1985). Motch & Pakull (1989) state that the galactic sources are probably formed with a wide range of metallicity. I suggest that the relatively high value of ζ in 4U0614+09 can be at least partially explained if the system has a higher than average metallicity relative to other galactic LMXB. This effect may be lead to an increased contribution of the non–fluorescence C III and O II lines to the λ4640–4660 blend. It might be possible to test this hypothesis by looking for lines of C III or O II in the spectrum. Unfortunately most of these lines are either weak or shortward of λ4000 where the spectra become too noisy to identify spectral features.

ii) Deguchi (1985) finds that the value of ζ can be increased if the electron collision mechanism (rather than the more usual electron recombination mechanism) is used to excite the He II Lyα line. This process has the effect of reducing the He II λ4686 flux by up to a factor $\sim$3 and could be operating in several LMXBs as well as in 4U0614+09 and may contribute to the excess of N III λ4640–4660 over He II λ4686.

One or both of these factors may cause the spectral feature at $\sim\lambda$4650 to be strengthened with respect to He II λ4686. A high resolution, high S/N spectrum of 4U0614+09 between λ3400–5000 would prove invaluable in understanding this system. This would permit a search for other Bowen fluorescence lines (especially for O III λ3444) so as to confirm that the Bowen process operates

here. Also it would be useful in looking for evidence of increased metallicity. However this will be difficult due to the intrinsic faintness of the source.

6.3.3 Long Timescale Photometric Variations

The November 1986 optical photometry of 4U0614+09 shows that the source faded and then subsequently brightened on a timescale of approximately 10 days. Also the December 1987 light curve exhibits two dips separated by 10 days. The absence of late type spectral features implies that the ~10 day optical variations are not orbital. The long period systems Cyg X–2 (P_{orb}~9.8 days; Cowley, Crampton & Hutchings 1979) and 2S0921–630 (P_{orb}~9 days; Branduardi-Raymont *et al.* 1983) both show stellar absorption features indicative of the secondary in these systems being an F–type sub–giant. Davidsen *et al.* (1974) estimate the distance of 4U0614+09 to be ~4–8 kpc. This indicates that 4U0614+09 is intrinsically fainter (V~18.8, d$\leq$8 kpc) than either Cyg X–2 (V~15, d~8 kpc) or 2S0921–630 (V~17, d~10 kpc). In the latter two systems the sub–giant secondary stars make substantial (or even dominant) contributions to the optical output. The absence of stellar absorption features and the intrinsic faintness of 4U0614+09 argue against the orbital period being 10 days.

If the 10 day variation is not orbital then what is it? The higher mass systems Her X–1 (P_{orb}=1.7 days; Gerend & Boynton 1976) and LMC X–4 (P_{orb}=1.4 days; Lang *et al.* 1981) have been extensively studied. Both display long term variations that are consistent with the precession of an accretion disc about the orbital plane with a period of ~30 days. These long timescale variations were first detected in large X–ray data sets (Tananbaum *et al.* 1972; Lang *et al.* 1981), with optical confirmation of these periods coming later (Deeter *et al.*

1976; Ilovaisky *et al.* 1984). I suggest that the 10 day modulation is caused by the precession of an accretion disc, the optical modulation arising from apparent changes in disc area. It is not clear how the 5 day X–ray periodicity detected by Marshall & Millit (1981) can be incorporated into this picture. It is possible to scale the precession period (P_{disc}) of Her X–1 to 4U0614+09 to infer the orbital period (P_{orb}) of 4U0614+09 by inverting the calculation of Priedhorsky & Terrell (1984),

$$P_{orb}=P_{disc}AR_n^{3/2}\rho^{3/2}\ q(1+q)^{-1/2} \qquad 6.1$$

where A=0.25 is a normalisation applicable to Her X–1, $q=M_{comp}/M_n$ and R_n is the ratio of the neutron star Roche lobe radius to the binary separation. R_n can be obtained from the equation $R_n=0.38-0.2\log_{10}(q)$ provided $0.05<q<3$ (Paczyński 1971). The radius of the Roche lobe is usually defined as an "average radius", r, so that $(4/3)\pi r^3$ is equal to the volume of the Roche lobe. The ratio of the neutron star Roche lobe radius to the disc radius, ρ is assumed to be $\sim$1 since the accretion disc is thought to fill the Roche lobe (van Paradjis 1981 and references therein). This gives an orbital period of between 7.2 and 8.5 hours (assuming $0.5\leq q\leq 0.7$). If ρ=0.5 then the orbital period range is 2.5 to 3.0 hours. Both orbital period ranges are consistent with the known binary period distribution of LMXBs (Parmar & White 1988). However, no periodic modulations on these timescales were detected. Any such modulations could be masked if they are at a low level when compared to the systems intrinsically high random optical variability. This could be the case if the inclination is low. Alternatively the orbital period could be very short ($\sim$30–60 minutes) in which case it would not be detected in this data because of poor time resolution. Equation 6.1 predicts that if the orbital period is short then the mass

ratio must be extreme. For example a period of 1 hour gives q<0.12 for ρ=0.5 and q<0.05 for ρ=1.

6.3.4 Short Timescale Photometric Variations

The December 1989 optical photometry of 4U0614+09 showed strong modulation on a ~1 hour timescale. This modulation could be the systems orbital period or possibly long timescale QPO. I consider both these possibilities, in reverse order, below. I then go on to discuss the implications, for 4U0614+09, of a short orbital period.

QPO

QPO is a common phenomena among LMXBs. It is usually manifest as fast (~Hz), quasi–coherent oscillations (for 10's to 1000's of cycles) in their X–ray light curves (van der Klis 1989). Several LMXBs show *long* timescale QPO (~mHz) notably 4U1626–67, Cyg X–3 and 4U1820–30 (van der Klis 1989). Also GX339–4 exhibits QPO on a ~50 mHz timescale in both in the optical and X–ray wavebands (Motch *et al.* 1983) though its oscillations are two orders of magnitude faster than those observed here. The oscillations that are present here are transient and therefore resemble long timescale QPO. This may not be a valid interpretation of the data because the period of oscillation (~0.3 mHz) is well outside the observed range of slow QPO (~0.7–20 mHz). Also the oscillations are coherent over two days which is not usually the case for QPO. Note that no satisfactory explanation has been put forward for the presence of these slow, transient oscillations. They are probably unrelated to the shorter timescale QPO (van der Klis 1989).

Orbital Modulations

Instead of slow QPO the ~1 hour optical modulation could reflect the orbital period of the system. The observed modulation could be caused by the changing aspect of an accretion disc bulge, the precession of an axisymmetric disc or the changing aspect of an X–ray heated secondary. I discuss these three possibilities, in turn, below.

4U0614+09 may be similar to the short period ($P_{orb}\simeq$50 minutes), bursting dipping LMXB 4U1916–05. Schmidtke (1988) using optical photometry derives a value of $M_V\simeq3.3\pm0.9$ (d=8.4 kpc, Smale *et al.* 1988) for the disc of 4U1916–05. The mean absolute magnitude for LMXBs is $M_V\sim1$ (van Paradjis 1981). 4U1916–05 is fainter than normal LMXBs because its disc is small. 4U0614+09 has a similarly faint disc with $4.9>M_V>3.3$ for a distance range of 4–8 kpc (Davidsen *et al.* 1974) and $A_V\sim1$. The intrinsic faintness of 4U0614+09 implies that it is a compact system with a short orbital period.

The orbital period of 4U1916–05 was obtained by studying the recurrence time of dips in its X–ray light curve (White and Swank 1982). Optical modulation on this timescale was subsequently discovered by Grindlay *et al.* (1988). From the absence of eclipses in the X–ray light curve of 4U1916–05 Smale *et al.* (1988) estimate its inclination to be $\leq$79°. Dips are not present in the EXOSAT light curves of 4U0614+09 (Corbet 1990 and Section 6.3.1) therefore its inclination must be lower than that of 4U1916–05. The absence of such features in these light curves imply an inclination of $\leq$70°.

Grindlay *et al.* (1988) suggest that the periodic optical modulation observed in the light curve of 4U1916–05 (amplitude δm~0.6) is caused by the partial

eclipse of an X–ray heated accretion disc bulge by the secondary star. Since the accretion disc bulge on the disc edge is a fixed feature in the binary reference frame, it reflects the binary motion of the system. The inner surface of the bulge (and also the inward facing accretion disk rim) is optically bright because it is heated by the central X–ray source (Mason 1990). 4U0614+09 has a lower inclination than 4U1916–05 and therefore no eclipse of its accretion disc bulge is possible. However periodic optical modulations will still be observable, though at a lower amplitude (for 4U0614+09 this is δm$\sim$0.1), because the X–ray heated inner surface of the bulge will change its projected area around the orbital cycle. *I suggest that the observed periodic modulation is produced in this way.* Such optical modulations, both the one described above and the more usual variation due to the X–ray heating of the secondary, are important for low i systems. This is because they are observable over a much wider range of inclination angle than X–ray modulations. This type of optical modulation has lead to the discovery of orbital periods for several low inclination LMXBs eg: Sco X–1 (Miyamoto and Matsuoka 1977) and 4U1636–536 (Smale and Mukai 1988).

The absence of the $\sim$1 hour modulation from the Night 2 data can be explained by assuming that the physical size of the vertical structure on the edge of the accretion disc is highly variable. Such variation is commonly observed in the X–ray light curves of dipping LMXBs (White 1989). For example Smale *et al.* (1988) found that the X–ray dips (caused by such structure) of 4U1916–05 were highly complex, varying dramatically in appearance from cycle to cycle. Their X–ray light curves sometimes displayed no dips whilst on other occasions they were continually subject to dipping events. The $\sim$1 hour optical modulation and its transient appearance can therefore be explained in terms of the above

model.

Smale *et al.* (1988) reports the presence of a second X–ray dip removed ~0.5–0.6 in phase from the first. This was interpreted by them as a second bulge on the accretion disc edge. This "duel dip" phenomena has been observed in other LMXBs (Mason 1990). The December 1989 folded light curve (Figures 6.11a–c) provides tentative evidence for two peaks in optical luminosity. The two peaks being separated by ~0.4 in phase (peak to peak). This could be interpreted as evidence for a second bulge on the accretion disc edge, the second maxima being produced when the second X–ray heated bulge moves into the observers line of sight. The large dip (amplitude ~0.06 magnitudes!) in the light curve is produced when the two bulges present their outer rims to the observer. Note that the reality of this "interdip" feature is questionable and only further extensive observations will confirm its existence.

The optical period (Grindlay 1990) of 4U1916–05 is ~1% longer than the X–ray dip period (Smale *et al.* 1988). Since the X–ray period derived for the dipping, *eclipsing* X–ray binaries has proved to be the orbital period, White (1989) has suggested that the X–ray period is the orbital period. He further speculated that the period difference may be related in some way to the superhump phenomena observed in SU UMa stars. The axisymmetric accretion discs (Whitehurst 1988) in these systems precess slowly, usually at a rate of a few percent of an orbital period per orbital period. Therefore the maximum projected area of the axisymmetric disc (and hence the maximum optical luminosity of the system) will recur periodically (from an observers point of view) on a timescale that is a few percent larger than the orbital period. This could explain the ~1% difference between the X–ray and optical periods observed for 4U1916–05. It

is possible that this "superhump" effect also produces the observed periodic optical modulation observed for 4U0614+09. This would mean that the actual orbital period would be slightly shorter than that observed here. These observations are consistent with both the bulge or the axisymmetric disc model. Distinguishing between these two models will be difficult. This is because the low inclination of 4U0614+09 prevents its orbital period being determined from X–ray observations. However if the 'superhump" phenomena causes the optical modulation then it should persist for several days (~10 days for SU UMa's). No periodic modulation was observable on Night 2. The transient nature of the modulation provides tentative evidence against it being produced by the superhump phenomena. The bulge model would be further supported if the colour of the object was observed to vary around the orbital cycle. This is because for some of the orbital cycle the bulge would present its cooler, and hence redder, side to the observer.

Alternatively it is possible that the modulation is "single wave" caused by the X–ray heated secondary changing its projected area around the orbital cycle. This type of modulation is observed in many LMXB systems, for example in: 4U1735–444 (Corbet *et al.* 1986), 4U1636–536 (Smale and Mukai 1988), XB1254–690 (Motch *et al.* 1987), Her X–1 and Sco X–1 (van Paradjis 1983). However the observed modulation is unlikely to be produced by this effect. Firstly one would expect the optical variability to be persistent: ie. to be visible in each nights data set, as in the light curves of 4U1735–444 (Corbet *et al.* 1986) and 4U1636–536 (Smale and Mukai 1988). The low level periodic modulations are not present in the Night 2 data. These may have been masked by the intrinsic variability of the X–ray source. However, the non periodic intrinsic

variability observed on Night 2 does not appear to be greater than that seen in the Night 1 or Night 3 data throwing some doubt on this explanation.
Secondly one would expect the periodic modulation to be sinusoidal if it was due to the changing aspect of a X–ray heated secondary. Such sinusoidal modulation is common to all systems where X–ray heating of the secondary is the major cause of the periodic modulation. The light curve of 4U0614+09 is distinctly non sinusoidal (Figure 6.11a,b and c) implying that X–ray heating of the secondary is NOT the cause of the modulation observed here.

The Short Orbital Period

What are the implications of a short orbital period? If it is assumed that the neutron star accretes from a Roche lobe filling secondary then the mass of the secondary can be found from $(R_{comp}/R_{\odot})=0.234(M_{comp}/M_{\odot})^{1/3}(P/1hr)^{2/3}$ with the mean mass radius relation for a lower main sequence dwarf being $(R_{comp}/R_{\odot})\simeq(M_{comp}/M_{\odot})^{0.88}$ (Patterson 1984). Solving these relations gives $M_{comp}\simeq 0.07M_{\odot}$. This is NOT a valid solution to these equations since stars with masses $<0.085M_{\odot}$ fail to ignite hydrogen in their core and hence never reach the main sequence (Graboske and Grossman 1973).
It has been found that for hydrogen rich (X>0.5) secondary stars the minimum orbital period possible is ~80 minutes (Paczyński and Sienkiewicz 1981). This minimum arises as follows. The secondary begins mass transfer whilst on the main sequence. The timescale for mass transference is much greater than the secondary stars thermal timescale ($\propto M^2$), and hence it remains in thermal equilibrium: ie. on the main sequence. When the stellar mass decreases to ~ 0.12–$0.15M_{\odot}$ these two timescales become comparable, the amount of energy being radiated away becoming approximately equal to that produced in the

stars interior by thermonuclear fusion. The secondary star is then driven out of thermal equilibrium and towards a non nuclear burning, degenerate state. As mass transfer continues the orbital period of the system begins to increase ($P_{orb} \propto R^3_{sec}/M_{sec}$, Section 1.3a) since the radius of degenerate stars increase as their mass decrease. However *it is possible* to obtain an orbital period shorter than 80 minutes. Nelson *et al.* (1986) have performed calculations for the evolution of ultra short period systems (P<80 minutes). They find that an orbital period of ~35 minutes is possible provided the secondary star is hydrogen deficient (X<0.5). From their results one finds that the secondary star in 4U0614+09 is only weakly hydrogen deficient 0.1<X<0.5, with the lower limit of hydrogen deficiency implying a mass and radius of about $0.15M_\odot$ and $0.15R_\odot$ respectively for an assumed $\dot{M}=10^{-10}$ $M_\odot$ yr^{-1}. Note that $\dot{M}$ is very uncertain for this system since its distance is poorly constrained. Using Keplers law the separation of the binary components is estimated to be $\sim 0.6R_\odot$ (assuming a mass for the neutron star of $1.4M_\odot$). The absence of hydrogen emission from any of the spectra of 4U0614+09 provides evidence that the mass donating star is highly evolved. Other "normal" LMXBs usually show weak hydrogen emission lines as well as He II λ4646 and the Bowen blend at $\sim\lambda$4640–4660 (Bradt and McClintock 1983).

Since X–ray heating of the secondary does not cause the optical modulation one can infer that the accretion disc in this system has a thick rim (Milgrom 1978), or alternatively the secondary is small. If the orbital separation is $\sim 0.6R_\odot$ and the radius of the secondary $\sim 0.15R_\odot$ then provided the disc has a rim that has an angular height of $\geq 15°$ from the neutron star the secondary is completely shadowed. This could indeed be the case for at least part of the orbital cycle since disc bulges often have projected vertical heights of $\geq 15°$.

4U0614+09 is probably the third LMXB whose orbital period is <80 minutes (the second possibly being the low inclination system, X1905+00, Chevalier and Ilovaisky 1990) and hence will be a crucial system for testing evolutionary theories.

6.4 Conclusions

Extensive optical monitoring of 4U0614+09 has revealed that the system is variable on two characteristic timescales: ~10 days and ~1 hour. A plausible interpretation for the former is this is precession of an accretion disc whilst the latter is probably the orbital period of the system. Assuming a one hour orbital period it is possible to infer that the secondary is hydrogen deficient with a mass and radius of $\sim 0.15 M_{\odot}$ and $\sim 0.15 R_{\odot}$ respectively with an orbital separation of $\sim 0.6 R_{\odot}$. The optical modulation is probably caused by the changing aspect of the inner surface of a X–ray heated bulge. But further observations are needed to confirm this.

During simultaneous X–ray and optical observations the fluxes are anticorrelated. No clear explanation for the observed X–ray and optical behaviour exists, however it is possible that the anticorrelation can be explained by assuming that in some circumstances the mass accretion rate (and hence the reprocessing area and optical flux) is anticorrelated with the X–ray luminosity.

The spectrum is unusual in that it does not display any He II λ4686 emission but *does* display the Bowen blend λ4640–4660 feature. This is probably due to a combination of high metallicity and electron collisional excitation of the Bowen process (instead of the more usual electron recombination) causing an enhancement of the λ4640–4660 flux over the He II flux.

6.5 References

Allen, C.W., 1973. *Astrophysical Quantities,* Section 125, p. 264, The Athlone Press, London.

Allington-Smith, J.R., Breare, J.M., Carrasco, B.E., Ellis, R.S., Parry, I.R., Webster, J., Gellatly, D.W., Gribbin, F.J., Ingle, M., Jorden, P.R., Lowne, C.M., Powell, J.R., Thorne, D.J., Taylor, C., van Breda, I.G., Waltham, N.R., Worswick, S.P. & Wynne, C.G., 1989. *Mon. Not. R. astr. Soc.,* **238,** 603.

Argyle, R.W., Mayer, C.J., Pike, C.D. & Jorden, P.R. 1988. In:*I.N.G. User Manual - No. XVIII. A User Guide to the JKT Camera (Version 1)*

Aurière, M., Le Fèvre, O. & Terzan, A., 1984. *Astron. Astrophys.,* **61,** 99.

Bradt, H.V.D. & McClintock, J.E., 1983. *Ann. Rev. Astron. Astrophys.,* **21,** 13.

Branduardi-Raymont, G., Corbet, R.H.D., Mason, K.O., Parmar, A.N., Murdin, P.G. & White, N.E., 1983. *Mon. Not. R. astr. Soc.,* **205,** 403.

Canizares, C.R., McClintock, J.E. & Grindlay, J.E., 1979. *Astrophys. J.,* **234,** 556.

Chevalier, C. & Ilovaisky, S.A., 1990. In:*Proceedings of the 23rd ESLAB Symposium,* Vol. 1, p. 345, eds. Hunt, J & Buttrick, B., ESA Publications Division, ESTEC, Noorwijk, The Netherlands.

Corbet, R.H.D., Thorstensen, J.R., Charles, P.A., Menzies, J.W., Naylor, T. & Smale, A.P., 1986. *Mon. Not. R. astr. Soc.,* **222,** 15P.

Corbet, R.H.D., Smale, A.P., Charles, P.A., Lewin, W.H.G., Menzies, J.W., Naylor, T., Pennix, W., Szajno, M., Thorstensen, J.R., Trümper, J. & van Paradjis, J., 1989. *Mon. Not. R. astr. Soc.,* **239,** 533.

Corbet, R.H.D., 1990. *Private Communication*

Cowley, A.P., Crampton, D. & Hutchings, J.B., , 1979. *Astrophys. J.,* **231,** 539.

Davidsen, A., Malina, R., Smith, H., Spinrad, H., Margon, B., Mason, K., Hawkins, F. & Sanford, P., 1974. *Astrophys. J.,* **193,** L25.

Deeter, J., Corosa, L., Gerend, D. & Boynton P.E., 1976. *Astrophys. J.,* **206,** 861.

Deguchi, S., 1985. *Astrophys. J.,* **291,** 492.

Fabian, A.C., Guilbert, P.W., Motch, C., Ricketts, M., Ilovaisky, S.A. & Chevalier, C., 1982. *Astron. Astrophys.* **111,** L9.

FitzGerald, P.M., 1968. *Astron. J.,* **73,** 988.

Forman, W., Jones, C., Cominsky, L., Julien, P., Murray, S., Peters, G., Tananbaum, H. & Giacconi, R., 1978. *Astrophys. J. Suppl.,* **38,** 357.

Fuller, N.M.J., 1989. *Science and Engineering Research Council, Rutherford Appleton Laboratory, Space and Astronomy Division, Starlink Project, Starlink User Note* **86.7.**

Gerend, D. & Boynton, P.E., 1976. *Astrophys. J.*, **209**, 562.

Graboske, Jr., H.C. & Grossman, A.S., 1971. *Astrophys. J.*, **170**, 363

Grindlay, J.E., 1990. In:*Proceedings of the 23rd ESLAB Symposium*, Vol. 1, p. 121, eds. Hunt, J & Buttrick, B., ESA Publications Division, ESTEC, Noorwijk, The Netherlands.

Grindlay, J.E., Bailyn, C.D., Cohn, H., Lugger, P.M., Thorstensen, J.R. & Wegner, G., 1988. *Astrophys. J.*, , **334**, L25.

Herbig, G.H., 1975. *Astrophys. J.*, , **196**, 129.

Horne, K.D., 1986. *Publs. astr. Soc. Pacif.*, **98**, 609.

Howarth, I.D. & Murray, J., 1988. *Science and Engineering Research Council, Rutherford Appleton Laboratory, Space and Astronomy Division, Starlink Project, Starlink User Note* **50.1**

Johnson, H.L., 1965. *Astrophys. J.*, **141**, 923.

Ilovaisky, S.A., Chevalier, C., Motch, C., Pakull, M., van Paradjis, J. & Lub, J., 1984. *Astr. Astrophys.*, **140**, 251.

Landolt, A.U., 1983. *Astron. J.*, **88**, 439.

Lang, F.L., Levine, A.M., Bautz, M., Hauskins S., Howe, S., Primini, F.A., Lewin, W.H.G., Baity, W.A., Knight, F.K., Rothschild, R.E. & Petterson, J.A., 1981. *Astrophys. J.*, **246**, L21.

Lehto, H. 1989. *Private Communication.*

Marshall, N. & Millit, J.M., 1981. *Nature*, **293**, 379.

Mason, K.O., Charles, P.A., White, N.E., Culhane, J.L., Sanford, P.W. & Strong, K.T., 1976. *Mon. Not. R. astr. Soc.*, **177**, 513.

Mason, K.O., 1990. In:*Proceedings of the 23rd ESLAB Symposium*, Vol. 1, p. 113, eds. Hunt, J & Buttrick, B., ESA Publications Division, ESTEC, Noorwijk, The Netherlands.

McClintock, J.E., Canizares, C.R. & Tarter, C.B., 1975. *Astrophys. J.*, **198**, 641.

Milgrom, M., 1978. *Astron. Astrophys.*, **67**, L25.

Miyamoto, S. & Matsuoka, M., 1977. *Space Sci. Rev.*, **20**, 687.

Motch, C., Ricketts, M.J., Page, C.G., Ilovaisky, S.A. & Chevalier, C., 1983. *Astron. Astrophys.*, **119**, 171.

Motch, C., Petersen, H., Beuermann, K., Pakull M.W. & Courvoisier, T.J.–L., 1987. *Astrophys. J.*, **313**, 792.

Motch, C. & Pakull M.W., 1989. *Astron. Astrophys.*, **214**, L1.

Mukai, K., 1990. *Publs. astr. Soc. Pacif.*, **102**, 183.

Murdin, P.G., Penston, M.J., Penston, M.V., Glass, I.S., Sanford, P.W., Hawkins, F.J., Mason, K.O. & Wilmore, A.P., 1974. *Mon. Not. R. astr. Soc.*, **169**, 25.

Naylor, T., Charles, P.A., Drew, J.E. & Hassall, B.J.M., 1988. *Mon. Not. R. astr. Soc.*, **233**, 285.

Nelson, L.A., Rappaport, S. & Joss, P.C., 1986. *Astrophys. J.*, **304**, 231

Oke, J.B., 1974. *Astrophys. J. Suppl.*, **27**, 21.

Paczyński, B., 1971. *Ann. Rev. Astron. Astrophys.*, **9**, 183.

Paczyński, B. & Sienkiewicz, R., 1981. *Astrophys. J.*, **248**, L27.

Parmar, A.N. & White, N.E., 1988. In:*X-ray Astronomy with EXOSAT*, eds. White, N.E. & Pallivicini, R., Memoria Soc. Astron. Ital., **59**, 147.

Patterson, J., 1984. *Astrophys. J. Suppl.* **54**, 443.

Priedhorsky, W.C., 1986. *Astrophys. J.*, **306**, L97.

Priedhorsky, W.C., Hasinger, G., Lewin, W.H.G., Middleditch, J., Parmer, A., Stella, L. & White, N. 1986. *Astrophys. J.*, **306**, L91.

Priedhorsky, W.C. & Terrell, J., 1984. *Astrophys. J.*, **280**, 661.

Roberts, D.H., Lehár, J. & Dreher, J.W., 1987. *Astron. J.*, **93**, 968.

Schmidtke, P.C., 1988. *Astron. J*, **95**, 1528.

Smale, A.P., Corbet, R.H.D., Charles, P.A., Menzies, J.W. & Mack, P., 1986. *Mon. Not. R. astr. Soc.*, **223**, 207.

Smale, A.P. & Mukai, K., 1988. *Mon. Not. R. astr. Soc.*, **231**, 663.

Smale, A.P., Mason, K.O., White, N.E. & Gottwald, M., 1988. *Mon. Not. R. astr. Soc.*, **232**, 647.

Stetson, P.B., 1987. *Pub. Astron. Soc. Pac.*, **99**, 191.

Swank, J.H., Becker, R.H., Boldt, E.A., Holt, S.S. & Seremitsos P.J., 1978. *Mon. Not. R. astr. Soc.*, **182**, 349.

Tananbaum, H., Gursky, H., Kellogg, E.M., Levinson, R., Schreier, E. & Giacconi, R., 1972. *Astrophys. J.*, **174**, L143.

Thorstensen, J.R. & Freed, I.W., 1985. *Astron. J.*, **90**, 2082.

Tritton, K., 1989. *Private Communication*

Turner M.J.L, Smith, A.S. & Zimmermann, H.U., 1981. *Space Sci. Rev.*, **30**, 513.

van der Klis, M., 1989. *Ann. Rev. Astron. Astrophys.*, **27**, 517.

van Paradjis, J., 1981. *Astr. Astrophys.*, **103**, 140.

van Paradjis, J., 1983. In:*The Evolution of Galactic X-ray Binaries.*, p. 189, eds. Lewin, W.H.G., & van den Heuvel, E.P.J., Cambridge University Press, Cambridge

Webbink, R.F., 1985. In:*Dynamics of Star Clusters, IAU Symp. No. 113*, p. 541, eds. Goodman, J., & Hut, P., Reidel, Dordrecht.

Westerlund, B.E., 1990. *Astron. Astrophys. Rev.*, **1**, 29.

White, N.E. & Swank, J.H., 1982. *Astrophys. J.*, **253**, L61.

White, N.E., 1989. *Astron. Astrophys. Rev.*, **1**, 85.

Whitehurst, R., 1988. *Mon. Not. R. astr. Soc.*, **232**, 35.

Concluding Notes

Although the formation of globular cluster CVs by various capture mechanisms has been discussed in the literature for over a decade (egs. Fabian *et al.* 1975, Verbunt & Meylan 1988) very few have ever been discovered. This is either because the very crowded observing fields have prevented the detection of CVs or because the calculations overestimate the number formed. With the advent of high sensitivity CCD detectors and reliable crowded field photometry packages (eg. DAOPHOT, Stetson 1987) the observational problems are, at last, being overcome.

This thesis contains the first detailed study of the two best known globular cluster CV candidates; V4 in M30 and V101 in M5. It is shown that the observational properties of V4 are incompatible with cluster membership. This leaves V101 as the only DN whose observational properties are consistent with cluster membership. Therefore further study of this system would now be useful. It should be relatively easy to determine the system's orbital period (probably ~5–8 hours) since its quiescent light curve displays humplike structure. Also, high resolution time resolved spectroscopy could be performed to determine the objects radial velocity curve and properly confirm cluster membership. Finally, since V101 is at a known distance, its luminosity is known. Therefore, provided the observational properties of V101 are unaffected by its metallicity, it might be possible to use this object as a "standard candle" for similar DN.

The most efficient technique of detecting CVs in globular clusters involves constructing a deep ($M_V \sim 10$) colour magnitude diagram of the cluster core (as described in Chapter 4). In the case of M71 no new CVs were found. It is thought that many CVs are formed in centrally condensed clusters (examples

of which are 47 Tuc and Ter 5, Verbunt & Meylan 1988, Verbunt & Hut 1987). This is because of the high stellar interaction rate within their core. However very few CVs may actually be found, thus supporting the recent suggestion by Bailyn, Grindlay and Garcia (1990) that few white dwarf binaries in globular clusters ever form CVs.

Obtaining deep colour magnitude diagrams for the cores of centrally condensed clusters is extremely difficult. This is because the seeing, which limits the resolution of even the best ground based telescopes to $\sim 1''$, severely blurs the stellar images. This situation would be improved enormously if higher resolution images could be obtained. The Hubble Space Telescope should have made a major contribution to this field. However its focussing problems have probably rendered it unsuitable for high resolution work. A more promising development is the advent of active optics on ground based telescopes. This technique, whilst not correcting for the effects of atmospheric turbulence, ensures that the telescope optics are always performing optimally. The New Technology Telescope uses active optics to routinely achieve $0.4''$ seeing (Wilson 1989). The improved resolution that results from the use of active optics should make it easier to detect faint, blue, quiescent CVs ($M_V \sim 9$) in globular clusters.

The ROSAT X–ray observatory should also make a significant contribution to the field of globular cluster CVs. Hertz and Grindlay (1983) suggested that the low luminosity X–ray sources (detected by the EINSTEIN X–ray observatory) in ω Cen and NGC6656 were CVs. This interpretation has been the cause of controversy for several years (eg. Margon and Bolte 1987, Verbunt and Meylan 1988). Observations with ROSAT should help resolve this controversy by providing the first accurate positions ($\sim 2''$) for these sources. This will then help in the search for their optical counterparts. In addition, as ROSAT will be able to

measure the X–ray spectra of the low luminosity sources it should be possible to compare them with the X–ray spectra of other CVs. This should then provide a powerful test as to whether these objects are CVs or not. Finally, ROSAT will be more sensitive than previous X–ray satellites enabling a deep search for other low luminosity globular cluster X–ray sources to be performed.

Radio observations of globular cluster LMXBs are still in their infancy. This is because instrumentation and data processing techniques have only recently become sufficiently advanced to detect these objects. The results reported in Chapter 5 represent the sum total of our knowledge of the radio properties of globular cluster LMXBs. These observations have established that, like their galactic counterparts, the globular cluster LMXBs emit radio radiation and that the emission regions appear extended. In addition improved positions for the detected globular cluster LMXBs have been found. Further VLA observations of these and other globular cluster LMXBs have recently been performed (Lehto, Callanan and McHardy 1990). It is hoped that these new observations will discover more LMXB radio counterparts and also establish the nature of the radio emission mechanism via spectral slope measurements. The former should further improve the possibility of discovering the elusive optical counterparts to the globular cluster LMXBs.

The galactic plane LMXB 4U0614+09 has been one of the least studied LMXBs in the galaxy. It does, however, display a number of interesting phenomena. Firstly, the absence of He II λ4686 but the presence of the "Bowen" blend feature λ4640–4660 is highly unusual. A high resolution spectrum, possibly obtained with the HST, ($\sim\lambda$3000–5000) is essential for investigating this behaviour. In particular it would permit a search for other Bowen fluorescence

lines. Secondly, the anti–correlated X–ray and optical behaviour reported in Chapter 6 needs further study. Angelini (1990) is currently analysing simultaneous optical and X–ray data (the latter obtained with GINGA). It is hoped that these observations will shed new light onto the physical mechanism behind the anti–correlation observed. Thirdly, its orbital period is probably short (~60 minutes); very close to the theoretical minimum allowed for systems with hydrogen rich secondaries (Paczyński and Sienkiewicz 1981). If further observations confirm the short orbital period then a detailed study of the system may place constraints on the evolution of short period LMXBs.

References to Concluding Notes

Angelini, L., 1990. *Private Communication.*

Bailyn, C.D., Grindlay, J.E. & Garcia, M.R., 1990. *Astrophys. J.*, **357**, L35.

Fabian, A.C., Pringle, J.E. & Rees, M.J., 1975. *Mon. Not. R. astr. Soc.*, **172**, 15P

Hertz, P. & Grindlay, J.E., 1983. *Astrophys. J.*, **275**, 105.

Lehto, H.J., Callanan, P.J. & McHardy, I.M. 1990. *Private Communication.*

Margon, B. & Bolte, M. 1987. *Astrophys. J.*, **321**, L61.

Paczyński, B. & Sienkiewicz, R., 1981. *Astrophys. J.*, **248**, L27.

Stetson, P.B., 1987. *Publs. astr. Soc. Pacif.*, **99**, 191.

Verbunt F. & Hut, P., 1987. In:*The Origin and Evolution of Neutron Stars*, p. 187, eds. D.J. Helfand & J.-H. Huang, D. Reidel Publishing Company, Dordrect, Holland.

Verbunt F. & Meylan, G., 1988. *Astr. Astrophys.*, **203**, 267.

Wilson, R., 1989. *The Messenger*, **56**, 1.

Appendix I

An Introduction to Hot Subdwarf Stars

Hot subdwarfs are thought to be the progenitors of white dwarfs. Early work by Greenstein and Sargent (1974) and Baschek and Norris (1975) showed that they fell into one of four distinct subgroups. These subgroups were defined in terms of an effective temperature, T_{eff}, and whether the optical spectra was hydrogen or helium dominated.

The Classification of Hot Subdwarfs

i) The horizontal branch B (HBB) stars, T_{eff}~20,000 K, He poor.

ii) The subdwarf B (sdB) stars, T_{eff}~30,000 K, He poor.

iii) The subdwarf OB (sdOB) stars, T_{eff}~30,000–40,000 K, He poor.

iv) The subdwarf O (sdO) stars, $T_{eff} \geq$40,000 K, He rich.

The HBB stars are formed as part of the normal stellar evolution process. A main sequence star evolves through the sub–giant and then the red giant branches of the HR diagram. Its life as a red giant ends with the so called He flash, that is when core He burning begins. The star then descends from the tip of the red giant branch onto the horizontal branch forming the He "main sequence". These stars are hotter and less luminous than red giants with their thermonuclear energy being produced by steady core He and shell H burning. The two burning regions generate similar amounts of energy. Globular clusters often have well populated horizontal branches.

The sdB and sdOB stars appear to be a blue extension of the horizontal branch. Their He burning core (~0.5 $M_{\odot}$) is very similar in mass and luminosity to the

core of a HBB star whilst their H burning shell has negligible mass and luminosity (Heber 1987). The sd stars are observed to be fainter than HBB stars. This probably reflects the absence of the H burning shell. The spectra of sdB stars are dominated by H absorption lines with little or no He being present. Spectra of sdOB stars are also dominated by H but some He II is also present. Both these classes of stars appear under-abundant in He. This apparent under-abundance is thought to be caused by the gravitational settling of He in the sd stars atmosphere. This leaves a very thin envelope ($\sim$0.02 $M_{\odot}$) of almost pure H on the stars surface.

The sdO stars form a heterogeneous mixture of very hot blue objects. They are found to populate the HR diagram to the left of sdB/OB stars and have a wide range of absolute magnitude. Their spectra are dominated by He lines with H being weak or absent. The evolutionary status of these objects is unclear though some are observed to be the central stars of planetary nebulae.

Since I suggest that the objects in M71 are sdB stars I summarise their main observational and demographic properties. These were compiled from the studies of faint blue stars by Downes (1986), Heber (1986) and Green *et al.* (1986).

The Observed Properties of sdB Stars

i) They have colours B–V$\sim$–0.3 and U–B$\sim$–1 which imply a temperature of $\sim$25,000 K.

ii) They have a $<M_V>\sim5\pm1$

iii) with spectroscopy indicating that their photospheres are helium poor.

iv) They form part of an old disc population,

v) with a scale height of 175–325 pc and a space density of $\sim 2\times10^{-6}$ pc^{-3}.

The observed properties of the other hot sd stars can be found in the references.

References to Appendix I

Baschek, B. & Norris, J., 1975. *Astrophys. J.*, **199**, 694.

Downes, R.A. 1986. *Astrophys. J. Suppl.*, **61**, 569.

Green, R.F., Schmidt, M. & Liebert, J., 1986. *Astrophys. J. Suppl.* **61**, 305.

Greenstein, J.L. & Sargent, A.I., 1974. *Astrophys. J. Suppl.*, **28**, 157.

Heber, U., 1986. *Astron. Astrophys.*, **155**, 33.

Heber, U., 1987. *Mitt. Astron. Ges.*, **70**, 79.

Appendix II

An Introduction to Radio Observations, the VLA and the Reduction of VLA Data

II–1.0 Introduction

The prime purpose of a radio telescope is to measure the radio brightness distribution across the sky. However the angular resolution ($\delta\theta \sim \lambda/d$) of early (1940s) radio telescopes was severely limited because the diameter of the aperture d, was often not much larger than the observing wavelength λ. This problem could not be solved by building larger single aperture telescopes since their size and cost would be prohibitive. A successful solution to this dilemma was the invention of aperture synthesis.

II–1.1 The Principle of Aperture Synthesis

Aperture synthesis is essentially the reconstruction or synthesis of one large aperture telescope by using two (or more) "smaller" aperture telescopes. It relies on the fact that a simple two element interferometer gives a response that is proportional to one Fourier component of the two dimensional sky brightness distribution. By varying the spacing (baseline) and the orientation of the interferometer it is possible to determine the two dimensional transform of the brightness distribution, then by Fourier inversion to derive the brightness distribution of the source to a given resolution. The resolution being determined by the largest interferometer pair spacing (Ryle and Hewish 1960).

Each Fourier component is known as the *visibility*. In radio astronomy this is

generally taken to be a complex number containing both phase and amplitude information. There may be many thousands of individual visibility records depending on the size and sophistication of the array.

One problem with a "fixed antenna" interferometer is that the source would only be in the sensitive areas (the beams) of the individual antenna for a limited length of time. If the array elements are able to track the source across the sky as the earth rotates this problem is solved. With a long enough observation the whole of the sky brightness distribution of the source (within the limits of the instrument) is sampled. This technique is known as "earth rotation aperture synthesis" and is the technique employed by several radio telescopes including the VLA. It is an extremely powerful technique for measuring many Fourier components of the sky brightness distribution in a relatively short time. Upon inversion of the two dimensional visibility distribution the measured sky brightness distribution is close to the true sky brightness distribution smoothed by the "synthesised beam" (which has an angular width of $\sim\lambda/$(largest spacing)).

II–2.0 The VLA

The practical situation is more complicated than the discussion given above. A description of the instrument is given and an outline of its operation.

II–2.1 Description of the VLA

The VLA is an earth rotation aperture synthesis radio telescope. It consists of 27 antennae (each of which has a 25 m diameter aperture) arranged in a three armed "Y" shaped array. It can be mounted in one of four configurations (A,

B, C and D) with the largest (A) array having antennae furthest from the array centre, the most distant being at ~21 km. Its sensitivity is ~100 μJy at 4885 MHz (1 Jy$\equiv 10^{-26}$ W m^{-2} Hz^{-1}) and in the A array configuration at 6 cm has an angular resolution (synthesised beam width) of ~0.6″. It has six operating wavelengths 90 cm, 20 cm, 6 cm, 3.6 cm, 2 cm and 1.3 cm (Thompson *et al.* 1980, Bridle 1989).

II–2.2 Use of the Instrument

There now follows a qualitative description of the action of the VLA. It is helpful to remember that the VLA just measures many Fourier components of the radio sources sky brightness.

Any two antenna of the VLA form an interferometric pair. Theoretically each Fourier component of the sky brightness distribution is determined by multiplying the output of any two antenna together and measuring the result. Practically however the determination of the Fourier components is a highly complex business. Fomalont and Wright (1974) give a good description as to how the Fourier components (the visibilities) are determined in practice. One important aspect of this is the mixing (multiplying) of the weak detected signal (frequency ν_{RF}) with a strong local oscillator signal (frequency ν_O) to produce a signal at a lower, intermediate frequency (ν_{IF}). This is performed immediately after the amplification of the ν_{RF} signal. When the observing frequency is changed the frequency of the local oscillator is also changed so that the mixer output signal is always at ν_{IF}. This enables the same post mixer electronic components (amplifiers, correlators and filters) to be used independently of the observing frequency.

The visibilities are defined as functions of the baselines projected onto the sky resolved into u (EW) and v (NS) components, ie. projected onto the so called u–v plane. In an ideal situation all possible visibilities would be measured. As the interferometer pair observes a source on the celestial sphere the rotation of the earth causes the u–v components of the baseline to trace out ellipses, thereby sampling different visibilities. The ensemble of elliptical loci is known as the transfer or visibility function. It is a function of antenna spacing and declination. Arrays are designed to sample the u–v plane as widely and uniformly as possible to get good coverage of the two dimensional visibility function. This is because the fuller the coverage in the u–v plane the more Fourier components that have been sampled and adequate sampling is essential if a good image is to result (Thompson 1989).

After the data has been corrected for instrumental and atmospheric effects (described in Chapter 5) it is inverted into the image plane via fast Fourier transform techniques; details of such schemes can be found in Hjellming and Basart (1982). However one simple result can be seen intuitively. If a point source is observed the Fourier transform of its transfer function gives the synthesized antenna response ie. the synthesised beam. A simple discussion of the details of image formation is given below.

II–3.1 Image Construction

The radio brightness distribution of a source is effectively the Fourier transform of the visibilities, calibrated for instrumental and atmospheric effects, that are recorded at various points in the u–v plane. However, before inversion, the data has to be "gridded" and choices have to be made as to how the visibilities

are "weighted" and "tapered". To apply fast Fourier transform techniques the visibility points are gridded, usually with powers–of–two points along each side of the grid (eg. 512×512 or 1024×1024) with cell sizes Δu and Δv chosen so as to get at least four points per synthesized beam width. A method must be found to assign visibility values to the grid points from the observed quantities. This is done by convolving the weighted, calibrated visibilities with a suitable function and then sampling the resultant convolution at the centre of the cell or grid. This "weighting and averaging" process gives a single complex visibility for each grid point.

For detection experiments it is found that to obtain the best signal to noise ratio in the map the gridded points should have a "natural weighting" applied to them. This means that all the data points are given equal weight. Or put another way they are assigned a weight proportional to the number of visibility points "averaged" together to determine the gridded visibility point. This has the effect of emphasizing the data from the short spacings. In other words it de–emphasizes the extremal parts of the u–v plane which are poorly sampled and hence prone to introduce artifacts into the image. A u–v taper can also be applied. This is generally taken to be an elliptical gaussian with a FWHM chosen so that the u–v points used in the Fourier inversion are well sampled ie. it is usually chosen so that the extremal parts of the u–v plane are reduced in significance. Once gridding of the calibrated, weighted, visibility points has been performed inversion can take place. Unfortunately even when weighting and tapering have been applied the direct transform of the gridded visibilities (known as the dirty map or image) display many artifacts mainly due to the incomplete sampling of sky brightness distribution in the u–v plane, ie. insufficient Fourier components are known for good image reconstruction. Note that

the Fourier transform of the convolved product of the weighting and tapering functions gives the dirty beam.

One way of alleviating this problem uses an algorithm developed by Högbom (1974) known as CLEAN. This is based on two assumptions. The first being that the estimated sky brightness distribution is the true sky brightness distribution convolved with a fully known antenna pattern. The second is that the field of view under observation contains a limited number of distinct features. In practice this enables the radio source to be represented by a number of point sources in an otherwise empty field. An iterative method is used to locate the position and strength of the point sources. The final "CLEAN" image is the sum of these point components convolved with a "CLEAN" beam (usually defined as an elliptical gaussian with the same FWHM as the central peak of the dirty beam but with no sidelobes). The algorithm proceeds as follows.

The largest amplitude point in the dirty image is found, the dirty beam is scaled to that point and then subtracted from the map. Only a fraction (10–25%) of the point is subtracted. This process is repeated until the maximum remaining amplitude is below a certain user specified threshold value. The map has now been effectively deconvolved into a series of δ functions, representing point sources at map grid positions. The map is then rebuilt using an artificial antenna pattern, ie. the "CLEAN" beam. The residuals of the dirty image are then added back into the "CLEAN" image. Note that "CLEAN" does not give a unique solution to the deconvolution problem but it does radically improve the solution derived from direct inversion (Brauw 1975, Cornwell and Braun 1989).

A way of improving further the observed map is by "self calibration". For this a reasonable model for the radio sky brightness distribution must be known.

Hence the CLEANed map is often used as the starting point for self calibration. Note that self calibration will lead to an improvement in image quality only if there is a bright source ($\geq 10\sigma$) in the observed field and the CLEAN components (remembering that the radio sky brightness distribution is described by a series of points by CLEAN) are a good representation of all the radio flux in the field. Self calibration then proceeds iteratively as follows. The CLEANed (or otherwise) map is taken as a model for the true radio sky brightness distribution, visibilities are calculated for this model. The ratios of the measured to the model visibilities are found (this is why a bright source is necessary otherwise this ratio would be dominated by noise) and correction factors derived for the calibration factors found from the observations of the external calibrators (Chapter 5) giving a new set of visibilities. These new visibilities are then inverted and CLEAN (or some other technique) is then used to obtain a better map. This procedure is then repeated until the input and output maps are the same (Pearson and Readhead 1984). Unfortunately this final improvement relies on there being a bright source present in the beam which is often not the case with detection experiments.

References to Appendix II

Brauw, W.N., 1975. In:*Image Processing Techniques in Astronomy,* p. 301, eds. De Jager, C. & p. Nieuwenhuijzen, H., D. Reidel Publishing Company, Dordrecht–Holland.

Bridle, A.H., 1989. In:*Synthesis Imaging in Radio Astronomy,* p. 443, eds. Perley, R.A., Schwab,F.R. & Bridle, A.H., Brigham Young University Print Services, Provo, Utah, USA.

Cornwell, T., & Braun, R., 1989. In:*Synthesis Imaging in Radio Astronomy,* p. 167, eds. Perley, R.A., Schwab, F.R. and Bridle, A.H., Brigham Young University Print Services, Provo, Utah, USA.

Fomalont, E.B. & Wright, M.C.H., 1974. In:*Galactic and Extragalactic Radio Astronomy,* p. 256., eds. Verschuur, G.L. & Kellermann, K.I., Springer–Verlag, USA.

Hjellming, R.M., & Basart, J.P., 1982. In:*An Introduction to the NRAO Very Large Array,* Ch. 2.

Högbom, J., 1974., *Astrophys. J. Suppl,* **15,** 417.

Kraus, J.D., 1984. In:*Radio Astronomy (2nd ed.,* p. 6–49, Cygnus–Quasar Books, Ohio, USA.

Ryle, M. & Hewish, A., 1960. *Mon. Not. R. astr. Soc.,* **120,** 220.

Pearson, T.J. & Readhead, A.C.S., 1984. *Ann. Rev. Astron. Astrophys.,* **22,** 97.

Thompson, A.R., 1989. In:*Synthesis Imaging in Radio Astronomy,* eds. Perley, R.A., Schwab,F.R. & Bridle, A.H., p. 11., Brigham Young University Print Services, Provo, Utah, USA.

Thompson, A.R., Clark, B.G., Wade, C.M. & Napier, P.J., 1980. *Astrophys. J. Suppl.,* **44,** 151.

Publications Resulting From this Thesis

From Chapters 2, 3 and 4

Machin, G., Callanan, P.J., Charles, P.A. & Naylor, T., 1990. *Accretion-Powered Compact Binaries; Proc. 11th North American Workshop on CVs and LMXBs.* p. 163, ed. C. W. Mauche, Cambridge University Press.
"WHT Spectroscopy of Globular Cluster CVs."

From Chapter 4

Machin, G., Allington-Smith, J., Callanan, P.J., Charles, P.A., Hassall, B.J.M., Mason, K.O., Naylor, T., Smale, A.P. & van Paradijs, J., 1990. *Mon. Not. R. astr. Soc.*, **242**, 9p.
"WHT Observations of Cataclysmic Variables in Globular Clusters – The CV Candidates in M71."

From Chapter 5

Machin, G., McHardy, I.M., Lehto, H.J., Callanan, P.J. & Charles, P.A., 1990. *Mon. Not. R. astr. Soc.*, **246**, 237.
"VLA Observations of four bright Globular Cluster X–ray Sources."

From Chapter 6

Machin, G., Callanan, P.J., Charles, P.A., Thorstensen, J., Mukai, K., Corbet, R., Harlaftis, E.T., Brownsberger, K. & Hamwey, R., 1990. *Mon. Not. R. astr. Soc.*, in press.
"Optical and X–ray observations of 4U0614+09."

Acknowledgements

I thank my "unofficial supervisor" Paul Callanan for all the help and encouragement he has given me during the course of this thesis, especially for "getting me started" back in the hut days. I would also like to thank Phil Charles (my "phantom supervisor") who exercised some mysterious force from La Palma which kept drawing me there. I would especially like to thank him for involving me with the FOS–2 commissioning run on the WHT. I also thank Ian McHardy (my "official supervisor") for his help with writing the VLA proposal and also for making comments on an earlier draft of this thesis. Also I would like to express my appreciation to "Radio Man" Harry Lehto for heroically continuing to help with observations at the VLA despite ill health. Also for initiating me into the mysteries of AIPS and VLA data reduction.

In addition, I am indebted to Koji Mukai for his assistance with the optimal extraction of CCD spectra. Also Robin Corbet who provided the reduced EXOSAT light curve of 4U0614+09 for me to think about. Thanks also to John Thorstensen and the students of the Dartmouth Off–Campus Astronomy program (undergraduates Chris Breg, Jim Bramson, Doug Borden, Josh Eisenthal, Eric Fischer, Dave Hamilton, Steve Huettner, Ken Kokko, Frank Miele, Steve Nichols, Paul Scheible, Adam Usadi, Rob Walsh, and Paul Wlodkowski) who helped collect the MDM data. Also to Paul Murdin who obtained ~600 INT images of 4U0614+09 for me.

I would like to thank the Science and Engineering Research Council for awarding me a postgraduate studentship and for funding my many observing trips. I am also grateful to Oxford University Department of Astrophysics for allowing me to make full use of their facilities.

Finally, I thank my parents for the love and support they have given me over the years. But most of all I thank Catherine Machin for all the encouragement and support she has given me during the writing of this thesis. I look forward to a continuing successful collaboration with her for years to come.

Errata

p. 60. Radial velocities in Table 2.3 should be POSITIVE not negative.

p. 68. Point (iii) should read:
iii) That the secondary star is probably of spectral type K5.

p. 84. (a) Replace the end of sentence 4 with:
....Echevarria (1983) one can infer a magnitude of $M_V(sec) \leq 7.3$ for the secondary and a spectral type K5 or later.
(b) Point (i) should be replaced by:
i) The secondary is probably a ZAMS since it is well below the turnoff point ($M_V(turnoff) \sim 4.3$) for M5 (Richer & Fahlman 1987).
(c) Delete sentence 3 from point (ii).

p. 86. (a) Replace the end of sentence 10 with:
....this indicates that the secondary is probably of K type.
(b) Replace the end of sentence 13 with:
....the secondary is probably a K5 type main sequence star.

p. 88. Replace the end of sentence 3 with:
....eight hours with a K5 type main sequence secondary.

p. 120. The spherical trigonometry formula should read:
$\mathrm{Cos}(\Delta\theta)=\mathrm{Sin}(\delta_1)\mathrm{Sin}(\delta_2)+ \mathrm{Cos}(\delta_1)\mathrm{Cos}(\delta_2)\mathrm{Cos}(\alpha_1-\alpha_2)$

p. 125. The luminosity was calculated incorrectly; the integral after the parameterization $\nu'=\nu/4885$ MHz should be:
$L=4\pi d^2(4885\times10^6)^{\alpha+1} \int_{0.002}^{20} S_0 \nu'^{\alpha}\, d\nu'$

This leads to revised estimates for L, B_{min}, E_{min} and the lifetime to synchrotron emission τ for both NGC7078 (p. 125 & p. 126) and NGC6712 (p. 129). These are:

–	NGC7078	NGC6712
L $\times10^{22}$ erg s^{-1}	3.64	0.663
B_{min} μGauss	$4.5f^{-2/7}$	$9.3f^{-2/7}$
E_{min} $\times10^{40}$ erg	$3.94f^{3/7}$	$0.268f^{3/7}$
τ $\times10^{15}$ s	6.18	2.30
τ $\times10^{8}$ yrs	2	0.72

The conclusions of the chapter remain unaltered.

p. 180–181. Wherever axisymmetric appears read asymmetric.